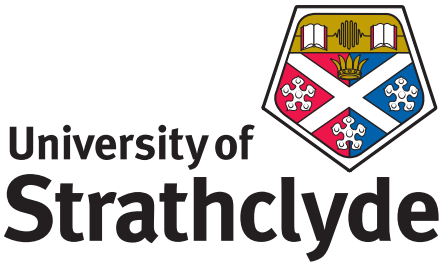

Island Nucleation and Growth during Submonolayer Deposition

K. P. O'Neill

Department of Mathematics and Statistics

University of Strathclyde

Glasgow, UK

June 2012

This thesis is submitted to the University of Strathclyde for the degree of Doctor of Philosophy in the Faculty of Science.

Acknowledgements

I would like to express my sincere gratitude to my three accomplished supervisors, Dr. Michael Grinfeld, Dr. Wilson Lamb and Dr. Paul A. Mulheran over the duration of this thesis. Without their guidance and support, it would have not been possible to write this thesis; because of this fact, I am eternally grateful to them.

I would also like to thank my family and friends for their help and support over the last three years.

Abstract

In this thesis, we develop a number of theoretical approaches that can be used to investigate the nucleation and growth of islands in submonolayer deposition. In particular, we consider initially a rate-equation approach in which we propose a system of differential equations as a mean-field model of the submonolayer deposition of monomers onto a surface. A key feature of these equations is that they depend explicitly on a parameter known as the critical island size. We use rigorous and novel mathematical techniques to obtain results on the asymptotic behaviour of the point island size distribution.

A fragmentation theory approach is also used in a one-dimensional model to obtain information on the asymptotic behaviour of the distribution of gaps between islands, the latter being represented by points on a line. This then leads to corresponding results for the capture zone distribution (CZD) associated with the islands. The CZD asymptotic forms that we obtain will be seen to differ from those of the Generalised Wigner Surmise (GWS) which has recently been proposed for island nucleation and growth models. The results predicted by our fragmentation approach and by the GWS are compared to kinetic Monte Carlo simulation data, and although this highlights both strengths and deficiencies in each approach, it also provides evidence that the fragmentation approach is more satisfactory than the GWS.

We conclude by presenting a model for the nucleation of point islands in one dimension that leads to distributional fixed point equations. This approach develops a new retrospective view of how the inter-island gaps and capture zones have developed from the fragmentation of larger entities. Solutions of these equations are compared to the simulation data, and to theoretical models based on more traditional fragmentation theory approaches. These comparisons confirm the competitive performance of the distributional fixed point equations.

Contents

1 Introduction **1**

1.1 Molecular Beam Epitaxy 3

1.2 The Need for Mathematical and Computational Modelling 8

1.3 Modelling Methodology 9

1.3.1 The Goal of Modelling 9

1.3.2 Rate Equations and the Island Size Distribution 10

1.3.3 Similarity Solutions 16

1.3.4 Attempts to Improve the ISD Approximation: the Capture Zone Distribution 20

1.3.5 Monte Carlo Simulation 25

1.3.6 Summary 27

1.4 Overview of Thesis 28

2 A Summary of Methods **31**

2.1 Introduction 31

2.2 Newton Polygon 32

2.3 The Mathematical Concept of a River 37

2.4 Watson's Lemma 43

2.5 One-Dimensional Laplace Integral 45

2.6 Bootstrap Method 47

3 Previous Work **49**

3.1 Analysis of the Island Size Distribution via Rate Equations 49

3.1.1 The Work of Bartelt & Evans and Blackman & Wilding . . 51

3.1.2 The Work of da Costa, van Roessel and Wattis 54

3.2 Analysis of the Gap Size Distribution in One-Dimensional Nucleation and Growth Model 59

3.2.1 The Blackman and Mulheran Theory 60

3.2.2 The Ziff and McGrady Fragmentation Equation 63

3.2.3 Similarity Solution of the Linear Fragmentation Equation . . 65

3.3 The Generalised Wigner Surmise 68

3.4 The Distributional Fixed Point Equation 72

4 Long Time Behaviour of Monomer and Point Island Size Distributions **74**

4.1 Introduction to the System 74

4.2 Asymptotic Behaviour of the Monomer and Total Island Distributions 82

4.3 Long Time Behaviour of the Island Size Distributions 88

4.4 Self-Similar Behaviour of the Coagulation System Outside the Characteristic Direction 95

4.4.1 Self-Similar Function 95

4.4.2 Monomeric Initial Data 96

4.4.3 Non-Monomeric Initial Data 101

4.5 Self-Similar Behaviour of the Coagulation System Along the Characteristic Direction 107

4.6 Conclusion 108

5 The Gap Evolution Equation **111**

5.1 Introduction 111

5.2 The Gap Evolution Equations 112

5.3 Asymptotics of Scaling Solutions for the Gap Size Distribution . . . 114

5.4 Asymptotics of Scaling Solutions for the Capture Zone Distribution 117

5.5 Conclusion: the Blackman and Mulheran Theory versus the Generalised Wigner Surmise 130

6 The Gap Size and Capture Zone Distributions in Monte Carlo Simulations **133**

6.1 Introduction 133

6.2 Monte Carlo Simulations 135

6.2.1 Full Simulation 136

6.2.2 Single-Gap Nucleation Rate Simulation 138

6.3 The Gap Evolution Equations Revised 139

6.4 Results 141

6.4.1 The Validity of Generalised Wigner Surmise 141

6.4.1.1 Case I: $d = 1$ 142

6.4.1.2 Case II: $d = 2$ 149

6.4.1.3 Case III: $d = 3$ 154

6.4.2 The Validity of Convolution Equation 160

6.4.3 Single-Gap Nucleation Rate 162

6.4.4 Full Simulation Behaviour 166

6.4.4.1 Small-Size Scaling of the Gap Size and Capture Zone Distributions 168

6.4.4.2 Large-Size Scaling of the Gap Size and Capture Zone Distributions 173

6.5 Conclusions 176

7 The Distributional Fixed Point Equation Approach 181

7.1 A Retrospective Approach 181

7.2 Analysis of the Scaled Gap Size Distribution 183

7.2.1 A DFPE without a Mean-Field Approximation Assumption for the Gap Size Distribution 190

7.2.2 Treat's Gap Size Distribution Function Revised 193

7.3 Analysis of the Scaled Capture Zone Distribution 194

7.4 Monte Carlo Simulation 198

7.5 Results 199

7.5.1 Comparisons of the Integral Equation and Monte Carlo Data for the Gap Size Distribution 199

7.5.2 Fragmentation Bias for the DFPE with a Non Mean-Field Approximation Assumption 201

7.5.3 Comparisons of the Integral Equation, Monte Carlo Data and the Generalised Wigner Surmise for the Capture Zone Distribution 203

7.5.4 Moments of the Gap Size Distribution 204

7.5.5 Moments of the Capture Zone Distribution 207

7.5.6 Small-Size Scaling of the Integral Equation 207

7.5.7 Large-Size Scaling of the Integral Equation 211

7.6 Conclusions 213

8 Conclusions and Future Directions 218

8.1 Conclusions 218

8.2 Future Directions 221

List of Figures

Chapter 1

1.1 The capture zone distributions at each different coverage 6

1.2 The Promixity and Voronoi cells 21

1.3 One-dimensional model of the capture zone distribution 21

Chapter 2

2.1 An example of Newton Polygon 37

2.2 Phase portrait of a river 38

2.3 Newton Polygon of a river 41

Chapter 4

4.1 Phase portrait of the system for n even and n odd 83

4.2 Newton Polygon of the system 83

Chapter 6

6.1 Monomers and island densities vs. coverage for 1-D extended islands 144

6.2 Monomers and island densities vs. coverage for 1-D point islands . . 145

6.3 The capture zone distributions for $i = 0$ and 1 in $d = 1$ 146

6.4 The capture zone distributions for $i = 2$ and 3 in $d = 1$ 147
6.5 Monomers and island densities vs. coverage for 2-D extended islands 150
6.6 Monomers and island densities vs. coverage for 2-D point islands . . 151
6.7 The capture zone distributions for $i = 0$ and 1 in $d = 2$ 152
6.8 The capture zone distributions for $i = 2$ and 3 in $d = 2$ 153
6.9 Monomers and island densities vs. coverage for 3-D extended islands 156
6.10 Monomers and island densities vs. coverage for 3-D point islands . . 157
6.11 The capture zone distributions for $i = 0$ and 1 in $d = 3$ 158
6.12 The capture zone distributions for $i = 2$ and 3 in $d = 3$ 159
6.13 The correlation of each two neighbouring gaps 161
6.14 Monomer density profile for $i = 1$ 163
6.15 Average time for a nucleation event to occur at all gaps 165
6.16 Histogram of the number of hops taken by the youngest monomer in an island for $i = 1$ 166
6.17 Monomers and island densities vs. coverage (up to 100%) for 1-D point islands 168
6.18 Small-size gap size distribution in logarithmic scale for $i = 0$, 1, 2 and 3 169
6.19 Small-size capture zone distribution in logarithmic scale for $i = 0$, 1, 2 and 3 170
6.20 Large-size gap size distribution in logarithmic scale for $i = 0$, 1, 2 and 3 173
6.21 Large-size capture zone distribution in logarithmic scale for $i = 0$, 1, 2 and 3 174

Chapter 7

7.1 One-dimensional model of the gap size distribution and capture zone distribution 183
7.2 The evolution of gap size distribution under iteration of the integral equation 188
7.3 The evolution of gap size distribution under iteration of the non mean-field integral equation 192
7.4 The sizes of capture zones of islands 195
7.5 The gap size distributions compared to histograms of MC data for various critical island size i 200
7.6 Comparison of the integral equations for the various gap size models 203
7.7 The capture zone distributions compared to histograms of MC data for various critical island size i 204
7.8 Small-size form of the integral equations for the gap size and capture zone distributions respectively in logarithmic scale 210
7.9 Large-size form of the integral equations for the gap size and capture zone distributions respectively in logarithmic scale 212

List of Tables

Chapter 2

2.1 Vertices using the Newton Polygon method 36

2.2 Vertices using the Newton Polygon method for the river example . . 41

Chapter 4

4.1 Vertices of the system using the Newton Polygon method 83

Chapter 6

6.1 Average island density for the 1-D simulation data 143

6.2 Best optimal values of β for $d = 1$ 148

6.3 Best optimal values of β for $d = 1$ using bootstrap methods 148

6.4 Average island density for the 2-D simulation data 149

6.5 Best optimal values of β for $d = 2$ 154

6.6 Best optimal values of β for $d = 2$ using bootstrap methods 154

6.7 Average island density for the 3-D simulation data 155

6.8 Best optimal values of β for $d = 3$ 160

6.9 Best optimal values of β for $d = 3$ using bootstrap methods 160

6.10 The average correlation of each two neighbouring gaps 162

6.11 Small gap nucleation rate exponents 165
6.12 Average island density for 1-D point islands 167
6.13 Average gradient for the small-size scaling of the gap size distribution using different bin-widths 170
6.14 Average gradient for the small-size scaling of the capture zone distribution using different bin-widths 171
6.15 Average gradient for the small-size scaling of the gap size distribution using bootstrap methods 171
6.16 Average gradient for the small-size scaling of the capture zone distribution using bootstrap methods 172
6.17 Average exponents for the large-size scaling of the gap size distribution using different bin-widths 174
6.18 Average exponents for the large-size scaling of the capture zone distribution using different bin-widths 175
6.19 Average exponents for the large-size scaling of the gap size distribution using bootstrap methods 175
6.20 Average exponents for the large-size scaling of the capture zone distribution using bootstrap methods 176

Chapter 7

7.1 Moments of the gap size distributions for $i = 0$, 1, 2 and 3 from the DFPE and from the MC simulations 205
7.2 Average moments of the gap size distributions for $i = 0$, 1, 2 and 3 from the DFPE and from the MC simulations 206
7.3 Moments of the capture zone distributions for $i = 0$, 1, 2 and 3 from the DFPE and from the MC simulations 208

7.4 Average moments of the capture zone distributions for $i = 0$, 1, 2 and 3 from the DFPE and from the MC simulations 209
7.5 Average gradient for the small-size scaling of the gap size distribution using different bin-widths 209
7.6 Average gradient for the small-size scaling of the capture zone distribution using different bin-widths 210
7.7 Average exponents for the large-size scaling of the gap size distribution using different bin-widths 212
7.8 Average exponents for the large-size scaling of the capture zone distribution using different bin-widths 213

List of Symbols

i	Critical island size	4
θ	Coverage	4
F	The deposition rate	4
k_b	Boltzmann's constant	4
T	The substrate temperature	4
E_d	The activation barrier for diffusion	5
v	The vibration frequency for hopping	5
D	The diffusion rate	5
l	The lattice connectivity	5
e	The hop length/lattice spacing	5
R	The ratio of deposition rate and diffusion rate	5
E_a	The adsorption energy	6
E_i	The bonding energy	6
t	The deposition time	7
j	The number of monomers	11
$c_j(t)$	The cluster density of size j at time t	11
$\sigma_{j,k}$	The coagulation/capture rate coefficients	11
a_j	The net rate of break-up of an cluster of size j	11
$b_{j,k}$	The average number of clusters	11
J_0	The source term of monomer input	12

γ_j Rate of release of monomers from an island of size j 12
κ_j Rate of direct impingement of monomers into an island of size j 12
n The smallest stable island size; $n := i + 1$ 13
α The deposition rate (same as F) 14
$u(x,t)$ The cluster density of size x at time t 14
$\sigma(x,y)$ The coagulation kernel/continuous version of $\sigma_{j,k}$ 14
$a(x)$ The fragmentation rate 14
$b(\cdot)$ The distribution of clusters of some size being produced 14
$H(\cdot,\cdot)$ The binary fragmentation kernel 15
λ The homogeneity index 15
$h(r)$ Homogeneous kernel 15
$\delta_{k,j}$ The Kronecker delta 16
$r(t)$ The typical island size 17
ϕ The scaling function 17
$M(t)$ The total mass 17
$N(t)$ The zeroth moment of $u(x,t)$ 19
$V(t)$ The first moment of $u(x,t)$ 19
$n_1(\cdot)$ The position dependent monomer density 20
$\phi(\cdot)$ The gap size distribution function 22
$P(\cdot)$ The capture zone distribution function 22
d Dimension 22
A The area of a capture zone 22
$\langle A \rangle$ The average area of a capture zone 22
β The sole parameter used in the Generalised Wigner Surmise 22
$P_\beta(s)$ The Generalised Wigner Surmise 23
$a_\beta,\ b_\beta$ Normalised constants for the Generalised Wigner Surmise 23

c_{st} The density of stable islands 23

$c_{j,A}$ The island density of size j and capture zone area A 23

X_d The distance between two parked cars 25

a Independent random variable 25

$f(a)$ The probability density 25

$\Gamma(\cdot)$ The Gamma function 46

c_1 The monomer density 53

c_0 The total island density of size $j \geq 1$ 55

$\tilde{c}_j(\tau)$ The cluster density of size j at time τ 57

$\Phi_1(\eta)$ The self-similar function with $\eta = j/\tau \neq 1$ 57

$\Phi_2(\xi)$ The self-similar function with $\xi = (j-\tau)/\sqrt{\tau}$ 58

E The average distance a monomer travels before being captured . 60

M The total number of traps on the line 62

$F_M(x)$ The number of gaps in the range x to $x + dx$ 62

$\mu_M(\cdot)$ The moment of $F_M(x)$ 62

$Q_\cdot$ The moment of the scaled gap size distribution function $\phi(X)$ .. 62

$u^*(x,t)$ Similarity solutions of $u(x,t)$ 65

$\mathcal{O}$ Big O notation 65

$G^{\cdot,\cdot}_{\cdot,\cdot}$ The Meijer G-function 66

$f_i(x)$ The empirical formula for the island size distribution 69

$C_i,\ a_i$ Normalisation constants for $f_i(x)$ 69

$w(t)$ The probability density function of X_d 72

$W(t)$ The cumulative density function of X_d 72

$\beta(\cdot,\cdot)$ The beta distribution 73

$B(\cdot,\cdot)$ The Beta function 112

ϕ_m The moments of Treat's ϕ 119

$\hat{\phi}_m$ The moments of the Ziff and McGrady ϕ 120

p_n A probability of spontaneous nucleation for the $i = 0$ case 136

$\langle c_j \rangle$ The average island density of size j 137

α_n The nucleation process 139

z The scaled gap size 140

Z_m The moments of the DFPE for the gap size distribution 189

T_m The moments of Treat's ϕ (same as ϕ_m) 193

S_m The moments of the DFPE for the capture zone distribution .. 197

G_m The moments of the Generalised Wigner Surmise 197

Chapter 1

Introduction

Coagulation and fragmentation processes are ubiquitous in nature and can often be found to lie at the heart of technological processes. Here by **coagulation** we mean the aggregation of smaller units of matter (which we call particles below) to create larger units. These units of matter can be objects as different as polymer molecules, clay particles, red blood cells or planetoids. **Fragmentation** processes are processes by which particles fall apart into smaller units. Though the main topic of this thesis is submonolayer deposition and growth, to be discussed in detail later, we start by presenting a number of examples from other areas where coagulation and fragmentation processes are important.

In *astrophysics*, the aggregation of dust particles is a common process in a variety of settings, such as the formation of protoplanetary disks. A protoplanetary disk is a rotating circumstellar disk of dense gas surrounding a young, newly formed star or a T Tauri star; it is the initial process in planet formation. The aggregation of dust particles can influence the appearance and evolution of a protoplanetary disk, and the subsequent planet [41, 88]. The coagulation-fragmentation processes were considered previously in this literature by Barrow [9].

In *medicine*, blood clotting provides an excellent example of coagulation-fragmentation dynamics. Red blood cells aggregate to form long, cylindrical shaped objects called rouleaux. A variety of diseases can cause strong adhesion between red blood cells which leads to blood vessel obstruction. For a model of the early stages of rouleaux formation, see [69].

Colloids are mixtures in which (colloidal) particles of one substance are dispersed in another. Colloidal particles are larger than those present in solutions but still invisible to the naked eye. Colloids exist in a number of forms, such as foams (whipped cream), emulsions (mayonnaise, milk) and aerosols, which will be described later. Processes such as the curdling of milk fall within the coagulation-fragmentation framework.

An *aerosol* is a suspension of fine solid particles, liquid droplets in a gas, or a combination of these, such as smoke, air pollution and smog [28, 34]. Understanding coagulation and fragmentation of soot particles under different conditions, is important in air pollution control; flame aerosol reactors are an emergent technology for the synthesis of nanoparticles [63].

In *polymer science*, processes of polymerisation such as step- and chain-growth polymerisation are clearly coagulation processes. Polymer chain breakage due to high shear mechanical action, chemical attack or radiation-induced chain scission [7] are examples of fragmentation in this industrially critical context.

In *molecular biology*, a molecule consisting of four key elements – carbon, hydrogen, oxygen and nitrogen – is known as an amino acid. Amino acids polyermise into polypeptides; polypeptides also polymerise into protein molecules (or simply proteins). Proteins consist of polymers built from a series of up to twenty different kinds of amino acids [58]. A protein is an example of a macromolecule (a large molecule). Other examples are deoxyribonucleic acid (DNA) and ribonucleic acid

(RNA). The polymerisation of proteins is a coagulation process and the method used to treat this polymerisation is similar to those for polymer science as discussed above.

Molecular beam epitaxy (MBE) is a process for growing thin films, which arise in a variety of applications such as optical coatings, corrosion protection, semiconductor devices and the self-assembly of nanostructures [5]. As this thesis deals with modelling and simulation of early stages of MBE, we will now discuss it in detail.

1.1 Molecular Beam Epitaxy

Epitaxy denotes the method of depositing a crystalline film on a crystalline substrate; such a deposited film is called an **epitaxial film**. If a film is deposited on a substrate of the same composition, the process is called **homoepitaxy**; otherwise it is called **heteroepitaxy**. MBE uses beams of atoms (or molecules) under ultra-high vacuum conditions. The reason for such conditions is to minimise the damage from the uncontrollable deposition of impurities such as H_2 and CO_2 [8].

Experimental techniques have been used to obtain data on the dynamics of MBE. Diffraction methods and direct imaging methods are the two main experimental techniques. The former involves the use of X-ray reflectivity and neutron scattering [73, 85]. Scanning tunnelling microscopy (STM) is the most commonly used direct imaging method, along with atomic force microscopy, scanning electron microscopy and transmission electron microscopy. In order to study epitaxial growth down to the atomic scale, STM snapshot images of epitaxial growth are taken at room temperature [80]. This provides the possibility of understanding growth processes. Despite the fact that STM has the ability to provide a res-

olution picture of a substrate at atomic scale, the scanning time is long, which leads to a limitation on the size of possible experimental systems. Note that the scanning time mainly means that we cannot directly view a nucleation process, and in general we can only observe the statistics of islands following nucleation. Therefore, we are concerned with the statistical consequences of various possible nucleation scenarios, and how these compare to experimental observations.

The **nucleation and growth** processes that characterise the growth of thin films, involve **deposition** of atoms on the surface, **surface diffusion**, and reversible chemical binding to other atoms and/or to the surface [78].

The first stage of MBE, when atoms or **monomers** are deposited onto a clean substrate, is called **submonolayer deposition**. It is of the utmost importance in MBE as the morphology and properties of the resulting multilayer film depend on the submonolayer structures. To describe submonolayer growth we will need the following concepts. We will call any cluster of monomers an **island**. A **stable island** is one from which no monomers can dissociate. If the smallest stable island contains $i+1$ monomers, the number i is the **critical island size**. **Coverage**, θ, is the percentage of substrate sites with monomers or islands on them.

The initial stage of MBE usually involves competition between nucleation and growth of islands due to monomer deposition, and diffusion of unattached monomers (**adatoms**). A minimal microscopic picture of submonolayer deposition may be described as follows [33]: monomers are deposited randomly with **deposition rate** F (in units of monolayers per unit time) onto a substrate surface. Isolated monomers diffuse along empty sites, hopping with Arrhenius rate

$$D_r = ve^{-E_d/(k_bT)}.$$

Here, k_b is Boltzmann's constant and T is the substrate temperature. The term

E_d is the activation barrier for diffusion and v is the pre-exponential factor. In the case of MBE, v is also known as the vibration frequency for hopping. D is subsequently the **diffusion rate** and so we have

$$D = \frac{D_r e^2}{l},$$

where l is the lattice connectivity (2 in one-dimension, 4 in two-dimensions and 6 in three-dimensions) and e is the hop length (lattice spacing).

New (immobile) islands are formed by aggregation of at least $i + 1$ diffusing monomers at a site, and growth of existing islands occurs by capturing monomers. To obtain a more realistic model [33] one may also include in this picture

- dynamics of (sub-stable) islands of size i or less;
- island mobility;
- direct impingement, that is, dynamics of monomers deposited on top of islands.

The monomer diffusion process can be described by a random walk on the substrate lattice with rate D. The dynamics of the process depend on the ratio $R = D/F$. The parameters θ and R together with the critical island size i and the temperature T play a crucial rôle in understanding the variation of island size and density.

Typically, it is found that for a fixed coverage θ, as R increases, the distance between the islands also increases. Similarly, for a fixed F, as coverage increases the island density also increases. In Figure 1.1, snapshots show in the two-dimensional case the growth of circular islands as the coverage increases; the region surrounding each island will be discussed in Subsection 1.3.4.

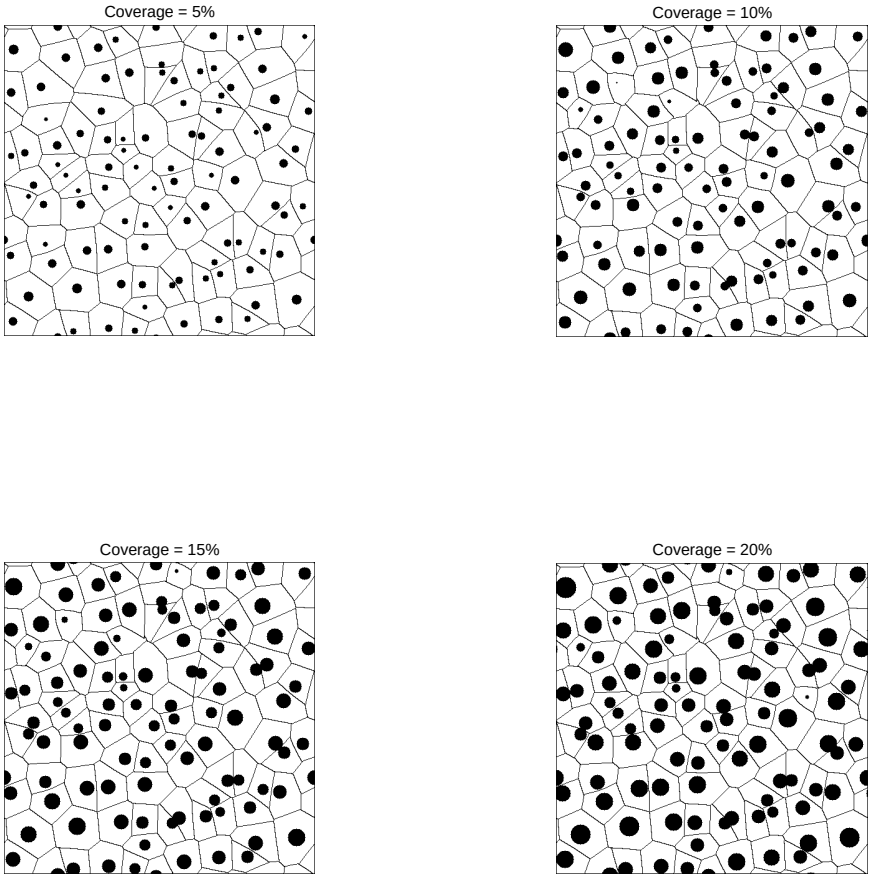

Figure 1.1: The coverage $\theta = 5\%$, 10%, 15% and 20% obtained by data from Monte Carlo simulations via MATLAB.

At high temperatures, monomers can re-evaporate, a process also known as **desorption**. The critical island size i is dependent on temperature, with i increasing as temperature increases. In this thesis, we assume $k_bT < E_a$ where E_a is the adsorption energy. Then $k_bT < E_d < E_a$ allows free monomer diffusion at reasonable rates. Note that if a monomer is attached to a stable island, it is bound there by E_i, say. So its barrier to diffusing away from the island is at least $E_i + E_d$ (it could, in principle, be larger). Therefore we might also say that

$k_bT \ll E_i$ for **irreversible aggregation**, in which the desorption process may be taken to be negligible during the stages of nucleation and growth of islands. Under such an assumption, in terms of F the coverage θ is given by $\theta = Ft$, where t is the deposition time [8, 12]. In terms of coverage, there are four distinct regimes, namely

1. Low coverage (L): at early times, the coverage and typical island size are both small. During the deposition process in this regime, the monomer density is much larger than the island density. There is a linear increase in the monomer density; island density is increasing due to the nucleation of new islands.

2. Intermediate coverage (I): the density of islands becomes comparable with the monomer density. The monomer density decreases as the island density increases due to significant nucleation of new islands.

3. Aggregation (A): here the island density increases slowly, and the monomer density decreases more rapidly – the fate of a monomer is much more likely to be aggregation into an island than nucleation of a new island.

4. Percolation or Coalescence (C): the island density decreases as islands coalesce. This causes the creation of a lattice-spanning cluster (percolation). Eventually second-layer growth occurs.

If we assume that either islands are mobile or that detachment of monomers is possible for an island of any size, then there are two different types of processes that can cause a reduction in the number of islands (known as coarsening) in the percolation regime : Ostwald and Smoluchowski ripening. **Ostwald ripening** is a phenomenon in which small clusters dissolve and redeposit their monomers into

larger islands. **Smoluchowski ripening** occurs when islands migrate until they collide and coalesce with other islands.

From now on, we focus only on the submonolayer deposition stage: it is vital to understand how the processes of deposition and diffusion affect the shape of islands and their size and spatial distributions, since the islands may be seen as the building blocks upon which the eventual film morphology depends.

1.2 The Need for Mathematical and Computational Modelling

From the above discussion, it should be clear that understanding submonolayer deposition dynamics is crucial if we want to be able to predict and control epitaxial film morphology. More precisely, given a system with parameters θ, R, T and i, an understanding is required of the following topics:

1. dependence of the island size distribution on the parameters of the system, in particular on the critical island size i;
2. island and monomer density evolution during the deposition process;
3. evolving island morphology;
4. dependence of the dynamics on system size.

Experimentally, the important parameters for a given combination of substrate and deposited material are deposition rate F, temperature T and time t. In terms of a simplified model these translate to the ratio $R = D/F$, coverage θ and i. The critical island size i will depend on both T and F; the rate at which islands can dissociate depends on the bonding energy, E_i, of the monomer to the island.

For stable islands this rate will be much lower than that at which new monomers impinge thus depending on F. In this thesis, these material aspects will not be considered in any further detail. Instead, we focus on the impact of the model parameters R, θ and i on the resultant statistics.

As we briefly noted above, experimental techniques (in addition to being expensive) are time-consuming and limited by experimental system size. Hence a need has long been felt for a theoretical and computational assault on this industrially important problem.

It has been found that kinetic Monte Carlo (MC) simulations are an invaluable way of generating numerical data that compare well with experimental data [15, 53]. This technique for the stages of nucleation and growth of islands will be discussed in detail in Chapter 6. For now it suffices to say that these simulations can yield realistic statistics for the nucleation and growth stages. However, not only are MC simulations restricted in the size of the system we can simulate by memory and execution time limitations of available computers, but it is also true that no simulations can by themselves explain how the growth might depend on deposition rate and/or temperature; only a theoretical analysis can do that. On the other hand, MC simulations provide a falsification framework for any theoretical work, since a theory's predictions can always be checked against the results of a MC simulation. This is the philosophy behind the present thesis.

1.3 Modelling Methodology

1.3.1 The Goal of Modelling

A considerable effort has been expended in trying to develop theories of nucleation and growth processes during submonolayer deposition. The goal is to provide a

comprehensive theory for the **island size distribution** (ISD). This is an important part of a more general aim of understanding and perhaps manipulating the formation of islands during the nucleation and growth stages. Despite the fact that the simple process of island formation during such stages has been extensively studied, the development of a formulation of a theory that would predict ISD consistent with experiments and computer simulations remains an important challenge.

Earliest attempts to compute the ISD have been in terms of rate equations which were developed in the 1960s; see [78] and the references therein. This approach was popular until the 1990s, when kinetic MC simulations were introduced. The comparison of results obtained from both approaches shows that rate equations fail to reproduce the ISD accurately despite the fact that average behaviour of densities, such as total island density (the sum of all islands), obtained by rate equations have been confirmed by MC simulations. Reasons for this failure will be discussed later in this section. This discrepancy prompts the challenge of finding an alternative modelling framework that allows one to predict experimentally and numerically obtained ISD.

1.3.2 Rate Equations and the Island Size Distribution

Rate equations often involve systems of ordinary differential equations (ODEs), or alternatively integro-differential equations. Much of the work in the present thesis is a contribution to this area of research.

We start by introducing a general discrete framework to describe the time evolution of clusters that takes into account binary coagulation and multiple fragmentation. This takes the form [13, 24, 83, 86]

$$\frac{dc_j(t)}{dt} = \frac{1}{2}\sum_{k=1}^{j-1} \sigma_{k,j-k} c_k(t) c_{j-k}(t) - \sum_{k=1}^{\infty} \sigma_{j,k} c_j(t) c_k(t) - a_j c_j(t) + \sum_{k=j+1}^{\infty} a_k b_{j,k} c_k(t), \quad j \geq 1, \tag{1.1}$$

where the first sum is interpreted as zero when $j = 1$. In (1.1), for each $j \in \mathbb{Z}^+$ and $t \geq 0$, $c_j(t)$ is the density of clusters of size j at time t. In many cases, a cluster of size j will be regarded as consisting of j identical atoms or monomers. The coagulation coefficients $\sigma_{j,k} = \sigma_{k,j}$ represent the rate at which a cluster of size j joins with a cluster of size k to form a cluster of size $j + k$. The terms a_j and $b_{j,k}$ are the net rate of break-up of a cluster of size j and the average number of clusters of size k created upon the break-up of a cluster of size j, respectively. Note that $a_1 = 0$.

Thus, the first term of the right-hand side of (1.1) describes the creation of clusters of size j by coagulation of clusters of sizes k and $j - k$. The factor $1/2$ is included since the first sum includes both a cluster of size $j - k$ coalescing with one of size k and vice versa. The second term corresponds to the depletion of clusters of size j due to their coalescence with other clusters. The third term is the rate at which clusters of size j vanish by fragmenting into clusters of smaller sizes. Finally, the fourth term corresponds to the rate at which the pool of clusters of size j is replenished by fragmentation of clusters of size $k > j$. It is also possible to consider a model that accounts for multiple coagulation, in which clusters may also be formed by collisions of more than two monomers. Such phenomena occur in ballistic aggregation; for more details see [39, 40].

Since coagulation through collisions of monomers features prominently in the growth of islands, it is not surprising that a standard tool in theoretical studies

for nucleation and growth stages is a system of equations based on (1.1) without fragmentation terms. Equation (1.1) can be adjusted by a source term $J_0(t)$, representing an external supply of monomers [25, 82]. In the simplest case, one may consider constant monomer input such as $J_0(t) \equiv F$ and this leads to several widely studied models [6, 42, 53, 66].

If we assume that islands (or clusters) evolve by capturing or releasing a single monomer, a physically realistic system of rate equations with critical island size $i = 1$, deposition rate F and diffusion rate of monomers D can be obtained by making the identifications $\sigma_{1,1} = 2D\sigma_1$, $\sigma_{1,j} = D\sigma_j$ for $j > 1$, $a_1 = 0$, $a_2 b_{1,2} = 2\gamma_2$ and $a_j b_{1,j} = \gamma_j$ for $j > 2$. Here, σ_j and γ_j are respectively the rates of capture and release of monomers from an island of size j. We have

$$\begin{aligned}
\frac{dc_1}{dt} &= F - 2D\sigma_1 c_1^2 - Dc_1 \sum_{j=2}^{\infty} \sigma_j c_j + 2\gamma_2 c_2 + \sum_{j=3}^{\infty} \gamma_j c_j \\
&\quad - 2F\kappa_1 c_1 - F \sum_{j=2}^{\infty} \kappa_j c_j \\
\frac{dc_j}{dt} &= Dc_1(\sigma_{j-1} c_{j-1} - \sigma_j c_j) + (\gamma_{j+1} c_{j+1} - \gamma_j c_j) \\
&\quad + F\kappa_{j-1} c_{j-1} - F\kappa_j c_j, \quad j \geq 2,
\end{aligned}$$

where we have also included direct impingement, with κ_j being the rate of direct impingement of monomers into an island of size j. The reason for the factor 2 is that the formation of a dimer results in the loss of two monomers. In the case of irreversible aggregation, which occurs at low temperatures, and negligibility of direct impingement, we set $\gamma_j = 0$ and $\kappa_j = 0$ to obtain

$$\frac{dc_1}{dt} = F - 2D\sigma_1 c_1^2 - Dc_1 \sum_{j=2}^{\infty} \sigma_j c_j \tag{1.2}$$

$$\frac{dc_j}{dt} = Dc_1(\sigma_{j-1}c_{j-1} - \sigma_j c_j), \quad j \geq 2. \tag{1.3}$$

For the general case of critical island size $i \geq 1$, corresponding to (1.2) and (1.3) we have a system of equations

$$\frac{dc_1}{dt} = F - nD\sigma_1 c_1^n - Dc_1 \sum_{j=n}^{\infty} \sigma_j c_j \tag{1.4}$$

$$\frac{dc_n}{dt} = D(\sigma_1 c_1^n - \sigma_n c_1 c_n) \tag{1.5}$$

$$\frac{dc_j}{dt} = Dc_1(\sigma_{j-1}c_{j-1} - \sigma_j c_j), \quad j > n, \tag{1.6}$$

in which we have set $n := i + 1$. Note that the stable islands of size j only exist when $j > i$. All the physics of the rate equations (1.2) and (1.3) is in the coefficients; different coefficients lead to different behaviour. Several choices for σ_j, such as $\sigma_j = 1$ and $\sigma_j = j^p$ where $p = 1/2$ or $1/3$ depending on the dimension of islands, have been considered; for more details see [16, 66].

A particularly simple case of these rate equations arises when we treat all islands as **point islands**, not having any spatial extent, and assume that all the coagulation constants can be taken to be equal. Choosing $D\sigma_j = 1$, we obtain a system that has been considered by Bartelt and Evans [11] and da Costa, van Roessel and Wattis [25], namely

$$\frac{dc_1}{dt} = \alpha - 2c_1^2 - c_1 \sum_{j=2}^{\infty} c_j \tag{1.7}$$

$$\frac{dc_j}{dt} = c_1 c_{j-1} - c_1 c_j, \quad j \geq 2, \tag{1.8}$$

where we have put $F = \alpha$ in order to stay consistent with the notation used by da Costa *et. al.* [25]. There are other approximations being made – namely, no spatial dependence, as discussed above, and in addition no time (or coverage) dependence. Moreover, in [6] the authors have developed a self-consistent rate-equation theory which accurately predicts the average quantities (average island size, average monomer density and average island density etc.) as a function of coverage for a given critical island size regardless of the shape of islands.

One could also take cluster size to be a continuous variable. The continuous counterpart of (1.1) [24, 45, 79, 86] is the integro-differential equation

$$\begin{aligned}\frac{\partial}{\partial t}u(x,t) = \frac{1}{2}\int_0^x \sigma(x-y,y)u(y,t)u(x-y,t)\,dy - \int_0^\infty \sigma(x,y)u(x,t)u(y,t)\,dy \\ - a(x)u(x,t) + \int_x^\infty a(y)b(x|y)u(y,t)\,dy,\end{aligned} \tag{1.9}$$

where the discrete sums of (1.1) have been replaced by integrals. Here, $u(x,t)$ stands for the density of clusters of size x at time t. The continuous version of the coefficient $\sigma_{j,k}$ is $\sigma(x,y)$, the **coagulation kernel**. The function $a(x)$ is the fragmentation rate. The function b accounts for the fragmentation of a cluster of size y into several daughter clusters; $b(x|y)$ describes the distribution of clusters of size x being produced when a cluster of size y fragments. For the **binary case** of the fragmentation process, according to Cheng and Redner [22], Lamb [45] and

Ziff and McGrady [87], a general continuous linear fragmentation equation in the absence of coagulation is in the form

$$\frac{\partial}{\partial t}u(x,t) = -\frac{1}{2}u(x,t)\int_0^x H(x-y,y)\ dy + \int_x^\infty H(x,y-x)u(y,t)\ dy, \qquad (1.10)$$

where $H(\cdot,\cdot)$, the binary **fragmentation kernel**, is assumed to be symmetric. Here $H(x,y)$ represents the rate at which a particle of size $x+y$ splits up into particles of sizes x and y. This is a special case of (1.9) with

$$\sigma \equiv 0; \quad a(x) = \frac{1}{2}\int_0^x H(x-y,y)\ dy; \quad b(x|y) = \frac{H(x,y-x)}{a(y)}.$$

If $a(x) = x^\lambda$, then we say that the fragmentation kernel is homogeneous with homogeneity index λ. Homogeneity requires the kernel b to have the form

$$b(x|y) = h\left(\frac{x}{y}\right)\frac{1}{y}, \qquad (1.11)$$

so that b is homogeneous of degree -1. This homogeneous form corresponds to the assumption that the distribution of daughter clusters is determined by the fraction (daughter size)/(parent size).

Note that when a parent cluster of size y fragments, the number of daughter particles formed, and their combined mass, are given by the integrals $\int_0^y b(x|y)dx$ and $\int_0^y xb(x|y)dx$ respectively. Consequently, in a mass-conserving, binary process, where each fragmentation produces only two daughter clusters with combined mass equal to the parent mass, we must have

$$\int_0^y b(x|y)\ dx = 2; \ \int_0^y xb(x|y)\ dx = y. \qquad (1.12)$$

In the homogeneous case, when $b(x|y)$ is given by (1.11), (1.12) can be expressed as

$$\int_0^1 h(r)\ dr = 2;\ \int_0^1 rh(r)\ dr = 1. \tag{1.13}$$

1.3.3 Similarity Solutions

What kind of results can one obtain from considering equations such as (1.1), (1.2), (1.3) and (1.9)? Explicit solutions of such equations are important in understanding the behaviour of the size distribution. However, exact solutions have been found only for very special rate coefficients, such as in the pure discrete coagulation equation case $\sigma_{j,k} = 1$, $\sigma_{j,k} = (j + k)/2$, $\sigma_{j,k} = jk$ and only for monodisperse initial conditions $c_j(0) = \delta_{1,j}$, where $\delta_{k,j}$ denotes the Kronecker delta (see [83] for details). Obtaining explicit solutions presents a difficult challenge, for which the use of elementary analytical methods is not usually suitable. However, we can use the infinite set of differential equations (1.1) for theoretical investigations into the long-term behaviour of island growth. This is done by applying a scaling approach which often allows us to identify solutions known as **scaling solutions**. This is particularly true for **homogeneous** kernels that are characterised by the property $\sigma_{\nu j,\nu k} = \nu^\lambda \sigma_{j,k}$ for some scalar λ if this property is followed by $\sigma_{j,k} = j^\lambda p(j/k)$ for some function $p(\cdot)$. In such a case, $\sigma_{\nu j,\nu k}$ is called **homogeneous of degree** λ. Dynamic **scaling solutions** (or similarity solutions) of (1.1) are sought in the form

$$c_j(t) = \frac{1}{r(t)^\tau}\phi\left(\frac{j}{r(t)}\right), \tag{1.14}$$

where $c_j(t)$ is the concentration of islands comprised of $j \geq 1$ monomers, τ is a positive exponent and

$$r(t) = \frac{\sum_{j=1}^{\infty} j c_j(t)}{\sum_{j=1}^{\infty} c_j(t)} \tag{1.15}$$

represents a typical island size; see the works of Leyvraz [46] and van Dongen and Ernst [77] for details. The function ϕ is the **scaling function**. Self-similar solutions of the form (1.14) are useful since they may describe the behaviour of general solutions of such equations. For example, it is conjectured – and in some cases proved – that solutions arising from a range of different initial data will approach a scaling solution in the long term [49, 50, 83].

For the case of mass-conserving solutions, we set $\tau = 2$ in (1.14) so that the total mass in the system remains constant for all time. The choice of $\tau = 2$ is determined by considering the total mass of the system

$$M(t) = \sum_{j=1}^{\infty} j c_j(t). \tag{1.16}$$

By introducing a continuous variable $\zeta = j/r(t)$, the sum in (1.16) is replaced by an integral over ζ and substituting (1.14) for $c_j(t)$, we obtain

$$M(t) = r(t)^{2-\tau} \int_0^{\infty} \zeta \phi(\zeta)\, d\zeta.$$

For $M(t)$ to be constant, we require $\tau = 2$. However, in the case of submonolayer growth, for monomer density mass is not conserved because of, for example, the presence of F in (1.2).

Dynamic scaling solutions of the form (1.14), but expressed in terms of coverage θ rather than t, are considered by several authors such as Amar *et. al.* [3]. We observe that in the case of irreversible aggregation $\theta = \sum_{j=1}^{\infty} j c_j(t)$ and we assume the scaling form

$$c_j(\theta) = G(\theta, r(\theta))\phi(j/r(\theta))$$

where r is the average island size and $G(\theta, r(\theta))$ is some function of θ and r. By a similar analysis for $M(t)$ to the one above, we obtain $G(\theta, r) = \theta/r^2$, where $\phi(\cdot)$ satisfies $\int_0^\infty \zeta\phi(\zeta)\, d\zeta = 1$. Thus, the scaling form for island density is

$$c_j(\theta) = \frac{\theta}{r^2}\phi\left(\frac{j}{r}\right),$$

which is the same as the dynamic scaling form of (1.14). The scaling form is only valid in low coverage (usually $\theta \leq 20\%$) before the coalescence stage where growing islands start to interact with each other [10, 12, 74]. The scaling function ϕ depends weakly on θ for realistic islands for up to $\theta = 20\%$ [12]. This means that the scaling function is consistent for any value of θ up to 20%. However, for the point-island case, ϕ is independent of θ. Another condition for the validity of the scaling form is that the ratio, $R = D/F$, must be large enough, say $R \geq 10^7$ or the average island size, $r = (\theta - c_1)/\sum_{j\geq i} c_j$ also needs to be sufficiently large.

Similarity solutions for the linear fragmentation equation

$$\frac{\partial}{\partial t}u(x,t) = -a(x)u(x,t) + \int_x^\infty a(y)b(x|y)u(y,t)\, dy, \tag{1.17}$$

(see equation (1.9)) have also been sought by a number of authors including Cheng and Redner [22, 23], Treat [75] and Ziff and McGrady [87]. These investigations have focussed on the homogeneous case

$$\frac{\partial}{\partial t}u(x,t) = -x^\lambda u(x,t) + \int_x^\infty y^{\lambda-1}h\left(\frac{x}{y}\right)u(y,t)\, dy, \tag{1.18}$$

described earlier, in which $a(x) = x^\lambda$ and $b(x|y)$ is given by (1.11) for some function h that satisfies the mass conservation condition $\int_0^1 rh(r)\, dr = 1$.

Such similarity solutions can be expressed in an analogous manner to (1.14) with $\tau = 2$. For example, in [75] Treat shows that similarity solutions can be

written as

$$u(x,t) = \frac{N^2(t)}{V}\phi\left(\frac{N(t)x}{V}\right) = V\left(\frac{N^2(t)}{V}\right)^2 \phi\left(\frac{N(t)x}{V}\right), \tag{1.19}$$

where the scaling function ϕ, referred to in [75] as the reduced distribution, is required to satisfy an integral equation and is normalised so that

$$\int_0^\infty \phi(y)\, dy = \int_0^\infty y\phi(y)\, dy = 1, \tag{1.20}$$

and

$$N(t) := \int_0^\infty u(x,t)\, dx,\ V(t) := \int_0^\infty xu(x,t)\, dx,$$

are, respectively, the zeroth and first moments of the similarity solution u. An explicit expression for ϕ involving the Meijer G-function, is derived in [75, Section 6] for the specific case when the function h in equation (1.11) takes the form

$$h(r) = r^\gamma(b_0 + b_1 r + \cdots + b_p r^p),$$

$p = 0, 1, \ldots$, γ and $b_0, b_1, \ldots, b_p \in \mathbb{R}$. We shall make use of the simple case $p = 1$ in Chapter 5. With regard to the question of existence of similarity solutions for more general homogeneous fragmentation equations, results have been obtained by Escobedo *et. al.* in [31].

The rate equations (1.2) and (1.3) can successfully predict the scaling behaviour of average quantities, such as the total island density $\sum c_j$, [6]. However, islands of the same size are assumed to grow at the same rate no matter where they are located and it is difficult to choose a large set of σ_j for $j \geq 1$ correctly. Consequently, with an incorrect choice of rate coefficients, a rate-equation approach is

likely to lead to predictions of ISD which differ substantially from results that are obtained experimentally or by MC simulations [11, 54].

Because of this, we have to (a) employ an experimental procedure that will give us realistic data on submonolayer growth and (b) try to find a modelling approach that will allow us to improve the approximation of the ISD to obtain results that agree with the data from MC simulations.

1.3.4 Attempts to Improve the ISD Approximation: the Capture Zone Distribution

There have been several attempts to improve the approximation of the ISD, which is the main goal here. In 1996 Mulheran and Blackman [54] suggested a way to model nucleation and growth of islands in various dimensions with $i = 1, 2, 3$ using the concept of a **capture zone distribution** (CZD). They defined the **capture zone** (CZ) associated with an island to be the substrate region surrounding the island that consists of all points closer to the island than to any other island. Figure 1.2 illustrates the CZD. In that figure, the CZs are indicated by the cell boundaries for one-dimensional (1-D) and two-dimensional (2-D) islands.

For the 1-D point-island model in the case of $i = 1$, Blackman and Mulheran [14] had the idea of using a fragmentation-based approach to analyse **gap size distributions** (GSDs) and, subsequently, CZDs. In the 1-D case, an island is an end-point of a gap. Nucleation of new islands during the deposition leads to the fragmentation of gaps and CZs. In Figure 1.3, we summarise the features of the model just described.

Blackman and Mulheran assumed that nucleation is rare in a gap of any size and derived an equation for the position dependent monomer density, $n_1(x)$ (its average is c_1), which is

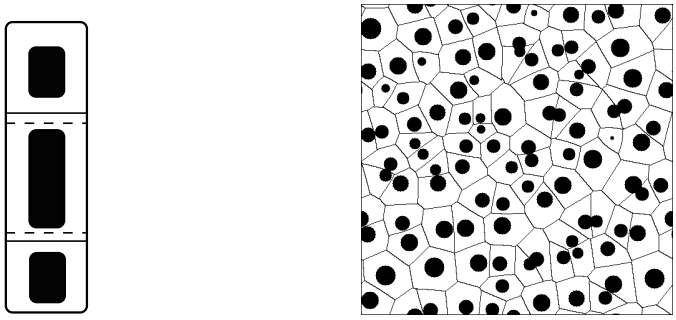

Figure 1.2: On the left-hand side, black rectangles correspond to 1-D islands. Horizontal lines mark the midpoints between the edges of two islands defining their CZs as the resulting proximity cells. If instead we use the midpoint between the centres of islands indicated by the dashed lines, we have Voronoi cells. On the right-hand side, the islands appear approximately circular and the CZs are indicated by the cell boundaries.

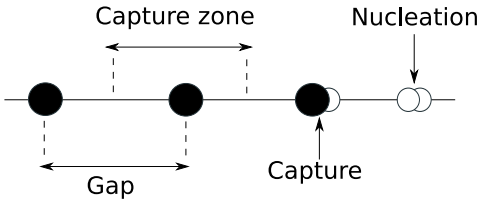

Figure 1.3: Summary of the features of the model. Solid circles represent an island; open circles are monomers. A capture zone is the separation of the bisectors of neighbouring gaps.

$$D\frac{d^2 n_1}{dx^2} + F \approx 0,$$

under the assumption that the monomer density is in an approximately steady state, that is, all time derivatives vanish. To obtain the GSD in this 1-D case, they describe the evolution of gap sizes as a fragmentation process. This is motivated by the observation that any new nucleation that occurs in a parent gap of width,

say, y, will result in the creation of two daughter gaps of widths, say, x and $y-x$. Due to the fact that the fragmentation of a parent gap leads to two gaps, this is the binary case of fragmentation process. With $n_1(x)$, Blackman and Mulheran derived a fragmentation equation for the GSD function in the case of $i = 1$. If there is no correlation between the sizes of two neighbouring gaps the connection between the GSD and CZD is given by [14],

$$P(s) = 2\int_0^{2s} \phi(x)\phi(2s-x)\ dx, \tag{1.21}$$

where $\phi(x)$ is the GSD function and $P(s)$ is the CZD function. The factor 2 is included to preserve the normalisation for $P(s)$ [14].

It was suggested by Pimpinelli and Einstein [61] that the Generalised Wigner Surmise (GWS) may accurately describe the CZD given in any dimension d for any critical island size i. The GWS is a simple expression generalising the Wigner Surmise from Random Matrix Theory that accounts for spacing distributions in a host of fluctuation phenomena such as energy levels of atomic nuclei, quantum chaos and distances between parked cars [1, 61]. Let $s(t) = A(t)/\langle A\rangle(t)$, where $A(t)$ and $\langle A\rangle(t)$ are, respectively, the area of a CZ and its average at fixed time t, and let $P(s)$ be the probability of finding an island with scaled CZ of area between s and $s+ds$. Then Pimpinelli and Einstein suggested the scaled CZD, depending on the sole parameter β, may be represented in the form

$$P_\beta(s) = a_\beta s^\beta \exp(-b_\beta s^2), \tag{1.22}$$

where

$$\beta = \begin{cases} \frac{2}{d}(i+1) & \text{if } d = 1, 2 \\ i+1 & \text{if } d = 3, \end{cases} \tag{1.23}$$

and a_β and b_β are constants chosen so that $\int_0^\infty P(s)\, ds = \int_0^\infty sP(s)\, ds = 1$. The GWS will be discussed in more detail later in this thesis.

There has been recent work on providing a suitable theory of capture zones in order to predict accurately the ISD. One may consider a **Joint Probability Distribution** (JPD) in order to develop an approach that describes the evolution of island sizes of j and CZ areas of A. This approach considers both the distributions of island size and CZ area; hence the name JPD. Such an approach was originally proposed by Mulheran and Robbie [55]. The basic JPD rate equations [33] are

$$\frac{dc_{j,A}}{dt} = FAc_{j-1,A} - FAc_{j,A} + P^+_{j,A}\frac{dc_{st}}{dt} - P_{j,A}\frac{dc_{st}}{dt},\ j \geq i, \tag{1.24}$$

where $c_{st} = \sum_{j \geq i} c_j$ is the density of stable islands and $c_{j,A}$ is the island density of size j and CZ area A. There are two growth rates that describe the rate at which monomers land within a specific CZ area of A and the growth rate of an island due to direct impingement. The former rate equals $F(A-j)$ and the latter equals Fj. Thus, the total growth rate is FA. In the right-hand side of (1.24), the first and second terms describe the total growth rate of island of size j and CZ of area A. In other words, the first and second terms, known as the gain and loss terms, describe the total growth rate for an island of size j and CZ area A. The term $P_{j,A}$ is the probability that a nucleation event occurs anywhere within the CZ of area, A, belonging to an island of size j. Thus, the CZ of the new island overlaps and reduces the original CZ of this existing island of size j, resulting in the loss of an original island of size s and area A. $P^+_{j,A}$ is similar to $P_{j,A}$ except that this probability will result in the gain of an island of size s and new area A. The term

dc_{st}/dt is approximately the nucleation rate of a stable island. The processes of nucleation are described in the latter two terms on the right-hand side of (1.24): the third term is the gain term since islands of size j and area A are being created by the fragmentation of larger CZs. Likewise, the fourth term is the loss term due to the reduction of the number of islands of size j and area A by nucleation events. Note that one can obtain the ISD and CZD by considering the equations of $\sum_A c_{j,A}$ and $\sum_j c_{j,A}$ respectively [32]. In terms of CZDs and subsequently ISD, the JPD is an advance because it allows us to capture local growth rates caused by different spatial environments around the islands. Further information can be found in [33].

The following question was raised in [66]: can the rate equations be successful in predicting the correct shape of the ISD if the capture numbers $\sigma_j(\theta)$ are allowed to depend on **both** j and the coverage, θ? To answer this question, in [42] Körner *et. al.* consider the following rate equations in the case of irreversible aggregation along with direct impingement of arriving monomers

$$\frac{dc_1}{dt} = (1-\theta)F - 2D\sigma_1 c_1^2 - Dc_1 \sum_{j=2}^{\infty} \sigma_j c_j - 2F\kappa_1 c_1 - F\sum_{j=2}^{\infty} \kappa_j c_j \tag{1.25}$$

$$\frac{dc_j}{dt} = Dc_1(\sigma_{j-1}c_{j-1} - \sigma_j c_j) + F\kappa_{j-1}c_{j-1} - F\kappa_j c_j, \quad j \geq 2. \tag{1.26}$$

The authors obtain the capture number $\sigma_j(\theta)$ which depends on both island size j and θ by collecting data for σ from MC simulations for constant θ, approximating the average σ as a function of j and θ and formulating rate equations using these averaged σ. They concluded that coefficients σ_j with no θ dependence lead to a poor prediction of ISD and thus there is a rate-equation model for submonolayer deposition that behaves just like the data from MC simulation if one takes into

account the correct dependence of σ_j on both j and θ. More details can be found in [42].

Seba [70] investigated a 1-D model aimed at describing the spacing distribution between cars parked in an infinitely long street to ensure the parking of as many cars as possible. The underlying strategy that is adopted for any particular parking attempt is as follows. A random position x on the street is selected. If a large enough interval centred at x is free, the car may park in the interval at x thereby fragmenting the interval. Otherwise, another random position x is chosen and so on. Cars are also allowed to leave, and new cars can then park in the vacated interval; this leads to an equilibrium model. As a means of describing the spacing distribution approximately, Seba derived the **distributional fixed point equation** (DFPE)

$$X_d \stackrel{\triangle}{=} a(1 + X_d). \tag{1.27}$$

Here X_d is the distance between two parked cars, a is an independent random variable with a probability density, $f(a)$, and the symbol $\stackrel{\triangle}{=}$ means that the left- and right-sides of (1.27) have the same distribution. One idea that we shall pursue in this thesis is to adapt the Seba model for the case of nucleation and growth on a 1-D substrate, where the distance between any two neighbouring cars may be interpreted as the gap between any two neighbouring islands. More details will be given later in Chapter 3.

1.3.5 Monte Carlo Simulation

MC methods form a family of algorithms that use pseudorandom numbers to conduct a statistical sampling experiment with a mathematical model. The idea was originally proposed in 1940s by Metropolis, Ulam and von Neumann [30, 51]. A MC method can be viewed as a type of simulation that uses repeated random

sampling to compute the behaviour of some process. However, it should be noted that there are many definitions of a MC simulation, such as in [18, 68]. Typically, one creates a model which describes a real-life random system and to do this, one must identify random variables. The resulting model can be run on a computer many times; these will generate different values of the random variables [48]. Once this is completed, the data from this model is analysed. Since the 1940s there have been many different versions of MC simulations which can solve various kinds of computational problems in a large range of applications in physics, statistics, computer science and other fields [48]. More details about MC simulations in the modelling of submonolayer deposition will be discussed in Chapter 6.

The following diagram illustrates how a MC simulation is related to the other approaches for submonolayer growth discussed in this work.

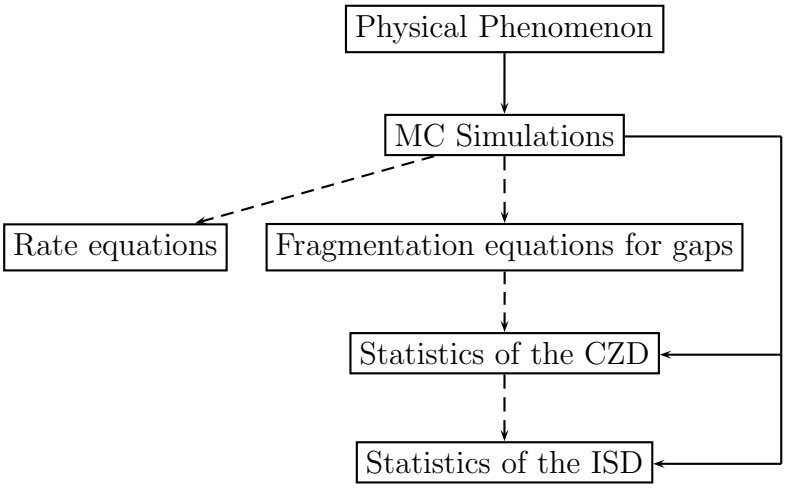

MC simulations provide the statistical data for the CZD, and, in the 1-D case only, also the GSD. Moreover, these simulations can yield realistic statistics of behaviour. It is natural for one to ask why we bother to develop mathematical theory such as rate equations at all. The answer is that MC simulations in them-

selves cannot explain how the growth might depend on deposition rate and/or temperature; only theoretical analysis is capable of doing this; hence the dashed arrows. It is important to note that MC simulations are the main way of falsifying theories concerning either the ISD or the CZD.

1.3.6 Summary

Despite several attempts at finding a reliable formulation for the ISD that allows one to predict the results from MC simulations accurately, such a formulation still remains an open, challenging problem. The main topics in this thesis are:

- To generalise the mean-field work of da Costa *et. al.* to the case $i > 1$.
- To generalise the Blackman and Mulheran model to the case of general $i \geq 0$.
- To study in more detail the validity of the GWS for other cases of i and d in addition to the case $i = 0$, 1 in $d = 1$, 2 considered in [61].
- To determine whether the predictions of the $d = 1$ Blackman and Mulheran fragmentation-nucleation theory for the CZD and the GWS are compatible.
- To adapt the DFPE approach to the non-equilibrium, dynamic scaling problem of island nucleation and growth in the 1-D model. This lays the foundations for a new approach to a more general understanding of nucleation and growth in higher dimensions.

It is important to note that there is a controversy in the literature over the definition of mean-field models and non mean-field models notably in [4, 81] where Amar *et. al.* claimed their work went beyond the mean field, and Vvedensky *et. al.* claimed it did not.

It is not clear what is the true definition of mean-field theory in the context of submonolayer deposition. Vvedensky *et. al.* seem to use the following definition: a model is mean-field if its dependent variables are space-independent. Amar *et. al.* used a more relaxed definition: a model is not mean-field if its parameters have been derived from a realistic (space-dependent) theory.

Nevertheless, the goal has always been to construct a theory that would predict the ISD results accurately.

1.4 Overview of Thesis

The thesis is divided into eight chapters. A summary of each of the subsequent chapters in the thesis is as follows.

In Chapter 2, we discuss techniques that will be of aid in later chapters, such as the concept of a river for Chapter 4 and Laplace's method for determining the asymptotic behaviour of solutions for Chapter 5.

In Chapter 3, we give a more detailed account of scaling solutions for discrete coagulation and continuous fragmentation equations. Moreover, we also discuss several established contributions to this area of research; although some of these topics may be reasonably well known, it is convenient to provide a summary of the key points for later reference.

In Chapter 4, we use the concept of a river to extend the results of da Costa *et. al.* [25] to the case when the critical island size i is larger than 1 and obtain analogous results to those presented in [25]. To the best of our knowledge, this is the first time that the idea of a river originating in the work of non-standard analysts such as the Dieners, has been used to solve an applied mathematical problem. In short, we can describe the ISD for $i > 0$ if we use rate equations (1.4)-

(1.6) with $\sigma_j = 1$.

In Chapter 5, we derive a generalised form of the Blackman and Mulheran formulation [14] for the GSD in the general case of $i \geq 0$ of the 1-D Blackman and Mulheran fragmentation-nucleation theory [14]. We extend this approach to the case of general critical island size $i \geq 0$. Moreover, we describe how the asymptotic behaviour of the 1-D Blackman and Mulheran theory for the CZD and the GWS conjectured by Pimpinelli and Einstein are compatible. After introducing a class of fragmentation kernels that depend on the critical island size, we highlight asymptotic results that we have obtained using the binary fragmentation equation (1.10). In deriving these asymptotic results, we use methods developed by Cheng and Redner, and Treat, together with a modified theorem of the 2-D Laplace method tailored specifically for the case $i = 0$. Our results establish that both models cannot be correct simultaneously.

After discussing the difference between the Blackman and Mulheran theory, and the GWS in Chapter 5, in Chapter 6 we discuss the model we have used in our MC simulations. These simulations provide the data that we compare with the predictions arising from the GWS to test the validity of the conjecture of Pimpinelli and Einstein. As stated earlier, it will be seen that it is only in the case of $d = 2$ that the GWS provides a good fit to the data. Shi *et. al.* [71] suggest otherwise in the case of point islands; however, the GWS may be more applicable for extended islands. Moreover, for the 1-D point islands case only, we shall investigate the large and small asymptotic behaviour of the GSD and CZD, and the nucleation rate for islands. After an extensive investigation on data from MC simulations, a summary of these results is given.

In Chapter 7, after discussing the Seba approach in detail for our problem of irreversible aggregation we conclude that this type of approach to fragmentation

problems is promising and merits further investigation. Moreover, we compare this approach with the Blackman and Mulheran model and the data from MC simulations.

In Chapter 8, a summary of the conclusions of each chapter is presented. We also propose new future directions and open, challenging problems that need to be investigated and solved in order to generalise the results of this thesis.

Chapter 2

A Summary of Methods

2.1 Introduction

In this chapter, we will discuss several key methods that prove to be crucial to the investigations into understanding the island size distribution (ISD) in this thesis. We begin, in Section 2.2, with a powerful tool called the Newton Polygon (NP). This method allows us to understand the asymptotic behaviour of solutions to polynomial equations and to ordinary and partial differential equations [20, 21, 36]. However, in this thesis, we will restrict our attention to ordinary differential equations only.

After discussing the NP method for ordinary differential equations (ODEs), we turn to the little-known concept of a 'river', which will be used in Chapter 4 to establish the asymptotic behaviour of monomer and island densities. As we shall point out, the concept of a river is similar to the NP method but also incorporates some convergence criteria [17, 19, 26, 27, 76]. It should be noted that our work in Chapter 4 is largely motivated by [25], where da Costa, van Roessel and Wattis use differential equation techniques, such as Centre Manifold theory, to determine

the asymptotic behaviour of solutions to a system of differential equations which can be obtained as a special case of the system we study in Chapter 4. The river concept plays an important role in our analysis as it overcomes the obstacle presented by our inability to apply, to the general system, some of the arguments used in [25], particularly those which rely on proving the existence of invariant regions in the phase plane associated with the system.

In Chapter 4 and beyond, we will analyse the ISD, the gap size distribution (GSD) and the capture zone distribution (CZD) with the aim of obtaining the small- and large-size asymptotic behaviour of each distribution. Our analysis will lead to certain problems which can be tackled by means of Watson's lemma and results on one-dimensional (1-D) Laplace integrals. For example, in Chapter 5, we will encounter a triple integral which requires the application of a combination of properties of one- and two-dimensional Laplace integrals. Watson's lemma and relevant results on 1-D Laplace integrals are given in Sections 2.4 and 2.5.

We will introduce the bootstrap method which can be used to overcome difficulties that can arise in situations where the theoretical distribution of a statistic is either complicated or unknown, or the sample size is too small for straightforward statistical inference. We will apply this method in Chapters 6 and 7 to calculate, for example, the average gradient of both small- and large-size behaviours of GSDs and CZDs, and the average moment of these distributions.

2.2 Newton Polygon

We aim to use the NP method in order to understand the asymptotic behaviour of solutions to ODEs. Therefore, in this section, we will give a description of the main techniques involved in investigating ODEs via NPs. Our account will be

based largely on that given by Cano in [21], and so we will define a polynomial F of the $n+1$ variables $y_0, y_1, \ldots, y_n$, with x dependent coefficients, by

$$F(y_0, y_1, \ldots, y_n) = \sum_{\gamma \in A} a_{\gamma,\underline{\rho}} x^{\gamma} y_0^{\rho_0} \ldots y_n^{\rho_n}. \tag{2.1}$$

In (2.1), the coefficient of the term $y_0^{\rho_0} \ldots y_n^{\rho_n}$ is $a_{\gamma,\underline{\rho}} x^{\gamma}$, where $\gamma \in A \subset \mathbb{R}$, $\underline{\rho} = (\rho_0, \ldots, \rho_n)$ and $a_{\gamma,\underline{\rho}}$ is a scalar. Associated with F is the ODE

$$F\left(y, \frac{dy}{dx}, \ldots, \frac{d^n y}{dx^n}\right) = 0, \tag{2.2}$$

which we shall abbreviate to $F(y) = 0$.

Example 2.2.1. *If we have the following equation in the form (2.2)*

$$F\left(y, \frac{dy}{dx}, \frac{d^2y}{dx^2}\right) = F(y) = 2xy'y'' - x^3y^2,$$

then we rewrite $F(y)$ in the form (2.1)

$$F(y_0, y_1, y_2) = 2xy_1y_2 - x^3y_0^2. \tag{2.3}$$

For the first term in the right-hand side of (2.3), i.e. $2xy_1y_2$, we have $\underline{\rho} = (\rho_0, \rho_1, \rho_2) = (0, 1, 1)$ and $\gamma = 1$. Similarly, for the second and last term, we have $\underline{\rho} = (2, 0, 0)$ and $\gamma = 3$. With $\gamma = 1$ and $\gamma = 3$ for each term, we have $A = \{1, 3\}$.

A set of planar points, known as the cloud of points of F, is defined in the following manner; see [21, p.19].

Definition 2.2.2 ([21])**.** *Let F be given by (2.1) and associate to each coefficient*

$a_{\gamma,\underline{\rho}}$ the point in $\mathbb{R}\times\mathbb{N}$ that is defined by

$$P_{\gamma,\underline{\rho}} := \left(\gamma - \sum_{j=1}^{n} j\rho_j,\ \sum_{j=0}^{n}\rho_j\right).$$

Then the cloud of points of F is the set

$$\mathcal{P}(F) := \left\{P_{\gamma,\underline{\rho}} \mid a_{\gamma,\underline{\rho}} \neq 0\right\}.$$

The next definition, describing the NP associated with F, can be found in [21, p.20].

Definition 2.2.3 ([21])**.** *The Newton Polygon $N(F)$ of F is the convex hull of the set*

$$\bigcup_{P\in\mathcal{P}(F)} \left(P + \{(a,0) \mid a \geq 0\}\right).$$

The following definition and remarks are used to obtain *necessary initial conditions* for the equation $F(y) = 0$

Definition 2.2.4. *Let L be a line in $\mathbb{R}^2$ with slope $-1/\mu$. Then μ is the inclination of L.*

The line $L(F;\mu)$ is defined to be the line with inclination $\mu\in\mathbb{R}$ such that $N(F)$ is contained in the left closed half-plane defined by $L(F;\mu)$, and $L(F;\mu)\cap N(F)\neq\emptyset$. In [21, Eq. (2)], for each $L(F;\mu)$ the author defines the polynomial

$$\Phi_{(F;\mu)}(c) = \sum_{P_{\gamma,\underline{\rho}}\in L(F;\mu)} a_{\gamma,\underline{\rho}} c^{\rho_0+\ldots+\rho_n} (\mu)_1^{\rho_1}\ldots(\mu)_n^{\rho_n},$$

where $(\mu)_k = \mu(\mu-1)\cdots(\mu-k+1)$ and $P_{\gamma,\underline{\rho}}$ is given in Definition 2.2.2. As in [21, p.20], the following statements can be made about $N(F)$.

- For each $\mu \in \mathbb{R}$, $L(F;\mu) \cap N(F)$ is either a side or a vertex of $N(F)$.
- If $L(F;\mu) \cap N(F)$ is a side, say S, then $\Phi_{(F;\mu)}(c)$ is the associated characteristic polynomial.
- Let $p = (a,h)$ be a vertex of $N(F)$ and let $\mu_1 < \mu_2$ be the inclinations of the adjacent sides at p. For any μ such that $\mu_1 < \mu < \mu_2$, $L(F;\mu) \cap N(F) = \{p\}$. Then $\Phi_{(F;\mu)}(c) = c^h \Psi_{(F;p)}(\mu)$ where

$$\Psi_{(F;p)}(\mu) = \sum_{P_{\gamma,\underline{\rho}}=p} a_{\gamma,\underline{\rho}}(\mu)_1^{\rho_1} \dots (\mu)_n^{\rho_n}.$$

Remark 2.2.5. *1. Suppose that (x_1,y_1) and (x_2,y_2) lie on a line with inclination μ. Then*

$$\frac{y_2 - y_1}{x_2 - x_1} = -\frac{1}{\mu} (\mu \neq 0) \Leftrightarrow x_1 + \mu y_1 = x_2 + \mu y_2.$$

2. Consider the term $a_{\gamma,\underline{\rho}} x^\gamma y_0^{\rho_0} \dots y_n^{\rho_n}$. Applying the differential operator associated with this term to $y = x^\mu$, we obtain the following equation

$$\begin{aligned} & a_{\gamma,\underline{\rho}} x^\gamma x^{\rho_0 \mu} (\mu)_1^{\rho_1} x^{\rho_1(\mu-1)} \dots (\mu)_n^{\rho_n} x^{\rho_n(\mu-n)} c^{\sum_{j=0}^n \rho_j} \\ &= \left[a_{\gamma,\underline{\rho}} (\mu)_1^{\rho_1} \dots (\mu)_n^{\rho_n} c^{|\underline{\rho}|} \right] x^{\gamma - \sum_{j=1}^n j\rho_j + \mu \sum_{j=0}^n \rho_j}, \end{aligned}$$

where $|\underline{\rho}| = \sum_{j=0}^n \rho_j$. So, all points on a side of $N(F)$ will contribute to the same power of x, i.e. if the inclination of S is μ, then each point $\left(\gamma - \sum_{j=1}^n j\rho_j, \sum_{j=0}^n \rho_j \right)$ on S satisfies

$$\gamma - \sum_{j=1}^{n} j\rho_j + \mu \sum_{j=0}^{n} \rho_j = constant.$$

3. *If $p = (a, h)$ is a vertex of $N(F)$ then for each term $a_{\gamma,\underline{\rho}} x^{\gamma} y_0^{\rho_0} \dots y_n^{\rho_n}$ in F that corresponds to p we must have $h = \sum_{j=0}^{n} \rho_j$. Hence $c^{\rho_0+\dots+\rho_n} = c^h$ for all such terms.*

More detail on necessary initial conditions can be found in [21, p.20]. A short example found in [36] will be illustrated using Cano's approach as described above

Example 2.2.6. *Let $F(y) = xyy'' - xy'' + yy' - y' - x(y')^2$. The corresponding polynomial $F(y_0, y_1, y_2)$ is then given by*

$$F(y_0, y_1, y_2) = xy_0y_2 - xy_2 + y_0y_1 - y_1 - xy_1^2. \tag{2.4}$$

In Table 2.1, A and B are defined as $\sum_{j=1}^{2} j\rho_j$ and $\sum_{j=0}^{2} \rho_j$ respectively. Note that γ and ρ_j represents the power of x and the power of y_j for $0 \le j \le 2$ respectively.

Term	γ	$\underline{\rho} = (\rho_0, \rho_1, \rho_2)$	A	B	$P_{\gamma,\underline{\rho}} := (\gamma - A, B)$
xy_0y_2	1	$(1, 0, 1)$	2	2	$(-1, 2)$
$-xy_2$	1	$(0, 0, 1)$	2	1	$(-1, 1)$
y_0y_1	0	$(1, 1, 0)$	1	2	$(-1, 2)$
$-y_1$	0	$(0, 1, 0)$	1	1	$(-1, 1)$
$-xy_1^2$	1	$(0, 2, 0)$	2	2	$(-1, 2)$

Table 2.1: Vertices of (2.4)

As seen in Figure 2.1, we have two vertices $(-1, 2)$ and $(-1, 1)$, and an edge. Consider the former vertex first

$$F(x^{\mu}) = x(x^{\mu})(x^{\mu})'' + x^{\mu}(x^{\mu})' - x[(x^{\mu})']^2 = (\mu^2 - \mu + \mu - \mu^2)x^{2\mu-1} = 0.$$

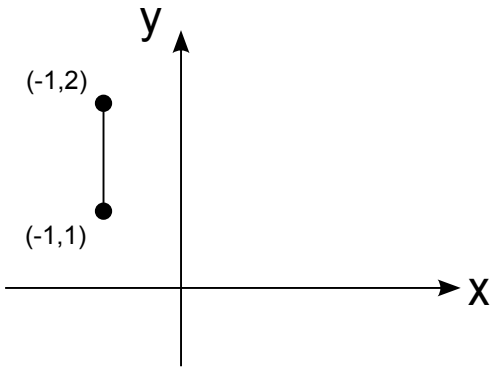

Figure 2.1: Newton Polygon for (2.4).

So, $\Phi_{(F,\mu)}(c) \equiv 0$ *and* $\Psi^{\mu}_{(F,p)} \equiv 0$ *for* $0 < \mu < \infty$. *Similarly, for* $(-1, 1)$

$$F(x^{\mu}) = -x(x^{\mu})'' - (x^{\mu})' = -\mu^2 x^{\mu-1}.$$

So, $\Phi_{(F,\mu)}(c) = -\mu^2 c$ *and* $\Psi^{\mu}_{(F,p)} = -\mu^2$ *for* $-\infty < \mu < 0$. *For the edge,* $\mu = 0$, *we have* $F(cx^0) = F(c) = 0$ *and so* $\Phi_{(F;0)}(c) = 0$.

For more details, we refer to [21, 36]. However, it is sufficient to know the method of finding vertices and edges, i.e. Definition 2.2.3, which is a key part of the analysis in Chapter 4 along with the concept of a river which we discuss next.

2.3 The Mathematical Concept of a River

The concept of *un fleuve* or a river will play a key role in establishing the asymptotic behaviour of monomer and island densities. As discussed earlier, we use the NP method to find rivers and we can obtain more information on asymptotic behaviour through convergence criteria associated with rivers. If one draws a phase portrait for the system of equations

$$\begin{aligned} \tfrac{dX}{dt} &= X'(t) = 3, \\ \tfrac{dY}{dt} &= Y'(t) = 3(Y(t)^2 - X(t)), \end{aligned} \tag{2.5}$$

then one will observe two concentrations of trajectories in a particular area of the phase portrait in Figure 2.2. These thick concentrations of trajectories are rivers (one is attracting and the other is repelling) which we will now explain in detail. Following [17, 19, 26, 76], we consider a two-dimensional system of polynomial differential equations,

$$\begin{aligned} X' &= P(X, Y), \\ Y' &= Q(X, Y). \end{aligned} \tag{2.6}$$

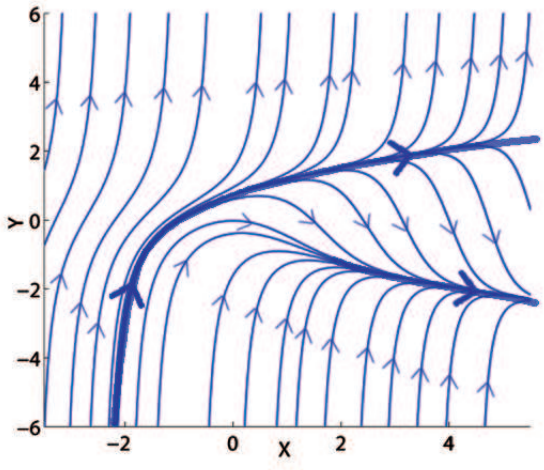

Figure 2.2: Phase portrait of (2.5). This figure is obtained from MATLAB via the *pplane* code.

Definition 2.3.1. *Given a polynomial $P(X, Y)$ and $r \in \mathbb{R}$, the r-degree of P, denoted by $\deg_r P$, is the highest power of X appearing in $P(X, X^r)$. We denote by*

$P_r(X,Y)$ the maximal polynomial obtained using monomials from $P(X,Y)$ such that $deg_r P = deg_r P_r$.

As an example, consider $Q(X,Y) = 3(Y^2 - X)$. If we set, say, $Y = X^2$, then we have $\deg_2 Q = 4$ and $Q_2(X,Y) = 3Y^2$.

Definition 2.3.2 ([26])**.** *A positive semi-orbit $(X(t), Y(t))$ of (2.6) which is such that $X(t) \to \infty$ as $t \to \infty$ is called a river of type (k,r) at $X = \infty$ if the following conditions are satisfied.*

1. $Q_r(1,k) = 0$;
2. $\lim_{t\to\infty} Y(t)/X(t)^r = k$;
3. $c(r) := 1 - r + deg_r Q - deg_r P > 0$;
4. $P_r(1,k) \neq 0$ *and* $[\partial Q_r/\partial Y](1,k) \neq 0$.

If a (k,r)-river exists, the integer $c(r)$ is called the **order of the river**. The significance of $c(r)$ is commented upon in [26]; in essence, the order provides a measure of the rate of convergence of other trajectories towards the river. Note that one may also define the analogous concept of a river of type (k,r) at $X = -\infty$, and, by changing the rôles of X and Y and replacing the condition $c(r) > 0$ by $c(r) < 0$, a river of type (k,r) at $Y = \infty$ or at $Y = -\infty$. To determine whether a river actually exists for a given system, it would appear that the first step would be to identify a semi-orbit against which the various conditions of Definition 2.3.2 can be tested. The question then arises as to how such a semi-orbit can be found. Fortunately, Definition 2.3.2 has been shown to be equivalent to an existence theorem, which we now state. This theorem is originally from [27] and also appears in various forms in [17, 19, 76].

Theorem 2.3.3. *The system (2.6) admits a (k, r)-river if and only if there is a pair (k, r) satisfying the definition of a (k, r)-river.*

Thus, the existence of a (k, r)-river is guaranteed if a pair (k, r) can be found satisfying conditions 1.-4. of Definition 2.3.2. In practice, the possible values of r are sought first by applying NP technique and the following lemma.

Lemma 2.3.4 ([27])**.** *If the positive semi-orbit $(X(t), Y(t))$ is a (k, r)-river for the system (2.6), then r must be a solution of the equation $(1, r) \cdot \mathbf{v}$, where $\mathbf{v}$ is a direction vector of a segment of the east-looking boundary of the Newton Polygon of $Q(X, Y)$.*

Once a (k, r)-river has been shown to exist, the next step is to identify how neighbouring trajectories behave. Fortunately, we have the following simple Liapunov stability criterion; see [17] for details.

Theorem 2.3.5 (Stability)**.** *Suppose that the system (2.6) admits a (k, r)-river and define $\Phi(X, Y) = Q(X, Y)/P(X, Y)$. Then the (k, r)-river is locally asymptotically stable in the Liapunov sense if*

$$\frac{\partial \Phi}{\partial Y}(X, kX^r) < 0. \tag{2.7}$$

Thus, if (2.7) holds, then any solution which is sufficiently close to the river at some finite time will, in the long term, become arbitrarily close to the river.

Example 2.3.6. *Consider the system of equations (2.5) in which $P(X, Y) = 3$ and $Q(X, Y) = 3(Y^2 - X)$. We begin by applying the NP approach to the function Q. If we set $X = x$, $Y = y_0$ and $Q = F$, then in terms of the notation used in Section 2.2, we have*

$$F(y_0) = 3(y_0^2 - x), \tag{2.8}$$

and so

Term	γ	$\underline{\rho} = (\rho_0)$	A	B	$P_{\gamma,\underline{\rho}} := (\gamma - A, B)$
$3y_0^2$	0	(2)	0	2	$(0, 2)$
$-3x$	1	(0)	0	0	$(1, 0)$

Table 2.2: Vertices of (2.8)

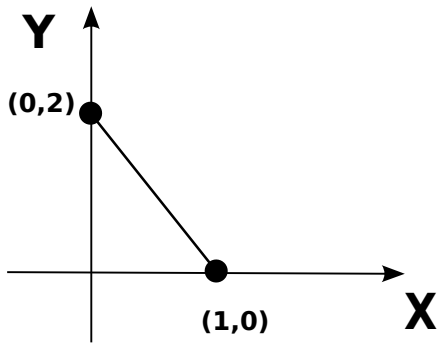

Figure 2.3: Newton Polygon for (2.5).

As seen in Figure 2.3, we have the single segment given by the straight line, with gradient -2*, connecting the points* $(1, 0)$ *and* $(0, 2)$*. Note that a direction vector of this segment is* $\mathbf{v} = (1, -2)$ *and so, from Lemma 2.3.4, we require* r *to satisfy the equation* $(1, r) \cdot (1, -2) = 0$*. It follows that the only possible value is* $r = 1/2$*. To establish that a* $(k, 1/2)$*-river exists for some value(s) of* k*, we now use Theorem 2.3.3. We begin by examining*

$$Q(X, X^{1/2}) = 3(X - X) = 0,$$

and so, by Definition 2.3.1, $deg_{1/2}Q = 0$ *and* $Q_{1/2}(X, Y) = 3(Y^2 - X)$*. From Definition 2.3.2, part 1, we see that* k *must satisfy*

$$Q_{1/2}(1, k) = k^2 - 1 = 0,$$

and therefore the only possible rivers are of types $(1, 1/2)$ *and* $(-1, 1/2)$. *Let us consider the case of* $(1, 1/2)$ *first. Since* $P_{1/2}(X, Y) = P(X, Y) = 3$ *and* $Q_{1/2}(X, Y) = Q(X, Y) = 3(Y^2 - X)$, *we obtain* $c(1/2) = 1 - 1/2 + 0 - 0 = 1/2 > 0$. *Moreover,*

$$P_{1/2}(1, 1) = 3 \neq 0 \text{ and } \frac{\partial Q_{1/2}}{\partial Y}(1, 1) = 6 \neq 0.$$

It follows from Theorem 2.3.3 that a $(1, 1/2)$*-river exists, and moreover, from part 2 of Definition 2.3.2, we have*

$$\lim_{t \to \infty} \frac{Y(t)}{(X(t))^{1/2}} = 1,$$

from which we deduce that

$$Y \sim X^{1/2} \text{ as } X \to \infty.$$

This shows that the river runs through the first quadrant of the (X, Y) *plane as* $X \to \infty$. *To determine whether or not it is locally asymptotically stable, we try to use Theorem 2.3.5. In this case,*

$$\Phi(X, Y) = Y^2 - X \Rightarrow \frac{\partial \Phi}{\partial Y}(X, X^{1/2}) = 2X^{1/2} - 1,$$

and we see that the stability criterion fails, since $2X^{1/2} - 1$ *is not always positive in the first quadrant. This is clearly reinforced by Figure 2.2 which shows that this river is repelling.*

Consider next the case of $k = -1$. *Once again we can apply Theorem 2.3.3 to establish that a river of type* $(-1, 1/2)$ *exists, with*

$$Y(t) \sim -X^{1/2} \text{ as } X \to \infty.$$

This river runs through the fourth quadrant of the (X, Y) *plane, and, since*

$$\frac{\partial \Phi}{\partial Y}(X, -X^{1/2}) = -2X^{1/2} - 1 < 0,$$

we can deduce that it is locally attractive.

In conclusion, we have

- *a repelling river with* $r = 1/2$ *and* $k = 1$ *that runs through the first quadrant of the* (X, Y) *plane;*
- *an attracting river with* $r = 1/2$ *and* $k = -1$ *that runs through the fourth quadrant,*

as seen in Figure 2.2.

The useful combination of the concept of a river and the NP method for finding rivers will be used in Chapter 4 to combat a problem, that is difficult to be solved by methods used by da Costa *et. al.* [25] in order to obtain asymptotic behaviour of monomer and island densities.

2.4 Watson's Lemma

Watson's lemma is a useful technique for deriving the asymptotic expansion of an exponentially decaying integral. As we shall require this technique in Chapter 4, it is convenient to include a statement of the lemma here; a proof can be found in [84, p.20].

Lemma 2.4.1 (Watson's lemma [84])**.** *If*

1. *$f(t)$ is analytic when $|t| \leq a+\sigma$, where $a > 0$, $\sigma > 0$, except at a branch-point at the origin, and*

$$f(t) = \sum_{m=1}^{\infty} a_m t^{m/r-1}, \tag{2.9}$$

   where $|t| \leq a$, r being positive

2. *$|f(t)| < Ke^{bt}$, where K and b are independent of t, when t is positive and $t \geq a$*

3. *$|\arg(z)| \leq \pi/2 - \Delta$, where $\Delta > 0$*

4. *$|z|$ is sufficiently large,*

then there exists an asymptotic expansion of $f(t)$ in the form (2.9) given by the formula

$$g(z) = \int_0^{\infty} f(t)e^{-zt}\, dt \sim \sum_{m=1}^{\infty} a_m \Gamma\left(\frac{m}{r}\right) z^{-m/r}. \tag{2.10}$$

Note that we have used the symbol $\sim$ in equation (2.10). Given two functions of $r(z)$ and $s(z)$, if

$$\lim_{z \to z_0} \frac{r(z)}{s(z)} \to K,$$

where K is a finite, non-zero limit then we obtain

$$r = \mathcal{O}(s).$$

This means r is asymptotically equivalent to the order of $s(z)$. If $K = 1$, then we write $r \sim s$.

A short example of the use of Watson's lemma is:

Example 2.4.2. *Consider the integral*

$$g(z) = \int_0^\infty \frac{e^{-zt}}{(1+t)}\, dt.$$

Here, for $t \geq 0$, $f(t) = (1+t)^{-1}$ *is continuous on* $(0, \infty)$ *and has the Maclaurin expansion*

$$f(t) = 1 - t + t^2 - t^3 + \cdots = \sum_{n=0}^{\infty} (-1)^n t^n, \ |t| < 1.$$

Then we have, by applying Watson's lemma, for $|z| \to \infty$ *and* $|\arg(z)| \leq \pi/2 - \sigma < \pi/2$

$$\begin{aligned} g(z) &= \int_0^\infty f(t) e^{-zt}\, dt = \int_0^\infty \sum_{n=0}^{\infty} (-1)^n t^n e^{-zt}\, dt \\ &\sim \sum_{n=0}^{\infty} (-1)^n \Gamma(n+1) z^{-(n+1)} \\ &= \sum_{n=0}^{\infty} (-1)^n \frac{n!}{z^{n+1}}. \end{aligned}$$

To the leading order term, we have

$$g(z) \sim \frac{1}{z},$$

which means that $g(z)$ *behaves like* $1/z$ *for large* z.

2.5 One-Dimensional Laplace Integral

When dealing with Laplace-type integrals of the form

$$I(\lambda) = \int_a^b g(z)e^{-\lambda S(z)}\, dz, \tag{2.11}$$

one is often interested in determining their asymptotic behaviour. As discussed in [84], one approach is to expand the function $S(z)$ as a Taylor series around a minimum point z_m, leading to

$$S(z) = S(z_m) + S'(z_m)(z - z_m) + S''(z_m)\frac{(z - z_m)^2}{2} + \cdots .$$

If the minimum z_m is such that $S'(z_m) = 0$ and $S''(z_m) > 0$, then

$$S(z) - S(z_m) = S''(z_m)\frac{(z - z_m)^2}{2} + \cdots .$$

In the case of a maximum point z_m, one replaces $-\lambda$ in (2.11) by λ. We can now estimate $I(\lambda)$ for large λ by

$$\begin{aligned} I(\lambda) &\approx \int_{z_m-\epsilon}^{z_m+\epsilon} g(z_m)e^{-\lambda(S(z_m)+S''(z_m)(z-z_m)^2/2)}\, dz \\ &\approx g(z_m)e^{-\lambda S(z_m)} \int_{-\infty}^{\infty} e^{-\lambda S''(z_m)(z-z_m)^2/2}\, dz \\ &\approx g(z_m)e^{-\lambda S(z_m)} \sqrt{\frac{2\pi}{\lambda S''(z_m)}}. \end{aligned} \tag{2.12}$$

For the case of a maximum point, the term 2π is replaced by -2π.

Example 2.5.1. *To illustrate this form of estimation of Laplace-type integrals, we consider the Gamma function, which for $\Re(x) > 0$ can be defined by*

$$\Gamma(x) = \int_0^\infty z^{x-1}e^{-z}\, dz.$$

It follows that

$$\Gamma(x+1) = \int_0^\infty z^x e^{-z}\ dz,$$

and, on substituting $z = xy$*, we obtain*

$$\Gamma(x+1) = x^{x+1}\int_0^\infty y^x e^{-xy}\ dy = x^{x+1}\int_0^\infty e^{xS(y)}\ dy,$$

where $S(y) = \ln(y) - y$*. From this, we obtain a maximum point* $y_m = 1$ *since* $S'(y) = 1/y - 1$ *and* $S''(y) = -1/y^2$ *and so by (2.12)*

$$\Gamma(x+1) \approx x^{x+1}e^{(-1)x}\sqrt{\frac{-2\pi}{(-1)x}} = x^{x+1/2}e^{-x}\sqrt{2\pi},$$

which is Stirling's approximation.

We shall require the results presented in this section in Chapters 4 and 5. In particular, the latter chapter contains our modified version of the original two-dimensional Laplace integral explained in [84] by Wong, that specifically allows us to obtain the large-size asymptotic behaviour of the CZD.

2.6 Bootstrap Method

There are sometimes situations where the theoretical distribution of a statistic is either complicated or unknown, or the sample size is too small for straightforward statistical inference. These problems can be easily solved by using the bootstrap method, which we describe next.

The bootstrap method (or bootstrapping) is a method for assigning measures of accuracy to sample estimates (mean, variance etc.) of the original data set, typically drawn from the Monte Carlo (MC) simulation [64]. The data set consists of N independent and identically distributed (iid) data points. The terminology

iid means that, in this case, each data point has the same probability distribution as the others and the sequential order of the data points is not important.

The bootstrap method uses the original data set, namely D_0, to generate, usually, a high number of synthetic data (or bootstrap data) sets, namely D_1, D_2, ... Each data set has N data points. The procedure is to draw N data points at a time with replacements from the original set D_0. We do not get the original set each time because of the replacement. Instead, we get bootstrap data sets in which some fraction of the original data points are replaced by *duplicated* original points. Since the bootstrap data sets are statistically similar to the original set, they make a good approximation to the (unknown) distribution of the original set.

This is not saying that the bootstrap method is infallible – there are some cases in which the method can fail, such as when the iid assumption is false and the sequential order of the data points is vital. Nevertheless, for a large class of problems, especially the ones in Chapters 6 and 7, the bootstrap methods do easily obtain the errors in an estimated parameter (mean, variance etc.) set drawn from the MC simulation.

Chapter 3

Previous Work

3.1 Analysis of the Island Size Distribution via Rate Equations

In this chapter, we will discuss several key papers that have either motivated or played a prominent rôle in the investigations into the island size distribution (ISD) that are presented in this thesis. We begin, in Section 3.1.1, with a significant contribution by Bartelt and Evans [11] who demonstrated that, in the case of point islands, and with critical island size $i = 1$, a rate-equation approach will fail to produce the ISD obtained by Monte Carlo (MC) simulations if one chooses an incorrect form for the capture rate coefficients. As explained in [11], this failure is due to the fact that the rate-equation approach is mean-field in nature, with all islands of the same size assumed to grow at the same rate, irrespective of their positions.

Prior to [11], Blackman and Wilding [16] presented a successful scaling analysis of the rate equations that enables the large-time behaviour of monomer, island and total island densities to be predicted for a class of capture rate coefficients,

including the constant rate coefficients that are customarily used for point-island models. Once again, the rate equations that were considered corresponded to the case of $i = 1$.

The case of constant capture rate coefficients and critical island size $i = 1$ was also the subject of a more recent investigation by da Costa, van Roessel and Wattis [25]. In contrast to the two earlier papers mentioned above, the authors in [25] were able to establish the long-term behaviour of monomer and island size distributions in a mathematically rigorous manner, albeit at the cost of dealing only with a relatively simple case of the rate equations. We shall comment below on how the results obtained in [25] compare with those given in [11] and [16].

In Section 3.2, we discuss a novel approach developed by Blackman and Mulheran [14] for introducing some spatial dependence into one-dimensional (1-D) models of nucleation and island growth. This approach involves the concepts of the gap size and capture zone distributions. Key to this is the recognition that the nucleation of a new island in a gap between two adjacent stable islands will result in the fragmentation of the gap. Thus the evolution of the gap sizes between stable islands caused by nucleation can be interpreted as a fragmentation process. After describing the fragmentation equation used in the work of Blackman and Mulheran, we go on to give some details of another common model used in the study of fragmentation processes, particularly in the work of Ziff and McGrady; see, for example, [87]. In this model, the evolution of a system of fragmenting particles is described by means of an integro-differential equation, and it is an equation of this type that we will use when extending the results of [14]. One advantage of using an integro-differential equation to describe the fragmentation of gaps, is that there are a number of well-established scaling theory results that we are then able to exploit. In particular, we shall give an account of a paper [75]

due to Treat.

In the last two sections, we survey some work of Pimpinelli and Einstein [61], in which the use of the Generalised Wigner Surmise plays a key part, before concluding with a discussion of a paper by Seba [70] on the spacing distribution between parked cars on an infinitely long street. We believe that the latter, which leads to a distributional fixed point equation, is intimately related to the gap size distribution problem and we explore this connection in Chapter 7.

3.1.1 The Work of Bartelt & Evans and Blackman & Wilding

In the case of irreversible aggregation, which occurs at low temperatures, if we assume that islands evolve by capturing a single monomer, then a physically realistic system of rate equations with critical island size $i = 1$, deposition rate F and diffusion rate D of monomers can be obtained. Recall from Chapter 1 that such a system of equations is given by

$$\frac{dc_1}{dt} = F - 2D\sigma_1 c_1^2 - Dc_1 \sum_{j=2}^{\infty} \sigma_j c_j \tag{3.1}$$

$$\frac{dc_j}{dt} = Dc_1(\sigma_{j-1}c_{j-1} - \sigma_j c_j), \quad j \geq 2. \tag{3.2}$$

Each term in the above system of equations has already been discussed in Section 1.3.2. Equations (3.1) and (3.2) have been used by a number of authors in investigations into the ISD in thin film growth. In this section we highlight the contributions made by Bartelt and Evans [11] and Blackman and Wilding [16].

In [11], the scaling form

$$c_j(\theta) = \frac{\theta}{r^2}\phi\left(\frac{j}{r}\right),$$

is assumed for solutions of (3.2), where, as noted in Section 1.3.3, r is the average island size, θ is the coverage and the function ϕ is the scaling function. In [11], Bartelt and Evans consider a point-island model, i.e. that each island occupies only a single site, with an additional label attached to indicate an island's size. In this case, the capture rates σ_j in the mean-field rate equations would customarily be chosen to be independent of j, with $\sigma_j = \sigma_{av} = r^{-1}\sum_{j\geq 2}\sigma_j c_j$. However, Bartelt and Evans use their simulation results to calculate size-dependent rates σ_j and derive a relationship of the form $\sigma_j = \sigma_{av}C(j/r)$, for some function C. Scaled ISDs ϕ are then obtained and plotted for each of the two cases, $\sigma_j = \sigma_{av}$ and $\sigma_j = \sigma_{av}C(j/r)$, and it is observed that these differ; see [11, Fig. 2]. In particular, the distribution for the former has a discontinuity at a scaled island size of 3/2.

In determining the size-dependent rates and in their analysis, Bartelt and Evans use the notion of a Voronoi tessellation of the substrate region containing the islands. Each cell in such a tessellation corresponds to the region of the substrate closer to an island than to any other island and so corresponds to the capture zone of an island described in Section 1.3.4. The assumption that most monomers deposited within a cell will aggregate with the associated island was exploited in [11] to obtain an appropriate form for the function C.

It should be noted that, prior to the work of Bartelt and Evans in [11], Blackman and Wilding [16] had also used a rate-equation approach to investigate the scaling behaviour of island growth in thin films, using (3.1) and (3.2). As in [11], described above, Blackman and Wilding took into account the possibility of the capture rates σ_j depending on j, but unlike the former, who used simulations to obtain σ_j, Blackman and Wilding assumed a power law dependence of the form

$$\sigma_j = j^p,$$

with $1/3 \leq p \leq 1/2$ representing the physically relevant range of p-values. It was also assumed in [16] that the decrease in the number of monomers is governed by another power law, namely

$$c_1(t) \sim t^{-w}, \text{ as } t \to \infty, \tag{3.3}$$

where the exponent w is to be determined. Assuming a scaling ansatz of the form

$$c_j(t) = \frac{1}{j^\tau} f\left(\frac{j}{t^z}\right),$$

it was shown [16, Eq. (9)] that, for $p < 1/2$,

$$z = 2(3-2p)^{-1}, \ \tau = \frac{1}{2} + p, \ w = (3-2p)^{-1},$$

and the time dependence of the n^{th} moment

$$M_n = t^{z(n+1-\tau)} \int_0^\infty x^{n-\tau} \, dx,$$

is therefore given by

$$M_n \sim t^{(2n+1-2p)/(3-2p)}; \tag{3.4}$$

see [16, Eq. (10)]. Analogous results are also obtained for the case $1/2 \leq p < 1$. Note, in particular, that when $p = 0$, in which case $\sigma_j = 1$ for all j, the above assumptions and subsequent results reduce to

$$c_1(t) \sim t^{-1/3}, \ M_n(t) \sim t^{(2n+1)/3} \ \text{ as } t \to \infty. \tag{3.5}$$

We shall return to (3.5) in the next section.

Moreover, in the same paper, Blackman and Wilding had also considered the case where islands of size $m+1$ are stable and all islands of size smaller than $m+1$ will dissociate. It should be noted that their parameter m is the critical island size, i.e. their m is the equivalent of our i in this thesis. By the same assumptions $\sigma_j = j^p$ and (3.3), it was shown [16, Eq. (19)] that, for $p < 1/(m+1)$,

$$z = (m+1)[(m+2)-(m+1)p]^{-1},\ \tau = \frac{m}{m+1} + p,\ w = [(m+2)-(m+1)p]^{-1},$$

and the time dependence of the n^{th} moment is given by

$$M_n \sim t^{[(m+1)n+1-(m+1)p]/[(m+2)-(m+1)p]}; \tag{3.6}$$

see [16, Eq. (20)]. Note that equation (3.6) is equivalent to (3.4) for the $m = 1$ case. As mentioned before, analogous results are also obtained for the case $1/(m+1) \leq p < 1$. In the case of $p = 0$, the above results reduce to

$$c_1(t) \sim t^{-1/(m+2)},\ M_n(t) \sim t^{[(m+1)n+1]/(m+2)} \ \text{ as } t \to \infty. \tag{3.7}$$

We shall return to (3.7) in Chapter 4.

3.1.2 The Work of da Costa, van Roessel and Wattis

We now turn our attention to a more recent investigation [25] by da Costa, van Roessel and Wattis. Once again, the rate equations that are studied are given by (3.1) and (3.2), but with the constant $\alpha > 0$ used instead of F and with

$$D\sigma_j = 1, \text{ for all } j. \tag{3.8}$$

Although (3.8) is a very restrictive assumption, the fact that the resulting equations simplify to

$$\frac{dc_1}{dt} = \alpha - 2c_1^2 - c_1 \sum_{j=2}^{\infty} c_j \tag{3.9}$$

$$\frac{dc_j}{dt} = c_1 c_{j-1} - c_1 c_j, \quad j \geq 2, \tag{3.10}$$

enables a number of results to be established using analytical arguments that are mathematically more rigorous than those employed in the two papers [11] and [16] summarised in the previous subsection.

In [25], da Costa *et. al.* begin by introducing a new variable c_0 defined by

$$c_0(t) = \sum_{j=1}^{\infty} c_j(t),$$

and make the assumption that $c_0(0) < \infty$. Note that c_0 corresponds to the zeroth moment M_0 and so, from (3.5), it is expected that

$$c_1(t) \sim t^{-1/3} \text{ and } c_0(t) \sim t^{1/3} \text{ as } t \to \infty. \tag{3.11}$$

In terms of c_0, equations (3.9) and (3.10) can be expressed as

$$\left.\begin{aligned} \dot{c}_0 &= \alpha - c_0 c_1, \\ \dot{c}_1 &= \alpha - c_1^2 - c_0 c_1, \\ \dot{c}_j &= c_1 c_{j-1} - c_1 c_j, \ j \geq 2. \end{aligned}\right\} \tag{3.12}$$

The advantage that (3.12) has over the system (3.9) and (3.10) is that, although

both are infinite-dimensional systems, the first two equations in (3.12) only involve the first two unknowns, c_0 and c_1 and this means that these can be studied separately using rigorous techniques on finite-dimensional systems of ordinary differential equations. The results obtained on c_0 and c_1 can then be used in conjunction with the third equation (3.12) to derive corresponding results on c_j, $j \geq 2$.

For notational convenience, da Costa *et. al.* replace c_0 and c_1 by $y \geq 0$ and $x \geq 0$ respectively. The two-dimensional (2-D) system of equations for x and y is then

$$\left.\begin{aligned} \dot{y} &= \alpha - xy, \\ \dot{x} &= \alpha - x^2 - xy. \end{aligned}\right\} \tag{3.13}$$

The first result established in [25] are

Proposition 3.1.1 ([25]). *For any solution (x, y) of (3.13) the following hold true, as $t \to \infty$,*

- $x(t) \to 0$;
- $y(t) \to \infty$;
- $x(t)y(t) \to \alpha$.

Poincaré compactification and Centre Manifold methods are then used to prove

Theorem 3.1.2 ([25]). *Let c_j be any non-negative solution of (3.9) and (3.10). Then, as $t \to \infty$, the following hold true*

- $\left(\frac{3}{\alpha}t\right)^{1/3} c_j(t) \to 1$ *for all* $j \geq 1$;
- $(3\alpha^2 t)^{-1/3} \sum_{j=1}^{\infty} c_j(t) \to 1$;

- $\left(\frac{3}{\alpha}t\right)^{2/3}\left(\alpha - c_1(t)\sum_{j=1}^{\infty} c_j(t)\right) \to 1.$

which are in agreement with equation (3.5) obtained by Blackman and Wilding for the case $p = 0$.

A scaling analysis is also carried out in [25] by means of a clever change of variables, which allows the third equation in (3.12) to become linear. First a new time scale is defined by

$$\tau(t) - \tau(t_0) = \int_{t_0}^{t} c_1(s)\, ds, \tag{3.14}$$

The variables c_j are then transformed to $\tilde{c}_j$ using $\tilde{c}_j(\tau) = c_j(t(\tau))$ where $t(\tau)$ is the inverse function of $\tau(t)$. In terms of $\tilde{c}_j$ and τ, the third equation in (3.12) becomes

$$\frac{d\tilde{c}_j}{d\tau} = \tilde{c}_{j-1} - \tilde{c}_j.$$

Theorem 3.1.3. *Let c_j be any non-negative solution of (3.9) and (3.10) with initial data satisfying $c_j(0) \le \rho/j^{\mu}$ for all j, where $\rho > 0$ and $\mu > 1/2$ are fixed constants. Let $\tau(t)$ and $\tilde{c}_j(\tau)$ be as given in (3.14). Then, with $\eta = j/\tau \neq 1$ fixed, the following holds*

$$\lim_{j,\tau\to\infty} \sqrt{\frac{2}{\alpha}\tau}\tilde{c}_j(\tau) = \Phi_1(\eta),$$

where

$$\Phi_1(\eta) := \begin{cases} (1-\eta)^{-1/2} & \text{if } \eta < 1, \\ 0 & \text{if } \eta > 1. \end{cases}$$

Note that the scaling solution in Theorem 3.1.3 is discontinuous. The case when $\eta = 1$ is also examined with the corresponding result being

Theorem 3.1.4. *Let c_j be any non-negative solution of (3.9) and (3.10) with monomeric initial data. Let $\tau(t)$ and $\tilde{c}_j(\tau)$ be as given in (3.14). Then, with $\xi = (j-\tau)/\sqrt{\tau} \in \mathbb{R}$ fixed, the following holds*

$$\lim_{j,\tau\to\infty} \left(\frac{\pi^2}{\alpha^2}\tau\right)^{1/4} \tilde{c}_j(\tau) = \Phi_2(\xi),$$

where

$$\Phi_2(\xi) := e^{-\xi^2/2} \int_0^\infty e^{-\xi w^2 - w^4/2}\, dw.$$

Note that, da Costa *et. al.* comment that Figures 1 and 2 which they produce in [25] using Φ_1 and Φ_2 are similar to Figure 2 obtained by Bartelt and Evans in [11].

As discussed earlier, equations (3.9) and (3.10) represent the case of island growth with critical island size $i = 1$. In Chapter 4, we shall adapt the arguments used by da Costa *et. al.* to produce analogous asymptotic results for a general critical island size $i \geq 1$ where the growth of islands is described by the rate equations (1.4)–(1.6) in Chapter 1, verifying in particular (3.7). We should stress, however, that our river-based approach leads to weaker versions of the $i = 1$ results obtained in [25] as we have only been able to establish the asymptotic behaviour for a restricted class of solutions and not for all non-negative solutions (as in Theorems 3.1.3 and 3.1.4).

3.2 Analysis of the Gap Size Distribution in One-Dimensional Nucleation and Growth Model

The mean-field nature of a rate-equation approach invariably leads to results that do not compare well with simulation data. Motivated by this, several attempts have been made to improve matters by introducing some measure of heterogeneity in the island growth process to reflect the variability in island environment. As described in Subsection 3.1.1, Bartelt and Evans [11] used the idea of a Voronoi tessellation when determining size-dependent capture rates. We now give a brief account of a fragmentation based approach used by Blackman and Mulheran [14] to investigate the distribution of gap sizes between neighbouring islands, and subsequently the capture zone distribution of islands, in a 1-D point island model with critical island size $i = 1$.

It should be noted that the fragmentation equation introduced in [14] as a means of describing the gap size evolution differs from the integro-differential version that is customarily used in studies of fragmentation processes. As we discuss in Subsection 3.2.2, in one such study, Ziff and McGrady [87] considered a binary fragmentation equation to study processes such as depolymerisation using a fragmentation kernel similar to the one Blackman and Mulheran used in their work [14]. Ziff and McGrady were able to obtain an explicit similarity solution of their fragmentation equation.

Despite the success of Ziff and McGrady, explicit solutions to integro-differential fragmentation equations with other, more complicated, kernels are notoriously difficult to obtain. However, we can apply a scaling approach which often allows us to identify similarity solutions. For example, in [75], Treat adopted a scaling

ansatz to produce similarity solutions. The latter were then used to obtain the small- and large-size asymptotic behaviour of general solutions. This is described in Subsection 3.2.3.

As mentioned earlier, influenced by the work of Blackman and Mulheran, and being aware of the fact that a number of asymptotic results are available for fragmentation equations of the type studied by Ziff and McGrady, we have been able to produce a modified fragmentation-based approach to the gap size distribution (GSD) which relies on the integro-differential formulation rather than the alternative equation used in [14]. By using methods presented in Chapter 2, particularly those relating to the Laplace integral, we have successfully extended the results in [14] from $i = 1$ to a general value of i. This will be discussed fully in Chapter 5.

3.2.1 The Blackman and Mulheran Theory

In the 1-D point island nucleation and growth model, with critical island size $i = 1$, Blackman and Mulheran noted that a nucleation occurring in a gap of width y will fragment the parent gap into two new daughter gaps of widths, say x and $y - x$. They then exploited this fact to model the evolution of gap sizes as a fragmentation process, and, from this, were able to determine the GSD. As the fragmentation of a parent gap leads to two daughter gaps, this is a binary fragmentation process. Note that this approach to the GSD applies only to the 1-D model, which is illustrated in Figure 1.3 (see Chapter 1).

Following the analysis of Bales and Chrzan [6], the position dependent monomer density $n_1(x, t)$, whose average is $c_1(t)$, satisfies the diffusion equation

$$\frac{\partial n_1}{\partial t} = D\frac{\partial^2 n_1}{\partial x^2} + F - DE^{-2}n_1, \tag{3.15}$$

where E is defined as the average distance a monomer travels before being captured

by an island or another monomer. As argued in [14, Sections 4 and 5], during the aggregation regime the monomer density between a pair of islands situated at $x = 0$ and $x = y$ is in an approximately steady state, and the monomer density is given approximately by the ordinary differential equation

$$D\frac{d^2 n_1}{dx^2} + F = 0. \tag{3.16}$$

The solution of (3.16) is

$$n_1(x) = \frac{1}{2R}x(y - x), \tag{3.17}$$

where x is the distance from an island located at one end of the gap, and $R = D/F$ is the ratio of monomer diffusion rate to deposition rate. Since the critical island size i is 1, we only require two monomers at a given x for nucleation to occur at x. According to (3.17), the probability of a new nucleation occuring in a gap of width y may be taken as being proportional to

$$a(y) = \int_0^y n_1(x)^2 \, dx = \left(\frac{1}{2R}\right)^2 \int_0^y [x(y - x)]^2 \, dx = \left(\frac{1}{2R}\right)^2 \frac{y^5}{30}. \tag{3.18}$$

Moreover, given that a nucleation event has taken place in a gap of width y, the probability that it will occur at a position x in the gap is proportional to $h(x/y)/y$ where

$$h(r) = \left(\frac{1}{2R}\right)^2 [r(1 - r)]^2, \ 0 \leq r \leq 1. \tag{3.19}$$

Blackman and Mulheran derive an equation [14, Eq. (30)] for describing the effect of a new nucleation, namely

$$F_{M+1}(x) = F_M(x)\left(1 - \frac{x^5}{\mu_M(5)}\right) + \int_x^\infty F_M(y)\left(\frac{y^5}{\mu_M(5)}\right)\left(h\left(\frac{x}{y}\right) + h\left(1 - \frac{x}{y}\right)\right)\frac{dy}{y}, \tag{3.20}$$

where M is the total number of traps on the line of length L, $F_M(x)$ is the number of gaps in the range x to $x + dx$ and $\mu_M(p)$ is the p^{th} moment of $F_M(x)$; see [14, Eq. (24)]. Moreover, they also derive an equation [14, Eq. (31)] for the scaled probability in the form

$$X\frac{d\phi}{dX} + \left(2 + \frac{X^5}{Q_5}\right)\phi = 2\int_X^\infty \left(\frac{Y^5\phi(Y)}{Q_5}\right) h\left(\frac{X}{Y}\right)\frac{dY}{Y}, \tag{3.21}$$

where $\phi(X)$ is the scaled GSD function with $X = x/\langle x\rangle$ and Q_p is the moment of $\phi(X)$; see [14, Eq. (26)].

Blackman and Mulheran have used different values of the ratio R and the coverage θ in their MC simulations for the GSD, confirming good scale invariance as in [14, Fig. 11]. Moreover, they compare these MC data for the GSD to (3.21). This is done by considering a line of length, L say, and, by using random number generation, generating an array of points on this line [14, p.688]. The selection of a pair of existing points (i.e. a gap) between which a new point is introduced is influenced by the fifth power of the separation of the points. The reason for the fifth power is due to (3.18). This procedure for $L = 1000 - 10000$ is repeated over 10000 runs. Blackman and Mulheran have commented on comparisons for the GSD that, though the fit is good, the MC data is more widening than the prediction of (3.21).

Under the assumption that nucleation has effectively mixed up the gaps so that nearest neighbours are not correlated, Blackman and Mulheran define the capture

zone distribution (CZD), $P(s)$, by the convolution equation

$$P(s) = 2\int_0^{2s} \phi(x)\phi(2s-x)\ dx, \tag{3.22}$$

where ϕ is the gap size scaling function, s is the scaled size of capture zones and the factor 2 ensures the normalisation of $P(s)$. More detail about the CZD discussed by Mulheran and Blackman [54] can be found in Chapter 1, Subsection 1.3.4.

Using MC simulations, as in the case for GSD, Blackman and Mulheran have again confirmed good scale invariance for the CZD using different values of R and θ as in [14, Fig. 12]. Moreover, they compare the MC data to the convolution equation (3.22) where the gap size scaling function, ϕ, is obtained from (3.21). In [14, Fig. 12], the comparison is excellent and this supports the assumption that the correlation of the two neighbouring gaps can be ignored and so, in the 1-D case only, we have a direct way of obtaining the function for the CZD.

3.2.2 The Ziff and McGrady Fragmentation Equation

Ziff and McGrady [87] used the binary fragmentation equation

$$\frac{\partial}{\partial t}u(x,t) = -\frac{1}{2}u(x,t)\int_0^x H(x-y,y)\ dy + \int_x^\infty H(x,y-x)u(y,t)\ dy, \tag{3.23}$$

to investigate the size distributions of polymer chains that arises as a result of polymer degradation. Each term in (3.23) is discussed in Section 1.3.2. To represent the situation when the breaking of bonds is more likely to occur in the middle of a chain, the fragmentation kernel H was chosen to be $H(x,y) = xy$, in which case (3.23) becomes

$$\frac{\partial}{\partial t}u(x,t) = -\frac{1}{6}x^3 u(x,t) + 2\int_x^\infty x(y-x)u(y,t)\ dy. \tag{3.24}$$

Ziff and McGrady derived an explicit solution of (3.24), subject to the monodisperse initial condition $u(x,0) = \delta(x-l)$, in the form

$$u(x,t) = e^{-tl^3/6}\delta(x-l) + tlx^2\int_x^l y^{-2}e^{-ty^3/6}\ dy, \tag{3.25}$$

and established that the scaling behaviour of (3.25) is given by

$$u(x,t) \sim xt\phi(xt^{1/3}), \tag{3.26}$$

where

$$\phi(x) = \frac{xl}{6^{1/3}3}\int_{x^3/6}^\infty n^{-4/3}e^{-n}\ dn. \tag{3.27}$$

It is important to note that the solution (3.25) may not be unique according to [72]. This is particularly due to the fact that this solution is not normalised, which will be discussed in Chapter 5.

If we follow the argument of Blackman and Mulheran, discussed earlier, but use the standard binary fragmentation equation (3.23) instead of (3.20), then we arrive at an integro-differential equation for describing the gap size evolution in the $i = 1$ case. We shall explore this in Chapter 5, where we shall also propose, and investigate, an appropriate binary fragmentation equation for the case of general i in which we set

$$a(y) = \int_0^y n_1(x)^{i+1}\ dx. \tag{3.28}$$

The equation (3.24) studied by Ziff and McGrady will be seen to correspond to

the case $i = 0$.

3.2.3 Similarity Solution of the Linear Fragmentation Equation

Equation (3.24) is a particular case of the linear, homogeneous fragmentation equation [75]

$$\frac{\partial}{\partial t}u(x,t) = -c_\rho x^\rho u(x,t) + c_\rho \int_x^\infty y^{\rho-1} h(x/y) u(y,t)\ dy, \tag{3.29}$$

where $\rho \geq 0$ and c_ρ is a constant; see Subsection 1.3.3 in Chapter 1. From [75, p.2524], similarity solutions of (3.29) can be written in the form

$$u^*(x,t) = \frac{N^{*2}(t)}{V}\phi\left(\frac{N^*(t)x}{V}\right), \tag{3.30}$$

where ϕ is normalised so that, as noted in Chapter 1,

$$\int_0^\infty \phi(x)\ dx = \int_0^\infty x\phi(x)\ dx = 1, \tag{3.31}$$

and

$$N^*(t) := \int_0^\infty u^*(x,t)\ dx,\ V := \int_0^\infty x u^*(x,t)\ dx,$$

are the zeroth and first moments of u^* respectively.

Asymptotic properties of ϕ have been established by Cheng and Redner [22, 23] and Treat [75]. In particular, it has been shown that there exists a constant $c > 0$ such that if γ is real, $\lim_{r\to 0} r^{-\gamma-2}\int_0^r \omega h(\omega)\ d\omega$ exists and is non-zero, then

$$\phi(x) = \mathcal{O}(x^\gamma) \text{ as } x \to 0, \tag{3.32}$$

$$\phi(x) = \mathcal{O}(x^{h(1)-2}\exp(-cx^{\rho})) \text{ as } x \to \infty, \tag{3.33}$$

where ρ is the exponent that appears in (3.29).

The scaled similarity variable $\eta = (x/\mu)^{\rho}$ is introduced in [75, Section 5] with $\phi(x) = \bar{\phi}(\eta)$. An explicit expression for similarity solutions, involving Meijer G-functions, is derived in [75, Section 6] for the specific case when the function h in equation (3.29) takes the form

$$h(r) = r^{\gamma}(b_0 + b_1 r + \cdots + b_p r^p),$$

where p is a non-negative integer, $b_0, \ldots, b_p \in \mathbb{R}$ and $0 \leq r \leq 1$. In the case of general p, Treat also derived the following expression for $\phi(\eta)$ [75, Eq. (6.13)]

$$\begin{aligned}\bar{\phi}(\eta) = &\frac{\Gamma(k_1/\rho)\Gamma(k_2/\rho)\cdots\Gamma(k_p/\rho)}{\Gamma((\gamma+1)/\rho)\Gamma((\gamma+2)/\rho)\cdots\Gamma((\gamma+1+p)/\rho)} \\ &\times \frac{\rho}{\mu}\eta^{\gamma/\rho}\, G^{p+1,0}_{p,p+1}\left(\frac{k_p-\gamma-1}{\rho};\ 0, \frac{p}{\rho};\ \eta\right),\end{aligned} \tag{3.34}$$

where, with $(k_p-\gamma-1)/\rho$ standing for $(k_1-\gamma-1)/\rho, (k_2-\gamma-1)/\rho, \ldots, (k_p-\gamma-1)/\rho$, and p/ρ for $1/\rho, 2/\rho, \ldots, p/\rho$, the Meijer G-function is defined [75, Eq. (6.15)] as

$$\begin{aligned}&G^{p+1,0}_{p,p+1}\left(\frac{k_p-\gamma-1}{\rho};\ 0, \frac{p}{\rho};\ \eta\right) \\ &= G^{p+1,0}_{p,p+1}\left(\frac{k_1-\gamma-1}{\rho}, \frac{k_2-\gamma-1}{\rho}, \ldots, \frac{k_p-\gamma-1}{\rho};\ 0, \frac{1}{\rho}, \frac{2}{\rho}, \ldots, \frac{p}{\rho};\ \eta\right) \\ &= \frac{1}{2\pi \mathrm{i}}\int_{\Omega-\mathrm{i}\infty}^{\Omega+\mathrm{i}\infty} \eta^{-z} \\ &\times \frac{\Gamma(z)\Gamma(z+(1/\rho))\cdots\Gamma(z+(p/\rho))}{\Gamma(z+(k_1-\gamma-1)/\rho)\Gamma(z+(k_2-\gamma-1)/\rho)\cdots\Gamma(z+(k_p-\gamma-1)/\rho)}\, dz,\end{aligned}$$

where $\Omega > 0$, and k_p, $p \in \mathbb{Z}^+$, are positive.

For the linear daughter distribution that corresponds to the case $p = 1$, from the function $h(r)$ the coefficients b_0 and b_1 can be expressed as [75, Eq. (7.5)],

$$b_0 = (2+\gamma)(k_1 - \gamma - 1); \quad b_1 = -(3+\gamma)(k_1 - \gamma - 2),$$

where k_1 is positive. In the $p = 1$ case, Treat also derived an alternative representation of the Meijer G-function [75, Eq. (6.26)]

$$G^{2,0}_{1,2}\left(\frac{k_1-\gamma-1}{\rho};\ 0, \frac{1}{\rho};\ \eta\right) = e^{-\eta}\psi\left(\frac{k_1-\gamma-2}{\rho};\ 1-\frac{1}{\rho};\ \eta\right), \tag{3.35}$$

where,

$$\psi\left(\frac{k_1-\gamma-2}{\rho};\ 1-\frac{1}{\rho};\ \eta\right) = \frac{\int_0^\infty z^{(k_1-\gamma-2)/\rho)-1}(1+z)^{-(k_1-\gamma-1)/\rho}e^{-\eta z}\,dz}{\Gamma((k_1-\gamma-2)/\rho)}. \tag{3.36}$$

In the simple case $p = 1$, as discussed in [75, Section 7.2], the integral form (3.34) of the solution ϕ simplifies via (3.35) to

$$\bar{\phi}(\eta) = \frac{\Gamma(k_1/\rho)}{\Gamma((\gamma+1)/\rho)\Gamma((\gamma+2)/\rho)}\frac{\rho}{\mu}\eta^{\gamma/\rho}e^{-\eta}\psi\left(\frac{k_1-\gamma-2}{\rho};\ 1-\frac{1}{\rho};\ \eta\right), \tag{3.37}$$

where

$$\mu = \frac{\Gamma((\gamma+1)/\rho)\Gamma((k_1+1)/\rho)}{\Gamma((\gamma+3)/\rho)\Gamma(k_1/\rho)},$$

and ψ is defined in (3.36). For the large-η expansion case, Treat derived, with ψ

being defined in (3.36),

$$\bar{\phi}(\eta) = \frac{(\gamma+2)}{\Gamma((\gamma+1)/\rho)\mu}\eta^{\gamma/\rho}\psi\left(1;\ 1-\frac{1}{\rho};\ \eta\right), \tag{3.38}$$

with

$$\mu = \frac{\Gamma((\gamma+1)/\rho)(\gamma+3)}{\Gamma((\gamma+2)/\rho)(\gamma+2)},$$

and $k_1 = \gamma + 2 + \mu$.

Since similarity solutions take the form (3.30), we are interested in obtaining the small and large x behaviour of $\phi(x)$. We also are interested in the large-η expansion [75, Section 7.2.2] that will be useful for the analysis in Chapter 5, where, as described earlier, we will obtain the small- and large-size asymptotics of the fragmentation equation with the arguments used in the work of Blackman and Mulheran.

3.3 The Generalised Wigner Surmise

Recently, Pimpinelli and Einstein introduced a new theory for the CZD, employing the Generalised Wigner Surmise (GWS) [61],

$$P(s) = a_\beta s^\beta \exp(-b_\beta s^2), \tag{3.39}$$

where

$$\beta = \begin{cases} \frac{2}{d}(i+1) & \text{if } d = 1, 2 \\ i+1 & \text{if } d = 3, \end{cases} \tag{3.40}$$

causing some controversy; more detail about (3.39) can be found in Chapter 1, Subsection 1.3.4. Despite the excellent visual comparisons between the GWS and MC data taken from the literature [61], the GWS has already been challenged.

Oliveira and Reis [57] have presented simulation results for point islands (at coverage $\theta = 10\%$), fractal islands (at $\theta = 20\%$) and square islands (at $\theta = 10\%$) grown on a 2-D substrate with critical island sizes $i = 1$ and 2 to study the ISD and the CZD numerically. Oliveira and Reis confirm good scale invariance for the CZD for point, fractal and square islands respectively in [57, Fig. 1(a), 2(a) & 2(b)] with different values of R. They compare these simulation data to the GWS, confirming excellent agreement and providing some support for the universal Gaussian tail of the CZD [61]. For the ISD, Oliveira and Reis use the empirical formula derived by Amar and Family [2]

$$f_i(x) = C_i x^i \exp(-i a_i x^{1/a_i}), \tag{3.41}$$

where x is the scaled island size, and C_i and a_i are normalisation constants. Equation (3.41) is used to investigate the peaks of ISDs and allows one to estimate i. However, because of its significant deviations from the point-island model as in [2, 33], the exact form of the ISD has yet to be found. As expected, Oliveira and Reis found that using (3.41) shows deviations from the simulated ISD for other types of islands.

In a short comment on [61], Li, Han and Evans [47] also question the $i = 1$, $d = 2$ GWS form for the CZD, proposing their own form based on a sophisticated theory for capture zone evolution in two dimensions [32]. They also presented an alternative theory which yields a modified form for the large-size behaviour of CZD, supported by data for the simulated growth of compact islands with $i = 1$. This form seems to agree with that found by Oliveira and Reis, contradicting the

GWS [57].

In other work, Shi, Shim and Amar [71] studied $i = 1$ point-island models in dimensions $d = 1, 2, 3, 4$. The shapes of the lattice for each d are a line ($d = 1$), square and triangle ($d = 2$), cubic ($d = 3$), and hypercubic ($d = 4$). Shi *et. al.* have used two simulation models, namely SSA (Shi, Shim and Amar) and EB (Evans and Bartelt). In the EB model, if a monomer diffuses to, or is deposited at, a site which has an occupied site as a neighbour, that monomer is immediately captured by another diffused monomer or an island. This short-range interaction does not exist in the SSA model, where if a monomer either hops onto an island or onto another monomer, then this particular monomer is captured by this island or a new island is nucleated, respectively. For $d = 2 - 4$, Shi *et. al.* confirm little dependence on θ for a fixed value of R. However, for a fixed $\theta = 10\%$, the peak of the simulated CZD decreases as the value of R increases. These are observed for $d = 3$ in [71, Fig. 1] and similar results are obtained for $d = 2$ and $d = 4$. It is noted that the dependence of the peak of the CZD on R is more sensitive for the EB model than the SSA model. This may be due to the interaction range in the EB model being larger than those of the SSA model.

Surprisingly, the conclusion for $d = 1$ is different. Firstly, SSA confirms good agreement of simulated data for different values of R with those of results in the work of Blackman and Mulheran [14]. For $\theta = 10\%$, the peak of the simulated CZD increases with R as the value of R increases, which is different from those results for $d = 2 - 4$. By investigating the peak of the simulated CZD, Shi *et. al.* find that the CZD is more sharply peaked and narrower than the GWS suggests, and a better choice of β is 3 rather than $\beta = 2$ for $d = 2, 3$. Moreover, for $d = 1$, it is notable that the peak height analysed by Shi *et. al.* suggests that the predicted value of $\beta = 4$ is not correct. Therefore it is by no means established whether the

GWS provides a good theoretical basis for understanding the CZD found in island nucleation and growth simulations.

Recent work by González, Pimpinelli and Einstein [35] has revisited the case of $i = 1$, developing the original fragmentation equation (3.21) [14] and the GWS arguments in response to deviations between prediction and simulation. As discussed earlier, Blackman and Mulheran proposed that $a(x) \approx x^5$ as in (3.18). However, González *et. al.* observe that exponents 3 and 4 instead of 5 give better agreement with their simulation data. But neither these values describe the large-size asymptotic behaviour of the scaled gap size x. They comment that the small-size asymptotic behaviour of the GSD may depend on the probability for the nucleation to occur in a specific position between two existing islands. In [35], the GSD decays like $\exp(-Bx^3)$, for some constant B, instead of $\exp(-Bx^5)$ as predicted by the Blackman and Mulheran fragmentation theory approach or $\exp(-Bx^2)$ as predicted by the GWS. González *et. al.* have concluded that the GWS with the suitable selection of β is a good approximation for the CZD.

It is interesting to note that the justification for the relationship between the parameter β and the critical island size is based on the same physical model analysed in this thesis. In [61], the island nucleation rate is discussed in terms of the monomer density n, and the probability of $(i + 1)$ monomers coinciding is used to give the nucleation rate as n^{i+1}. This is the same physical basis Blackman and Mulheran have used for their fragmentation theory in the case of $i = 1$ [14].

Therefore, in Chapter 5 we will conclude the work presented in this thesis with a discussion of how the Blackman and Mulheran theory and the GWS approaches differ and how they might be reconciled. Also, in Chapter 6 confrontation with the MC simulation and experiment will ultimately arbitrate between these theories. Along these lines, we note the recent analysis of the case of $i = 1$ in [35], and our

own detailed comparisons with extensive simulation data for $i = 0, 1, 2, 3$.

3.4 The Distributional Fixed Point Equation

Seba [70] investigated a 1-D model of spacing distribution between cars parked in an infinitely long street to ensure the parking of as many cars as possible. The underlying strategy that is adopted for any particular parking attempt is as follows. A random position x on the street is selected. If a large enough interval centred at x is free, the car may park in the interval at x thereby fragmenting the interval. Otherwise, another random position x is chosen and so on. Cars may leave as well and new ones immediately park in the interval. As a means of describing the spacing distribution approximately, Seba derived the distributional fixed point equation (DFPE)

$$X_d \stackrel{\triangle}{=} a(1 + X_d). \tag{3.42}$$

Here X_d is the distance between two parked cars, a is an independent random variable with a probability density, $f(a)$, and the symbol $\stackrel{\triangle}{=}$ means that the left- and right-hand sides of (3.42) have the same distribution. It is assumed that $f(a)$ is symmetric such that $f(a) = f(1 - a)$. The DFPE (3.42) can be solved by iteration. If we define $w(t)$ of X_d as the probability density of the distance X_d, then the cumulative density function $W(t)$ of X_d can be written as an integral equation in the form [70, Eq. (8)]

$$W(t) = \int_0^1 W\left(\frac{t}{a} - 1\right) f(a)\, da = t \int_{t-1}^{\infty} W(s) f\left(\frac{t}{s+1}\right) \frac{ds}{(s+1)^2}. \tag{3.43}$$

Seba chooses the beta distribution with two parameters being equal to 2, i.e. $\beta(2,2)$, for $f(a)$ which leads to $f(a) = a^{2-1}(1-a)^{2-1}/B(2,2) = 6a(1-a)$ where $B(\cdot,\cdot)$ is the Beta function. He then differentiates (3.43) with respect to t four times to obtain the delay differential equation [70, Eq. (14)]

$$t^3 \frac{d^2}{dt^2}\left(\frac{w(t)}{t}\right) = 6w(t-1). \tag{3.44}$$

In [70], Seba compares the prediction results from (3.42) and (3.44) with experimental data obtained by measuring the distances between cars parked in a street and observed that the prediction compares well with experimental data.

The idea we pursue later in the thesis is to adapt the Seba model for the case of nucleation and growth on a 1-D substrate as a way of describing the ISD accurately. The connection between our model and the Seba model is that we may interpret the distance between any two neighbouring cars as the gap between any two neighbouring islands. This may be also a way of describing both GSDs and CZDs which may allow us to analyse the DFPE and its counterpart integral equation. More details will be given later in Chapter 7.

Chapter 4

Long Time Behaviour of Monomer and Point Island Size Distributions

4.1 Introduction to the System

In Chapter 3, we described how equations (3.9) and (3.10), with constant capture rate coefficients, have been the subject of rigorous mathematical analysis aimed at determining the asymptotic behaviour of monomer and island size distributions and proving the convergence of island size distribution (ISD) to a similarity solution. As indicated earlier, this rigorous analysis has been carried out under the assumption that the critical island size is given by $i = 1$. In this chapter, our aim is to relax this rather restrictive condition by extending the $i = 1$ results obtained by da Costa, van Roessel and Wattis in [25] to the case when $i > 1$. In achieving this aim, we shall use techniques associated with the Newton Polygon and the notion of a river, as outlined in Chapter 2. This is in contrast to the approach that relied

upon the Centre Manifold and Tubular Flow theorems that was adopted in [25]. Our reasons for using this alternative approach are two-fold. Firstly, we have been unable to apply the approach used by da Costa *et. al.* to the case $i > 1$. Secondly, we believe that the method which we use is easier to apply than that adopted in [25] even in the $i = 1$ case. Moreover, our results for a general i immediately yield those of [25], albeit for a restricted class of solutions, on setting $i = 1$ and provide confirmation of the results of Blackman and Wilding for the case of constant capture rate coefficients and a general critical island size. Further motivation for our work in this chapter is also provided by the fact that an important objective in the modelling of the submonolayer nucleation and growth regime is to identify how the critical island size i influences the scaling properties of the resulting ISD.

We generalise the model of [25] to the case of submonolayer deposition with point islands of critical size $i \geq 1$. We assume that islands of size $1 < j \leq i$ simply do not arise and as such that islands of size $j > i$ cannot fragment into monomers. Under these assumptions and the assumptions of da Costa *et. al.* [25], we consider a system of equations

$$\left.\begin{aligned} \dot{c}_1 &= \alpha - nc_1^n - c_1 \sum_{j=n}^{\infty} c_j, \\ \dot{c}_n &= c_1^n - c_1 c_n, \\ \dot{c}_j &= c_1 c_{j-1} - c_1 c_j, \ j > n, \end{aligned}\right\} \tag{4.1}$$

where $c_j(t)$ is the expected number of islands of size j, $n(:= i + 1)$ is the smallest stable island size and $\alpha \in \mathbb{R}$ is the constant monomer input.

The advantage of the system of equations (4.1) is, as in the work of da Costa *et. al.*, that the analysis of the long-time behaviour of solutions reduces to a study of a two-dimensional system of ordinary differential equations. Let $Y(t) = c_1(t)$

and formally set $X(t) = \sum_{j=n}^{\infty} c_j(t)$. Then, substituting in the equation for $\dot{c}_1$ leads to

$$\dot{Y} = \alpha - nY^n - YX.$$

We differentiate X with respect to (w.r.t) t to obtain,

$$\dot{X} = \sum_{j=n}^{\infty} \dot{c}_j = Y^n - Yc_n + Y \sum_{j=n+1}^{\infty} (c_{j-1} - c_j) = Y^n.$$

Thus, we have a system of equations

$$\left.\begin{aligned} \dot{Y} &= \alpha - nY^n - XY, \\ \dot{X} &= Y^n, \\ \dot{c}_n &= Y^n - Yc_n, \\ \dot{c}_j &= Y(c_{j-1} - c_j),\ j > n. \end{aligned}\right\} \tag{4.2}$$

One can recover the equations (3.9) and (3.10) analysed by da Costa *et. al.* in [25] by setting $n = 2$ and noting that $c_0 = X + Y$. We notice that there is no factor $n = 2$ in equation (3.9). We show that this is not inconsistent. Recall, from Chapter 3, the system of equations investigated by da Costa *et. al.*

$$\left.\begin{aligned} \dot{c}_0 &= \alpha - c_0c_1, \quad c_0(t) = \sum_{j=1}^{\infty} c_j(t), \\ \dot{c}_1 &= \alpha - c_1^2 - c_0c_1, \\ \dot{c}_j &= c_1(c_{j-1} - c_j),\ j \geq 2. \end{aligned}\right\} \tag{4.3}$$

Let us write the $\dot{c}_1$ equation as

$$\dot{c}_1 = \alpha - c_1^2 - c_1^2 - c_1 \sum_{j=2}^{\infty} c_j(t) = \alpha - 2c_1^2 - c_1X, \quad X = \sum_{j=2}^{\infty} c_j(t).$$

Then differentiate X w.r.t t to obtain

$$\dot{X} = \sum_{j=2}^{\infty} \dot{c}_j = \sum_{j=2}^{\infty} (c_1 c_{j-1} - c_1 c_j) = c_1 \sum_{j=2}^{\infty} c_{j-1} - c_1 \sum_{j=2}^{\infty} c_j = c_1^2.$$

Hence, letting $Y = c_1$, we recover

$$\left.\begin{aligned} \dot{Y} &= \alpha - 2Y^2 - XY, \\ \dot{X} &= Y^2, \end{aligned}\right\}$$

since we have the following relation $c_0 = \sum_{j=1}^{\infty} c_j = X + Y$.

Note that the first two equations in (4.2) decouple from the rest and that once the behaviour of $Y(t)$ is known for large t, we can recover the long-time behaviour of $c_j(t)$ by solving, one by one, linear equations.

As in [25], we can establish the equivalence of solutions to (4.1) and (4.2). Following the approach used in [25], we first introduce a new timescale

$$\tau(t) := \int_0^t Y(s)\, ds, \tag{4.4}$$

along with scaled variables, $\tilde{c}_j(\tau) := c_j(t(\tau))$. Since $Y(t) > 0$, $\tau(t)$ is positive and monotonic increasing, and so has an inverse which we denote by $t(\tau)$. Using the new timescale, we derive for $j \geq n$

$$\tilde{c}_j'(\tau) = \frac{dc_j}{dt}\frac{dt}{d\tau} = \frac{c_1 c_{j-1} - c_1 c_j}{c_1} \Leftrightarrow \tilde{c}_j' = \tilde{c}_{j-1} - \tilde{c}_j.$$

By using the variation of constants formula, we obtain

$$\tilde{c}_j = e^{-\tau} \int_0^{\tau} e^s \tilde{c}_{j-1}(s)\, ds + K e^{-\tau} = \int_0^{\tau} e^{-s} \tilde{c}_{j-1}(\tau - s)\, ds + K e^{-\tau},$$

where $K \equiv \tilde{c}_j(0)$ is a constant. Note that the equation $\dot{c}_n = c_1^n - c_1 c_n$ becomes

$$\tilde{c}_n' = \tilde{c}_1^{n-1} - \tilde{c}_n \Rightarrow \tilde{c}_n = e^{-\tau}\tilde{c}_n(0) + \int_0^\tau e^{-(\tau-s)}[\tilde{c}_1(s)]^{n-1}\, ds.$$

For $j = n+1$, we have

$$\begin{aligned}\tilde{c}_{n+1}(\tau) &= e^{-\tau}\int_0^\tau e^s\tilde{c}_n(s)\, ds + e^{-\tau}\tilde{c}_{n+1}(0) = \int_0^\tau e^{-s}\tilde{c}_n(\tau-s)\, ds + e^{-\tau}\tilde{c}_{n+1}(0)\\ &= \int_0^\tau se^{-s}[\tilde{c}_1(\tau-s)]^{n-1}\, ds + e^{-\tau}[\tau\tilde{c}_n(0) + \tilde{c}_{n+1}(0)].\end{aligned}$$

We now use induction to establish a formula for $\tilde{c}_j$ in the general case $j \geq n$.

Proposition 4.1.1. *For $j \geq n$,*

$$\tilde{c}_j(\tau) = e^{-\tau}\sum_{k=n}^{j}\frac{\tau^{j-k}}{(j-k)!}\tilde{c}_k(0) + \frac{1}{(j-n)!}\int_0^\tau s^{j-n}e^{-s}[\tilde{c}_1(\tau-s)]^{n-1}\, ds. \qquad (4.5)$$

Proof. When $j = n$, we have $\tilde{c}_n(\tau) = e^{-\tau}\tilde{c}_n(0) + \int_0^\tau e^{-s}[\tilde{c}_1(\tau-s)]^{n-1}ds$ and so the formula holds for $j = n$. Suppose the formula for $\tilde{c}_j$ holds for some fixed $j \geq n$. Then

$$\begin{aligned}\tilde{c}_{j+1}(\tau) &= e^{-\tau}\tilde{c}_{j+1}(0) + \int_0^\tau e^{-(\tau-s)}\tilde{c}_j(s)\, ds\\ &= e^{-\tau}\tilde{c}_{j+1}(0) + \int_0^\tau e^{-(\tau-s)}\left[e^{-s}\sum_{k=n}^{j}\frac{s^{j-k}}{(j-k)!}\tilde{c}_k(0)\, ds\right.\\ &\left.+\frac{1}{(j-n)!}\int_0^s (s-r)^{j-n}e^{-(s-r)}[\tilde{c}_1(r)]^{n-1}\, dr\right] ds. \qquad (4.6)\end{aligned}$$

By changing the order of integration, from (4.6) we obtain

$$\begin{aligned}
\tilde{c}_{j+1}(\tau) &= e^{-\tau}\tilde{c}_{j+1}(0) + e^{-\tau}\int_0^\tau \sum_{k=n}^{j} \frac{s^{j-k}}{(j-k)!}\tilde{c}_k(0)\ ds \\
&\quad + \frac{1}{(j-n)!}\int_0^\tau \left[\int_r^\tau e^{-(\tau-r)}(s-r)^{j-n}[\tilde{c}_1(r)]^{n-1}\ ds\right] dr \\
&= e^{-\tau}\tilde{c}_{j+1}(0) + e^{-\tau}\sum_{k=n}^{j}\frac{\tau^{j-k+1}}{(j-k+1)!}\tilde{c}_k(0) \\
&\quad + \frac{1}{(j-n)!}\int_0^\tau e^{-(\tau-r)}[\tilde{c}_1(r)]^{n-1}\frac{(\tau-r)^{j-n+1}}{(j-n+1)}\ dr \\
&= e^{-\tau}\sum_{k=n}^{j+1}\frac{\tau^{j+1-k}}{(j+1-k)!}\tilde{c}_k(0) + \frac{1}{(j+1-n)!}\int_0^\tau e^{-(\tau-r)}(\tau-r)^{j+1-n}[\tilde{c}_1(r)]^{n-1}\ dr \\
&= e^{-\tau}\sum_{k=n}^{j+1}\frac{\tau^{j+1-k}}{(j+1-k)!}\tilde{c}_k(0) + \frac{1}{(j+1-n)!}\int_0^\tau e^{-s}s^{j+1-n}[\tilde{c}_1(\tau-s)]^{n-1}\ ds,
\end{aligned}$$

as required. □

Now, we obtain a theorem about the equivalence of solutions of (4.1) and (4.2)

Theorem 4.1.2. *If $X(0) < \infty$, then a solution of system (4.2) will also be a solution of (4.1).*

Proof. We begin by introducing the following generating function,

$$\begin{aligned}
F(\tau, z) &= \sum_{m=n}^{\infty}\tilde{c}_m(\tau)z^m = e^{-\tau}\sum_{m=n}^{\infty}\sum_{k=n}^{m}\frac{\tau^{m-k}}{(m-k)!}z^m\tilde{c}_k(0) \\
&\quad + \sum_{m=n}^{\infty}\frac{z^m}{(m-n)!}\int_0^\tau s^{m-n}e^{-s}[\tilde{c}_1(\tau-s)]^{n-1}\ ds \\
&= G(\tau, z) + H(\tau, z).
\end{aligned}$$

Rearranging, we obtain

$$\begin{aligned} G(\tau, z) &= e^{-\tau} \sum_{m=n}^{\infty} \sum_{k=n}^{m} \frac{\tau^{m-k}}{(m-k)!} z^m \tilde{c}_k(0) \\ &= e^{-\tau} \sum_{k=n}^{\infty} \sum_{m=k}^{\infty} \frac{\tau^{m-k}}{(m-k)!} z^m \tilde{c}_k(0) \\ &= e^{-\tau} \sum_{k=n}^{\infty} \sum_{m=0}^{\infty} \frac{\tau^m}{m!} z^{m+k} \tilde{c}_k(0) \\ &= e^{-\tau(1-z)} \sum_{k=n}^{\infty} z^k \tilde{c}_k(0). \end{aligned}$$

The series above converges for $|z| \leq 1$ since the series $\sum_{k=n}^{\infty} \tilde{c}_k(0)$ is convergent presumably because $X(0) < \infty$. The series $\sum_{k=n}^{\infty} |\tilde{c}_k(0)| < \infty$ is also convergent because $\tilde{c}_k(0) \geq 0$. Also, $|z||\tilde{c}_k(0)| \leq |\tilde{c}_k(0)|$ if $|z| \leq 1$. Thus,

$$\sum_{k=n}^{\infty} |z^k||\tilde{c}_k(0)| \leq \sum_{k=n}^{\infty} |\tilde{c}_k(0)| = \sum_{k=n}^{\infty} \tilde{c}_k(0),$$

which converges by comparison test (non-limit version). For $\tau = 0$, $F(0, z) = \sum_{m=n}^{\infty} \tilde{c}_k(0) z^m$ and therefore we have

$$G(\tau, z) = e^{-\tau(1-z)} F(0, z) \quad \text{for } |z| \leq 1. \tag{4.7}$$

If we now examine $H(\tau, z)$, then, on rearranging, we obtain

$$\begin{aligned} H(\tau, z) &= \sum_{m=n}^{\infty} \frac{z^m}{(m-n)!} \int_0^{\tau} [\tilde{c}_1(\tau - s)]^{n-1} s^{m-n} e^{-s} \, ds \\ &= \sum_{m=n}^{\infty} z^n \int_0^{\tau} [\tilde{c}_1(\tau - s)]^{n-1} \frac{(sz)^{m-n}}{(m-n)!} e^{-s} \, ds \\ &= z^n \int_0^{\tau} [\tilde{c}_1(\tau - s)]^{n-1} e^{-s+sz} \, ds \\ &= z^n \int_0^{\tau} [\tilde{c}_1(s)]^{n-1} e^{-(\tau-s)(1-z)} \, ds. \end{aligned}$$

Thus,

$$F(\tau, z) = e^{-\tau(1-z)} F(0, z) + z^n \int_0^{\tau} [\tilde{c}_1(s)]^{n-1} e^{-(\tau-s)(1-z)} \, ds,$$

which, at $z = 1$, yields

$$F(\tau, 1) = F(0, 1) + \int_0^{\tau} [\tilde{c}_1(s)]^{n-1} \, ds = F(0, 1) + \int_0^{\tau} [\tilde{Y}(s)]^{n-1} \, ds. \tag{4.8}$$

Recall $\dot{X}(t) = Y(t)^n$ such that

$$\tilde{X}'(\tau) = \tilde{Y}(\tau)^{n-1}, \tag{4.9}$$

and the fact that $F(\tau, 1) = \tilde{X}(\tau)$. Differentiate (4.8) w.r.t τ

$$F(\tau, 1)' = F(0, 1)' + \tilde{Y}(\tau)^{n-1} \Leftrightarrow \tilde{X}'(\tau) = \tilde{Y}(\tau)^{n-1},$$

which satisfies (4.9). □

4.2 Asymptotic Behaviour of the Monomer and Total Island Distributions

Our aim now is to determine the asymptotic behaviour of solutions to the system (4.2). For this we can apply the theory discussed in Chapter 2 to the equations for X and Y in (4.2) to investigate whether any (k, r)-rivers exists, and, if so, determine their stability. We begin by using the Newton Polygon (NP) method to find the possible river exponents r, and define $\Phi(X, Y)$ by

$$\Phi(X, Y) := \frac{Q(X, Y)}{P(X, Y)},$$

where $Q(X, Y) = \alpha - nY^n - XY$ and $P(X, Y) = Y^n$. It follows that

$$\frac{dY}{dX} = \alpha Y^{-n} - n - XY^{1-n} := \Phi(X, Y). \tag{4.10}$$

It can be shown that the NP of $\Phi(X, Y)$, which is a generalised polynomial, provides the same information as that of $Q(X, Y)$. The former is as in Figure 4.1. Following the approach explained in Chapter 2, we take

$$F(y_0) = \alpha y_0^{-n} - n - xy_0^{1-n} \tag{4.11}$$

and then examine each term in turn. This is set out in Table 4.1 with $A = 0$ and $B = \underline{\rho}$

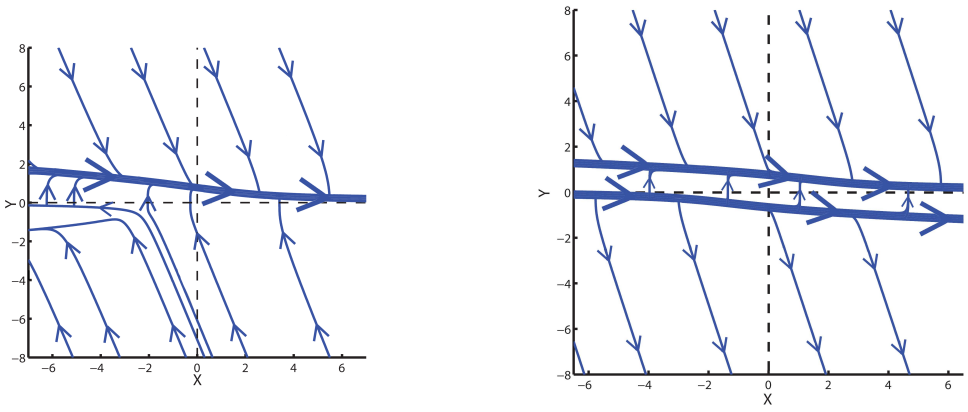

Figure 4.1: Phase portrait of (4.10) for n even (on the left-hand side of this figure) and odd (on the right-hand side).

Term	γ	$\underline{\rho} = (\rho_0)$	A	B	Point (γ, B)
αy_0^{-n}	0	$(-n)$	0	$-n$	$(0, -n)$
$-n$	0	(0)	0	0	$(0, 0)$
$-xy_0^{1-n}$	1	$(1-n)$	0	$1-n$	$(1, 1-n)$

Table 4.1: Vertices of the system using the Newton Polygon method

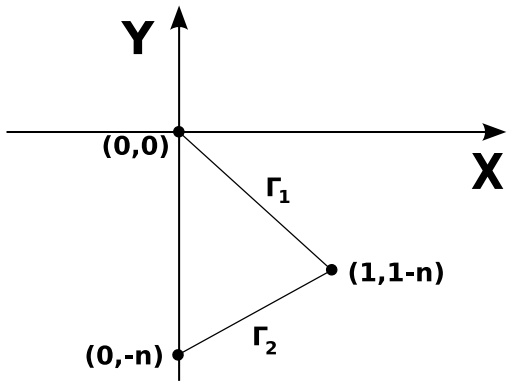

Figure 4.2: Newton Polygon for (4.10).

We want to find the real numbers r such that the vector $(1, r)$ is perpendicular to the direction vectors of the segments Γ_1 or Γ_2. Let us consider the case of the segment Γ_1 first. This segment connects $(0, 0)$ to $(1, 1-n)$, and its gradient is $(1-n)$. Thus, we have $r_1 = 1/(n-1)$ for Γ_1. For Definition 2.3.2 part 1, we start with

$$\Phi(X, X^{1/(n-1)}) = \alpha X^{-n/(n-1)} - n - 1,$$

and so $\deg_{r_1} \Phi = 0$, and $\Phi_{r_1}(X, Y) = -n - XY^{1-n}$. By Definition 2.3.2 part 1, we have (note that $\Phi_r(1, k) = Q_r(1, k) = 0$)

$$\Phi_{r_1}(1, k) = 0 \Leftrightarrow -n - k^{1-n} = 0,$$

i.e. $k \in \mathbb{R}$ has to satisfy

$$k^{1-n} = -n,$$

from which it follows that when n is odd, say $n = 2l + 1$, where $l \in \mathbb{Z}^+$, then we have $k = [-(2l+1)]^{-1/2l}$. In other words, there are no solutions. In the case of even integer $n = 2l$, we have k is obtained as an odd root of a negative number and so k is negative. This implies that the only real solution is negative, i.e. the river runs through the fourth quadrant of the (X, Y) plane. Moreover, we have

$$P(X, X^{1/(n-1)}) = X^{n/(n-1)} \Rightarrow P_{r_1}(X, Y) = Y^n;$$
$$Q(X, X^{1/(n-1)}) = \alpha - nX^{n/(n-1)} - X^{n/(n-1)} \Rightarrow Q_{r_1}(X, Y) = -nY^n - XY,$$

and, by Definition 2.3.2 part 3, $c(r) = (n+2)/(n-1) \geq 0$. Finally, we have

$$P_{r_1}(1,k) = k^n \neq 0 \text{ and } \frac{\partial Q_{r_1}}{\partial Y}(1,k) = n-1 \neq 0.$$

Hence, by Theorem 2.3.3, the river with $r_1 = 1/(n-1)$ exists. Next, we want to determine whether this river is attractive or repulsive using Theorem 2.3.5. We differentiate $\Phi(X,Y)$ with respect to Y, setting $Y \sim kX^{1/(n-1)}$,

$$\Phi_Y(X,Y) = -n\alpha Y^{-n-1} - (1-n)XY^{-n},$$

i.e.

$$\Phi_Y(X, kX^{1/(n-1)}) = -n\alpha^{-n}k^{-(n+1)}X^{-(n+1)/(n-1)} - (1-n)k^{-n}X^{-1/(n-1)}.$$

Since $\Phi_Y(X, kX^{1/(n-1)})$ is not always negative for all $X > 0$, this river with $r_1 = 1/(n-1)$ is repulsive.

The segment Γ_2 connects $(1, 1-n)$ to $(0, -n)$, and its gradient is 1. Thus $r_2 = -1$ for all $n \geq 2$. We use the value $r_2 = -1$ to determine k and, by Definition 2.3.2 part 2, we set

$$Y = R(X) \sim kX^{-1}.$$

The term $\deg_{r_2}\Phi = n$ leads to $\Phi_{r_2}(X,Y) = \alpha Y^{-n} - XY^{1-n}$. By Definition 2.3.2 part 1, we obtain

$$\Phi_{r_2}(1,k) = \alpha k^{-n} - k^{1-n} = 0,$$

which leads to $k = \alpha$. Moreover, we have

$$P(X, X^{-1}) = X^{-n} \Rightarrow P_{r_2}(X, Y) = Y^n;$$
$$Q(X, X^{-1}) = \alpha - nX^{-n} - 1 \Rightarrow Q_{r_2}(X, Y) = \alpha - XY,$$

and, by Definition 2.3.2 part 3, $c(r) = n + 2 > 0$. Finally, we have

$$P_{r_2}(1, k) = \alpha^n \neq 0 \text{ and } \frac{\partial Q_{r_2}}{\partial Y}(1, k) = -1 \neq 0.$$

Hence, by Theorem 2.3.3, the river $R(X)$ corresponding to $r_2 = -1$ exists. Moreover, since $Y = R(X) \sim \alpha X^{-1}$, where $\alpha > 0$ and $X \to \infty$ as $t \to \infty$, we can state that $R(X)$ is in the first quadrant of the XY plane. Next we want to determine whether $R(X)$ is locally attractive by applying Theorem 2.3.5. We differentiate $\Phi(X, Y)$ with respect to Y, setting $Y \sim \alpha X^{-1}$, to obtain

$$\Phi_Y(X, Y) = -n\alpha Y^{-n-1} - (1 - n)XY^{-n} \Leftrightarrow \Phi_Y(X, \alpha X^{-1}) = -\alpha^{-n} X^{n+1}.$$

Since $\Phi_Y(X, \alpha X^{-1}) < 0$ for positive X, we have by Theorem 2.3.5 that the river is locally attractive.

In conclusion, we have

- an attracting river with $r_2 = -1$ and $k = \alpha$ that runs through the first quadrant of the (X, Y) plane;
- for even integer of n, a repelling river with $r_1 = 1/(n-1)$ and $k = (-n)^{1/(1-n)}$ that runs through the fourth quadrant;
- for odd integer of n, a river with $r_1 = 1/(n-1)$ and $k = (-n)^{1/(1-n)}$ does

not exist,

as seen in Figure 4.1.

Having established that the river $R(x)$ is locally attractive, the next step would be that of proving that all solutions in the first quadrant are attracted to the river. Unfortunately, we have been unable to establish this more global asymptotic result.

In conclusion, we have shown that the rivers with $r_1 = 1/(n-1)$ and $r_2 = -1$, respectively, are repulsive and attractive. Since we have the locally attractive river $R(x)$ which is relevant for $X(t) \geq 0$ and $Y(t) \geq 0$, we can go back to the system of equations (4.2) and determine the asymptotic behaviour of solutions that start off in the basin of attraction of $R(X)$. Note that solutions $X(t)$ and $Y(t)$ must be non-negative because $X(t)$, total stable island density, and $Y(t)$, monomer density, cannot be physically negative. Since $Y \sim \alpha X^{-1}$, so that $\dot{X} = Y^n \sim \alpha^n X^{-n}$, for X we have

$$X(t) \sim t^{1/(n+1)}[(n+1)\alpha^n]^{1/(n+1)}. \tag{4.12}$$

Similarly, since $Y(t) \sim \alpha/X(t)$ for large time, we have

$$Y(t) \sim t^{-1/(n+1)} \left[\frac{\alpha}{n+1}\right]^{1/(n+1)}. \tag{4.13}$$

Clearly, we have $XY \to \alpha$ for any solution of (4.2) as $t \to \infty$. To obtain the rate of convergence of XY, we differentiate the Y equation in (4.2) with respect to time and rearrange it as

$$(\dot{XY}) = -n^2 Y^{n-1}\dot{Y} - \ddot{Y}.$$

By rearranging the $Y(t)$ equation i.e. $XY = -\alpha - nY^n - \dot{Y}$, if $XY \sim \alpha + at^s$ for large time, we have

$$ast^{s-1} \sim \frac{n^2}{n+1} t^{-(2n+1)/(n+1)} \left[\frac{\alpha}{n+1}\right]^{n/(n+1)} - \frac{(n+2)}{(n+1)^2} t^{-(2n+3)/(n+1)} \left[\frac{\alpha}{n+1}\right]^{1/(n+1)}$$
$$\sim \frac{n^2}{n+1} t^{-(2n+1)/(n+1)} \left[\frac{\alpha}{n+1}\right]^{n/(n+1)}.$$

Integrating w.r.t t gives us

$$at^s \sim -n \left[\frac{\alpha}{n+1}\right]^{n/(n+1)} t^{-n/(n+1)},$$

and so, as $XY \sim \alpha + at^s$, we have

$$X(t)Y(t) \sim \alpha - n \left[\frac{\alpha}{n+1}\right]^{n/(n+1)} t^{-n/(n+1)}. \tag{4.14}$$

4.3 Long Time Behaviour of the Island Size Distributions

In this section we have a theorem which describes the long-term behaviour of $c_j(t)$ with $j \geq n$. Before we proceed, we are required to prove the following proposition

Proposition 4.3.1. *Let τ be given by (4.4), so that*

$$\tau(t) - \tau(t_0) = \int_{t_0}^{t} Y(s)\, ds, \tag{4.15}$$

and define $\tilde{Y}(\tau) = Y(t(\tau))$, where $t(\tau)$ is the inverse function of $\tau(t)$ and Y satisfies (4.13). Then the relation between t and τ, and the long time behaviour of $\tilde{Y}(\tau)$ are, respectively,

(i) $\left(\frac{n}{n+1}\right)\left(\frac{n+1}{\alpha}\right)^{1/(n+1)} t^{-n/(n+1)}\tau(t) \to 1$ *as* $t \to \infty$*;*

(ii) $\left(\frac{n\tau}{\alpha}\right)^{1/n} \tilde{Y}(\tau) = \left(\frac{n\tau}{\alpha}\right)^{1/n} \tilde{c}_1(\tau) \to 1$ *as* $\tau \to \infty$.

Proof. From (4.13), $\forall \epsilon > 0\ \exists\ T = T(\epsilon)$ s.t $\forall\ t > T$

$$\left[\frac{(n+1)t}{\alpha}\right]^{1/(n+1)} Y(t) \in [1-\epsilon, 1+\epsilon].$$

Let us focus on the upper bound case. Then $\forall\, t > T, Y(t) \leq (1+\epsilon)\left[\frac{(n+1)t}{\alpha}\right]^{-1/(n+1)}$. Substituting into (4.15), for $t > t_0 \geq T$, we have

$$\begin{aligned}\tau(t) - \tau(t_0) &\leq \int_{t_0}^{t} (1+\epsilon)\left[\frac{(n+1)s}{\alpha}\right]^{-1/(n+1)} ds \\ &= (1+\epsilon)\left[\frac{(n+1)}{\alpha}\right]^{-1/(n+1)} \left(\frac{n+1}{n}\right)\left(t^{n/(n+1)} - t_0^{n/(n+1)}\right).\end{aligned}$$

Multiplying this inequality by $\left(\frac{n+1}{n}\right)^{-1}\left[\frac{(n+1)}{\alpha}\right]^{1/(n+1)} t^{-n/(n+1)}$ and then leads to

$$\limsup_{t\to\infty} \left(\frac{n}{n+1}\right)\left(\frac{n+1}{\alpha}\right)^{1/(n+1)} t^{-n/(n+1)}\tau(t) \leq 1+\epsilon.$$

Similarly, for the lower bound,

$$\liminf_{t\to\infty} \left(\frac{n}{n+1}\right)\left(\frac{n+1}{\alpha}\right)^{1/(n+1)} t^{-n/(n+1)}\tau(t) \geq 1-\epsilon.$$

By the sandwich theorem with $\epsilon > 0$, we get, as $t \to \infty$

$$\left(\frac{n}{n+1}\right)\left(\frac{n+1}{\alpha}\right)^{1/(n+1)} t^{-n/(n+1)}\tau(t) = 1 + o(1). \tag{4.16}$$

Furthermore,

$$
\begin{aligned}
1+o(1) &= \left(\frac{n}{n+1}\right)\left(\frac{n+1}{\alpha}\right)^{1/(n+1)} t^{-n/(n+1)}\tau \left(\frac{\tilde{Y}(\tau)}{Y(t)}\right)^n \\
&= \left(\frac{\tilde{Y}(\tau)}{Y(t)}\right)^n \left(\frac{n\tau}{\alpha}\right)\left(\frac{(n+1)t}{\alpha}\right)^{-n/(n+1)} \\
&= \left(\frac{\tilde{Y}(\tau)}{Y(t)}\right)^n \left[\frac{\left(\frac{n\tau}{\alpha}\right)^{1/n}}{\left(\frac{(n+1)t}{\alpha}\right)^{1/(n+1)}}\right]^n,
\end{aligned}
$$

and so

$$
\left(\frac{n\tau}{\alpha}\right)^{1/n}\tilde{Y}(\tau) = \left(\frac{(n+1)t}{\alpha}\right)^{1/(n+1)} Y(t)[1+o(1)] = 1+o(1). \tag{4.17}
$$

□

Next, we will need to obtain the long time behaviour of $\tilde{c}_j(\tau)$ for $j \geq n$, as this is required before Proposition 4.3.1 can be used to obtain the long time behaviour of $c_1(t)$ and $c_j(t)$ with $j \geq n$.

Proposition 4.3.2. *With τ being defined by (4.15) and Y satisfying (4.13), the long time behaviour of $\tilde{c}_j(\tau)$ is*

$$
\left(\frac{n\tau}{\alpha}\right)^{(n-1)/n}\tilde{c}_j(\tau) \to 1 \text{ as } \tau \to \infty,\ j \geq n. \tag{4.18}
$$

Proof. We recall the $\tilde{c}_j(\tau)$ equation (4.5), with $\tilde{c}_1(\tau) \equiv \tilde{Y}(\tau)$, and multiplying (4.5) by $\left(\frac{n\tau}{\alpha}\right)^{(n-1)/n}$ gives

$$\left(\frac{n\tau}{\alpha}\right)^{(n-1)/n}\tilde{c}_j(\tau) = \left(\frac{n\tau}{\alpha}\right)^{(n-1)/n} e^{-\tau}\sum_{k=n}^{j}\frac{\tau^{j-k}}{(j-k)!}\tilde{c}_k(0) + \left(\frac{n\tau}{\alpha}\right)^{(n-1)/n}\frac{1}{(j-n)!}\int_0^\tau s^{j-n}e^{-s}[\tilde{Y}(\tau-s)]^{n-1}\,ds.$$

The first term in the right-hand side of the above expression is the contribution due to the non monomeric initial data and since j is fixed, we have

$$\begin{aligned}\tau^{(n-1)/n}e^{-\tau}\sum_{k=n}^{j}\frac{\tau^{j-k}}{(j-k)!}\tilde{c}_k(0) &= \tau^{(n-1)/n}e^{-\tau}\left[\frac{\tau^{j-n}}{(j-n)!}\tilde{c}_n(0) + \frac{\tau^{j-n-1}}{(j-n-1)!}\tilde{c}_{n+1}(0) + \cdots\right]\\ &= \mathcal{O}(\tau^{j+(n-1-n^2)/n}e^{-\tau})\\ &= o(e^{\iota\tau}) \text{ as } \tau\to\infty,\end{aligned}$$

for every $\iota < 1$ since $\tau^{j+(n-1-n^2)/n}e^{(\iota-1)\tau} \to 0$ as $\tau \to \infty$. In order to study the remaining integral term, change the integration variable to $s = y\tau$. Then

$$\begin{aligned}&\left(\frac{n\tau}{\alpha}\right)^{(n-1)/n}\frac{1}{(j-n)!}\int_0^\tau s^{j-n}e^{-s}[\tilde{Y}(\tau-s)]^{n-1}\,ds\\ &= \left(\frac{n\tau}{\alpha}\right)^{(n-1)/n}\frac{1}{(j-n)!}\int_0^1 (y\tau)^{j-n}e^{-y\tau}[\tilde{Y}(\tau-y\tau)]^{n-1}(\tau dy)\\ &= \left(\frac{n\tau}{\alpha}\right)^{(n-1)/n}\frac{1}{(j-n)!}\int_0^1 \left[\frac{\tau(1-y)}{\tau(1-y)}\right]^{(n-1)/n}(y\tau)^{j-n}e^{-y\tau}[\tilde{Y}(\tau(1-y)]^{n-1}(\tau dy)\\ &= \frac{\tau^{j-n+1}}{(j-n)!}\int_0^1 \frac{[(n/\alpha)\tau(1-y)]^{(n-1)/n}}{(1-y)^{(n-1)/n}}y^{j-n}e^{-y\tau}[\tilde{Y}(\tau(1-y)]^{n-1}\,dy\\ &= \frac{\tau^{j-n+1}}{(j-n)!}\int_0^1 \frac{\psi(\tau(1-y))}{(1-y)^{(n-1)/n}}y^{j-n}e^{-y\tau}\,dy,\end{aligned}$$

where $\psi(\tau(1-y)) = [(n/\alpha)\tau(1-y)]^{(n-1)/n}[\tilde{Y}(\tau(1-y)]^{n-1}$.

Let $0 < \epsilon < 1$ be fixed and write $\int_0^1 = \int_0^{1-\epsilon} + \int_{1-\epsilon}^1$. Since $\psi(s)$ is a continuous function and is $1+o(1)$ as $s \to \infty$ by Proposition 4.3.1 (ii), it is bounded in $[0,\infty)$ and so there exists a positive constant M_ψ such that $0 \leq \psi(s) \leq M_\psi \ \forall s$. From this

$$\begin{aligned}
\frac{\tau^{j-n+1}}{(j-n)!}\int_{1-\epsilon}^1 \frac{\psi(\tau(1-y))}{(1-y)^{(n-1)/n}} y^{j-n}e^{-y\tau}\,dy &\leq M_\psi \tau^{j-n+1}\int_{1-\epsilon}^1 \frac{y^{j-n}}{(1-y)^{(n-1)/n}}e^{-y\tau}\,dy \\
&\leq M_\psi \tau^{j-n+1}e^{-(1-\epsilon)\tau}\int_{1-\epsilon}^1 \frac{y^{j-n}}{(1-y)^{(n-1)/n}}\,dy \\
&< M_\psi \tau^{j-n+1}e^{-(1-\epsilon)\tau}\int_{1-\epsilon}^1 \frac{1}{(1-y)^{(n-1)/n}}\,dy \\
&= \epsilon^{1/n} n M_\psi \tau^{j-n+1}e^{-(1-\epsilon)\tau},
\end{aligned}$$

and, by the arguments of da Costa *et. al.* in [25, p.382], the term above tends to zero as $\tau \to \infty$. For the integral over $(0, 1-\epsilon)$, we have $y < 1-\epsilon \Rightarrow \tau(1-y) > \tau\epsilon \to \infty$ as $\tau \to \infty$. By Proposition 4.3.1 (ii), we conclude that $\psi(s) = 1 + o(1)$ in the region of integration provided τ is sufficiently large. Thus, $\forall \delta > 0 \ \exists \ T(\delta)$ such that $\forall \tau > T(\delta),\ \psi(\tau(1-y)) \in [1-\delta, 1+\delta]$ and as $\tau \to \infty$, with

$$I_{0,j}(\tau) := \int_0^{1-\epsilon} \frac{y^{j-n}}{(1-y)^{(n-1)/n}} e^{-\tau y}\,dy,$$

we obtain

$$(1-\delta)I_{0,j}(\tau) \leq \int_0^{1-\epsilon} \frac{\psi(\tau(1-y))}{(1-y)^{(n-1)/n}} y^{j-n}e^{-y\tau}\,dy \leq (1+\delta)I_{0,j}(\tau). \tag{4.19}$$

We can expand $(1-y)^{-(n-1)/n}$ straight away by using the binomial series, i.e.

$$(1-y)^{-(n-1)/n} = \sum_{k=0}^{\infty} \begin{pmatrix} \frac{1}{n}-1 \\ k \end{pmatrix} (-y)^k.$$

Thus,

$$I_{0,j}(\tau) = \int_0^{1-\epsilon} \frac{y^{j-n}}{(1-y)^{(n-1)/n}} e^{-\tau y}\, dy = \int_0^{1-\epsilon} y^{j-n} e^{-\tau y} \sum_{k=0}^{\infty} \begin{pmatrix} \frac{1}{n}-1 \\ k \end{pmatrix} (-1)^k y^k\, dy.$$

Let $g(y) = \sum_{k=0}^{\infty} (-1)^k \begin{pmatrix} \frac{1}{n}-1 \\ k \end{pmatrix} y^{j+k-n}$. Then, by Watson's lemma (see Chapter 2 for more detail),

$$\begin{aligned} \int_0^{1-\epsilon} g(y) e^{-\tau y}\, dy &\sim \sum_{k=0}^{\infty} (-1)^k \begin{pmatrix} \frac{1}{n}-1 \\ k \end{pmatrix} \Gamma(j+k-n+1)\tau^{-(j+k-n+1)} \\ &= \frac{\Gamma(j-n+1)}{\tau^{j-n+1}} + \frac{n-1}{n}.\frac{\Gamma(j-n+2)}{\tau^{j-n+2}} + \cdots . \end{aligned}$$

Thus,

$$I_{0,j}(\tau) = \frac{\Gamma(j-n+1)}{\tau^{j-n+1}} + \mathcal{O}(\tau^{-j+n-2}) \text{ as } \tau \to \infty.$$

Equation (4.19) now gives

$$\begin{aligned} (1-\delta)\left[\frac{\Gamma(j-n+1)}{\tau^{j-n+1}} + \mathcal{O}(\tau^{-j+n-2})\right] &\le \int_0^{1-\epsilon} \frac{\psi(\tau(1-y))}{(1-y)^{(n-1)/n}} y^{j-n} e^{-y\tau}\, dy \\ &\le (1+\delta)\left[\frac{\Gamma(j-n+1)}{\tau^{j-n+1}} + \mathcal{O}(\tau^{-j+n-2})\right], \end{aligned}$$

and, by multiplying each term by $\dfrac{\tau^{j-n+1}}{\Gamma(j-n+1)}$,

$$\begin{aligned}(1-\delta)[1+\mathcal{O}(\tau^{-1})] &\leq \frac{\tau^{j-n+1}}{\Gamma(j-n+1)}\int_0^{1-\epsilon}\frac{\psi(\tau(1-y))}{(1-y)^{(n-1)/n}}y^{j-n}e^{-y\tau}\,dy \\ &\leq (1+\delta)[1+\mathcal{O}(\tau^{-1})].\end{aligned}$$

Thus,

$$\begin{aligned}\frac{\tau^{j-n+1}}{\Gamma(j-n+1)}\int_0^{1-\epsilon}\frac{\psi(\tau(1-y))}{(1-y)^{(n-1)/n}}y^{j-n}e^{-y\tau}\,dy &= \frac{\tau^{j-n+1}}{(j-n)!}\int_0^{1-\epsilon}\frac{\psi(\tau(1-y))}{(1-y)^{(n-1)/n}}y^{j-n}e^{-y\tau}\,dy \\ &= 1+\mathcal{O}(\tau^{-1}).\end{aligned}$$

Hence, as in [25, p.382], we have

$$\left(\frac{n\tau}{\alpha}\right)^{(n-1)/n}\tilde{c}_j(\tau)\to 1 \text{ as } \tau\to\infty,\ j\geq n,$$

as expected. □

For the long time behaviour of $c_1(t)$ and $c_j(t)$, we have the following theorem

Theorem 4.3.3. *Let $(X(0),Y(0))$ be in the basin of attraction for $R(X)$. Then the long time behaviour of $c_1(t)$ and $c_j(t)$, respectively, are*

(i) $\left(\frac{n+1}{\alpha}\right)^{1/(n+1)}t^{1/(n+1)}c_1\to 1$;

(ii) $\left(\frac{(n+1)t}{\alpha}\right)^{(n-1)/(n+1)}c_j\to 1,\ \forall j\geq n,$

as $t\to\infty$.

Proof. From Proposition 4.3.1, we first recall

$$\tau \sim \left(\frac{n+1}{n}\right)\left(\frac{\alpha}{n+1}\right)^{1/(n+1)} t^{n/(n+1)},$$

and then, by Proposition 4.3.1 (ii), we obtain

$$\left[\left(\frac{n+1}{\alpha}\right)^{1-1/(n+1)} t^{n/(n+1)}\right]^{1/n} c_1 = \left(\frac{n+1}{\alpha}\right)^{1/(n+1)} t^{1/(n+1)} c_1 \to 1 \text{ as } t \to \infty.$$

Similarly, Proposition 4.3.2 gives

$$\left(\frac{(n+1)t}{\alpha}\right)^{(n-1)/(n+1)} c_j \to 1 \text{ as } t \to \infty \ \forall j \geq n.$$

□

4.4 Self-Similar Behaviour of the Coagulation System Outside the Characteristic Direction

4.4.1 Self-Similar Function

Our objective now is to find a function $\Phi_1(\eta)$, $\eta \neq 1$, such that

$$\lim_{j,\tau\to\infty} \left[\frac{n\tau}{\alpha}\right]^{(n-1)/n} \tilde{c}_j(\tau) = \Phi_1(\eta),$$

where $\eta = j/\tau$ is fixed. with $\eta \neq 1$. To this end, we shall require Propositions 4.1.1 and 4.3.1 as well as the Stirling formula for the Gamma function,

$$\Gamma(x) = \sqrt{2\pi} x^{x-1/2} e^{-x} [1 + \mathcal{O}(x^{-1})] \text{ as } x \to \infty;$$

see Example 2.5.1 in Chapter 2. Note that Proposition 4.3.1 (ii) gives

$$\left(\frac{n\tau}{\alpha}\right)^{(n-1)/n} [\tilde{c}_1(\tau)]^{n-1} \to 1 \text{ as } \tau \to \infty.$$

Once again we assume throughout that $(X(0), Y(0))$ is in the basin of attraction of the river $R(X)$, where $X(0) = \sum_{j=n}^{\infty} c_j(0)$ and $Y(0) = c_j(0)$.

4.4.2 Monomeric Initial Data

For monomeric initial data with $j \geq n$, we have

$$\left(\frac{n\tau}{\alpha}\right)^{(n-1)/n} \tilde{c}_j(\tau) = \frac{\left(\frac{n\tau}{\alpha}\right)^{(n-1)/n}}{(j-n)!} \int_0^\tau s^{j-n} e^{-s} [\tilde{c}_1(\tau - s)]^{n-1} \, ds. \tag{4.20}$$

Consider the function ϕ_1 defined on $[n, \infty) \times [0, \infty)$ by

$$\phi_1(x, \tau) = \frac{\left(\frac{n\tau}{\alpha}\right)^{(n-1)/n}}{\Gamma(x - n + 1)} \int_0^\tau s^{x-n} e^{-s} [\tilde{c}_1(\tau - s)]^{n-1} \, ds. \tag{4.21}$$

Let $x = \eta\tau$. Then, from (4.21), we obtain

$$\phi_1(\eta\tau, \tau) = \frac{\left(\frac{n\tau}{\alpha}\right)^{(n-1)/n}}{\Gamma(\eta\tau - n + 1)} \int_0^\tau s^{\eta\tau-n} e^{-s} [\tilde{c}_1(\tau - s)]^{n-1} \, ds.$$

The change of variable $s = y\tau$ now leads to

$$\phi_1(\eta\tau,\tau) \tag{4.22}$$
$$= \frac{\left(\frac{n\tau}{\alpha}\right)^{(n-1)/n}}{\Gamma(\eta\tau-n+1)}\int_0^1 (\tau y)^{\eta\tau-n}e^{-\tau y}[\tilde{c}_1(\tau-\tau y)]^{n-1}(\tau dy)$$
$$= \frac{\left(\frac{n}{\alpha}\right)^{(n-1)/n}\tau^{(n-1)/n}\tau^{\eta\tau-n+1}}{\Gamma(\eta\tau-n+1)}\int_0^1 y^{\eta\tau-n}e^{-\tau y}[\tilde{c}_1(\tau(1-y)]^{n-1}\,dy$$
$$= \frac{\tau^{\eta\tau-n+1}}{\sqrt{2\pi}}\left(\frac{n}{\alpha}\right)^{(n-1)/n}(\eta\tau-n+2)^{n-3/2-\eta\tau}(\eta\tau-n+1)e^{\eta\tau}e^{2-n}\times(1+\mathcal{O}((\eta\tau+2-n)^{-1}))$$
$$\times\ \tau^{(n-1)/n}\int_0^1 y^{\eta\tau-n}e^{-y\tau}[\tilde{c}_1(\tau(1-y)]^{n-1}\,dy \quad \text{[using Stirling's formula]}$$
$$= \frac{\eta^{n-1/2-\eta\tau}\tau^{\eta\tau-n+1+n-3/2-\eta\tau+1}e^{\eta\tau}\left(\frac{n}{\alpha}\right)^{(n-1)/n}}{\sqrt{2\pi}e^{n-2}}(1+\mathcal{O}(\tau^{-1}))$$
$$\times\ \tau^{(n-1)/n}\int_0^1 y^{\eta\tau-n}e^{-y\tau}[\tilde{c}_1(\tau(1-y)]^{n-1}\,dy$$
$$= \frac{e^{\eta\tau}\eta^{n-1/2-\eta\tau}\tau^{1/2}\left(\frac{n}{\alpha}\right)^{(n-1)/n}}{\sqrt{2\pi}e^{n-2}}(1+\mathcal{O}(\tau^{-1}))\int_0^1 y^{\eta\tau-n}e^{-y\tau}\tau^{(n-1)/n}[\tilde{c}_1(\tau(1-y)]^{n-1}\,dy$$
$$= \frac{\eta^{n-1/2-\eta\tau}\tau^{1/2}\left(\frac{n}{\alpha}\right)^{(n-1)/n}}{\sqrt{2\pi}e^{n-2}}(1+\mathcal{O}(\tau^{-1}))\int_0^1 \frac{e^{\tau(\eta\ln(y)-y+\eta)}\tau^{(n-1)/n}[\tilde{c}_1(\tau(1-y)]^{n-1}}{y^n}\,dy$$
$$= \frac{\eta^{n-1/2-\eta\tau}\tau^{1/2}}{\sqrt{2\pi}e^{n-2}}(1+\mathcal{O}(\tau^{-1}))\int_0^1 \frac{\psi(\tau(1-y))e^{\tau(\eta\ln(y)-y+\eta)}}{y^n(1-y)^{(n-1)/n}}\,dy, \tag{4.23}$$

where $\psi(\tau)=\left(\frac{n\tau}{\alpha}\right)^{(n-1)/n}[\widetilde{c_1}(\tau)]^{n-1}$. Note that in the above calculation,

$$\frac{1}{1+\mathcal{O}(x^{-1})}=\frac{1}{1+1/x+\cdots}\approx 1-\frac{1}{x}+\cdots=1+\mathcal{O}(x^{-1}).$$

Let

$$I_n(\eta,\tau):=\eta^{-\eta\tau}\tau^{1/2}e^{\eta\tau}\int_0^1\frac{\psi(\tau(1-y))e^{\tau(\eta\ln(y)-y)}}{y^n(1-y)^{(n-1)/n}}\,dy,$$

ignoring constants as $\tau\to\infty$ for the time being. There are two cases, $\eta>1$ and $\eta\in(0,1)$, to be considered to seek the function $\Phi_1(\eta)$ as described earlier in this

section. If we consider the case $\eta > 1$ first, then we have the following proposition.

Proposition 4.4.1. *If $\eta > 1$, then $\Phi_1(\eta) = 0$.*

Proof. We examine the term in the integral $I_n(\eta, \tau)$ given by

$$y^{-n} e^{\tau(\eta \ln(y) - y)} = e^{(\eta\tau - n)\ln(y) - y\tau} = e^{g_1(y)},$$

where $g_1(y)$ is defined by

$$g_1(y) = (\eta\tau - n)\ln(y) - y\tau.$$

For all $y \in (0, 1]$ and $\tau > \frac{n}{\eta - 1}$, the function $g_1(y)$ satisfies

$$g_1'(y) = \frac{1}{y}(\eta\tau - n) - \tau \geq (\eta\tau - n) - \tau > 0.$$

For $y \in (0, 1]$, we have $g_1(y) \leq g_1(1) = -\tau$. This leads to

$$\int_0^1 \psi(\tau(1-y)) \frac{e^{\tau(\eta \ln(y) - y)}}{y^n (1-y)^{(n-1)/n}}\, dy \leq M_\psi e^{-\tau} \int_0^1 \frac{dy}{(1-y)^{(n-1)/n}} = n M_\psi e^{-\tau}.$$

Thus, following da Costa *et. al.*'s argument [25, p.384], for $\eta > 1$ we have $I_n(\eta, \tau) \to 0$ as $\tau \to \infty$. □

Consider the case $\eta \in (0, 1)$ next.

Proposition 4.4.2. *If $\eta \in (0, 1)$ then $\Phi_1(\eta) = (1 - \eta)^{-(n-1)/n}$.*

Proof. The exponential term inside the integral $I_n(\eta, \tau)$ is $e^{f(y)}$ where

$$f(y) = \tau(\eta \ln(y) - y) \;\Rightarrow f'(y) = \tau\left(\frac{\eta}{y} - 1\right) \;\Rightarrow f''(y) = -\frac{\eta\tau}{y^2}.$$

Now $f'(y) = 0 \Leftrightarrow y = \eta$ and $f''(\eta) = -\frac{\tau}{\eta} < 0$. So, the exponential term has a unique maximum at $y = \eta$. To seek the asymptotic behaviour of $I_n(\eta, \tau)$, we write

$$\begin{aligned} I_n(\eta,\tau) &= \eta^{-\eta\tau}\tau^{1/2}e^{\eta\tau}\left(\int_0^{\epsilon} + \int_{\epsilon}^{1-\epsilon} + \int_{1-\epsilon}^{1}\right)\psi(\tau(1-y))\frac{e^{\tau(\eta\ln(y)-y)}}{y^n(1-y)^{(n-1)/n}}\,dy \\ &=: I_{n,1}(\eta,\tau) + I_{n,2}(\eta,\tau) + I_{n,3}(\eta,\tau). \end{aligned} \tag{4.24}$$

Consider $I_{n,1}(\eta, \tau)$ first. The calculation is similar to that used for the case $\eta > 1$. Since we have $0 < y < \epsilon < \eta e^{-1}$, for all $\tau > \frac{n}{(1-e^{-1})\eta}$, we obtain $g_1(y) = (\eta\tau - n)\ln(y) - y\tau$ and

$$g_1'(y) = \frac{\eta\tau - n}{y} - \tau = \frac{\tau(\eta - y) - n}{y} > 0.$$

Thus, $g_1(y) \le g_1(\epsilon) \le g_1(\eta e^{-1}) = (\eta\tau - n)\ln(\eta) - (\eta\tau - n) - \tau\eta e^{-1}$. Following da Costa *et. al.*'s argument [25, p.385], we have

$$I_{n,1}(\eta,\tau) \to 0 \ \text{ as } \tau \to \infty. \tag{4.25}$$

Next, consider the case $I_{n,3}(\eta, \tau)$. The exponential term is

$$e^{\tau(\eta\ln(y)-y)}e^{\eta\tau}e^{-\eta\tau\ln(\eta)} =: e^{-\tau g_3(y)},$$

where the function $g_3(y) = (\eta\ln(\eta) - \eta) - (\eta\ln(y) - y)$. By da Costa *et. al.*'s argument [25, p.385], we again have

$$I_{n,3}(\eta,\tau) \to 0 \quad \text{as } \tau \to \infty. \tag{4.26}$$

By (4.25) and (4.26), we have

$$I(\eta,\tau) = I_{n,2}(\eta,\tau) + o(1) \quad \text{as } \tau \to \infty. \tag{4.27}$$

Consider the final case $I_{n,2}(\eta,\tau)$. We need to make a few minor modifications to da Costa *et. al.*'s argument. As they state, since $y < 1-\epsilon \Rightarrow \tau(1-y) > \tau\epsilon \to \infty$ as $\tau \to \infty$, then $\psi(\tau(1-y)) = 1 + o(1)$ for large τ. So, $\forall\delta > 0$, $\exists\ T(\delta)$ such that $\forall\tau > T(\delta)$, $\psi(\tau(1-y)) \in [1-\delta, 1+\delta]$ and, with

$$J_n(\eta,\tau) := \int_\epsilon^{1-\epsilon} \frac{e^{-\tau\phi(y)}}{y^n(1-y)^{(n-1)/n}}\, dy \quad \text{and } \phi(y) = y - \eta\ln(y) - \eta,$$

we have

$$(1-\delta)\eta^{-\eta\tau}\tau^{1/2}J_n(\eta,\tau) \le I_{n,2}(\eta,\tau) \le (1+\delta)\eta^{-\eta\tau}\tau^{1/2}J_n(\eta,\tau). \tag{4.28}$$

Since $\phi(y)$ is smooth and has a unique minimum $y = \eta \in (\epsilon, 1-\epsilon)$ with $\phi(\eta) = -\eta\ln(\eta)$ and $\phi''(\eta) = \eta^{-1}$, we can use Laplace's method for the asymptotic evaluation of integrals; see Section 2.5. We obtain, via this method,

$$J(\eta,\tau) \approx \frac{e^{\eta\tau\ln(\eta)}}{\eta^n(1-\eta)^{(n-1)/n}}\sqrt{\frac{2\pi}{\tau/\eta}}. \tag{4.29}$$

By (4.22), (4.27), (4.28) and (4.29), we obtain

$$\begin{aligned}
\phi_1(\eta\tau,\tau) &= \frac{\eta^{n-1/2}e^{2-n}}{\sqrt{2\pi}}\frac{\eta^{-\eta\tau}\tau^{1/2}e^{\eta\tau\ln(\eta)}}{\eta^n(1-\eta)^{(n-1)/n}}\sqrt{\frac{2\pi}{\tau/\eta}}(1+\mathcal{O}(\tau^{-1})) \\
&= \frac{e^{2-n}}{(1-\eta)^{(n-1)/n}}(1+\mathcal{O}(\tau^{-1})) \\
&= \frac{1}{(1-\eta)^{(n-1)/n}}(1+\mathcal{O}(\tau^{-1})).
\end{aligned}$$

□

By Proposition 4.4.1 and 4.4.2, for monomeric initial data we have

Theorem 4.4.3.

$$\Phi_1(\eta) := \begin{cases} (1-\eta)^{-(n-1)/n} & \text{if } 0 < \eta < 1, \\ 0 & \text{if } \eta > 1. \end{cases}$$

4.4.3 Non-Monomeric Initial Data

For non-monomeric initial data, we have

$$\left(\frac{n\tau}{\alpha}\right)^{(n-1)/n} \tilde{c}_j(\tau) = \phi_1(j,\tau) + \left(\frac{n\tau}{\alpha}\right)^{(n-1)/n} e^{-\tau} \sum_{k=n}^{j} \frac{\tau^{j-k}}{(j-k)!} \tilde{c}_k(0),$$

where $\phi_1(\eta)$ is defined in the previous subsection. Since we already have established that the term ϕ_1 is related to the term Φ_1 defined by Theorem 4.4.3, all that is required is to show that the second part of the non-monomeric solution goes to zero. This establishes that the asymptotic behaviour for monomeric initial conditions also holds for the non-monomeric case.

We define $v := \frac{1}{\eta}$, $\tau = jv$ and assume $\tilde{c}_k(0) \leq \rho k^{-\mu}$. Then

$$\begin{aligned} \left(\frac{n\tau}{\alpha}\right)^{(n-1)/n} e^{-\tau} \sum_{k=n}^{j} \frac{\tau^{j-k}}{(j-k)!} \tilde{c}_k(0) &\leq \rho \left(\frac{njv}{\alpha}\right)^{(n-1)/n} e^{-jv} \sum_{k=n}^{j} \frac{(jv)^{j-k}}{(j-k)!\ k^{\mu}} \\ &=: \rho \left(\frac{n}{\alpha}\right)^{(n-1)/n} \phi_2(v,j), \end{aligned}$$

where $\phi_2(v,j) = (jv)^{(n-1)/n} e^{-jv} \sum_{k=n}^{j} \frac{(jv)^{j-k}}{(j-k)!\ k^{\mu}}$. Note that $v \neq 1$ since $\eta \neq 1$. We now prove the next proposition.

Proposition 4.4.4. *For $v \in (0,1)$ and $v > 1$,*

$$\phi_2(v,j) \to 0 \quad \textit{as } j \to \infty.$$

Proof. Consider first the case $v > 1$. Let us change the summation variable by setting $l := j - k$ to obtain

$$\phi_2(v,j) = (jv)^{(n-1)/n} e^{-jv} \sum_{l=0}^{j-n} \frac{(jv)^l}{l!(j-l)^\mu} \leq \frac{(jv)^{(n-1)/n}}{n^\mu} e^{-jv} \sum_{l=0}^{j-n} \frac{(jv)^l}{l!}. \tag{4.30}$$

Considering $u_l := (jv)^l/l!$ and by studying the sign of

$$u_{l+1} - u_l = \frac{(jv)^l}{l!}\left(\frac{jv}{l+1} - 1\right),$$

we see that the maximum of u_l is attained at $l = \lfloor jv \rfloor > jv - 1 > j - 1 > j - n$. From (4.30)

$$\frac{(jv)^{(n-1)/n}}{n^\mu} e^{-jv} \sum_{l=0}^{j-n} \frac{(jv)^l}{l!} < \frac{(jv)^{(n-1)/n}}{n^\mu} e^{-jv} (j-n+1) \frac{(jv)^{j-n}}{(j-n)!}. \tag{4.31}$$

Note that

$$\begin{aligned}
\frac{1}{(j-n)!} &= \frac{(j-n+1)}{(j-n+1)!} \\
&= \frac{(j-n+1)(j-n+2)}{(j-n+2)!} \\
&\vdots \\
&= \frac{(j-n+1)(j-n+2)\ldots(j-1)}{(j-1)!} \\
&\approx (j-n+1)\frac{j^{n-2}}{\Gamma(j)} \\
&= \frac{(j-n+1)j^{n-2}}{\sqrt{2\pi}j^{j-1/2}e^{-j}}(1+o(1)).
\end{aligned}$$

Thus, from (4.31) we conclude that

$$\begin{aligned}
&\frac{(jv)^{(n-1)/n}}{n^{\mu}}e^{-jv}\sum_{l=0}^{j-n}\frac{(jv)^l}{l!} \\
&< \frac{(jv)^{(n-1)/n}}{n^{\mu}}(j-n+1)^2e^{-jv}\frac{j^{n-2}(jv)^{j-n}}{\sqrt{2\pi}j^{j-1/2}e^{-j}}(1+o(1)) \\
&= \frac{v^{(n-1)/n-n+j}}{n^{\mu}\sqrt{2\pi}}(j-n+1)^2j^{(n-1)/n+n-2-j+1/2+j-n}e^{j-jv}(1+o(1)) \\
&= \frac{v^{(n-1)/n-n}}{n^{\mu}\sqrt{2\pi}}(j-n+1)^2j^{(n-1)/n-3/2}e^{j-jv+j\ln(v)}(1+o(1)) \\
&= \frac{v^{(n-1)/n-n}}{n^{\mu}\sqrt{2\pi}}\left(\frac{j-n+1}{j}\right)^2 \\
&\times e^{-j(v-1-\ln(v))+[(n-1)/n+1/2]\ln(j)}(1+o(1)). \qquad (4.32)
\end{aligned}$$

Following da Costa *et. al.*'s argument [25, p.388], we can state that (4.32) tends to zero as $j \to \infty$.

Consider the case $v \in (0,1)$. Let $\beta \in (ve^{1-v}, \min\{ve, 1\})$ be fixed and write

$$\phi_2(v,j) = (jv)^{(n-1)/n} e^{-jv} \left[\sum_{0 \le l \le \beta_j} \frac{(jv)^l}{l!(j-l)^\mu} + \sum_{\beta j \le l \le j-n} \frac{(jv)^l}{l!(j-l)^\mu} \right] =: S_1(j) + S_2(j).$$

First, we concentrate on $S_1(j)$. Then we obtain

$$\begin{aligned} S_1(j) &\le (jv)^{(n-1)/n} e^{-jv} \sum_{0 \le l \le \beta_j} \frac{(jv)^l}{l!(j-\beta j)^\mu} \\ &= \frac{(jv)^{(n-1)/n}}{j^\mu (1-\beta)^\mu} e^{-jv} \sum_{0 \le l \le \beta_j} \frac{(jv)^l}{l!} \\ &\le \frac{(jv)^{(n-1)/n}}{j^\mu (1-\beta)^\mu} e^{-jv} e^{jv} \\ &= \frac{v^{(n-1)/n}}{(1-\beta)^\mu} j^{(n-1)/n-\mu}, \end{aligned}$$

and so we have

$$S_1(j) \to 0 \ \text{ as } j \to \infty \ \text{ if } \mu > \frac{n-1}{n}.$$

By Stirling's expansion, for large l,

$$l! = \sqrt{2l\pi} \left(\frac{l}{e} \right)^l (1 + \mathcal{O}(l^{-1})) \ge e^{-l} l^{l+1/2}.$$

Therefore, since in S_2 we have $(j-l)^\mu \ge n^\mu \ge 1$,

$$
\begin{aligned}
S_2(j) &\le (jv)^{(n-1)/n} e^{-jv} \sum_{\beta j \le l \le j-n} \frac{(jv)^l}{e^{-l} l^{l+1/2}} \\
&= (jv)^{(n-1)/n} e^{-jv} \sum_{\beta j \le l \le j-n} l^{-1/2} \left(\frac{jve}{l}\right)^l \\
&< (jv)^{(n-1)/n} e^{-jv} (j\beta)^{-1/2} \sum_{\beta j \le l \le j-n} \left(\frac{jve}{l}\right)^l \\
&< v^{(n-1)/n} j^{(n-1)/n-1/2} \beta^{-1/2} e^{-jv} \left(\frac{ve}{\beta}\right)^{\lfloor \beta j \rfloor + 1} \frac{1-(ve/\beta)^{j-n-\lfloor \beta j \rfloor}}{1-ve/\beta} \\
&< v^{(n-1)/n} j^{(n-1)/n-1/2} e^{-jv} \left(\frac{ve}{\beta}\right)^{j-n+1} \frac{\beta^{1-1/2}}{ve-\beta} \\
&= \frac{v^{(n-1)/n} \beta^{1/2}}{ve-\beta} j^{(n-2)/2n} \left(\frac{ve}{\beta}\right)^{1-n} \left(\frac{ve^{1-v}}{\beta}\right)^j \\
&\to 0 \quad \text{as } j \to \infty.
\end{aligned}
$$

Thus, since (4.32), $S_1(j)$ and $S_2(j)$ all tends to zero as j tend to infinity, we have

$$
\lim_{j,\tau \to \infty} \left(\frac{n\tau}{\alpha}\right)^{(n-1)/n} e^{-\tau} \sum_{k=n}^{j} \frac{\tau^{j-k}}{(j-k)!} \tilde{c}_k(0) = 0.
$$

□

Hence, by Theorem 4.4.3 and Proposition 4.4.4,

Theorem 4.4.5. *With $\eta = \frac{j}{\tau}$ fixed, $\eta \neq 1$ and $(X(0), Y(0))$ in the basin of attraction of the river $R(X)$, we have*

$$
\lim_{j,\tau \to \infty} \left(\frac{n\tau}{\alpha}\right)^{(n-1)/n} \tilde{c}_j(\tau) = \Phi_1(\eta),
$$

where

$$\Phi_1(\eta) := \begin{cases} (1-\eta)^{-(n-1)/n} & \text{if } \eta < 1, \\ 0 & \text{if } \eta > 1. \end{cases}$$

Suppose we want to find a self-similar function for $c_j(t)$. Recall the following relations from Proposition 4.3.1, equation (4.12) and Theorem 4.3.3 respectively,

$$\tau \sim \left(\frac{n+1}{n}\right)\left(\frac{\alpha}{n+1}\right)^{1/(n+1)} t^{n/(n+1)}; \tag{4.33}$$

$$X = \sum_{j=n}^{\infty} c_j(t) \sim [(n+1)\alpha^n t]^{1/(n+1)}; \quad c_1 \sim \left[\left(\frac{n+1}{\alpha}\right)t\right]^{-1/(n+1)}. \tag{4.34}$$

By (4.34), for large t we obtain (note that $c_1 \to 0$ as $t \to \infty$)

$$\langle j\rangle = \frac{\sum_{j=1}^{\infty} j c_j(t)}{\sum_{j=1}^{\infty} c_j(t)} \sim \frac{\alpha t}{[(n+1)\alpha^n t]^{1/(n+1)}} = \left(\frac{\alpha}{n+1}\right)^{1/(n+1)} t^{n/(n+1)}. \tag{4.35}$$

By (4.35), (4.33) becomes

$$\tau \sim \left(\frac{n+1}{n}\right)\left(\frac{\alpha}{n+1}\right)^{1/(n+1)} t^{n/(n+1)} \sim \left(\frac{n+1}{n}\right)\langle j\rangle.$$

This leads to the following main result.

Theorem 4.4.6. *As $t \to \infty$, we have, for $(X(0), Y(0))$ in the basin of attraction of the river $R(X)$,*

$$\lim_{t\to\infty}\left[\left(\frac{n+1}{\alpha}\right)\langle j\rangle\right]^{(n-1)/n} c_j(t) = \Phi_1\left(f_1\left(\frac{j}{\langle j\rangle}\right)\right),$$

where $f_1\left(\frac{j}{\langle j\rangle}\right) = \left(\frac{n}{n+1}\right)\frac{j}{\langle j\rangle}$.

This implies that solutions have the self-similar asymptotic behaviour

$$c_j(t) \sim \langle j \rangle^{-(n-1)/n} \Phi_1 \left(f_1 \left(\frac{j}{\langle j \rangle} \right) \right),$$

provided that $f_1(j/\langle j \rangle) \neq 1$. Thus, we obtain a discontinuous scaling solution for $i \geq 1$.

4.5 Self-Similar Behaviour of the Coagulation System Along the Characteristic Direction

The case $\eta = 1$, which has been mentioned briefly in the previous section, was investigated by da Costa *et. al.* [25, p.21]. We were able to obtain analogous results to these obtained by da Costa *et. al.* However, in the modelling of submonolayer deposition, we were unable to determine whether these results do or do not have any physical meaning in terms of both monomer and island size distributions. Therefore, we will summarise a few key results that will collapse into the results obtained by da Costa *et. al.* when one sets $n = 2$, rather than show full calculations for obtaining these results. As in [25, p.21], our objective is to find a function $\Phi_2(\xi)$ such that

$$\lim_{j,\tau \to \infty} \left[\frac{n}{\alpha} \right]^{(n-1)/n} \frac{\sqrt{2\pi}}{n} \tau^{1/2 - 1/(2n)} \tilde{c}_j(\tau) = \Phi_2(\xi),$$

where $\xi = \frac{j-\tau}{\sqrt{\tau}}$ is fixed. In the case of monomeric initial data, we have the following theorem.

Theorem 4.5.1. *With $\xi = \frac{j-\tau}{\tau^{1/2}}$ fixed, $\xi \in \mathbb{R}$ and $(X(0), Y(0))$ in the basin of attraction of $R(X)$, we have, as j, $\tau \to \infty$,*

$$\left(\frac{n}{\alpha} \right)^{(n-1)/n} \frac{\sqrt{2\pi}}{n} \tau^{1/2 - 1/(2n)} \tilde{c}_j(\tau) \to \Phi_2(\xi),$$

where

$$\Phi_2(\xi) := e^{-\xi^2/2} \int_0^\infty e^{-\xi w^n - w^{2n}/n} dw.$$

As in the previous section, we want to find a self-similar function for $c_j(t)$. Recall the following relation

$$\tau \sim \left(\frac{n+1}{n}\right) \langle j \rangle.$$

This leads to the following key result.

Theorem 4.5.2. *As $t \to \infty$, we have, for $(X(0), Y(0))$ in the basin of attraction of the river $R(X)$,*

$$\lim_{t\to\infty} \sqrt{2\pi}\alpha^{-(n-1)/n} n^{-(n+1)/2n} ((n+1)\langle j \rangle)^{(n-1)/2n} c_j(t) = \Phi_2(f_2(j, \langle j \rangle)),$$

where $f_2(j, \langle j \rangle) = \left(\dfrac{n}{n+1}\right)^{1/2} \left(\dfrac{j - \left(\frac{n+1}{n}\right)\langle j \rangle}{\langle j \rangle^{1/2}}\right)$.

4.6 Conclusion

For the point-island case of general $i \geq 1$, we have obtained the long time behaviour of a class of solutions to (4.2). To the best of our knowledge, this is the first time that the idea of rivers has been used to solve an applied mathematical problem. This method allows us to obtain the asymptotic behaviour of the monomer and island size distributions easier than the use of the Centre Manifold and Tubular Flow theorems that was adopted in the work of da Costa *et. al.* Moreover, we have proved the convergence to a self-similar profile $\Phi_1(\eta)$, see Theorem 4.4.6 where there is a discontinuity at $\eta = j/\tau = 1$, i.e. $f(j/\langle j \rangle) = 1$. It is important to note

that if one sets $i = 1$ such that $n = 2$, then one will recover restricted versions of the results obtained by da Costa *et. al.* in [25]. To fully recover the results in [25] requires the first quadrant to be in the basin of attraction of the river $R(X)$, and this has not yet been established.

Our results (4.12) and (4.13) are consistent with equation (3.7) obtained by Blackman and Wilding; more detail can be found in Chapter 3 along with the work of Bartelt and Evans, which we will discuss next. The model studied in this chapter is closely related to the one studied by Bartelt and Evans in [11] for the $i = 1$ point-island case. They derived an equation for the scaled island size distribution (ISD) and obtained a divergence at 3/2. In this chapter, we provide a short analysis of divergence at $j/\tau = 1$. Let j be the island size and $\langle j \rangle$ be the average island size such that

$$\langle j \rangle = \frac{\sum_{j \geq n} j c_j(t)}{\sum_{j \geq n} c_j(t)} = \frac{\theta - \sum_{j=1}^{n-1} j c_j(t)}{\sum_{j \geq n} c_j(t)}, \quad \left(\theta = Ft = \sum_{j \geq 1} j c_j \right).$$

Now, recall that we simply do not allow islands of size $1 < j \leq i$ to arise. This implies that $c_k(t) = 0$ for $k = 2, 3, \ldots, n-1$. Then we have, with $\alpha = F$,

$$\langle j \rangle = \frac{\alpha t - c_1(t)}{\sum_{j \geq n} c_j(t)}.$$

Recalling, from (4.34) and (4.35), that

$$\tau \sim \left(\frac{n+1}{n} \right) \left(\frac{\alpha}{n+1} \right)^{1/(n+1)} t^{n/(n+1)} \sim \left(\frac{n+1}{n} \right) \langle j \rangle.$$

We see that there is the discontinuity (at $j/\tau = 1$) is at

$$\frac{j}{\left(\frac{n+1}{n}\right) \langle j \rangle} \sim 1 \Leftrightarrow \frac{j}{\langle j \rangle} \sim \frac{n+1}{n}. \tag{4.36}$$

Equation (4.36) confirms the divergence obtained by Bartelt and Evans for $i = 1$ ($n = 2$). However, as explained in [11, p.54] and [53, p.89], since there is no divergence in the results obtained from Monte Carlo simulations the comparisons with ISDs based on (4.2) fail and thus the divergence in $\Phi_1(\eta)$ is not observed in reality. One of the reasons for this is that under a system of equations (4.2), they neglect local growth caused by islands' spatial environments.

Therefore, we are required to improve the approximation of the ISD and several attempts to improve this approximation have been considered in the past such as the capture zone distribution (CZD) by Mulheran and Blackman [54], the fragmentation approach for the $i = 1$ point-island case by Blackman and Mulheran [14] and the Joint Probability Distribution (JPD) [32, 55]. These (and other attempts) have been discussed in Subsection 1.3.5.

Because of the failure behind (4.2), we attempt to improve the approximation of the ISD by modifying the fragmentation approach for the case of a general $i \geq 0$ in the next chapter.

However, two important consideration which is raised by this chapter are to formulate conditions on the coefficients of rate equations which ensure a continuous scaling solution and to determine the physical meaning of $\Phi_2(\xi)$ as seen in Theorem 4.5.2 for the nucleation and growth stages in the submonolayer deposition.

Chapter 5

The Gap Evolution Equation

5.1 Introduction

In this chapter, our main aim is to derive the equivalent of the Blackman and Mulheran (BM) formulation [14] for the gap size distribution (GSD) in the case of a general critical island size $i \geq 0$ and then use this to obtain the capture zone distribution (CZD) via the convolution identity

$$P(s) = 2\int_0^{2s} \phi(x)\phi(2s-x)\ dx, \tag{5.1}$$

as discussed in Chapter 3. We shall use asymptotic results on solutions of fragmentation equations due to Treat, together with properties of Laplace-type integrals, to obtain qualitative information on both the GSD and CZD. Our fragmentation-based results are compared with those obtained from the Generalised Wigner Surmise (GWS)

$$P_\beta(s) = a_\beta s^\beta \exp(-b_\beta s^2), \tag{5.2}$$

to determine whether they are compatible.

5.2 The Gap Evolution Equations

We recall from Chapter 3 that the main idea of the BM theory is that, since any new nucleation that occurs in a parent gap of width, say y, will result in the creation of two daughter gaps of widths, say x and $y - x$, the evolution of gap sizes can be considered as a fragmentation process, from which we can obtain the GSD. As the fragmentation of a parent gap leads to two daughter gaps, this is a binary fragmentation. We follow the BM model and assume that in the regime of aggregation (the regime where island density remains constant while the monomer density decreases; see Chapter 1, Section 1.1), the monomer density at x in a gap of width y is given by

$$n_1(x) = \frac{1}{2R}x(y - x), \tag{5.3}$$

where x is the distance from an island located at one end of the gap, and $R = D/F$ is the ratio of monomer diffusion rate to deposition rate. If the critical island size is i, we require $i + 1$ monomers at a given x for nucleation to occur at x. On the basis of assumption (5.3), the probability of a new nucleation occuring in a gap of width y may be taken as being proportional to

$$\begin{aligned} a(y) = \int_0^y n_1(x)^{i+1}\, dx &= \left(\frac{1}{2R}\right)^{i+1} \int_0^y [x(y-x)]^{i+1}\, dx \\ &= \left(\frac{1}{2R}\right)^{i+1} B(i+2, i+2)y^{2i+3}, \end{aligned} \tag{5.4}$$

where $B(\cdot, \cdot)$ is the Beta function. Moreover, given that a nucleation event has taken place in a gap of width y, the probability that it will occur at a position x in the gap is proportional to $h(x/y)/y$ where

$$h(r) = \left(\frac{1}{2R}\right)^{i+1} [r(1-r)]^{i+1},\ 0 \le r \le 1. \tag{5.5}$$

Therefore, we take $b(x|y) = lh(x/y)/y$ where the constant l is chosen so that

$$\int_0^y xb(x|y)\ dx = y;\ \int_0^y b(x|y)\ dx = 2; \tag{5.6}$$

see Chapter 1 Section 1.3. We obtain

$$\int_0^y xb(x|y)\ dx = l\int_0^y \frac{x}{y}h\left(\frac{x}{y}\right) dx = \frac{ly}{(2R)^{i+1}}\int_0^1 r^{i+2}(1-r)^{i+1}\ dr = \frac{lB(i+3,i+2)}{(2R)^{i+1}}y,$$

and so, in order to satisfy $\int_0^y xb(x|y)dx = y$, we require

$$l = \frac{(2R)^{i+1}}{B(i+3,i+2)}.$$

This leads to

$$b(x|y) = \frac{[x(y-x)]^{i+1}}{B(i+3,i+2)y^{2i+3}}. \tag{5.7}$$

Note that with this choice of b, the binary fragmentation condition (1.12) (see Chapter 1)

$$\int_0^y b(x|y)\ dx = \int_0^y \frac{x^{i+1}(y-x)^{i+1}}{B(i+3,i+2)y^{2i+3}}\ dx = \frac{B(i+2,i+2)}{B(i+3,i+2)} = 2,$$

is satisfied as expected. Thus, equation (1.10), with (5.4) and (5.7), becomes

$$\frac{\partial}{\partial t}u(x,t) = -\frac{B(i+2,i+2)}{(2R)^{i+1}}x^{2i+3}u(x,t) + \frac{2}{(2R)^{i+1}}\int_x^\infty [x(y-x)]^{i+1}u(y,t)\ dy,$$

and a simple re-scaling of the time variable then yields the evolution equation for gap sizes $u(x,t)$

$$\frac{\partial}{\partial t}u(x,t) = -B(i+2,i+2)x^{2i+3}u(x,t) + 2\int_x^\infty [x(y-x)]^{i+1}u(y,t)\ dy. \tag{5.8}$$

Equation (5.8) is a particular case of the linear, homogeneous fragmentation equation

$$\frac{\partial}{\partial t}u(x,t) = -c_\rho x^\rho u(x,t) + c_\rho \int_x^\infty y^{\rho-1}h(x/y)u(y,t)\ dy, \tag{5.9}$$

where $\rho \geq 0$ and c_ρ is a constant; see [75] and Section 3.2 of Chapter 3. To obtain (5.8) from (5.9) we set

$$\rho = 2i+3,\ c_\rho = B(i+2,i+2),\ h(r) = \frac{2}{c_\rho}(1-r)^{i+1}r^{i+1}. \tag{5.10}$$

5.3 Asymptotics of Scaling Solutions for the Gap Size Distribution

The next step is to find the small- and large-size asymptotics of similarity solutions of the gap evolution equation (5.8). As noted in Chapter 3, such similarity solutions can be written in the form

$$u^*(x,t) = \frac{N^{*2}(t)}{V}\phi\left(\frac{N^*(t)x}{V}\right), \tag{5.11}$$

where ϕ is normalised so that

$$\int_0^\infty \phi(x)\ dx = \int_0^\infty x\phi(x)\ dx = 1, \tag{5.12}$$

and

$$N^*(t) := \int_0^\infty u^*(x,t)\ dx,\ V := \int_0^\infty xu^*(x,t)\ dx,$$

are the zeroth and first moments of u^* respectively.

Since similarity solutions take the form (5.11), we require the small and large x behaviour of $\phi(x)$. An explicit expression, involving a Meijer G-function, is shown in Chapter 3 for the specific case when the function h in equation (5.9) takes the form

$$h(r) = r^\gamma(b_0 + b_1 r + \cdots + b_p r^p),$$

$p = 0, 1, 2, \ldots,$ γ and $b_0, \ldots, b_p \in \mathbb{R}$ to be determined. We shall make use of the simple case $p = 1$, discussed in Chapter 3 in the next section. As noted in Chapter 1, asymptotic properties of ϕ have also been established for more general homogeneous functions h. In particular, recall equations (3.32) and (3.33) in Chapter 3 where it is shown that there exist constants k, m and $c > 0$ such that

$$\phi(x) \sim kx^\gamma \text{ as } x \to 0, \tag{5.13}$$

provided that $\lim_{r\to 0} r^{-\gamma-2} \int_0^r sh(s)\ ds$ exists and is non-zero, and

$$\phi(x) \sim mx^{h(1)-2} \exp(-cx^\rho) \text{ as } x \to \infty. \tag{5.14}$$

In the case of the gap evolution equation (5.8), (5.10), (5.13) and (5.14) lead immediately to the following result

Theorem 5.3.1 (Asymptotics of scaling solutions for the one-dimensional (1-D) GSD)**.** *Let*

$$u^*(x,t) = \frac{N^{*2}(t)}{V}\phi(x),$$

be the similarity solution of (5.8). Then, for each critical island size $i \geq 0$, we have

1. $\phi(x) \sim kx^{i+1} = \mathcal{O}(x^{i+1})$ *as* $x \to 0$ *for some constant* k*;*

2. $\phi(x) \sim mx^{-2}\exp(-cx^{2i+3}) = \mathcal{O}(x^{-2}\exp(-cx^{2i+3}))$ *as* $x \to \infty$ *for constants* $c > 0$ *and* m*.*

Proof. From (5.10), $h(r) = 2r^{i+1}(1-r)^{i+1}/c_\rho$ and the stated results follow since $h(1) = 0$, $\rho = 2i+3$ and

$$\begin{aligned}\frac{2}{c_\rho}r^{-i-3}\int_0^r s^{i+2}(1-s)^{i+1}\,ds &= \frac{2}{c_\rho}r^{-i-3}\sum_{j=0}^{i+1}\int_0^r \frac{(i+1)!}{j!(i+1-j)!}(-1)^j s^{i+j+2}\,ds \\ &= \frac{2}{c_\rho}\sum_{j=0}^{i+1}\frac{(i+1)!}{j!(i+1-j)!}\frac{(-1)^j r^j}{(i+j+3)} \\ &\to \frac{2}{c_\rho(i+3)} \text{ as } r \to 0.\end{aligned}$$

□

We may use Theorem 5.3.1 to obtain the asymptotic behaviour of the CZD, $P(s)$. As shown in the next section, we determine the asymptotics of $P(s)$ as $s \to 0$ for all $i \geq 0$ and as $s \to \infty$ for $i = 0$ only.

5.4 Asymptotics of Scaling Solutions for the Capture Zone Distribution

Under the assumption that nucleation has effectively mixed up the gaps so that nearest neighbours are not correlated, we define the CZD function, $P(s)$, by the convolution identity

$$P(s) = 2\int_0^{2s} \phi(x)\phi(2s-x)\, dx, \tag{5.15}$$

where ϕ is the gap size scaling function considered in the previous section.

Following Theorem 5.3.1 part 1, for small s we have the following theorem.

Theorem 5.4.1 (Small asymptotics of the 1-D CZD)**.** *For each critical island size $i \geq 0$, we have*

$$P(s) = \mathcal{O}(s^{2i+3}) \quad as\ s \to 0,$$

where $P(s)$ is the one-dimensional capture zone distribution.

Proof. We have, for small s and $0 < x < 2s$,

$$\phi(x) \leq Mx^{i+1}, \quad \phi(2s-x) \leq M(2s-x)^{i+1},$$

where M is a constant. Hence

$$\begin{aligned} P(s) &\leq 2M^2 \int_0^{2s} x^{i+1}(2s-x)^{i+1}\, dx \\ &= M^2 2^{2i+4} s^{2i+3} \int_0^1 t^{i+1}(1-t)^{i+1}\, dt \\ &= M^2 2^{2i+4} B(i+2, i+2) s^{2i+3}. \end{aligned}$$

Hence, $P(s) = \mathcal{O}(s^{2i+3})$ as $s \to 0$. □

The next aim is to understand the asymptotic behaviour of $P(s)$ as $s \to \infty$. This is more of a challenge, as it is not clear how to use part 2 of Theorem 5.3.1 for general i. So, as $s \to \infty$, we only consider the case $i = 0$ and subsequently the equation

$$\frac{\partial}{\partial t}u(x,t) = -\frac{x^3}{6}u(x,t) + 2\int_x^\infty x(y-x)u(y,t)\ dy, \tag{5.16}$$

which is the equation analysed by Ziff and McGrady [87]. The homogeneous function h for equation (5.16) can be obtained from the general linear daughter distribution,

$$h(r) = r^\gamma(b_0 + b_1 r) = \frac{2}{c_\rho}(1-r)^{i+1}r^{i+1}, \tag{5.17}$$

with $c_\rho = B(i+2, i+2)$. So when $i = 0$, $c_\rho = 1/6$ and $h(r) = 12(1-r)r = r(12-12r)$ as seen in (5.10). From this, we set $\gamma = 1$, $b_0 = 12$ and $b_1 = -12$. On applying (3.37) or (3.38) in Chapter 3, we deduce that $\phi(x) = \bar{\phi}(\eta)$, where $\eta = (x/\mu)^3$,

$$\mu = \frac{\Gamma(2/3)\Gamma(7/3)}{\Gamma(4/3)\Gamma(2)} = \frac{4}{3}\Gamma\left(\frac{2}{3},\right)$$

and

$$\bar{\phi}(\eta) = \frac{3}{\Gamma(\frac{2}{3})\mu}e^{-\eta}\eta^{1/3}\int_0^\infty (1+s)^{-4/3}e^{-s\eta}\ ds = \frac{3}{\Gamma(\frac{2}{3})\mu}\eta^{1/3}\int_0^\infty (1+s)^{-4/3}e^{-(1+s)\eta}\ ds.$$

Substituting $z = 1 + s$, we have

$$\bar{\phi}(\eta) = \frac{3}{\Gamma(\frac{2}{3})\mu}\eta^{1/3}\int_1^\infty z^{-4/3}e^{-z\eta}\,dz.$$

Now we set $z\eta = u$ to obtain

$$\bar{\phi}(\eta) = \frac{3}{\Gamma(\frac{2}{3})\mu}\eta^{2/3}\int_\eta^\infty u^{-4/3}e^{-u}\,du,$$

and therefore the GSD, ϕ, is given explicitly by the formula

$$\phi(x) = \frac{3x^2}{\Gamma(\frac{2}{3})\mu^3}\int_{(x/\mu)^3}^\infty u^{-4/3}e^{-u}\,du. \tag{5.18}$$

Note that this $\phi(x)$ is similar to the Ziff and McGrady equation (3.27) with the constant $\mu^3 \approx 5.88$ on the lower limit of integration in (5.18) replaced by 6. This key difference occurs because Treat [75, p.2524] imposes the normalisation conditions (5.12) on ϕ where the zeroth and first moments of ϕ are required to be 1. Observe that the moments of (5.18) are

$$\begin{aligned}\phi_m &= \int_0^\infty x^m\phi(x)\,dx = \frac{3}{\mu^3\Gamma(\frac{2}{3})}\int_0^\infty\int_{(x/\mu)^3}^\infty x^{m+2}u^{-4/3}e^{-u}\,du\,dx \\ &= \frac{3}{\mu^3\Gamma(\frac{2}{3})}\int_0^\infty\int_0^{u^{1/3}\mu} x^{m+2}u^{-4/3}e^{-u}\,dx\,du = \frac{3\mu^{m+3}}{\mu^3(m+3)\Gamma(\frac{2}{3})}\int_0^\infty u^{(m-1)/3}e^{-u}\,du,\end{aligned}$$

and thus

$$\phi_m = \frac{3\mu^m\Gamma(\frac{1}{3}(m+2))}{(m+3)\Gamma(\frac{2}{3})}. \tag{5.19}$$

It follows from (5.19) that the normalisation and mean conditions (5.12) are satisfied, since we have $\phi_0 = 1$ and $\phi_1 = 1$ as required. If we follow the same analysis for the Ziff and McGrady formula

$$\hat{\phi}(x) = Ax^2 \int_{x^3/6}^{\infty} u^{-4/3} e^{-u}\, du,$$

where A is some normalising constant, then

$$\hat{\phi}_m = \frac{A6^{(m+3)/3}}{(m+3)} \Gamma\left(\frac{m+2}{3}\right).$$

It follows that

$$\hat{\phi}_0 = \frac{6A}{3} \Gamma\left(\frac{2}{3}\right),$$

and so, for $\hat{\phi}_0 = 1$, we require $A = (2\Gamma(2/3))^{-1}$. However, for this choice of A, we obtain

$$\hat{\phi}_1 = \frac{6^{4/3}}{8} \frac{\Gamma(1)}{\Gamma(2/3)} \approx 1.0064.$$

Consequently, with the Ziff and McGrady formula, no normalising constant A can be found for which both $\hat{\phi}_0 = 1$ and $\hat{\phi}_1 = 1$

With (5.18) we can now determine the asymptotic behaviour of $P(s)$ as $s \to \infty$. To do this, we first let $u = x^3 v/\mu^3$. Then, (5.18) becomes

$$\begin{aligned} \phi(x) &= \frac{3x^2}{\mu^3 \Gamma(\frac{2}{3})} \int_1^{\infty} e^{-v(x/\mu)^3} \left(\frac{x^3 v}{\mu^3}\right)^{-4/3} \left(\frac{x^3}{\mu^3}\right) dv \\ &= \frac{3x}{\mu^2 \Gamma(\frac{2}{3})} \int_1^{\infty} e^{-v(x/\mu)^3} v^{-4/3}\, dv. \end{aligned} \tag{5.20}$$

Substituting (5.20) into (5.15), we have

$$P(s) = 2\int_0^{2s} \left(\frac{3x}{\mu^2\Gamma(\frac{2}{3})} \int_1^\infty e^{-v(x/\mu)^3} v^{-4/3}\, dv \, \frac{3(2s-x)}{\mu^2\Gamma(\frac{2}{3})} \int_1^\infty e^{-w((2s-x)/\mu)^3} w^{-4/3}\, dw \right) dx.$$

Let $x = 2sz$. Then we obtain

$$\begin{aligned} P(s) &= \frac{18}{\mu^4\Gamma(\frac{2}{3})^2} \int_0^1 \left(2sz \int_1^\infty e^{-v(2sz/\mu)^3} v^{-4/3}\, dv \right. \\ &\quad \left. \times (2s-2sz) \int_1^\infty e^{-w((2s-2sz)/\mu)^3} w^{-4/3}\, dw \right) 2s\, dz \\ &= \frac{144s^3}{\mu^4\Gamma(\frac{2}{3})^2} \int_1^\infty \int_1^\infty (vw)^{-4/3} \\ &\quad \times \int_0^1 z(1-z) e^{-(2s/\mu)^3(z^3v+(1-z)^3w)}\, dz\, dv\, dw. \end{aligned} \tag{5.21}$$

Our strategy is to use the usual 1-D Laplace's method to estimate the inner integral, which will give us a new two-dimensional (2-D) Laplace integral with respect to v and w on $\bar{D} = [1,\infty) \times [1,\infty)$. We have the following proposition.

Proposition 5.4.2. *As $s \to \infty$, the inner integral of (5.21),*

$$\int_0^1 z(1-z) e^{-(2s/\mu)^3 S(z)}\, dz,$$

satisfies

$$\int_0^1 z(1-z) e^{-(2s/\mu)^3 S(z)}\, dz \sim \left(\frac{2s}{\mu}\right)^{-3/2} \eta(v,w) e^{-(2s/\mu)^3 S(z_+)} \quad \text{as } s \to \infty,$$

where $S(z) = z^3v + (1-z)^3w$, $z_+ = \sqrt{w}/(\sqrt{w}+\sqrt{v})$ and

$$S(z_+) = \frac{vw}{(\sqrt{v}+\sqrt{w})^2}; \quad \eta(v,w) = z_+(1-z_+)\sqrt{\frac{2\pi}{S''(z_+)}}. \tag{5.22}$$

Proof. Since $S'(z) = 3z^2v - 3(1-z)^2w$, to find critical points of $S(z)$ we must have $z^2v - (1-z)^2w = 0$, i.e. $(v-w)z^2 + 2wz - w = 0$. There are two cases to be considered: $v \neq w$ and $v = w$. Let us consider the former case first. We have

$$z_\pm = \frac{-2w \pm \sqrt{4w^2 + 4w(v-w)}}{2(v-w)} = \frac{-w \pm \sqrt{vw}}{v-w}, \ v \neq w.$$

At a minimum point, $S''(z) = 6zv + 6(1-z)w \geq 0$. Now,

$$S''(z_+) = 6v\left(\frac{-w+\sqrt{vw}}{v-w}\right) + 6w\left(\frac{v-\sqrt{vw}}{v-w}\right) = \frac{6\sqrt{vw}(v-w)}{v-w} = 6\sqrt{vw} > 0,$$

since $v \geq 1$ and $w \geq 1$. Note that

$$z_+ = \frac{-w+\sqrt{vw}}{v-w} = \frac{\sqrt{w}}{\sqrt{w}+\sqrt{v}} \ \in (0,1). \tag{5.23}$$

Expanding $S(z)$ around z_+ [84], we have

$$S(z) - S(z_+) = S''(z_+)\frac{(z-z_+)^2}{2} + \mathcal{O}((z-z_+)^3).$$

Then, for $(2s/\mu)^3 \gg 1$, in the neighborhood of z_+ we have

$$\int_0^1 g(z)e^{-(2s/\mu)^3 S(z)}\, dz \sim g(z_+)e^{-(2s/\mu)^3 S(z_+)}\sqrt{\frac{2\pi}{(2s/\mu)^3 S''(z_+)}} \text{ as } s \to \infty,$$

by the Laplace method, where $g(z) = z(1-z)$ and $S(z_+)$ is given in (5.22). Thus, for the case of $v \neq w$ to the leading order term as $s \to \infty$ the inner integral in

(5.21) becomes

$$\int_0^1 z(1-z)e^{-(2s/\mu)^3 S(z)}\, dz \sim \left(\frac{2s}{\mu}\right)^{-3/2} \eta(v,w)e^{-(2s/\mu)^3 S(z_+)},$$

with $\eta(v,w)$ defined in (5.22) and $S''(z) = 6\sqrt{vw}$.

For the case of $v = w$, there exists only one critical point, $z_+ = 1/2$ with $S(1/2) = v/4$ and $S''(1/2) = 6v > 0$ since $v \geq 1$. Note that these can be obtained from equation (5.23) on setting $v = w$ in the formulae involving z_+. Thus, by a similar analysis to that used for the case $v \neq w$, to the leading order term as $s \to \infty$, the inner integral in (5.21) becomes

$$\int_0^1 z(1-z)e^{-(2s/\mu)^3 S(z)}\, dz \sim \left(\frac{2s}{\mu}\right)^{-3/2} \eta(v)e^{-(2s/\mu)^3 S(z_+)} \quad \text{as } s \to \infty,$$

with $\eta(v)$ defined in (5.22).

□

Hence (5.21) becomes, as $s \to \infty$,

$$P(s) \sim s^{3/2} \int_1^\infty \int_1^\infty \eta(v,w)(vw)^{-4/3} e^{-(2s/\mu)^3 S(z_+)}\, dv\, dw. \tag{5.24}$$

The integral in (5.24) can be obtained as a special case of the general 2-D Laplace integral

$$J(m) = \iint_D g(v,w)e^{-mf(v,w)}\, dv\, dw, \tag{5.25}$$

by setting

$$\left.\begin{aligned} &\bar{D} = [1,\infty)\times[1,\infty);\\ &g(v,w) = \eta(v,w)(vw)^{-4/3} = \sqrt{\tfrac{\pi}{3}}\tfrac{(vw)^{1/4}}{(\sqrt{v}+\sqrt{w})^2};\\ &m = \left(\tfrac{2s}{\mu}\right)^3, \end{aligned}\right\} \tag{5.26}$$

and

$$f(v,w) = S(z_+) = \frac{vw}{(\sqrt{v}+\sqrt{w})^2}. \tag{5.27}$$

Consequently, any results on the large m behaviour of (5.25) can be used to deduce the large s behaviour of $P(s)$. The large m behaviour of the integral (5.25) is discussed by Wong [84, Chapter VIII, Sections 10, 11]. As pointed out by Wong [84, p.459–460], the major contribution to the asymptotic expansion comes from points where $f(v,w)$ attains its absolute minimum. The case where the global minimum occurs at an interior stationary point of $\bar{D}$ is examined in [84, Chapter VIII, Section 10] while the case of the minimum being attained on the boundary of $\bar{D}$, either at a stationary point or a critical point of the second kind, is dealt with in [84, Chapter VIII, Section 11].

If we consider the function f given by (5.27) then we see that the minimum value of $f(v,w)$ on $[1,\infty)\times[1,\infty)$ occurs at the corner point $(1,1)$, which is neither a stationary point of f nor a critical point of the second kind. Instead, $(1,1)$ is a so-called critical point of f of the **third kind**.

Proposition 5.4.3. *The function $f(v,w)$ has a global minimum of $1/4$ on $\bar{D}$ attained at the corner point $(1,1)$.*

Proof. We differentiate $f(v,w)$ with respect to v and w respectively to obtain

$$f_v = \frac{w^{3/2}}{(\sqrt{v}+\sqrt{w})^3};\ f_w = \frac{v^{3/2}}{(\sqrt{v}+\sqrt{w})^3}.$$

Since the region $\bar{D}$ is $[1,\infty)\times[1,\infty)$, f has no stationary point in $\bar{D}$. Suppose we consider the region $\bar{D}_R=[1,R]\times[1,R]$ for some constant R. In $\bar{D}_1$, $f(v,w)$ is continuous and so has a global minimum which is attained at either an interior stationary point or at a boundary point. Since there are no stationary points, the minimum occurs on the boundary which consists of the four line segments:

- a: $v=1$, $1\leq w\leq R$ and $f(1,w)=w(1+\sqrt{w})^{-2}$;
- b: $w=1$, $1\leq v\leq R$ and $f(v,1)=v(\sqrt{v}+1)^{-2}$;
- c: $v=R$, $1\leq w\leq R$ and $f(R,w)=Rw(\sqrt{R}+\sqrt{w})^{-2}$;
- d: $w=R$, $1\leq v\leq R$ and $f(v,R)=Rv(\sqrt{v}+\sqrt{R})^{-2}$.

Since $f_v>0$ and $f_w>0$ on $\bar{D}$, and hence also on $\bar{D}_R$, it follows that the minimum value of $f(v,w)$ on lines a and b is $f(1,1)=1/4$. Similarly, the minimum value on lines c and d is $f(R,1)=f(1,R)=R(1+\sqrt{R})^{-2}$. Hence, for each $R>1$, the global minimum value of $f(v,w)$ on $\bar{D}_R$ is $f(1,1)=1/4$ and the result follows.

□

Returning to the more general case of (5.25), we say that (v_0,w_0) is a critical point of the third kind for $f(v,w)$ if it is a point on the boundary of $\bar{D}$ at which the boundary has two intersecting tangent lines, but neither tangent line coincides with that of the level curve $f(v,w)=f(v_0,w_0)$; see [84, Chapter VIII, Section 8]. Equivalently, there is some parameterisation of the boundary which has a discontinuous derivative of some order at (v_0,w_0); see [84, Chapter VIII, Section 2]. Unfortunately, Wong does not give any details of the large m behaviour of $J(m)$ when the global minimum of f occurs at a critical point of the third kind.

However, this case can also be treated by adapting the arguments used in [84]. As explained in [84, p.448-449], by making appropriate changes of variables, we

can assume that the critical point on the boundary is located at $(0,0)$, and at this point the boundary coincides with the coordinate axes in the vw-plane. Expanding f in a Maclaurin series then yields

$$f(v,w) = f_{00} + f_{10}v + f_{01}w + f_{20}v^2 + f_{11}vw + f_{02}w^2 + \cdots,$$

where

$$f_{jk} = \frac{\partial^{j+k}}{\partial v^j \partial w^k} f(0,0).$$

Since the constant term f_{00} merely contributes a factor $e^{-mf_{00}}$ to $J(m)$ we can also assume, again without loss of generality, that $f_{00} = 0$.

Consequently, we can write

$$\begin{aligned} f(v,w) &= f_{10}v + f_{01}w + \cdots, \quad f_{10} \neq 0, \quad f_{01} \neq 0. \\ &= f_{10}v[1 + P(v,w)] + f_{01}w[1 + Q(v,w)], \end{aligned} \tag{5.28}$$

where $P(v,w)$ and $Q(v,w)$ are power series in v and w, with $P(0,0) = Q(0,0) = 0$; see [84, p.449, Eq. (8.3)].

Theorem 5.4.4. *Let $f(v,w)$, $g(v,w)$ be smooth functions on a domain $\bar{D}$ and let $f(v,w)$ attain its minimum value of 0 at the critical point $(0,0)$ of the third kind and satisfy $f_v(0,0) > 0$ and $f_w(0,0) > 0$. Moreover, assume that the boundary of $\bar{D}$ at $(0,0)$ coincides with the coordinate axes in the vw-plane. Then*

$$J(m) = \iint_{\bar{D}} g(v,w)e^{-mf(v,w)}\, dv\, dw \sim \frac{g_{00}}{f_{10}f_{01}} m^{-2} = \mathcal{O}(m^{-2}) \quad \text{as } m \to \infty,$$

where $g_{00} = g(0,0)$.

Proof. As indicated above (equation (5.28)) we can write

$$\begin{aligned} f(v,w) &= f_{10}v(1+P(v,w)) + f_{01}w(1+Q(v,w)),\ f_{10} \neq 0,\ f_{01} \neq 0, \\ &= f_{10}V + f_{01}W, \end{aligned}$$

where $V = v(1+P(v,w))$ and $W = w(1+Q(v,w))$. Let $\bar{D}'$ denote the image of $\bar{D}$ under this change of variables. Then

$$J(m) = \iint_{\bar{D}'} G(V,W)e^{-mF(V,W)}\ dV\ dW, \tag{5.29}$$

where

$$G(V,W) = g(v,w)\frac{\partial(v,w)}{\partial(V,W)},\ F(V,W) = f_{10}V + f_{01}W.$$

By [84, Chapter V, Theorem 9], the double integral in (5.29) can be written as

$$J(m) = \int_0^M h(t)e^{-mt}\ dt, \tag{5.30}$$

where 0 and M denote the infimum and supremum of F in $\bar{D}'$ (or equivalently, of f in $\bar{D}$) respectively, and

$$h(t) = \int_{F(V,W)=t} \frac{G(V,W)}{\sqrt{F_V^2 + F_W^2}}\ d\sigma,$$

σ being the arc length of the curve $F(V,W) = t$.

Following the argument used in [84, p.449], we now make the transformation

$$V = \frac{\xi}{f_{10}} \cos^2(\eta);\ W = \frac{\xi}{f_{01}} \sin^2(\eta),$$

which gives $\xi = f_{10}V + f_{01}W = F(V, W)$. Since $f_{10} > 0$ and $f_{01} > 0$ (by assumption), the line $F(V, W) = t$ lies outside $\bar{D}'$ whenever $t < 0$ and so $h(t) = 0$ for $t < 0$. For $t > 0$, we have

$$h(t) = \int_0^{\pi/2} \Phi(t, \eta)\ d\eta,$$

where

$$\Phi(t, \eta) = \frac{2}{f_{10}f_{01}} \sum \Phi_{jk} t^{j+k+1} \cos^{2j+1}(\eta) \sin^{2k+1}(\eta), \tag{5.31}$$

with

$$\Phi_{jk} = \frac{G_{jk}}{f_{10}^j f_{01}^k} \text{ and } G_{jk} = \frac{\partial^{j+k}}{\partial v^j \partial w^k} G(0, 0). \tag{5.32}$$

Hence

$$h(t) \sim \sum b_{jk} t^{j+k+1} \text{ as } t \to 0^+, \tag{5.33}$$

where

$$b_{jk} = \frac{\Phi_{jk} j!k!}{(j + k + 1)! f_{10} f_{01}}, \tag{5.34}$$

since

$$\begin{aligned}\int_0^{\pi/2} \cos^{2j+1}(\eta)\sin^{2k+1}(\eta)\ d\eta &= \int_0^{\pi/2} (1-\sin^2(\eta))^j(\sin^2(\eta))^k\cos(\eta)\sin(\eta)\ d\eta \\ &= \frac{1}{2}\int_0^1 (1-u)^j u^k\ du \\ &= \frac{1}{2}B(j+1,k+1);\end{aligned}$$

see [84, p.450]. It follows from (5.30) and Watson's lemma that

$$J(m) \sim \sum b_{jk}\Gamma(j+k+2)m^{-(j+k+2)} \quad \text{as } m \to \infty.$$

Since $b_{00} = g_{00}/(f_{10}f_{01})$, the stated result follows.

□

Theorem 5.4.5 (Large size asymptotics of the 1-D CZD)**.** *Let the critical island size $i = 0$. Then*

$$P(s) = \mathcal{O}(s^{-9/2}e^{-2(s/\mu)^3}) \quad as\ s \to \infty.$$

Proof. From (5.24) and (5.25),

$$P(s) = \mathcal{O}\left(s^{3/2}\iint_{\bar{D}} g(v,w)e^{-mf(v,w)}\ dv\ dw\right),$$

where $\bar{D} = [1,\infty) \times [1,\infty)$, $m = (2s/\mu)^3$, $g(v,w) = \sqrt{\pi/3}(vw)^{1/4}(\sqrt{v}+\sqrt{w})^{-2}$ and $f(v,w) = vw(\sqrt{v}+\sqrt{w})^{-2}$.

As discussed earlier, f attains a minimum value of $1/4$ at the corner point $(1,1)$, which is a critical point of the third kind. Note that the boundary of $\bar{D}$ at $(1,1)$ consists of two perpendicular lines $v = 1$ and $w = 1$. Moreover, $f_v(1,1) > 0$ and $f_w(1,1) > 0$. Consequently, from Theorem 5.4.4, we deduce that

$$P(s) = \mathcal{O}(s^{3/2}e^{-mf(1,1)}m^{-2}) = \mathcal{O}\left(s^{3/2}e^{-(2s/\mu)^3/4}\left(\frac{2s}{\mu}\right)^{-6}\right)$$
$$= \mathcal{O}(s^{-9/2}e^{-2s^3/\mu^3}) \text{ as } s \to \infty.$$

□

5.5 Conclusion: the Blackman and Mulheran Theory versus the Generalised Wigner Surmise

In the case of the one-dimensional (1-D) point-island model only, by Theorem 5.4.1, the exponent of $2i+3$ is odd for all $i \geq 0$ which differs from the Generalised Wigner Surmise (GWS) prediction (5.2) that we should have $P_\beta(s) \sim s^\beta = s^{2(i+1)}$ as $s \to 0$ in $d = 1$. By Theorem 5.4.5, GWS does not hold for $i = 0$ also asymptotically as $s \to \infty$. Hence, it follows that the Blackman and Mulheran (BM) model and the GWS **cannot** be simultaneously correct.

Here we will discuss the differences between the two theoretical approaches presented in this chapter. It is interesting to note that the analysis of GWS and the BM theory are based on the same physical model. In [61], the authors discuss the nucleation rate in terms of the monomer density and just as in the BM theory, the probability of $(i+1)$ monomers coinciding is required. This leads to the nucleation rate, approximately n_1^{i+1}. This is essentially the same as the physical basis we have used in this chapter. Similarly, despite the fact both approaches are based on the same physical model there is a conflict of GWS with the BM theory. So, the question is why do these two theoretical approaches exhibit different behaviour for small- and large-sizes of capture zones?

In small-size scaling, the authors in [61] consider the nucleation rate within capture zones of size s. Moreover, they reconsider such a nucleation rate using the locally averaged monomer density. They argue that the capture zone distribution $P_\beta(s) \sim s^{2i+2} = s^{2(i+1)} = s^\beta$ for small s in the 1-D case. However, the justification of the nucleation rate using locally averaged monomer density within a capture zone is not clear.

In [62], the authors use a spatially dependent monomer density within a capture zone instead to derive the nucleation rate for two-dimensional substrates. This involves integrating the monomer density to the power of $(i+1)$ over the capture zone which results in a different $\beta = i + 2$.

We can use this type of modification for our case here. By the same argument, using (5.3), we take the local monomer density in a capture zone of small size s which is obtained by two gaps of size $s/2$. If we do this, we recover $\beta = 2i + 3$ which is in agreement with Theorem 5.4.1. The argument used in [62] is heuristic at best and the more rigorous methods adopted in this chapter may be viewed as more satisfactory.

In this chapter we have proved that for $i = 0$ in large-size scaling, the large-size dependence of the capture zone distribution (CZD) following equation (5.15) mirrors the corresponding gap size distribution (GSD) $\phi(x)$ – instead of the Gaussian tail of equation (5.2), we have $P(s) \sim \exp(-2s^3/\mu^3)$. It can be conjectured, unlike the Gaussian tail, that the CZD for larger values of i will follow $\exp(-c_i s^{2i+3})$ for some constants c_i, following the asymptotics of the corresponding GSD.

Essentially, when dealing with one dimension, we show that the GWS of [61] does not correspond with the asymptotic solutions to the BM theory analysis of point island nucleation and growth. As the physical basis of these two approaches is the same, we therefore believe that failings of the GWS have led to such differences.

This does not necessarily imply that we take the BM model to be correct – we will now discuss this.

Since the BM theory is based on (5.3) and (5.15), we need to discuss the validity of these equations. Equation (5.3) says that nucleation events are rare in a gap of any size x so that monomers equilibrate between nucleations. This assumption is true if in the aggregation regime the monomer density is assumed to be approximately steady state, that is, if we neglect any effect of nucleation.

One could argue that a nucleation event is likely to occur roughly at the centre of any existing gap. From this, such a gap will have similar size to the left and to the right of a new island. However, when such an island is nucleated in an existing gap, correlations in both new gaps tend to vanish. Assuming there is no correlation between the sizes of the two neighbouring gaps, we have (5.15).

Note that equations (5.3) and (5.15) are independent of each other, one of them being false does not imply that the other is also false.

In Chapter 6, we will discuss whether the MC simulations can confirm that (5.3) and (5.15) are valid or not and determine whether the BM theory or GWS is true. In brief, equation (5.3) needs modification for large gap size x. This may suggest a better fragmentation kernel for the gap evolution equation.

Also, the fact that we have shown that the correlation coefficient between each gap is almost zero tells us that there is no relationship between each gap prior to nucleation events. This seems to almost confirm the assumption behind (5.15).

However, since (5.3) is true for small x, and if (5.15) is true then these tell us that GWS with the original definition of $\beta = 2(i + 1)$ cannot be true in at least the 1-D point-island case.

Chapter 6

The Gap Size and Capture Zone Distributions in Monte Carlo Simulations

6.1 Introduction

As noted in Chapter 3, Pimpinelli and Einstein introduced a new theory for the capture zone distribution (CZD) employing the Generalised Wigner Surmise (GWS) from Random Matrix Theory [61], causing some controversy. Oliveira and Reis [57] have presented simulation results for islands grown on a two-dimensional substrate with critical island size $i = 1$ and 2, providing some support for the proposed Gaussian tail of the CZD [61]. However, Li *et. al.* [47] presented an alternative theory which yields a modified form for the large-size CZD behaviour, supported by data for the simulated growth of compact islands with $i = 1$. This form seems to agree with that found by Oliveira and Reis, contradicting the GWS [57]. In other work, Shi *et. al.* [71] studied $i = 1$ models in $d = 1, 2, 3, 4$ dimen-

sions, finding that the CZD is more sharply peaked and narrower than the GWS suggests. Therefore it is by no means established whether the GWS provides a good theoretical basis for understanding the distribution of capture zones found in island nucleation and growth simulations.

The simplified case of point island nucleation and growth in one dimension has proven to be a good test case for theories. Blackman and Mulheran [14] studied the system with critical island size $i = 1$, using a fragmentation equation approach. In this system, we can view the substrate as a string of inter-island gaps, and new island nucleation caused by the deposited monomers as a fragmentation of these gaps. Thus in order to understand the CZD, it is important first to be able to describe the gap size distribution (GSD).

In the previous chapter we have extended the analysis of the fragmentation equations of [14] to the case of general $i \geq 0$. We have been able to derive the small- and large-size asymptotics of the GSD, and by assuming random mixing of the gaps caused by the nucleation process, we have also derived the small-size asymptotics for the CZD for general i and the large-size behaviour for $i = 0$.

One key feature to emerge from the gap evolution equations as discussed in the previous chapter is that the asymptotic behaviour of the CZD is different to that of the GWS [61]. It therefore is appropriate to ask what support, further to that in [14], for the fragmentation equation approach is offered by Monte Carlo (MC) simulations of the system. Recent work by González *et. al.* [35] has revisited the case of $i = 1$, developing the original fragmentation equation [14] and GWS arguments in response to deviations between prediction and simulation. In this work we will explore simulation results for the one-dimensional model with $i = 0, 1, 2, 3$, and consider the relative merits of the fragmentation theory [37] and GWS [61] approaches.

The aims of this chapter are, using MC simulations,

- To investigate the validity of the GWS discussed in Chapter 3 for one-, two- and three-dimensional (1-D, 2-D and 3-D respectively) nucleation and growth models;
- To investigate the correlations between neighbouring gaps in a 1-D model;
- To investigate the GSD and CZD in more detail, especially at small- and large-size scaling. Moreover, we compare their results to two theories – the GWS and gap evolution equations – and comment on whether these theories agree, or otherwise, with data from MC simulations.

6.2 Monte Carlo Simulations

Firstly, a decision must be made about shapes of islands; point or extended. Here, by **point island** we mean islands that have no spatial extent, such that a stable island of any size greater than the critical island size i will always occupy a single lattice site. Alternatively, **extended island** shapes are allowed; such islands grow by capturing monomers that diffuse to their locations. The shape of these islands depends on the dimension d; an island with $2 \times radius$ as the length for $d = 1$, a circular island for $d = 2$ and a spherical island for $d = 3$. However, it is possible that the dimension of an island could be different from the substrate and still be physical, such as hemispherical islands growing on a flat 2-D surface. Dendritic (or fractal) is another possibility for the island shape; such an island has a characteristic tree-like structure, growing predominantly in the direction from which monomers diffuse [3, 54]. In this chapter we will not consider dendritic islands in favour of the cases of point and extended islands. In this thesis, MC

simulations were programmed in FORTRAN, and the results of the simulations were analysed and visualised in MATLAB.

6.2.1 Full Simulation

Within the full simulation, monomers are deposited onto an initially empty 1-D array of sites representing the substrate at deposition rate F monolayers per unit time. Deposited monomers perform random hops between nearest neighbour lattice sites within periodic boundary conditions; this diffusion occurs at the constant monomer rate D. In the case $i > 0$, a new island is nucleated when the number of monomers at any one site exceeds the critical island size. The $i = 0$ case represents spontaneous nucleation, and in this case monomers have a small probability p_n of nucleating a new island whenever they hop. Note that the lower the value of p_n, the lower the nucleation rate and the larger the gaps, which delays the onset of the monomer density saturation we assume in this thesis. However, if p_n is too high, then we obtain a high density of islands and the granularity of the lattice becomes an issue for modelling in the gaps. Once nucleated, the new island absorbs monomers that hop onto it from a nearest neighbour site, therefore increasing in size. These processes are illustrated for the 1-D case in Figure 1.3 of Chapter 1, Section 1.3.

As the rate F increases, there is a decrease in the average time a monomer diffuses before it meets another monomer or island. As diffusion and deposition are occuring as competing processes the statistical properties depend on the ratio $R = D/F$.

The deposition process can be measured by the nominal substrate coverage, $\theta = Ft$. Note that in the case of point islands, the coverage can exceed 100% even whilst most of the substrate remains free for monomer diffusion. For a fixed value

of θ, the average distance between islands increases in relation to an increase in R – and for fixed R, the island density increases as coverage increases. We are interested in the scaling properties of the aggregation regime [3] where the island density exceeds the monomer density. The value of θ for which the regime starts is dependent on i and R; we check that the values for θ are sufficiently high to ensure that we are in the aggregation regime.

An important point raised by Ratsch *et. al.* [65] needs consideration for the point-island model. In the work of Ratsch *et. al.*, the island size distribution (ISD) for point island models, where the process of nucleation is endless, does not scale in the asymptotic limit. In other words, the ISD has to become singular for $\theta \to \infty$ for any R, so that scaling breaks down at large coverage. The reason for this is that the lattice becomes saturated with islands and all the capture zones have become size one. Note that the connection between size of island and its capture zone area is vital for the ISD to scale.

Interestingly, for extended islands Ratsch *et. al.* confirm that the ISD do scale in the scaling limit. This may be due to the fact that islands usually coalesce at around $\theta = 20\%$ and at this point there is no more nucleation. However, for extended islands, scaling will break down at θ beyond 20%, i.e. when coalescence plays a major role. This leads to the lattice being covered by islands and so capture zone becomes size one.

In the Results section, we provide average island densities, $\langle c_j \rangle$, from extended- and, more importantly, point-island MC simulations for each value of $i = 0 - 3$. Note that c_j is the number density of island size j, and $\langle c_j \rangle$ is its average which varies with θ and R. This allows us to ensure that, according to these results, the lattice does not become saturated with islands and, thus, are long way short of the limit referred by Ratsch *et. al.*

6.2.2 Single-Gap Nucleation Rate Simulation

In the 1-D single-gap simulation, we simulate point island nucleation events in gaps ranging from size $g = 50$ to $g = 500$ which proves to be adequate to illustrate the nucleation mechanisms at play. In this case, monomers can diffuse as usual on a lattice of length g, but if they attempt to hop beyond the length of the lattice the monomers are removed from the simulation.

A monomer deposition increments the simulated time by $1/g$ when the nominal monolayer deposition rate F is set to unity – recall that what is important is the ratio $R = D/F$, rather than the absolute value of either F or D. At each step of the algorithm, either a new monomer is deposited at a randomly chosen site in the gap or an existing monomer is diffused, according to the relative rate of such processes. Explicitly, a monomer is deposited into the gap with probability $Fg/(Fg + Dn) = 1/(1 + Rn/g)$, where n represents the number of monomers present in the gap. If deposition does not occur, a randomly chosen monomer then hops to a nearest neighbour site. For $i = 1$, 2 and 3, if $i + 1$ monomers coincide at a site to form a stable island, the simulation ends and the time to the nucleation event is recorded. Repeat runs always start with an empty lattice, and we obtain reliable statistics on the nucleation times within each gap size.

We use $R = 10^6$ for $i = 1$, 2, and $R = 10^5$ for $i = 3$ due to simulation time constraints. In the single-gap simulations we also monitor the average monomer density profile across the gaps and the number of hops each monomer makes. The latter will indicate whether deposition events influence island nucleation. If nucleation is caused solely by the diffusional fluctuations of monomers, then stable islands should only include monomers that have taken many hops. However, if nucleation closely follows a deposition event then the island will contain monomers that have only made few hops since being deposited.

6.3 The Gap Evolution Equations Revised

The data from MC simulations can be used as a benchmark against which to test predictions of theories for the GSD and CZD. In this subsection we will revise the fragmentation approach considered in the previous chapter.

A nucleation that occurs in a parent gap of width y will result in the creation of two daughter gaps of widths x and $y - x$. The probability that the nucleation occurs at position $x < y$ is taken from the long-time (steady state) monomer density profile in the gap,

$$n_1(x) = \frac{1}{2R} x(y - x), \tag{6.1}$$

where, as before, $R = D/F$. In particular, we assume that the nucleation probability is obtained from this monomer density $n_1(x)^{\alpha_n}$, with the value of α_n reflecting the nucleation process. We then obtain

$$\frac{\partial}{\partial t} u(x,t) = -B(\alpha_n + 1, \alpha_n + 1) x^{\lambda} u(x,t) + 2 \int_x^{\infty} [x(y-x)]^{\alpha_n} u(y,t) dy, \tag{6.2}$$

where $B(\cdot, \cdot)$ is the Beta function and $\lambda = 2\alpha_n + 1$. Here, $u(x,t)$ is the number of gaps of size x at time t. Each term in (6.2) has already been discussed in the previous chapter.

In Chapter 5 we set $\alpha_n = i + 1$ under the assumption that nucleation is a rare event solely driven by the diffusion of the monomers. In doing this we implicitly assume that the $i + 1$ monomers necessary to create the nucleus are all in some sense *mature*, each separately obeying the long-time steady-state density profile $n_1(x)$. However, we shall also have need to consider the case when nucleation is triggered by a deposition event. Here a newly deposited monomer either lands

close to (or even directly onto) a pre-existing cluster of $i > 0$ mature monomers. In this case, we set $\alpha_n = i$.

By a similar analysis to that used for $\alpha_n = i + 1$ in Chapter 5, the following asymptotics for the 1-D GSD are then found:

$$\phi(z) \sim kz^{\alpha_n} \text{ as } z \to 0; \tag{6.3}$$

$$\phi(z) \sim kz^{-2} \exp(-cz^{\lambda}) \text{ as } z \to \infty, \tag{6.4}$$

for constants $c > 0$ and k. Here $z = x/\bar{x}(t)$ is the scaled gap size where $\bar{x}$ is the average gap size.

We may use this information to understand the scaling asymptotics of the CZD $P(s)$ where s is the scaled capture zone size. It follows that

$$P(s) \sim ks^{2\alpha_n+1} \text{ as } s \to 0, \tag{6.5}$$

for some constant k. The large-size scaling of $P(s)$ can be computed only for the special case $\alpha_n = 1, i = 0$. It has been shown that, for some constant k,

$$P(s) \sim ks^{-9/2} e^{-2s^3/\mu^3} \text{ as } s \to \infty, \tag{6.6}$$

where μ is a positive constant.

As seen in the previous chapter, we note here that the large-size asymptotics of the GSD and the CZD are thus the same for spontaneous nucleation ($i = 0$) using (5.1). Given the form of (5.1) for $P(s)$, we conjecture that the correspondence between the GSD and CZD large-size asymptotics will hold for other values of $i \geq 1$ although it has not been proved.

Here we note that the asymptotics of the fragmentation equation approach above and the GWS, with β, the sole parameter in the GWS, do not agree (see the conclusion section in the previous chapter for more detail), which in part motivates the present MC study.

6.4 Results

In Subsection 6.4.1, we consider the validity of the GWS for the case of all 1-D, 2-D and 3-D models by comparing the GWS to the MC data visually and comment on whether the expected value of a parameter used in the GWS form is correct or not. In Subsection 6.4.2 and subsequent ones, the 1-D point-island model will be considered for the relationship between the GSD and CZD, and the small- and large-size scaling of both the GSD and CZD. Moreover, we compare these results to the prediction of the fragmentation theory approach as discussed in the previous section.

6.4.1 The Validity of Generalised Wigner Surmise

Here, we are comparing the data from MC simulations to the GWS

$$P_\beta(s) = a_\beta s^\beta \exp(-b_\beta s^2), \tag{6.7}$$

conjectured by Pimpinelli and Einstein where β is given by (3.40) in Chapter 3. In these simulations, we consider both extended (at $\theta = 5 - 20\%$) and point islands (at $\theta = 20\%$) for the case of $i = 0 - 3$. CZDs were obtained and fitted to the GWS functional form, with β no longer restricted to the values in (3.40).

As noted in Chapter 3, Shi *et. al.* have carried out simulations of point-island models of irreversible nucleation and growth in $d = 1$–4 in the $i = 1$ case.

Their model is similar to our point-island simulation except that if a monomer is deposited directly on or, hops onto, an island, then this monomer aggregate to an island. In this subsection, we compare our results to those of Shi *et. al.*

6.4.1.1 Case I: $d = 1$

Our simulations were performed on lattices with 10^6 sites, with $R = 8 \times 10^6$ up to coverage $\theta = 20\%$, averaging results over 100 runs. For $i = 0$ we set the spontaneous nucleation probability to $p_n = 10^{-7}$. As discussed in Section 6.2, we must ensure that point island densities for each i are much less than unity. In Table 6.1, where *len* is defined as the length of the lattice, we confirm that these island densities are well short of the limit referred as in [65]. This means that the lattice in our MC simulations is not completely occupied by islands and hence the scaling does not break down. As discussed in Section 1.1, there are four distinct regimes – low coverage, intermediate coverage, aggregation and coalescence regimes. We are interested in intermediate coverage and aggregation regimes. Intermediate coverage is the regime where the island density increases as the monomer density decreases due to significant nucleation of new islands. The aggregation regime occurs when the island density still increases (slowly) and the monomer density reduces. This is where a diffused monomer is more likely to be captured by an island rather than joining another monomer to nucleate a new island.

The MC simulation has entered the intermediate coverage when there is a crossover between the monomer and island densities. In Figure 6.1, we see that the crossover for the case of $i = 0$ occurs at $\theta \approx 15\%$. In Figures 6.1 and 6.2, there is a clear crossover between both monomer and island densities within coverage $\theta = 20\%$ except for the $i = 3$ point-island case. This is due to rarity of nucleation of islands in the $i = 3$ model. However, since we are dealing with point islands,

the coverage can be large and eventually there is a crossover beyond $\theta = 20\%$. Of course, this is true as long as the island density does not reach the limit as discussed earlier.

i	$\langle c_j \rangle / len^{\mathrm{a}}$	$\langle c_j \rangle / len^{\mathrm{b}}$
0	0.259%	0.282%
1	0.879%	0.954%
2	0.384%	0.416%
3	0.202%	0.215%

[a] Extended islands, $\theta = 20\%$
[b] Point islands, $\theta = 20\%$

Table 6.1: Average island density, $\langle c_j \rangle$, at coverage $\theta = 20\%$ for $d = 1$.

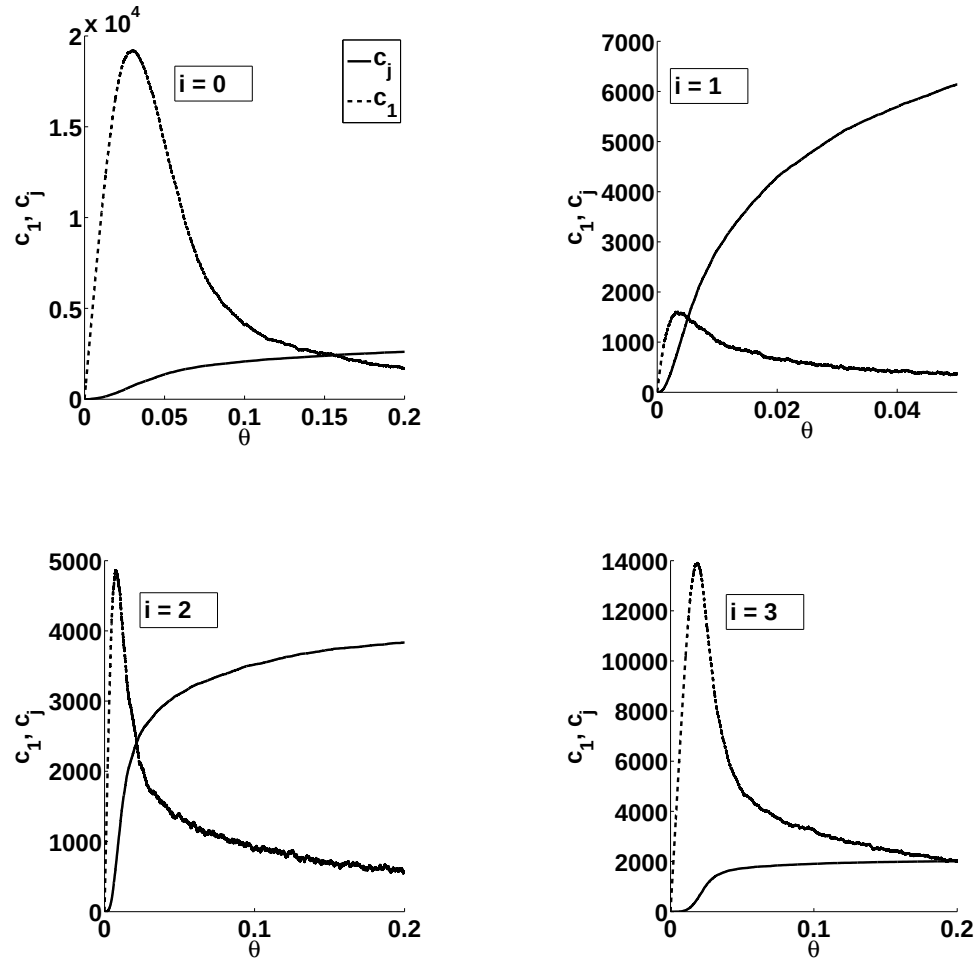

Figure 6.1: Monomers (c_1) and island (c_j) densities vs. coverage (up to $\theta = 20\%$) for 1-D extended islands.

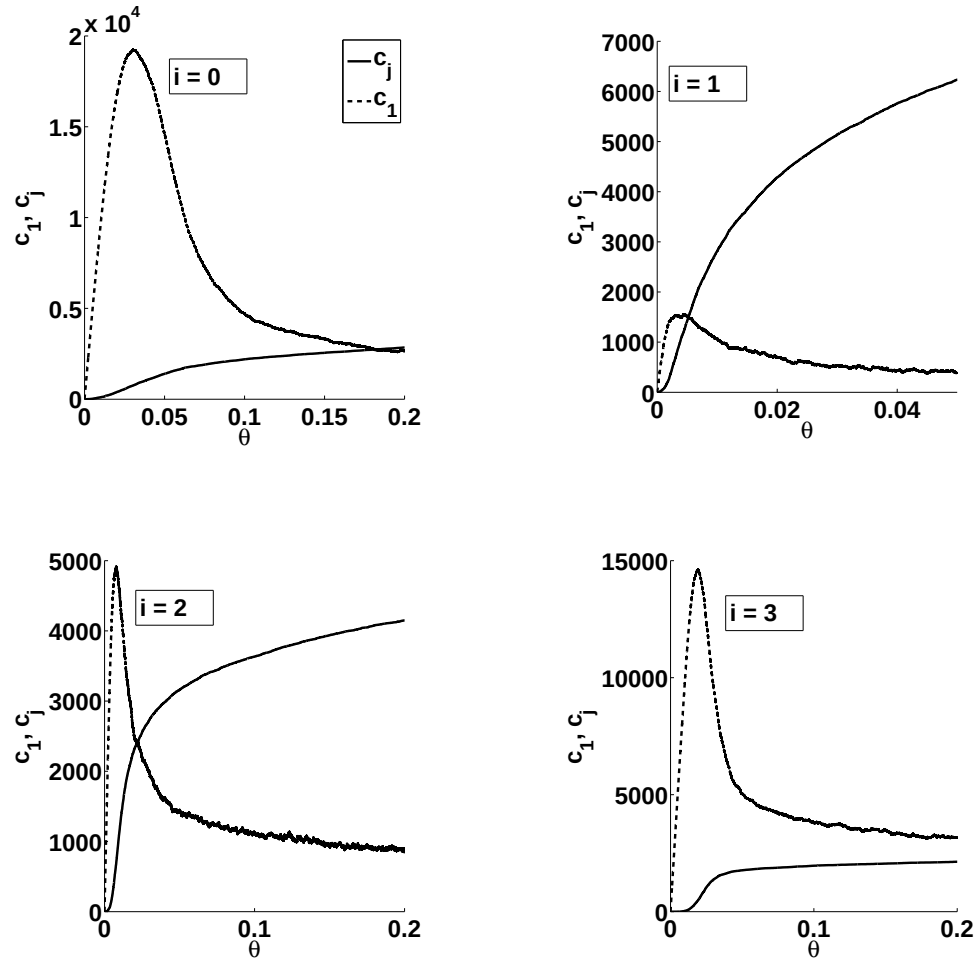

Figure 6.2: Monomers (c_1) and island (c_j) densities vs. coverage (up to $\theta = 20\%$) for 1-D point islands.

In Figures 6.3 and 6.4, we plot the CZDs from the MC data at $\theta = 5\%$, 10%, 15% and 20% for extended islands, and 20% for point islands. Moreover, we compare the GWS to these figures for the CZD. as illustrated in Figures 6.3 and 6.4. We allow β to be a real (not necessarily integer-valued) parameter by calculating the deviation between the MC data and the GWS for various β, and identify the value that minimises this deviation. In other words, assuming the GWS is true we want to know whether the data does fit $\beta = \frac{2}{d}(i+1)$ for any i and

d better than any other integer values of β. The best optimal values of β are used in the right-hand plots of Figures 6.3 and 6.4.

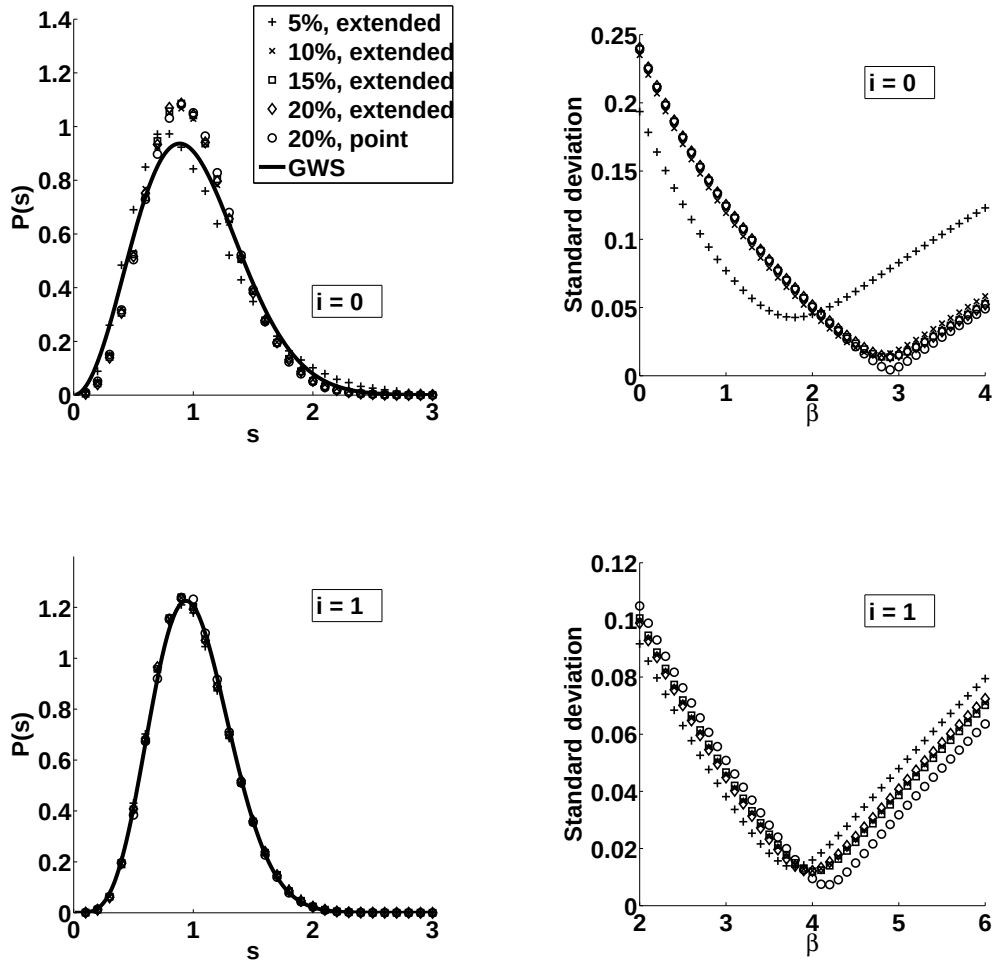

Figure 6.3: CZDs and the deviation between MC data and the GWS for various β, with for $i = 0$ and 1 in $d = 1$.

In order to provide an estimate of the error in fitting of β to the MC data, we adopt a strategy to bin the data using binwidths of size $0.01v$ with $v = 1, 2, ..., 20$. This allows us to calculate the average of these deviation between MC data and the GWS for various β, and an approximate 95% confidence interval. The results of this fitting procedure are presented in Table 6.2 for the CZD.

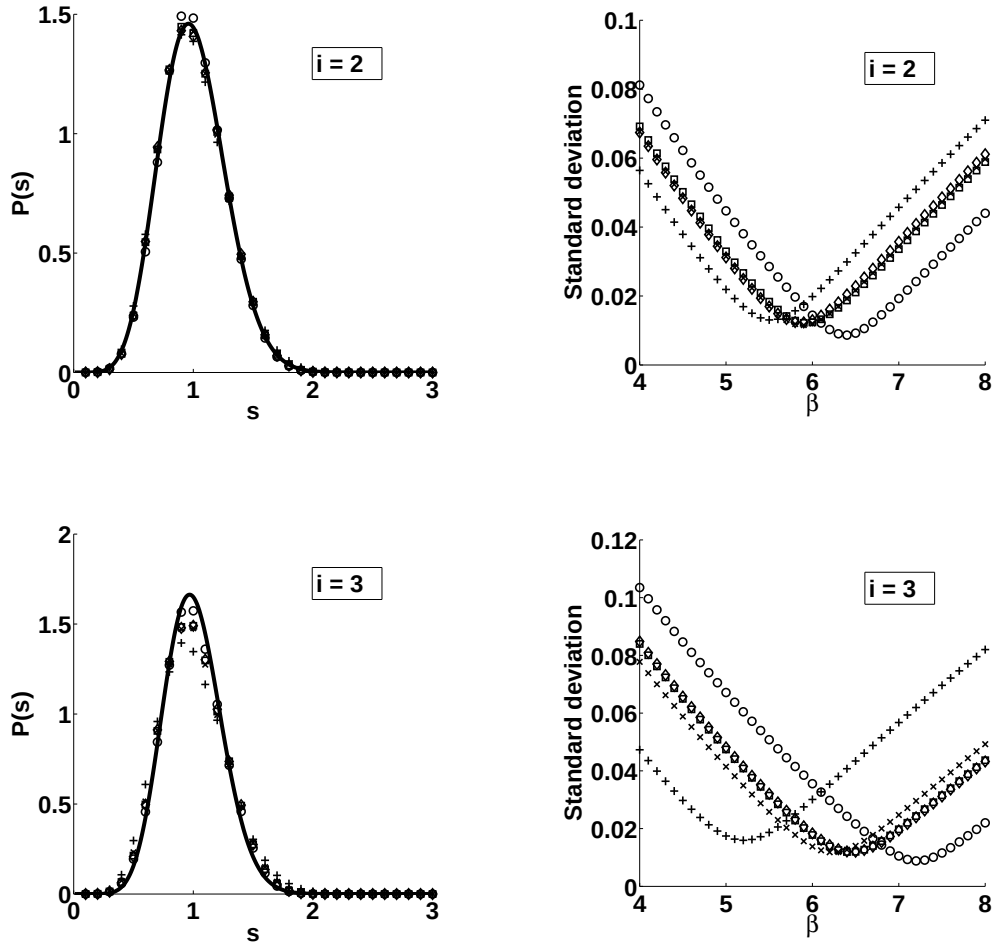

Figure 6.4: CZDs and the deviation between MC data and the GWS for various β, with $i = 2$ and 3 in $d = 1$.

i	GWS	CZD[a]	CZD[b]	CZD[c]
0	2	2.785 ± 0.007	2.904 ± 0.010	2.930 ± 0.011
1	4	4.021 ± 0.017	3.998 ± 0.017	4.187 ± 0.019
2	6	5.934 ± 0.030	5.895 ± 0.028	6.422 ± 0.034
3	8	6.282 ± 0.032	6.507 ± 0.034	7.260 ± 0.043

[a] Extended islands, $\theta = 10\%$
[b] Extended islands, $\theta = 20\%$
[c] Point islands, $\theta = 20\%$

Table 6.2: Best optimal values of β for $d = 1$.

Utilising bootstrap methods (see Chapter 2 for detail) with 1000 samples of size as big as the original sample size we consider the average value of β for the general case of $i \geq 0$, and therefore find the approximate 95% confidence interval of these averages. Moreover, we have confirmed that these bootstrap results in Table 6.3 (with much smaller errorbars due to very large number of bootstrap samples) are consistent with the results in Table 6.2.

i	GWS	CZD[a]	CZD[b]	CZD[c]
0	2	2.760 ± 0.001	2.882 ± 0.001	2.900 ± 0.001
1	4	3.993 ± 0.001	3.966 ± 0.001	4.156 ± 0.001
2	6	5.890 ± 0.001	5.864 ± 0.001	6.388 ± 0.001
3	8	6.238 ± 0.002	6.464 ± 0.002	7.215 ± 0.002

[a] Extended islands, $\theta = 10\%$
[b] Extended islands, $\theta = 20\%$
[c] Point islands, $\theta = 20\%$

Table 6.3: Best optimal values of β for $d = 1$ using bootstrap methods.

As we see in Table 6.2, in the extended-island case for $i = 1$ and 2 the data fit the expected values of $\beta = 4$ and $\beta = 6$ respectively better than other integer values of β. The results for point islands in the cases of $i = 1$ and $i = 2$ are similar to these for realistic islands. For $i = 0$, the data seems to fit $\beta = 3$ rather than the expected value of $\beta = 2$. Likewise, for $i = 3$, the data fit $\beta = 6$ and $\beta = 7$ rather than the expected value of $\beta = 8$ for extended and point islands respectively. In

[71], Shi *et. al.* found that the peak height of the CZD in $d = 1$ with $i = 1$, and at very large R, is higher than the GWS with $\beta = 4$ despite the fact that their simulation data is close to the predicted $\beta = 4$.

6.4.1.2 Case II: $d = 2$

Our simulations were performed on lattices with 1581×1581 sites, with $R = 10^7$ up to coverage $\theta = 20\%$, averaging results over 100 runs. For $i = 0$ we set the spontaneous nucleation probability to $p_n = 10^{-7}$. As before, in Table 6.4, we confirm that these point island densities are well short of the limit referred as in [65] and thus the scaling for the ISD does not break down. In Figures 6.5 and 6.6, there is a clear crossover between both monomer and island densities within coverage $\theta = 20\%$ except for the $i = 3$ case. This may be due to the fact that it is much rarer to nucleate a new island by joining four monomers than any case of lower i. As before, in Figures 6.7 and 6.8, we plot the CZDs from the MC data at $\theta = 5\%$, 10%, 15% and 20% for extended islands, and 20% for point islands. Moreover, we compare the GWS to these figures for the CZD and use the same approach as for the $d = 1$ case to find optimal β values.

i	$\langle c_j \rangle / len^{\mathrm{a}}$	$\langle c_j \rangle / len^{\mathrm{b}}$
0	0.019%	0.041%
1	0.155%	0.322%
2	0.012%	0.030%
3	0.002%	0.006%

[a] Extended islands, $\theta = 20\%$
[b] Point islands, $\theta = 20\%$

Table 6.4: Average island density, $\langle c_j \rangle$, at coverage $\theta = 20\%$ for $d = 2$.

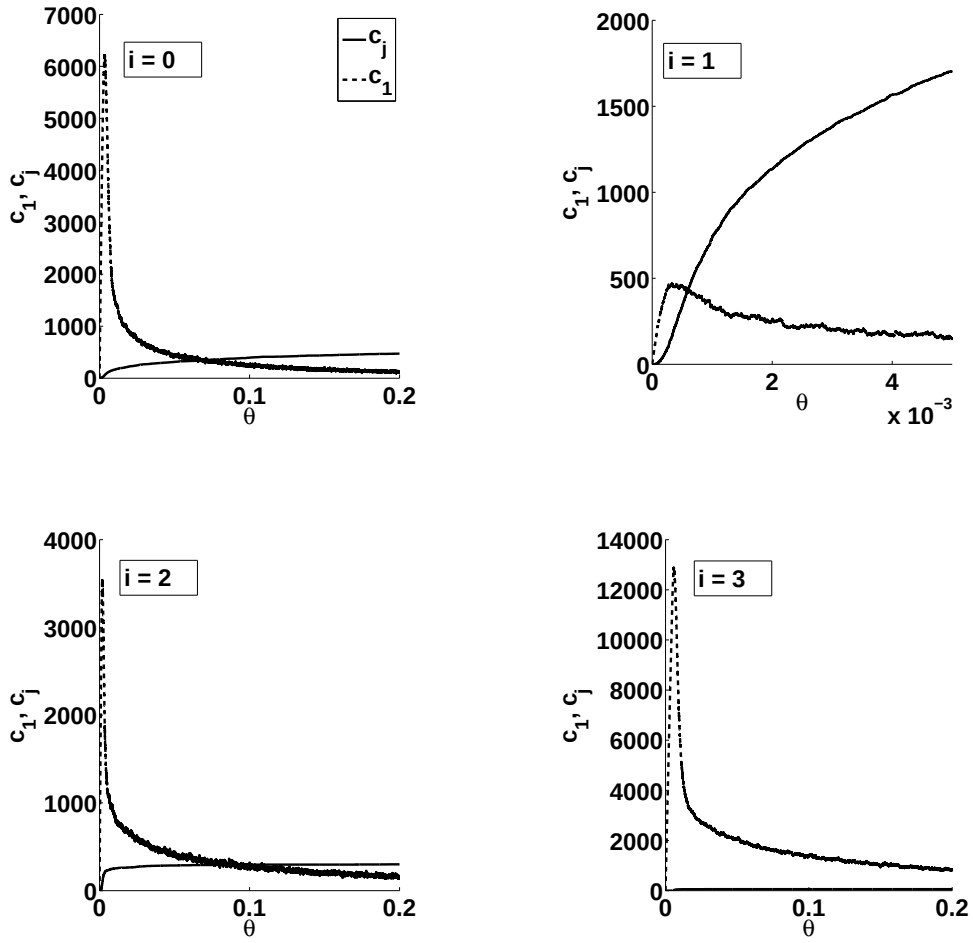

Figure 6.5: Monomers (c_1) and island (c_j) densities vs. coverage (up to $\theta = 20\%$) for 2-D extended islands.

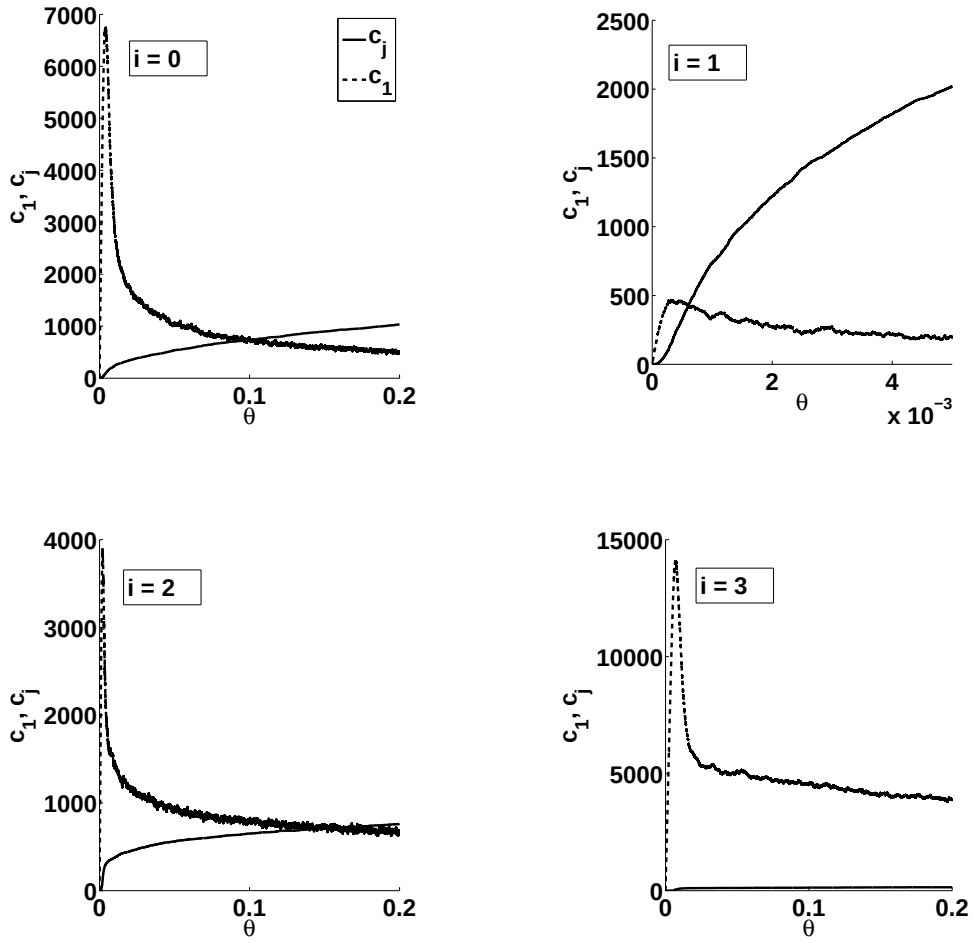

Figure 6.6: Monomers (c_1) and island (c_j) densities vs. coverage (up to $\theta = 20\%$) for 2-D point islands.

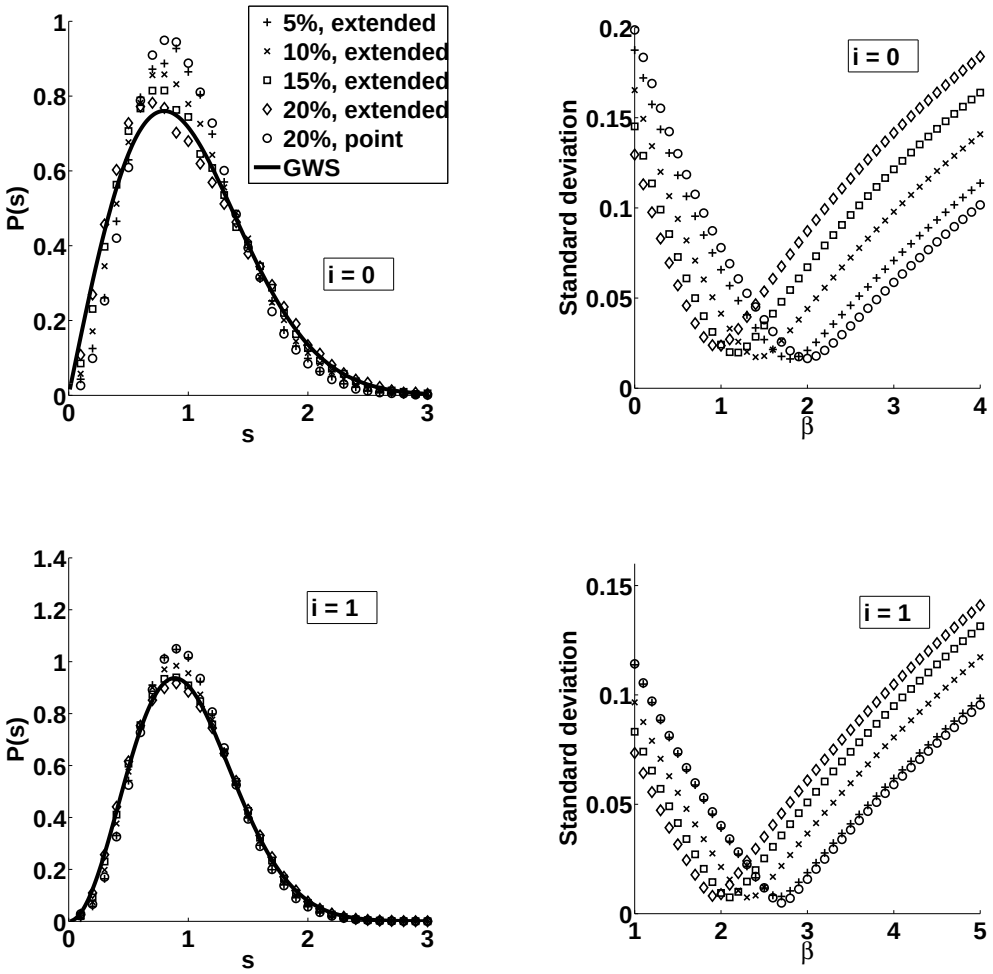

Figure 6.7: CZDs and the deviation between MC data and the GWS for various β, with $i = 0$ and 1 in $d = 2$.

As before, we adopt a strategy to bin the data using binwidths of size $0.01v$ with $v = 1, 2, ..., 20$ in order to obtain the average of the deviations between MC data and the GWS for various β, and an approximate 95% confidence interval. The results of this fitting procedure are presented in Table 6.5 for the CZD.

As before, we have used bootstrap methods with 1000 samples of size as big as the original sample size, we considered the average value of β for the general case of $i \geq 0$ and have found the approximate 95% confidence interval of these

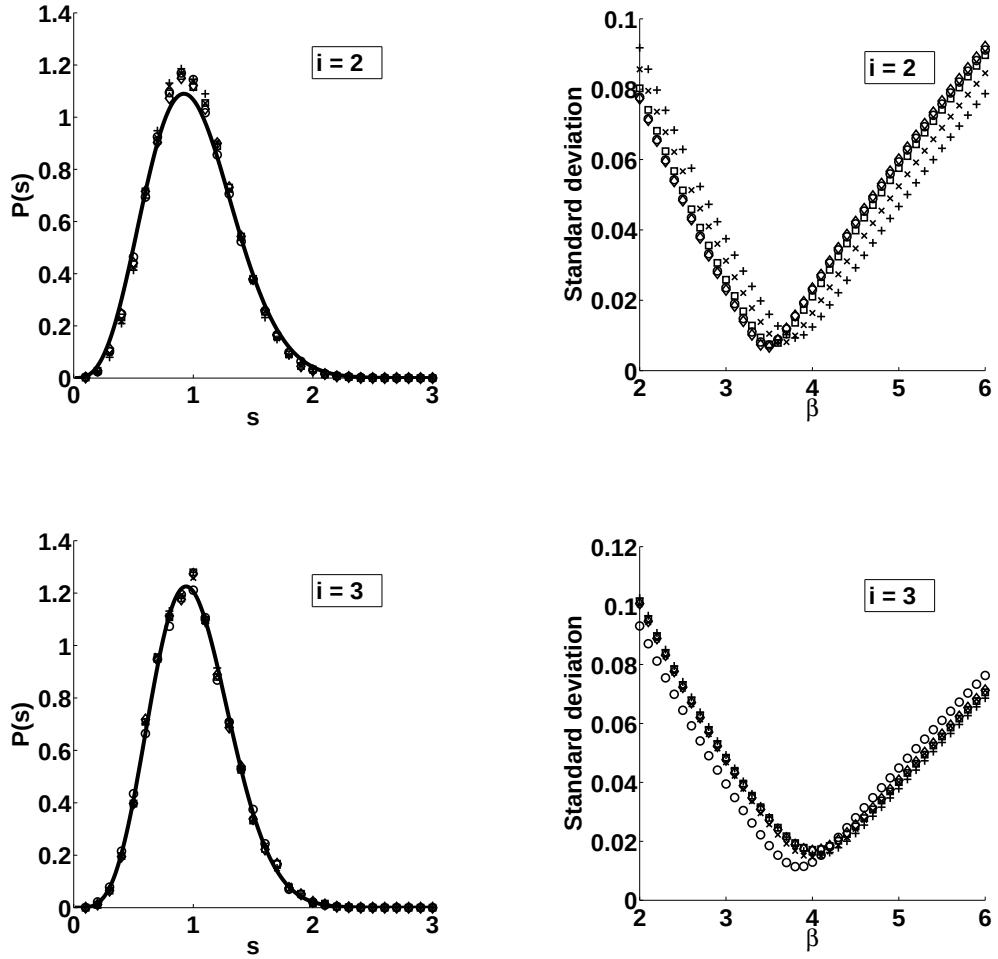

Figure 6.8: CZDs and the deviation between MC data and the GWS for various β, with $i = 2$ and 3 in $d = 2$.

i	GWS	CZD[a]	CZD[b]	CZD[c]
0	1	1.450 ± 0.006	0.959 ± 0.005	2.012 ± 0.008
1	2	2.351 ± 0.009	1.952 ± 0.007	2.726 ± 0.011
2	3	3.683 ± 0.015	3.484 ± 0.015	3.516 ± 0.014
3	4	4.041 ± 0.018	4.037 ± 0.019	3.868 ± 0.021

[a] Extended islands, $\theta = 10\%$
[b] Extended islands, $\theta = 20\%$
[c] Point islands, $\theta = 20\%$

Table 6.5: Best optimal values of β for $d = 2$.

averages. Moreover, we have confirmed that these bootstrap results in Table 6.6 are consistent with the results in Table 6.5.

i	GWS	CZD[a]	CZD[b]	CZD[c]
0	1	1.433 ± 0.001	0.956 ± 0.001	1.991 ± 0.001
1	2	2.329 ± 0.001	1.934 ± 0.001	2.702 ± 0.001
2	3	3.658 ± 0.002	3.469 ± 0.002	3.483 ± 0.001
3	4	4.007 ± 0.006	4.011 ± 0.006	3.846 ± 0.004

[a] Extended islands, $\theta = 10\%$
[b] Extended islands, $\theta = 20\%$
[c] Point islands, $\theta = 20\%$

Table 6.6: Best optimal values of β for $d = 2$ using bootstrap methods.

As we see in Table 6.5, the data for extended islands agree with the GWS. Though the case $i = 2$ for both point and extended islands is questionable as the best fit β could be 4 and the case $i = 1$ for point islands found better agreement with $\beta = 3$. In [71], Shi *et. al.* found that in the case of $i = 1$, the data from the models agree with $\beta = 3$ rather than $\beta = 2$ which confirms our results.

6.4.1.3 Case III: $d = 3$

Our simulations were performed on lattices with $189 \times 189 \times 189$ sites, with $R = 4.5 \times 10^6$ up to coverage $\theta = 20\%$, averaging results over 100 runs. For $i = 0$ we set the spontaneous nucleation probability to $p_n = 10^{-7}$. In Table 6.7, we also

confirm that these point island densities are well short of the limit referred as in [65]. Recall that the intermediate coverage regime occurs when monomer and island densities are intersected over a certain coverage. In Figures 6.9 and 6.10, apart from the $i = 1$ case, the crossover of both monomer and islands densities is much more likely to occur at later coverage for point islands. Comparably, for the extended-island case, the MC simulation has entered the intermediate coverage regime well within $\theta = 20\%$ except for $i = 3$. For the $i = 3$, the intermediate coverage regime does not occurs because of quite low number of islands. This may be due to the fact that it is much rarer to nucleate a new island by joining four monomers. In Figures 6.11 and 6.12, we plot the CZDs from the MC data at $\theta = 5\%$, 10%, 15% and 20% for extended islands, and 20% for point islands. As in the case of $d = 1$ and $d = 2$, we compare the GWS to these figures for the CZD and find the best optimal values of β.

i	$\langle c_j \rangle / len^{\mathrm{a}}$	$\langle c_j \rangle / len^{\mathrm{b}}$
0	0.004%	0.027%
1	0.141%	0.310%
2	0.002%	0.020%
3	0.001%	0.003%

[a] Extended islands, $\theta = 20\%$
[b] Point islands, $\theta = 20\%$

Table 6.7: Average island density, $\langle c_j \rangle$, at coverage $\theta = 20\%$ for $d = 3$.

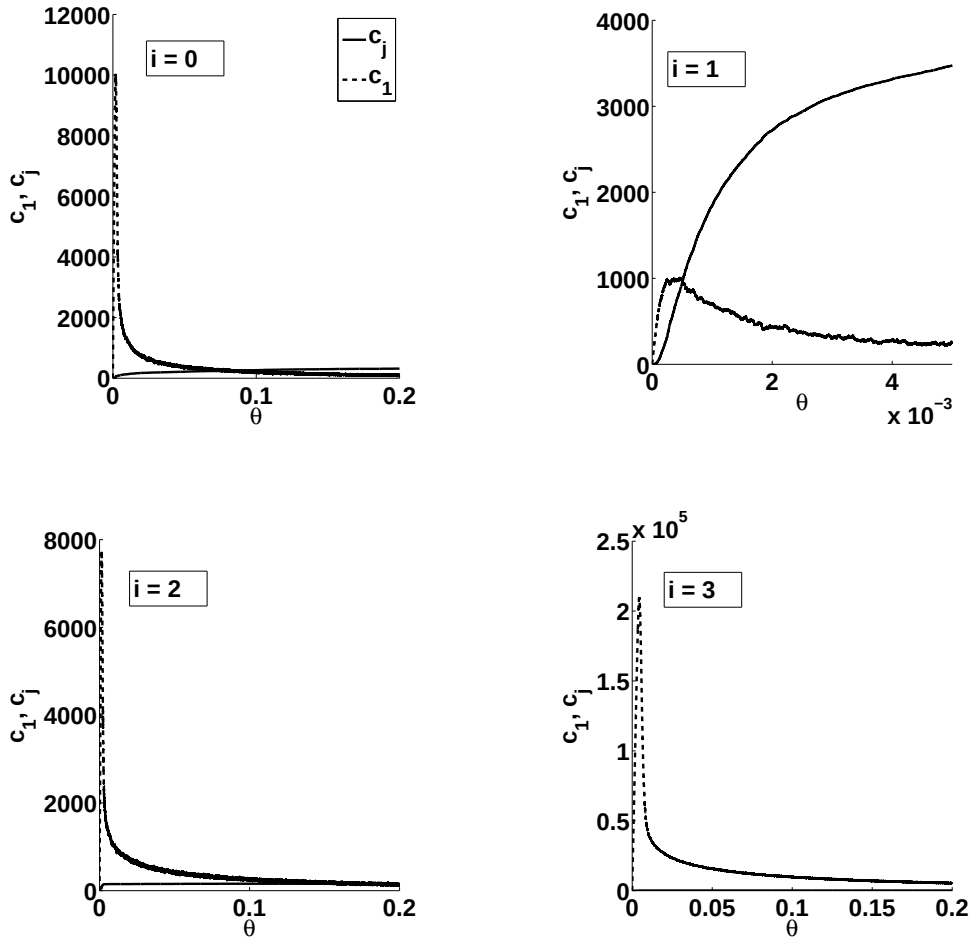

Figure 6.9: Monomers (c_1) and island (c_j) densities vs. coverage (up to $\theta = 20\%$) for 3-D extended islands.

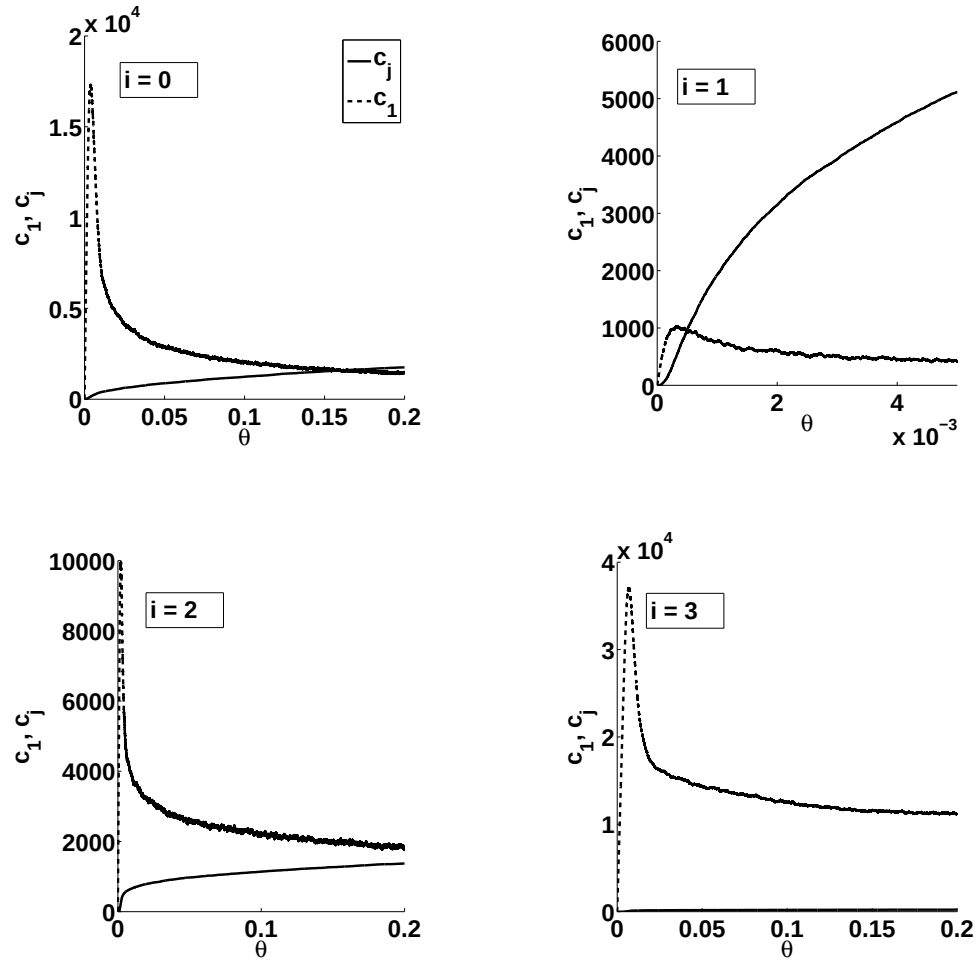

Figure 6.10: Monomers (c_1) and island (c_j) densities vs. coverage (up to $\theta = 20\%$) for 3-D point islands.

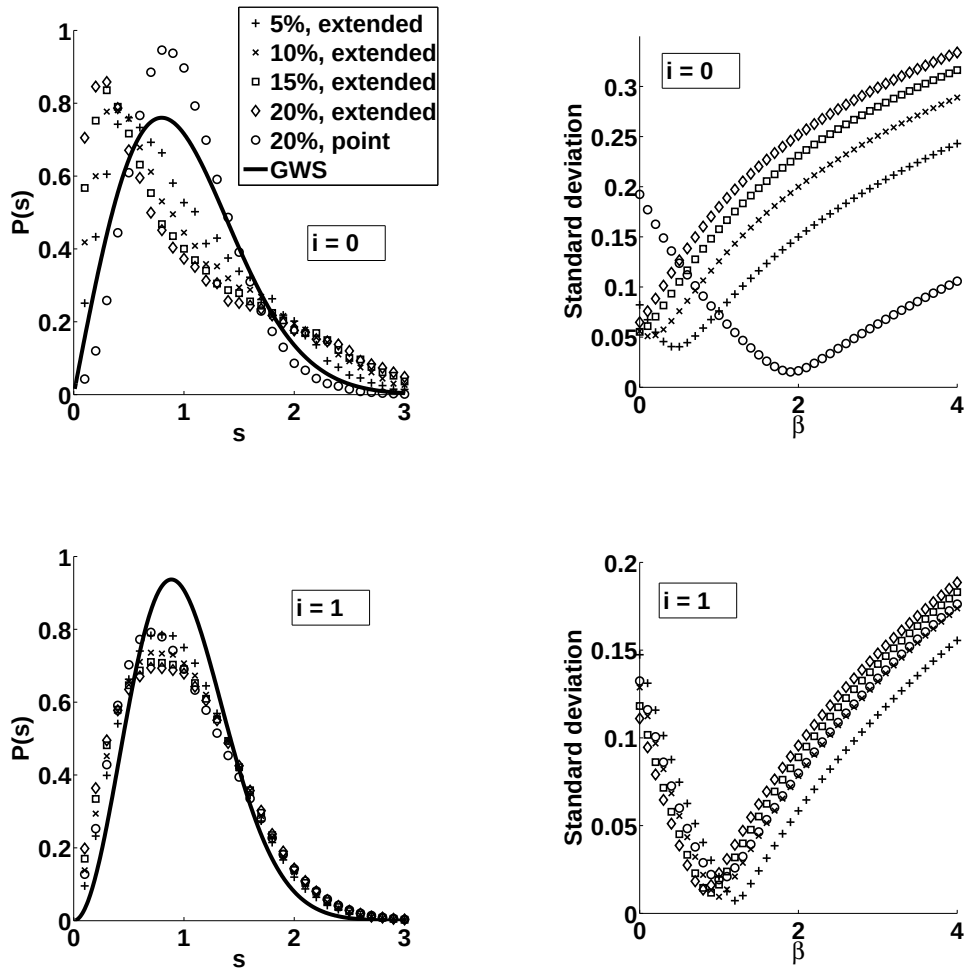

Figure 6.11: CZDs and the deviation between MC data and the GWS for various β, with $i = 0$ and 1 in $d = 3$.

We adopt the same strategy as in the previous subsection for the average of the deviations between MC data and the GWS. The results of this fitting procedure are presented in Table 6.8 for the CZD. Using bootstrap methods as before, we have confirmed that these bootstrap results in Table 6.9 are consistent with the results in Table 6.8.

As we see in Table 6.8, the data for both point and extended islands completely disagree with the GWS. It is interesting to note that, in [71], Shi *et. al.* found that

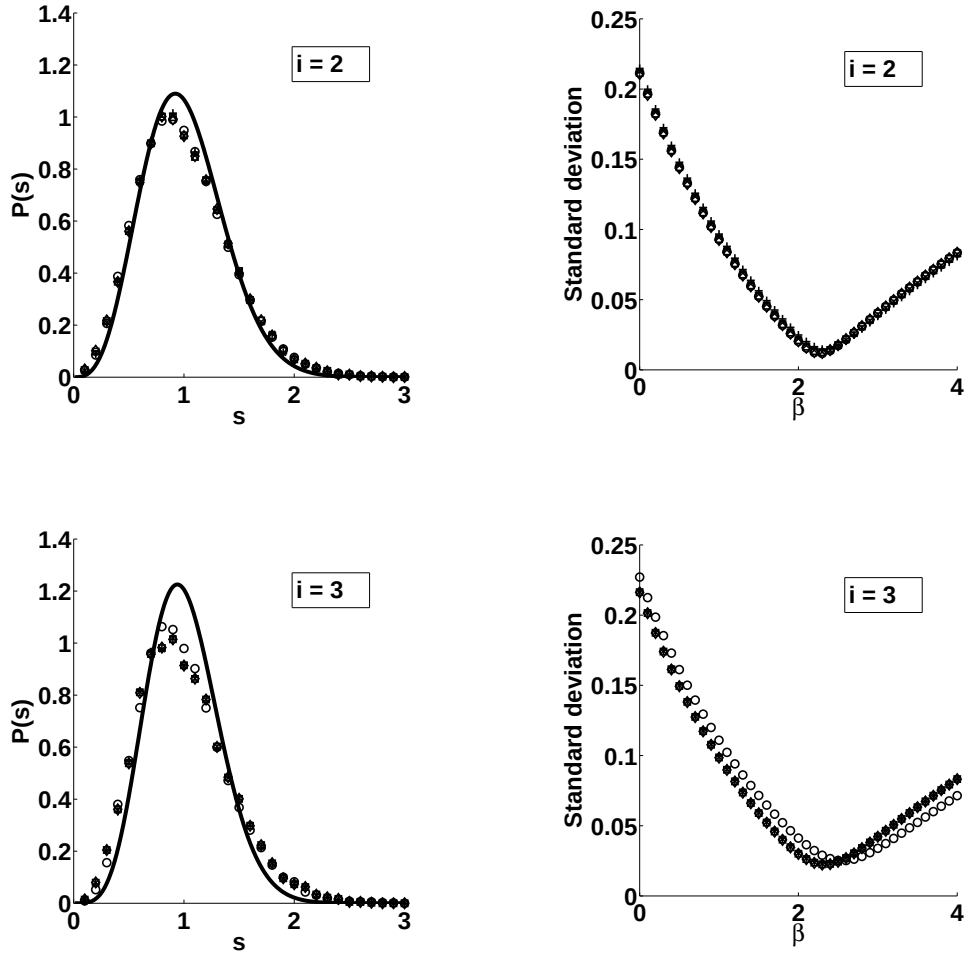

Figure 6.12: CZDs and the deviation between MC data and the GWS for various β, with $i = 2$ and 3 in $d = 3$.

i	GWS	CZD[a]	CZD[b]	CZD[c]
0	1	0.126 ± 0.027	0.002 ± 0.003	1.951 ± 0.008
1	2	0.867 ± 0.006	0.688 ± 0.008	0.790 ± 0.007
2	3	2.139 ± 0.008	2.110 ± 0.009	2.127 ± 0.008
3	4	2.070 ± 0.008	2.065 ± 0.009	2.527 ± 0.009

[a] Extended islands, $\theta = 10\%$
[b] Extended islands, $\theta = 20\%$
[c] Point islands, $\theta = 20\%$

Table 6.8: Best optimal values of β for $d = 3$.

i	GWS	CZD[a]	CZD[b]	CZD[c]
0	1	0.133 ± 0.001	0.000 ± 0.000	1.906 ± 0.001
1	2	0.995 ± 0.001	0.814 ± 0.001	1.011 ± 0.001
2	3	2.298 ± 0.002	2.273 ± 0.002	2.273 ± 0.001
3	4	2.332 ± 0.003	2.330 ± 0.003	2.557 ± 0.001

[a] Extended islands, $\theta = 10\%$
[b] Extended islands, $\theta = 20\%$
[c] Point islands, $\theta = 20\%$

Table 6.9: Best optimal values of β for $d = 3$ using bootstrap methods.

in the case of $i = 1$, the data from the models agree with $\beta = 3$ rather than $\beta = 2$. According to Table 6.8, in the $i = 1$ point island case the data is closer to 1. In other words, the data from our simulations suggests that $\beta = 1$ rather than the GWS's $\beta = 2$ or $\beta = 3$ as suggested by Shi *et. al.* After checking our simulation methods again, we are still unable to understand why these results differ.

6.4.2 The Validity of Convolution Equation

At this point, it is wise to mention that we consider only the 1-D point-island model for the rest of this chapter. This is because we are now investigating the GSD which is relevant for the 1-D model. In the case of the 1-D point-island model, assuming there is no correlation between the sizes of the two neighbouring gaps, then we recall the convolution equation for $P(s)$, the CZD with s being the

scaled capture zone size,

$$P(s) = 2\int_0^{2s} \phi(z)\phi(2s-z)dz, \tag{6.8}$$

where $\phi(z)$ is the GSD function with z being the scaled gap size. Here, we have used the data from MC simulations to determine whether there is correlation between the sizes of the two neighbouring gaps or not. In Figure 6.13, we have shown almost zero correlation between the sizes of two gaps for the $i = 1$ point-island case. The graphical representation for other values of i in the case of point and extended islands are similar to Figure 6.13.

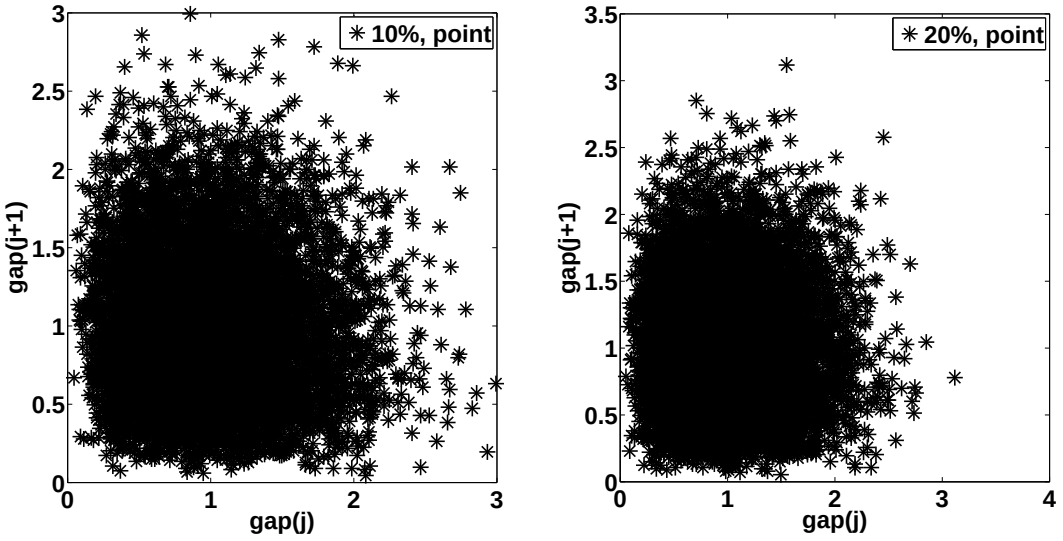

Figure 6.13: gap(j) vs. gap($j+1$) for $j \in \mathbb{Z}^+$ in the case of $i = 1$ and $d = 1$.

As we see in Table 6.10, there is **almost** zero correlation in the 1-D case. It is interesting to note that, at $\theta = 20\%$, the correlation of gaps for extended islands is consistently lower than those of point islands for the case of $i = 0$–3. We may need to revise equation (6.8) (equation (3.22) in Chapter 3): If there is weak correlation between the sizes of the two neighbouring gaps, then we have

i	20% [a]	20% [b]	40% [a]	100% [a]
0	-0.0737 ± 0.0035	-0.0420 ± 0.0034	-0.0782 ± 0.0028	-0.0746 ± 0.0023
1	-0.0519 ± 0.0017	-0.0267 ± 0.0019	-0.0520 ± 0.0017	-0.0540 ± 0.0012
2	-0.0567 ± 0.0026	-0.0383 ± 0.0028	-0.0536 ± 0.0024	-0.0537 ± 0.0025
3	-0.0523 ± 0.0036	-0.0362 ± 0.0041	-0.0569 ± 0.0032	-0.0627 ± 0.0034

[a] Point islands
[b] Extended islands

Table 6.10: Average correlation coefficients of sizes of two neighbouring gaps for $d = 1$.

$$P(s) \approx 2 \int_0^{2s} \phi(z)\phi(2s - z)dz, \tag{6.9}$$

as confirmed in the work of González *et. al.* [35].

6.4.3 Single-Gap Nucleation Rate

In Figure 6.14 we show the results for the average monomer density profile within gaps of size $g = 100$ and $g = 300$ for $i = 1$. For the smaller gap size, we see that the profile agrees well with the assumption made in the fragmentation equation approach, coinciding with the long-time steady-state solution of the diffusion equation with random deposition (6.1). This is typical for the lower end of the range of gap sizes that occur in the full simulation at higher coverage, for all the values of i that we have studied.

However, for the larger gap size $g = 300$ shown in Figure 6.14, we see that the monomer density profile falls a long way below the long-time prediction. This behaviour is typical for all values of i at the upper end of gap sizes found in our full simulations. The reason for the shortfall is the higher nucleation rate in the larger gaps; the average monomer density profile does not have sufficient time to reach its saturated level in (6.1) before a nucleation event occurs. As stated, the range of

gap sizes g used in the single-gap simulation is determined by the range typically seen in our full simulations. Therefore, this failure to reach the saturated monomer density profile with the large gaps can also be seen in our full simulation results (data not shown). This will have direct consequences for how the nucleation rate varies with gap size for larger gaps, as we now show.

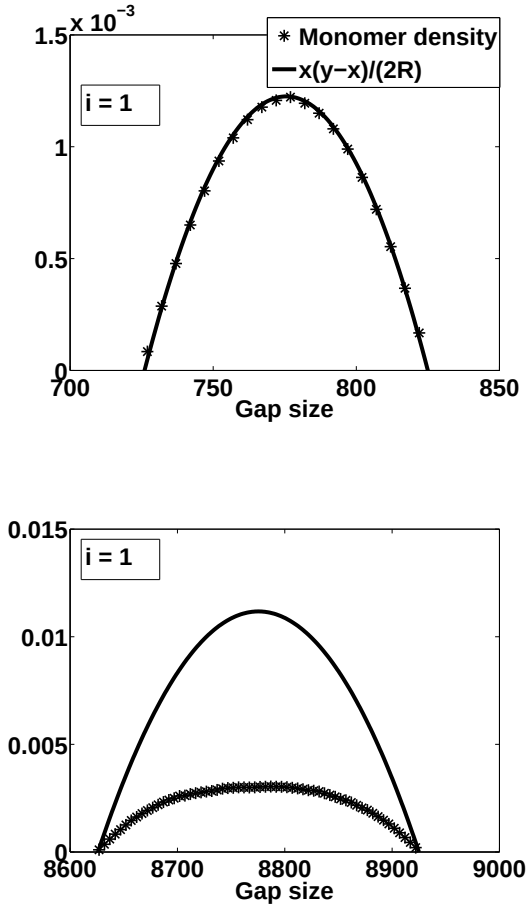

Figure 6.14: Monomer density profile in a single gap of size $g = 100$ (top) and $g = 300$ (bottom) for $i = 1$

In Figure 6.15 we show the average time for a nucleation event to occur $\langle t_{nuc} \rangle$ for all single gaps in the case of $i = 1$, 2 and 3 (note that the data for $i = 2$ and $i = 3$ have been shifted horizontally to avoid overlapping curves). We note

that the data obeys the power-law form predicted by the fragmentation equation approach for small gap sizes g, but as expected deviates strongly for larger gaps. In fact, the average time to nucleation becomes much higher than predicted by the use of the saturated monomer density profile, since the actual profile for the larger gaps is lower, therefore presenting slower than expected nucleation rates (but still fast compared to the time it takes for the monomer density to grow from zero to its saturation level).

The straight line fits in Figure 6.15 are for the small gap size data only ($g \in [50, 150]$). We use these to estimate how the nucleation rate varies with gap size g through $1/\langle t_{nuc} \rangle \propto g^{\gamma}$, with the values of the power γ reported in Table 6.11. We have used bootstrap methods with 1000 samples of size as large as the original to find an approximate 95% confidence interval in Table 6.11.

The fragmentation equation approach (as mentioned in Section 6.3 above) suggests that this power should be $2i + 1$ or $2i + 3$, depending on whether island nucleation is driven by monomer deposition or solely by monomer diffusion respectively. The results in Table 6.11 suggest that the simulation reflects both these mechanisms, with the small gap size nucleation rate exponent lying between these two possibilities.

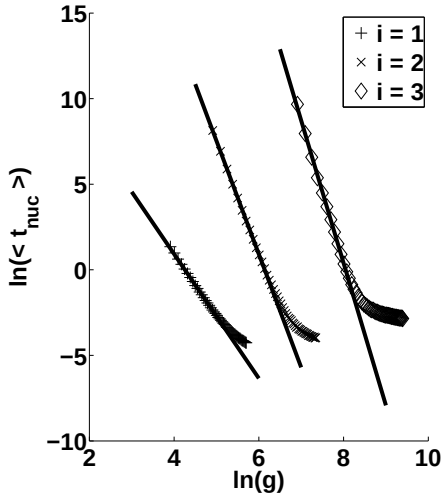

Figure 6.15: Average time for a nucleation event to occur at all gaps.

i	λ^{a}	λ^{b}	Simulation
1	3	5	3.630 ± 0.028
2	5	7	6.615 ± 0.097
3	7	9	8.296 ± 0.219

[a] $\lambda = 2i + 1$
[b] $\lambda = 2i + 3$

Table 6.11: Small gap nucleation rate exponents from the single gap simulations.

In Figure 6.16 we present histograms for the number of hops taken by the youngest monomer in an island for the $g = 100$ and $g = 300$ $i = 1$ simulations. The histogram has a long tail, showing that in many cases all the monomers in the island are indeed mature in the sense that they have diffused many times since their deposition. However, there is also a sharp increase in likelihood of a monomer only taking very few diffusive steps before being caught up in a nucleation event. In other words, there are a significant number of nucleation events driven by fluctuations due to deposition. This supports the conclusion that nucleation in these simulations is driven by a combination of deposition and diffusion fluctuations in

monomer density, helping to explain the intermediate values for the nucleation rate exponents in Table 6.11.

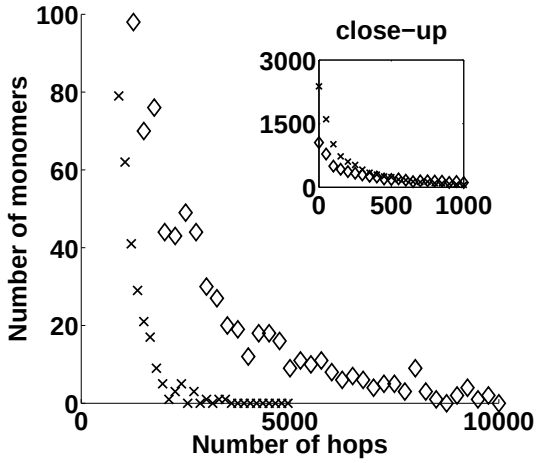

Figure 6.16: Histogram of the number of hops taken by the youngest monomer in an island for $i = 1$, for gap size $g = 100$ (crosses) and $g = 300$ (diamonds). In the main figure the number of monomers is truncated at 100. The inset shows the same result at the lower number of hops without truncation of the number of monomers in the histogram.

6.4.4 Full Simulation Behaviour

We can now look at our full MC simulations results as we have established the nucleation behaviour in single gaps. It is quite difficult to obtain exact solutions for the fragmentation equation approach, but such an approach provides concrete predictions for the small- and large-size behaviours of the GSD and CZD. We can establish which of the two theories is the better basis on which to understand the observed behaviour, by comparing the CZD properties with those of the GWS.

Our simulations were performed on lattices with 10^6 sites, with $R = 8 \times 10^6$ up to coverage $\theta = 100\%$, averaging results over 100 runs. For $i = 0$ we set the spontaneous nucleation probability to $p_n = 10^{-7}$. Recall that, in Section 6.2, we

need to ensure that point island densities at $\theta = 20\%$ and $\theta = 100\%$ for each i are less than the lattice of size 10^6. In Table 6.12, we confirm that these island densities are well short of the limit referred as in [65] and so the scaling for the ISD does not break down. As before, in Figure 6.17, there is a clear crossover between both monomer and island densities well within coverage $\theta = 100\%$ especially the $i = 3$ point-island case (occurs at $\theta \approx 50\%$).

i	$\langle c_j \rangle / len^{\mathrm{a}}$	$\langle c_j \rangle / len^{\mathrm{b}}$
0	0.282%	0.487%
1	0.954%	1.467%
2	0.416%	0.540%
3	0.215%	0.256%

[a] Point islands, $\theta = 20\%$
[b] Point islands, $\theta = 100\%$

Table 6.12: Average point island density, $\langle c_j \rangle$, at both coverage $\theta = 20\%$ and $\theta = 100\%$ for $d = 1$.

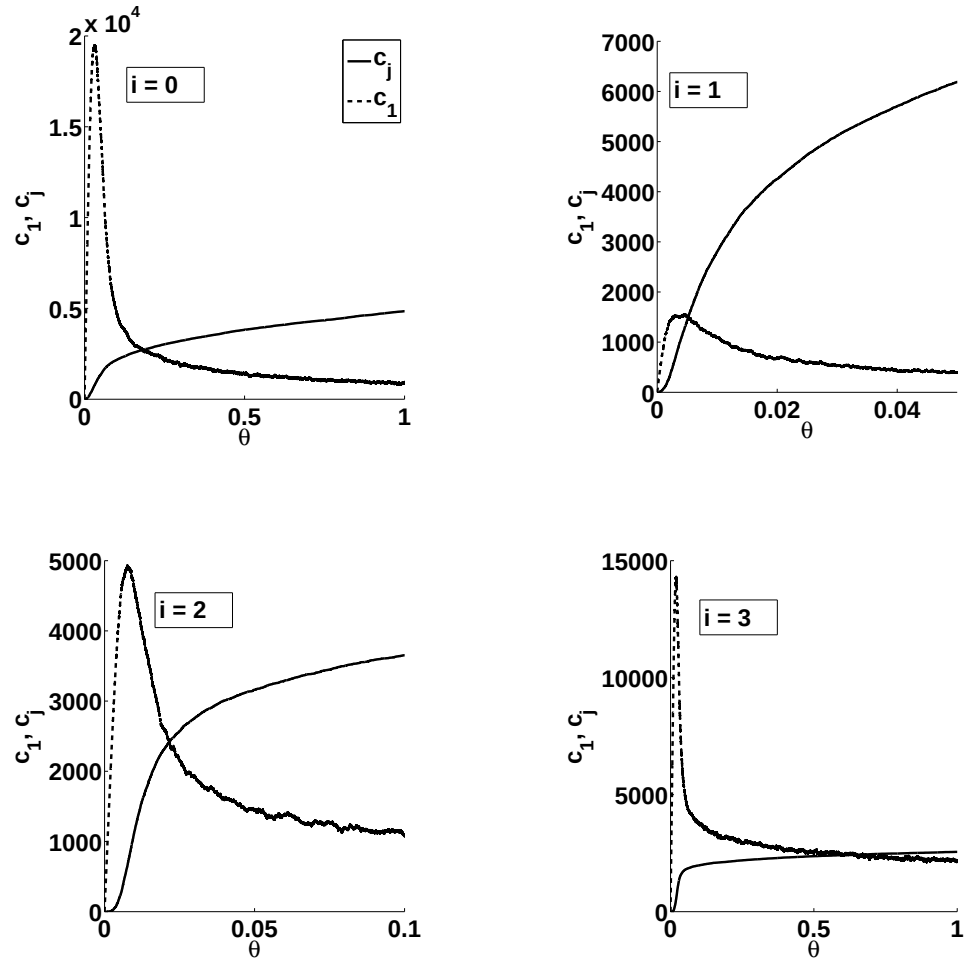

Figure 6.17: Monomers (c_1) and island (c_j) densities vs. coverage (up to $\theta = 100\%$) for 1-D point islands

6.4.4.1 Small-Size Scaling of the Gap Size and Capture Zone Distributions

In Figures 6.18 and 6.19, we report the small size behaviour of the GSD ($\phi(z)$) and CZD ($P(s)$) in logarithmic scale at $\theta = 20\%$. In order to fit the slopes in these plots, and obtain reliable error estimates, we adopt the following numerical technique. The size data are binned using regularly spaced bins on the logarithmic abscissa, with bin widths $b^m r$ where b and r are fixed constants and $m \geq 0$. By

choosing a range of values for $b = 1.1$, 1.2, 1.3 and 1.4, and $r = 0.0125$, 0.025 and 0.05, all of which provide reasonable choices for binning the data, we obtain a number of straight-line fits. This allows us to calculate the average of these gradients and a 95% confidence interval. The results of this fitting procedure are shown in Tables 6.13 and 6.14.

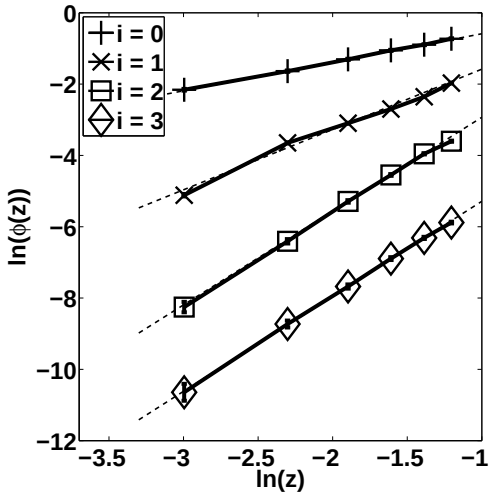

Figure 6.18: Small-size GSD in logarithmic scale for $i = 0$, 1, 2 and 3 at coverage $\theta = 20\%$. The dashed line is the straight-line fit to data.

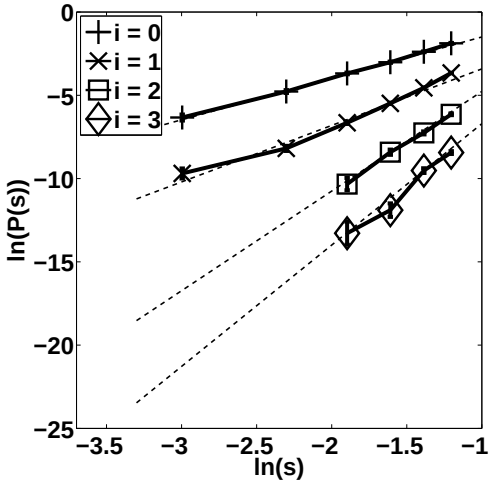

Figure 6.19: Small-size CZD in logarithmic scale for $i = 0$, 1, 2 and 3 at coverage $\theta = 20\%$. The dashed line is the straight-line fit to data.

For the small-size asymptotic behaviour of the GSD and CZD we compare the data from MC simulations with the fragmentation equation approach predictions of Section 6.3. For the GSD, the dominant term is z^{α_n} as $z \to 0$ (see (6.3)). Likewise, for the CZD the dominant term is $s^{2\alpha_n+1}$ (see (6.5)). For the latter, we also have the competing prediction of the GWS which is s^{β} (see (6.7)). The values from these theories are also displayed in Tables 6.13 and 6.14.

i	α_n [a]	α_n [b]	GSD[c]	GSD[d]
0	-	1	0.876 ± 0.033	0.905 ± 0.029
1	1	2	1.701 ± 0.045	1.579 ± 0.105
2	2	3	2.789 ± 0.080	2.718 ± 0.074
3	3	4	2.719 ± 0.082	3.271 ± 0.056

[a] $\alpha_n = i$
[b] $\alpha_n = i + 1$
[c] $\theta = 20\%$
[d] $\theta = 100\%$

Table 6.13: Average gradient for the small-size scaling of the GSD using different bin-widths at coverages $\theta = 20\%$ and 100%.

i	$2\alpha_n + 1$[a]	$2\alpha_n + 1$[b]	GWS[c]	CZD[d]	CZD[e]
0	-	3	2	2.730 ± 0.030	2.751 ± 0.086
1	3	5	4	4.187 ± 0.050	4.372 ± 0.149
2	5	7	6	5.883 ± 0.207	5.957 ± 0.187
3	7	9	8	7.200 ± 0.382	6.138 ± 0.124

[a] $\alpha_n = i$
[b] $\alpha_n = i + 1$
[c] $\beta = 2(i + 1)$
[d] $\theta = 20\%$
[e] $\theta = 100\%$

Table 6.14: Average gradient for the small-size scaling of the CZD using different bin-widths at coverages $\theta = 20\%$ and 100%.

Utilising bootstrap methods with 1000 samples of size as big as the original sample size we consider the average gradient of small GSD and CZD, and therefore find the approximate 95% confidence interval of these averages. Moreover, we have confirmed that these bootstrap results in Tables 6.15 and 6.16 (with much smaller errorbars due to the very large number of bootstrap samples) are consistent with the results in Tables 6.13 and 6.14.

i	${\alpha_n}$[a]	${\alpha_n}$[b]	GSD(20%)[c]	GSD(100%)[c]
0	-	1	0.946 ± 0.002	0.868 ± 0.001
1	1	2	1.741 ± 0.002	1.521 ± 0.001
2	2	3	2.893 ± 0.009	2.795 ± 0.008
3	3	4	2.638 ± 0.009	3.133 ± 0.014

[a] $\alpha_n = i$
[b] $\alpha_n = i + 1$
[c] $b^m r$ with $r = 0.0125$ & $b = 1.3$ ($i = 0$–2) & $b = 1.4$ ($i = 3$)

Table 6.15: Average gradient for the small-size scaling of the GSD using bootstrap methods at coverage $\theta = 20\%$ and 100%.

The results for the small-size scaling exponent of the GSD in Table 6.13 show that the fragmentation equation approach provides a reasonably sound framework for understanding the island nucleation and growth process. For $i = 1$, 2 and 3

i	$2\alpha_n + 1$[a]	$2\alpha_n + 1$[b]	GWS[c]	CZD(20%)[d]	CZD(100%)[d]
0	1	3	2	2.763 ± 0.008	2.585 ± 0.009
1	2	5	4	4.089 ± 0.013	4.356 ± 0.014
2	5	7	6	5.976 ± 0.030	6.133 ± 0.032
3	7	9	8	6.768 ± 0.021	6.181 ± 0.025

[a] $\alpha_n = i$
[b] $\alpha_n = i + 1$
[c] $\beta = 2(i + 1)$
[d] $b^m r$ with $r = 0.0125$ & $b = 1.3$ ($i = 0$–2) & $b = 1.4$ ($i = 3$)

Table 6.16: Average gradient for the small-size scaling of the CZD using bootstrap methods at coverage $\theta = 20\%$ and 100%.

we see that the exponent at $\theta = 100\%$ lies between the two possible values $\alpha_n = i$ and $\alpha_n = i + 1$ suggested by the theory. This is as expected following the single-gap nucleation results presented above, which show that both the deposition- and diffusion-driven nucleation mechanisms are at play in the simulations. We note that the $\theta = 20\%$ results for $i = 3$ lie below $\alpha_n = i = 3$, but we believe that this is due to the fact that the MC simulation has only just entered the aggregation regime in this case. We also see that for $i = 0$, the exponent is close to the $\alpha_n = i + 1 = 1$ prediction ($\alpha_n = 0$ is not a viable possibility), being closer at $\theta = 100\%$.

The trends shown in the small-size scaling exponent of the CZD in Table 6.14 are rather similar. We see the $i = 0$ data are close to the $\lambda = 2i + 3 = 3$ prediction of the fragmentation equation approach, being somewhat larger than the $\beta = 2(i+1) = 2$ predicted by the GWS. For $i = 1$ and 2 the data are bracketed by the two alternatives suggested by the fragmentation theory, as indeed is the GWS exponent which appears to present a reasonable compromise given the two alternative nucleation mechanisms. The case of $i = 3$ provides an exception, which hints at the breakdown of the relation in (6.9) between the GSD and the CZD. This will be discussed further in the conclusion section.

6.4.4.2 Large-Size Scaling of the Gap Size and Capture Zone Distributions

In Figures 6.20 and 6.21 we present the large-size behaviour of the GSD and CZD from the full simulations. The data are plotted in order to test the common large-size functional form suggested by the fragmentation equation approach for the GSD and by the GWS for the CZD, namely $\exp(-cz^p)$ (see (6.4) and (6.7)). In all cases, the data do conform well to this functional form. In addition, we perform fits to find the gradients p on these plots. In order to provide an estimate of the error in these fits, we adopt a similar strategy to that used above for the small-size scaling and bin the data using binwidths of size $0.01v$ with $v = 1, 2, ..., 20$. The results of this fitting procedure are presented in Tables 6.17 and 6.18 for the GSD and CZD respectively.

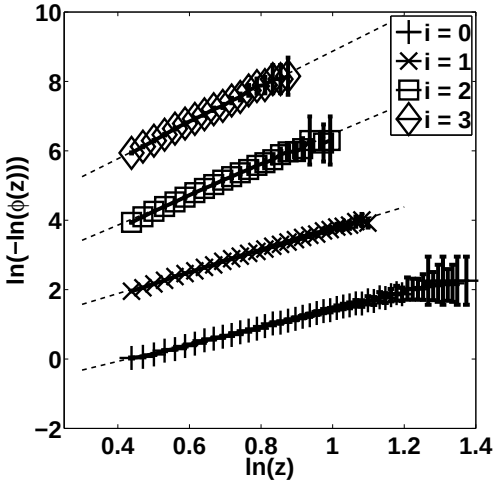

Figure 6.20: Large-size GSD in logarithmic scale for $i = 0$, 1, 2 and 3 at $\theta = 20\%$. The dashed line is the straight-line fit to data.

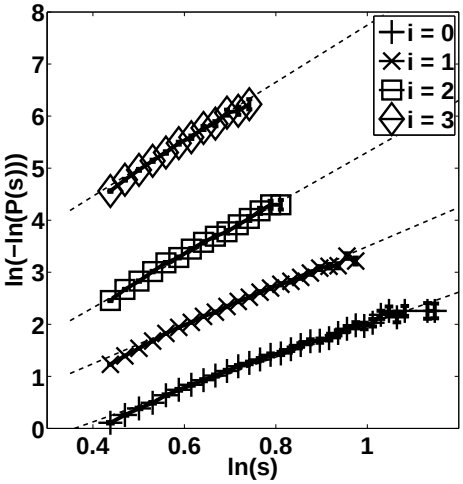

Figure 6.21: Large-size CZD in logarithmic scale for $i = 0$, 1, 2 and 3 at $\theta = 20\%$. The dashed line is the straight-line fit to data.

Once again we compare the exponents p from the MC simulation data with the theoretical predictions. For the GSD, the fragmentation equation approach predicts values of $2\alpha_n+1$ for p. For the CZD, the fragmentation equation prediction is $p = 3$ for $i = 0$ (see (6.6)) and we conjecture that the values for $i > 0$ will match those of the GSD. In contrast, the GWS prediction for the CZD is the universal value $p = 2$. The values from these theories are displayed in Tables 6.17 and 6.18.

i	α_n [a]	α_n [b]	GSD[c]	GSD[d]
0	-	3	2.515 ± 0.006	2.665 ± 0.007
1	3	5	3.130 ± 0.009	3.383 ± 0.008
2	5	7	4.364 ± 0.020	5.112 ± 0.025
3	7	9	5.094 ± 0.026	6.437 ± 0.034

[a] $\alpha_n = i$
[b] $\alpha_n = i + 1$
[c] $\theta = 20\%$
[d] $\theta = 100\%$

Table 6.17: Average exponents for the large-size scaling of the GSD using different bin-widths at coverage $\theta = 20\%$ and 100%.

i	$2i+3$[a]	GWS	CZD[b]	CZD[c]
0	3	2	3.108 ± 0.012	3.043 ± 0.043
1	-	2	3.721 ± 0.020	3.826 ± 0.021
2	-	2	4.946 ± 0.029	5.536 ± 0.033
3	-	2	5.464 ± 0.041	6.530 ± 0.042

[a] $\lambda = 2i + 3$
[b] $\theta = 20\%$
[c] $\theta = 100\%$

Table 6.18: Average exponents for the large-size scaling of the CZD using different bin-widths at coverage $\theta = 20\%$ and 100%.

Again, as before, to stay consistent with the results in Tables 6.17 and 6.18, we have calculated the gradient of large-size scaling of GSD and CZD using the bootstrap methods. In Tables 6.19 and 6.20, we also have confirmed good consistency between both set of results.

i	$2\alpha_n + 1$[a]	$2\alpha_n + 1$[b]	GSD[c]	GSD[d]
0	1	3	2.513 ± 0.001	2.656 ± 0.001
1	3	5	3.121 ± 0.001	3.372 ± 0.001
2	5	7	4.384 ± 0.004	5.139 ± 0.003
3	7	9	5.192 ± 0.004	6.504 ± 0.005

[a] $\alpha_n = i$
[b] $\alpha_n = i + 1$
[c] $\theta = 20\%$
[d] $\theta = 100\%$

Table 6.19: Average exponents for the large-size scaling of the GSD using bootstrap methods at coverage $\theta = 20\%$ and 100%.

In Table 6.17 we see that the fragmentation equation approach provides a useful point of reference to the observed large-size scaling exponents of the GSD. Again we see values that are bracketed by the two possible nucleation mechanisms for $i = 1$ and 2, whilst the behaviour for $i = 0$ is a little below the predicted exponent of $p = 3$. For $i = 3$ the data's exponent is below even that of the deposition-induced nucleation case. However, we have shown in Subsection 6.4.3 above that

i	$2i+3$[a]	GWS	CZD[c]	CZD[d]
0	3	2	3.131 ± 0.003	3.219 ± 0.007
1	-	2	3.762 ± 0.002	3.885 ± 0.003
2	-	2	4.981 ± 0.006	5.581 ± 0.005
3	-	2	5.511 ± 0.008	6.506 ± 0.008

[a] $\lambda = 2i + 3$
[b] $\theta = 20\%$
[c] $\theta = 100\%$

Table 6.20: Average exponents for the large-size scaling of the CZD using bootstrap methods at coverage $\theta = 20\%$ and 100%.

the monomer density profile does not reach its saturation value in larger gaps, so that the nucleation rate in these gaps is lower than predicted by the theory. This seems to provide a rational explanation for the discrepancies.

The results in Table 6.18 for the large-size scaling behaviour of the CZD are rather informative. We firstly observe that the MC data exponents do indeed mirror those of the GSD in Table 6.17 quite well. This means that the universal GWS prediction for $p = 2$ is always wrong. We also see that the concrete prediction for $i = 0$ from the fragmentation equations, namely $p = 3$, is well supported by the simulation data.

6.5 Conclusions

It was proposed that the capture zone distributions (CZDs) are described well by the Generalised Wigner Surmise (GWS). Therefore, it is of interest to study in more detail the validity of the GWS for the one-dimensional (1-D), two-dimensional (2-D) and three-dimensional (3-D) nucleation and growth models for point and extended islands.

As we see in Table 6.2, in the 1-D extended-island case for $i = 1$ and 2 the data fit the expected values of $\beta = 4$ and $\beta = 6$ respectively better than other integer

values of β. The results for point islands in the cases of $i = 1$ and $i = 2$ are similar to these for realistic islands. Monte Carlo (MC) data have also confirmed that for $i = 0$, β could be 3 rather than the expected value of $\beta = 2$. In [71], Shi *et. al.* found that the peak height of the CZD in $d = 1$ is higher than the GWS with $\beta = 4$ despite the fact that their simulation data is close to the predicted $\beta = 4$. Moreover, for $i = 3$, the data fit, respectively, $\beta = 6$ and $\beta = 7$ rather than $\beta = 8$ for extended and point islands.

As we see in Table 6.5, in the case of the 2-D model we have confirmed that the data for both point and extended islands agree with the GWS except that for the case of $i = 2$ the MC data suggested that β could be 4. Similarly, the case $i = 1$ for point islands found better agreement with $\beta = 3$. In [71], Shi *et. al.* found that in the case of $i = 1$, the data from the models agree with $\beta = 3$ rather than $\beta = 2$ which confirms our results.

Moreover, in Table 6.8, in the case of the 3-D model we have confirmed that the data for both point and extended islands disagree with the GWS. Also, in the case of the $i = 1$ point island model, we have found that the data is closer to $\beta = 1$ rather than the GWS's prediction $\beta = 2$. Note that in [71] Shi *et. al.* have found that β is closer to 3 according to their point island simulations. Despite the fact that our results are consistent with the results of Shi *et. al.* for the 1-D and 2-D cases, we were unable to agree with their result for the 3-D case and the explanation for this difference is unknown.

We have considered the convolution equation (6.8) for $P(s)$ in terms of $\phi(z)$ for the (1-D) model, under the assumption that the nucleation events have mixed up the gaps effectively so that nearest neighbour gaps are not correlated. By calculating the average correlation coefficients, we have found that there is almost zero correlation and this indicates that (6.8) may be approximate rather than

exact, albeit a rather good approximation

We have also investigated the 1-D point island nucleation and growth simulations in order to test out predictions for the asymptotics of the gap size and capture zone distributions. The work shows that the fragmentation equation approach provides a good framework in which to understand the MC simulation results. The theory can be used to investigate two cases for the nucleation process for $i > 0$, the first where nucleation is driven by deposition events, the second where fluctuations caused solely by monomer diffusion induce nucleation.

Firstly we presented single-gap simulation results which show that both these nucleation processes are active, so that the observed nucleation rates are bracketed by these two extremes. Furthermore, we showed that for larger gaps the average monomer density profile does not reach the long-time steady state assumed in the fragmentation equation. As a result, the nucleation rates in large gaps are slower than predicted by the theory, with the shortfall increasing with gap size. Therefore, the simple power-law scaling of the nucleation rate with gap size breaks down at larger sizes, with obvious consequences for the fragmentation equation predictions for the gap size distribution (GSD).

We note here that deviations from the original Blackman and Mulheran [14] predictions for the nucleation rate dependence on gap size have recently been observed for the $i = 1$ 1-D model [35]. In this work, the authors report that the nucleation rate has two regimes; for small sizes, it approximately obeys s^4, whilst at larger sizes it approximately follows s^3. The latter power-law feeds into the asymptotic form of the GSD and hence the CZD, yielding the functional form $\exp(-s^3)$. We note here that these values are close to those we find for $i = 1$ in Table 6.11 for the small gap nucleation rates and Tables 6.17 and 6.18 for the large-size GSD and CZD scaling. We therefore propose that the explanations

presented here in terms of competing nucleation mechanisms and unsaturated monomer density profiles will also explain the results reported in [35].

We then presented data for the full island nucleation and growth simulation. For the small-size GSD scaling, we found results consistent with the fragmentation equation predictions for $i = 0$. For $i = 1$, 2 and 3 the exponents were bracketed by the values for the alternative nucleation mechanisms as expected. For the large gap size scaling, the MC data followed the functional form suggested by the fragmentation theory, with the exponents again being largely bracketed by the predicted values, although the breakdown of the nucleation rate scaling is apparent, especially for larger i.

In the case of the CZD, we once again successfully placed the observed simulation data into the context provided by the fragmentation equation. Interestingly, the GWS predictions for the small-size CZD scaling work extremely well since they bisect the exponents from the alternative nucleation mechanisms. As discussed elsewhere [37], the predicted formula for the parameter β of the GWS can be brought into line with either nucleation mechanism following the arguments of Pimpinelli and Einstein [62], but the original prediction of these authors, (3.40), does seem to speak well for their physical intuition [61].

However, the predicted GWS form for the large-size CZD scaling fails badly when confronted with our 1-D point island simulation results. This is in contrast to recent tests performed using two-dimensional (2-D) substrates [57], which suggests that there is something unique to the 1-D case, possibly due to the topological constraints in how capture zones are constructed from the inter-island gaps. This aspect is worthy of further investigation.

In order to predict the asymptotics of the CZD, we have assumed that the capture zones can be constructed from pairs of gaps sampled randomly for the

GSD (see (6.8)). This is valid provided that the nucleation has effectively mixed up the gaps so that nearest neighbours are no longer correlated [14]. One consequence is that the small-size exponents of the CZD (say p_1) are related to those of the GSD (say p_2) through $p_1 = 2p_2 + 1$. Looking at the results in Tables 6.13 and 6.14, we see that this relationship is reasonably obeyed for $i = 0$ and 1 but starts to break down for $i = 2$ and 3. This is perhaps understandable, since for the higher critical island sizes, the nucleation rate slows down dramatically over time suggesting less well-mixed systems. This is another point for further consideration in future theory development work.

Despite the limitations of the fragmentation equation approach used in this work, such as its failure to capture the time-dependent nature of the monomer density profile within gaps, it has provided an excellent theoretical framework from which to consider the island nucleation process. Hence, alongside the points discussed above, future work might also look at how the fragmentation kernels can incorporate this time dependence, and how the two nucleation mechanisms can be combined into a consistent set of fragmentation equations.

Chapter 7

The Distributional Fixed Point Equation Approach

7.1 A Retrospective Approach

The island size and capture zone distributions (ISD and CZD respectively) that underlie the island growth rates evolve towards scaling forms despite the on-going nucleation of new islands with continued fragmentation of the existing capture zones [52]. Furthermore, the form of the scaling functions depends on the critical island size i, where $i+1$ is the smallest stable island size. A number of theoretical approaches, such as the rate-equation approach considered in Chapter 4, have been used to model this behaviour, ranging from rate equations which neglect the variation in capture zone sizes [3, 6, 10, 67] due to spatial arrangements of the islands, to those which attempt to include this information explicitly [4, 11, 14, 32, 54, 55]. An example of this latter approach is the fragmentation theory approach considered originally by Blackman and Mulheran, and extended in Chapters 5 and 6. All these approaches can be characterised as forward-looking in the sense

that they are based on predicting how the size distributions evolve as new islands nucleate.

In this chapter we present an alternative, retrospective point of view where we ask how the capture zones present in the system came to be created. This approach was inspired by Seba [70] where he investigated a one-dimensional (1-D) model aimed at describing the spacing distribution between cars parked in an infinitely long street to ensure that any gap which is large enough for a car to park in according to the probability $f(a)$, described below. To describe this spacing distribution approximately in the 1-D car-parking problem, Seba derived the distributional fixed point equation (DFPE)

$$X_d \stackrel{\triangle}{=} a(1 + X_d).$$

Here X_d is the distance between two parked cars, a is an independent random variable with a probability density $f(a)$ and the symbol $\stackrel{\triangle}{=}$ means that the left- and right-sides of the above DFPE have the same distribution. More details about this model can be found in Chapter 3.

In this thesis, we focus on the case of point island nucleation in a 1-D system since this allows for more complete analysis and comparisons with results from a more traditional fragmentation theory approach in Chapters 5 and 6. This new perspective provides interesting insight into why scaling occurs as well as yielding excellent comparisons with our simulation data.

The aim of this chapter is to investigate the effectiveness of the integral equation (IE) counterpart of the DFPE for the gap size and capture zone distributions. We do this by comparing solutions to the IE with data from Monte Carlo (MC) simulations, and investigating the moments and small/large-size asymptotics of the IE. We have also included Treat's function for the gap size distribution (GSD), as

derived in Chapter 5, as a useful benchmark in comparing the MC data and the IE in the case of $i = 0$ only. Once we have carried out the analysis for both the GSD and CZD, we compare these to the MC data and determine how well the IEs fare.

7.2 Analysis of the Scaled Gap Size Distribution

A point island approximation is often used both for clarity and because it approximates the growth of small, well-separated islands, and 1-D systems occur experimentally during island growth at substrate steps. Here we employ the same 1-D model as in Chapters 5 and 6.

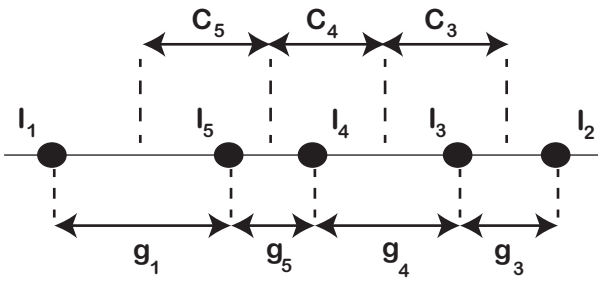

Figure 7.1: The islands numbered I_1–I_5 on the 1-D substrate. The gaps between the islands are labelled g_1, g_5, g_4 and g_3, and the capture zones of islands I_5, I_4 and I_3 are labelled C_5, C_4 and C_3 respectively.

Figure 7.1 illustrates some islands nucleated on the lattice, which are numbered by the times of their birth. In other words, the island I_1 is the oldest. Each island has its own capture zone with its size being the bisection of this island's two neighbouring gaps.

The creation of gap g_5 was formed by the nucleation of the young island, I_5, in Figure 7.1, which occurred in the gap of size $(g_1 + g_5)$ between older islands I_1 and I_4. In general, any randomly chosen gap with scaled size z in the system will

occur by the fragmentation of a larger gap formed by the combination of $z + z_n$ where z_n (say) is a neighbouring gap size. In general we do not have the benefit of the chronological ages to guide us, so we make a mean field approximation for the size of the neighbouring gap, namely $z_n = 1$. Then we have the following DFPE [70] for the gap size distribution (GSD) $\phi(z)$

$$z \stackrel{\triangle}{=} a(1 + z), \tag{7.1}$$

where gap splits into proportions a and $1 - a$.

Before we progress further, we note that in Seba's 1-D car-parking problem [70], any car is free to leave - this renders this model reversible, which is not the same as in the 1-D nucleation and growth of irreversible islands studied in this thesis. However, we suggest the following argument in considering reversibility versus irreversibility. First, we consider the 1-D model and the population of gaps once we have reached the scale-invariant regime. The ongoing nucleation in any system will cause the mixing of gaps; this in itself presents an opportunity. In a well-mixed system it is common to make a mean-field approximation. Say we are to choose any existing gap – created by the fragmentation of a larger gap of size $z + z_s$ – we can then capture the essential physics of the system by replacing z_s by the average size $\langle z_s \rangle = 1$. We then arrive at the DFPE as described above. An interesting point to note is that the DFPE is as much an approximation to Seba's 1-D car-parking problem as it is to the island nucleation system.

As noted in Chapter 5 and [14], in the aggregation regime, we derive the probability $f(a)$ of fragmenting a gap into proportions a and $(1 - a)$ from the steady-state monomer density profile. We obtain $f(a)$ in the form of the normalised beta distribution

$$f(a) = \frac{a^{\alpha_n}(1-a)^{\alpha_n}}{B(\alpha_n+1,\alpha_n+1)} = \frac{(2\alpha_n+1)!}{(\alpha_n!)^2}\ a^{\alpha_n}(1-a)^{\alpha_n}, \tag{7.2}$$

where α_n reflects the dominant nucleation mechanism. Recall, from Chapter 6, that we define $\alpha_n = i+1$, $i \geq 0$ for nucleation resulting from the diffusion of mature monomers, and $\alpha_n = i$, $i \geq 1$ for nucleation triggered by deposition of monomers. Note that for the $i = 0$ spontaneous nucleation, only the $\alpha_n = i + 1$ model is physically reasonable, since there is no possibility of a monomer depositing close to a pre-existing critical island size of i in this case.

Following the analysis in [59, 70], we obtain an IE which is equivalent to the DFPE (7.1)

Proposition 7.2.1. *For the gap size distribution, $\phi(z)$, the following integral equation*

$$\phi(z) = \int_0^{\min(z,1)} \phi\left(\frac{z}{a} - 1\right) \frac{f(a)}{a} da, \tag{7.3}$$

is derived from the distributional fixed point equation (7.1).

Proof. Suppose we have a cumulative density function (CDF), $\Phi(z) = 0$ (say) if

$z < 0$. Then we have

$$\begin{aligned}
\Phi(z) &= Prob[z_1 \le z] \\
&= Prob[a(1+z_1) \le z] \quad \text{[from (7.1)]} \\
&= E[\ Prob[a(1+z_1) \le z \mid a]\ ] \quad \text{[by the properties of conditional expectations]} \\
&= \int_0^1 Prob[a(1+z_1) \le z] f(a) da \quad \text{[by the definition of } E\text{]} \\
&= \int_0^1 Prob[z_1 \le z/a - 1] f(a) da \\
&= \int_0^1 \Phi(z/a - 1) H(z/a - 1) f(a) da,
\end{aligned}$$

where $H(\cdot)$ is the Heaviside function since $\Phi(z_1) = Prob[z_1 \le a]$ and since $\Phi(z) = 0$ if $z < 0$. Hence the CDF satisfies

$$\Phi(z) = \int_0^{\min(z,1)} \Phi\left(\frac{z}{a} - 1\right) f(a) da. \tag{7.4}$$

Now, since the probability density function is the derivative of the CDF, we would like to differentiate $\Phi(z)$ with respect to z and use the Leibniz rule. However, it is not clear whether $\Phi(z)$ is differentiable or not. Since we know that $f(a)$ is differentiable, we change variables to $w = z/a - 1$ to obtain

$$\Phi(z) = z \int_{\max(0,z-1)}^{\infty} \Phi(w) f\left(\frac{z}{w+1}\right) \frac{1}{(w+1)^2}\ dw.$$

We can differentiate the right-hand side of the above equation for all z and so we can also differentiate the left-hand side. Having established that we can differentiate $\Phi(z)$ with respect to z, we return to (7.4). However, it is not clear whether equation (7.4) is differentiable at $z = 1$. So, we carefully consider two cases $z < 1$ and $z > 1$. In the case of $z < 1$, we obtain

$$\Phi(z) = \int_0^z \Phi\left(\frac{z}{a} - 1\right) f(a)da,$$

and, by differentiation, we also obtain

$$\Phi'(z) = \phi_l(z) = \Phi(0)f(z) + \int_0^z \phi\left(\frac{z}{a} - 1\right) \frac{f(a)}{a}\, da.$$

Similarly, for the case of $z > 1$, we obtain

$$\Phi(z) = \int_0^1 \Phi\left(\frac{z}{a} - 1\right) f(a)da,$$

and, by differentiation, we also obtain

$$\Phi'(z) = \phi_r(z) = \int_0^1 \phi\left(\frac{z}{a} - 1\right) \frac{f(a)}{a}\, da.$$

Taking left-sided and right-sided limits, we have

$$\lim_{z\to 1^-} \phi_l(z) = \int_0^1 \phi\left(\frac{z}{a} - 1\right) \frac{f(a)}{a}\, da,$$

and

$$\lim_{z\to 1^+} \phi_r(z) = \int_0^1 \phi\left(\frac{z}{a} - 1\right) \frac{f(a)}{a}\, da.$$

Thus, by the sandwich theorem, we obtain

$$\phi(z) = \int_0^{\min(z,1)} \phi\left(\frac{z}{a} - 1\right) \frac{f(a)}{a}\, da.$$

□

In Figure 7.2 we show the convergence of iterates of equation (7.3), with $f(a)$ given by equation (7.2). The limit satisfies the DFPE (7.1), and so is the form (7.3)

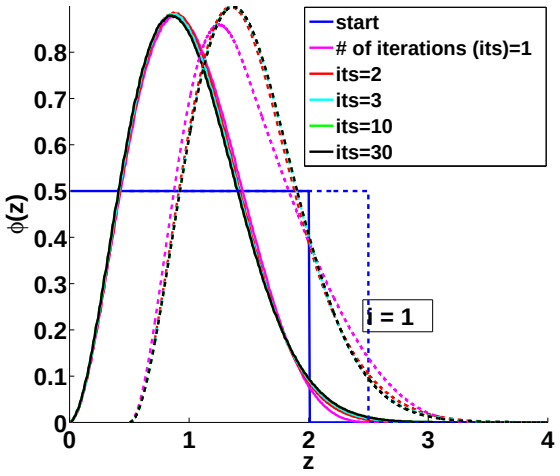

Figure 7.2: The evolution of gap size distribution under iteration of (7.3) with $i = 1$. The solid lines are for $\alpha = i + 1$ in (7.2), and the broken lines for $\alpha = i$, where the broken lines are shifted along the abscissa for clarity.

that we wish to compare to the scale-invariant GSD found in the MC simulations.

Moreover, if we let $w = z/a - 1$, then we can rewrite (7.3) as

$$\begin{aligned}\phi(z) &= \int_{\infty}^{\max(0,z-1)} \phi(w) f\left(\frac{z}{w+1}\right)\left(\frac{w+1}{z}\right)\left(-\frac{z}{(w+1)^2}\right)\, dw \\ &= \int_{\max(0,z-1)}^{\infty} \phi(w) f\left(\frac{z}{w+1}\right)\frac{1}{w+1}\, dw.\end{aligned}$$

It is interesting to see how the solutions to the DFPE (7.3) compare to those of the fragmentation theory, for which the asymptotic behaviours are known in Chapters 5 and 6. In fact, if $f(a) = a^{\alpha_n}(1-a)^{\alpha_n}/B(\alpha_n+1, \alpha_n+1)$, then for small z

$$f\left(\frac{z}{w+1}\right) = \frac{1}{B(\alpha_n+1,\alpha_n+1)}\frac{z^{\alpha_n}}{(w+1)^{\alpha_n}}\left(1-\frac{z}{w+1}\right)^{\alpha_n} \sim \frac{1}{B(\alpha_n+1,\alpha_n+1)}\frac{z^{\alpha_n}}{(w+1)^{\alpha_n}},$$

and so

$$\phi(z) \sim \frac{z^{\alpha_n}}{B(\alpha_n+1,\alpha_n+1)}\int_0^\infty \frac{\phi(w)}{(w+1)^{\alpha_n+1}}\,dw.$$

Hence, for small z we obtain

$$\phi(z) = \mathcal{O}\left(f\left(\frac{z}{w+1}\right)\right),$$

which shows that ϕ has the same behaviour as f. In other words, for small z we have $\phi(z) \sim kz^\alpha$ for some constant k.

We can quantify the performance of the solutions using the m^{th} moments Z_m of the distributions. Following the analysis (and the notation used) in [44], from (7.1) we have

$$\begin{aligned} Z_m = \langle z^m\rangle = \langle (a(1+z))^m\rangle &= \langle \sum_{k=0}^{m} \frac{m!}{k!(m-k)!}\, a^m z^k\rangle \\ &= \sum_{k=0}^{m} \frac{m!}{k!(m-k)!}\langle a^m\rangle\langle z^k\rangle, \end{aligned} \tag{7.5}$$

where

$$\langle a^m \rangle = E[a^m] = \int_0^1 a^m f(a)\, da \quad = \frac{1}{B(\alpha_n + 1, \alpha_n + 1)} \int_0^1 a^{m+\alpha_n} (1-a)^{\alpha_n}\, da$$

$$= \frac{B(m + \alpha_n + 1, \alpha_n + 1)}{B(\alpha_n + 1, \alpha_n + 1)} \tag{7.6}$$

$$:= B_m. \tag{7.7}$$

Hence, from (7.5) we find the following recursive relationship, with $\langle z^k \rangle = Z_k$,

$$Z_m = B_m \sum_{k=0}^{m} \frac{m!}{k!(m-k)!} Z_k, \tag{7.8}$$

and B_m as defined above.

7.2.1 A DFPE without a Mean-Field Approximation Assumption for the Gap Size Distribution

In deriving equations (7.1) and (7.3) in the previous section, we invoke a mean-field approximation for the size of the neighbouring gap, putting $y = 1$. We could instead find the fixed point of the following DFPE that does not make a mean-field assumption:

$$z \stackrel{\triangle}{=} a(z_1 + z_2), \tag{7.9}$$

where the gaps z_1 and z_2 are, independently, drawn from the same distribution as z. As before a is drawn from the probability distribution $f(a)$ of equation (7.2). Then instead of (7.3) we have the integral equation

Proposition 7.2.2. *For the gap size distribution, $\phi(z)$, the following integral equation*

$$\phi(z) = \int_0^1 \int_0^{z/a} \phi\left(\frac{z}{a} - z_1\right) \phi(z_1) \frac{f(a)}{a} \, dz_1 \, da, \tag{7.10}$$

is derived from the distributional fixed point equation (7.9).

Proof. As before, suppose we have a cumulative density function (CDF), $\Phi(z)$ (say). Then we have

$$\begin{aligned}
\Phi(z) &= Prob[a(z_1 + z_2) \leq z] \\
&= E[\ Prob[a(z_1 + z_2) \leq z \mid a]\ ] \quad \text{[by the properties of conditional expectations]} \\
&= \int_0^1 Prob[a(z_1 + z_2) \leq z] f(a) \, da \quad \text{[by the definition of } E \text{ and } z \in [0, \infty)] \\
&= \int_0^1 E[\ Prob[a(z_1 + z_2) \leq z] \mid z_1] f(a) \, da \\
&= \int_0^1 \int_0^{z/a} Prob[a(z_1 + z_2) \leq z] \phi(z_1) f(a) \, dz_1 \, da \quad \text{[since } z/a - z_1 \geq 0] \\
&= \int_0^1 \int_0^{z/a} Prob[z_2 \leq z/a - z_1] \phi(z_1) f(a) \, dz_1 \, da \\
&= \int_0^1 \int_0^{z/a} \Phi(z/a - z_1) \phi(z_1) f(a) \, dz_1 \, da.
\end{aligned}$$

We differentiate with respect to z to obtain

$$\phi(z) = \int_0^1 \int_0^{z/a} \phi\left(\frac{z}{a} - z_1\right) \phi(z_1) \frac{f(a)}{a} \, dz_1 \, da.$$

□

Convergence of iterates of (7.10) are shown in Figure 7.3, we show the limit satisfies the DFPE (7.1).

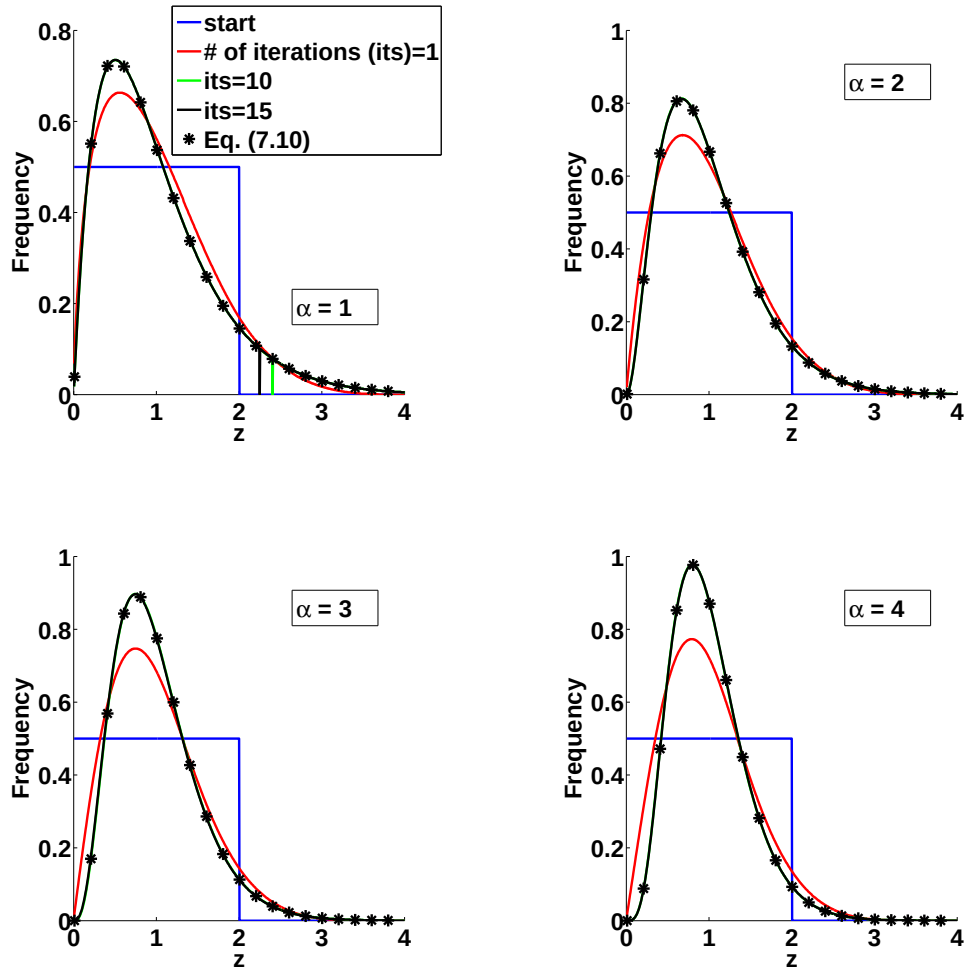

Figure 7.3: The evolution of gap size distribution under iteration of (7.10) with $\alpha = 1 - 4$.

Equation (7.9) with $f(a)$ as in (7.2) is considered by Dufresne in [29, p.289], where it is shown that the fixed point is given by a gamma distribution. Explicitly the fixed point probability distribution is

$$\Gamma(\alpha+1,\nu,z) = \frac{z^{\alpha}\exp(-z/\nu)}{\Gamma(\alpha+1)\nu^{\alpha+1}}.$$

The mean of the above gamma distribution is $(\alpha+1)\nu$ and so, by setting $(\alpha+1)\nu = 1$, we rescale z to unity to obtain

$$\Gamma\left(\alpha+1, \frac{1}{\alpha+1}, z\right) = \phi_\alpha(z) = \frac{(\alpha+1)^{\alpha+1}}{\Gamma(\alpha+1)} z^\alpha \exp(-(\alpha+1)z). \tag{7.11}$$

Note that if we assume (7.11), then for small z we obtain $\phi(z) \sim kz^\alpha$ for some constant k. In Figure 7.3, this gamma distribution is shown by the stars. It is apparent that the iterations converge to the form (7.10), confirming the result obtained by Dufresne in [29].

7.2.2 Treat's Gap Size Distribution Function Revised

Recall that in Chapter 5, for the $i = 0$ case we were able to use the fragmentation approach combined with Treat's results to obtain

$$\phi(x) = \frac{3x^2}{\Gamma(\frac{2}{3})\mu^3} \int_{(x/\mu)^3}^{\infty} u^{-4/3} e^{-u}\, du, \tag{7.12}$$

where

$$\mu = \frac{4}{3}\Gamma\left(\frac{2}{3}\right).$$

The moments of (7.12) T_m (note the different notation, T_m being used rather than ϕ_m as introduced in Chapter 5) are

$$T_m = \frac{3\mu^{m+3}}{\mu^3(m+3)\Gamma(\frac{2}{3})} \int_0^{\infty} u^{(m-1)/3} e^{-u}\, du,$$

i.e.

$$T_m = \frac{3\mu^m \Gamma(\frac{1}{3}(m+2))}{(m+3)\Gamma(\frac{2}{3})}, \tag{7.13}$$

where the calculation for (7.13) has already been done in Chapter 5. Also, in

that chapter, we have confirmed that the zeroth and first moments of (7.13) are 1 as expected. Now, in the case of $i = 0$ we can compare (7.12) and its moment (7.13) to the IE (7.3) and its moments (7.8) respectively. In the Result section of the current chapter, we discuss how well the moments, small- and large-size asymptotics of (7.3) compare with those of the MC data for the GSD.

7.3 Analysis of the Scaled Capture Zone Distribution

We recall that one possible way of obtaining the CZD is from the GSD via the convolution equation (3.22) assuming that there is no correlation between the size of two neighbouring gaps. In turn, we know that the CZD can be obtained from the GSD through the random pairing of gaps such that

$$s \stackrel{\triangle}{=} \frac{1}{2}(z_1 + z_2),$$

where s is the scaled capture zone size and, for two gap sizes z_1 and z_2,

$$z_1 \stackrel{\triangle}{=} a(z_1 + z_{n_1});\ z_2 \stackrel{\triangle}{=} b(z_2 + z_{n_2}),$$

where z_{n_1} and z_{n_2} are neighbours to be replaced by averages and we have a and $b \neq a \in (0, 1)$ with the identical distribution (7.2). Invoking a mean field approximation such that z_{n_1} and z_{n_2} may be replaced by the average $\langle z \rangle = 1$ in the above equation yielding

$$s \stackrel{\triangle}{=} \frac{1}{2}(a(1 + z_1) + b(1 + z_2)) \stackrel{\triangle}{=} \frac{1}{2}(a + aa_1 + aa_1a_2 + \cdots + b + bb_1 + bb_1b_2 + \cdots),$$

where $a \neq a_1 \neq a_2 \neq \cdots$ and $b \neq b_1 \neq b_2 \neq \cdots \in (0,1)$ as defined earlier, and the latter relation is obtained by the iterations.

However, in Chapter 6 and [35], there are weak correlations between the sizes of two neighbouring gaps. We need to carefully consider the evolution of the capture zones in the system. In Figure 7.4 (akin to Figure 7.1), each island has its own capture zone with its size, s_1, s_2, s, s_4 and s_2 respectively, being the bisection of this island's two neighbouring gaps.

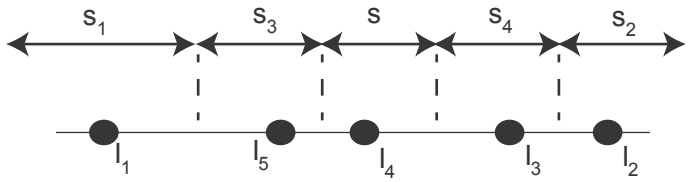

Figure 7.4: The sizes of capture zones of islands (black circles) are labelled s_1, s_2, s, s_4 and s_2 respectively.

From Figures 7.1 and 7.4, the capture zone of size s was created by the fragmentation of the parent capture zone of size $(s_3 + s + s_4)$ caused by the nucleation of an island I_5. Since s can be viewed as the fragmentation of part of s_3 (to the right of an island I_3) and part of s_4 (to the left of an island I_4) we may write on average

$$s \stackrel{\triangle}{=} \frac{a}{2}(s + s_3) + \frac{b}{2}(s + s_4). \tag{7.14}$$

However, as the nucleation and growth of islands stage has progressed, we do not know how much of the neighbouring capture zones to take, nor indeed how large these zones are. Moreover, as discussed for the GSD, we too do not have the benefit of the chronological ages to assist us. So, we can again invoke a mean field approximation, $s_3 = 1$ and $s_4 = 1$ for these nearest neighbour correlations to find

the following DFPE for a general (scaled) capture zone

$$s \stackrel{\triangle}{=} \frac{1}{2}(a+b)(1+s), \tag{7.15}$$

where we must emphasise that the DFPE (7.15) uses a mean field approximation. Equation (7.15) can be solved by iterations

$$s \stackrel{\triangle}{=} \frac{1}{2}\left[(a+b) + \frac{1}{2}(a+b)(a_1+b_1) + \frac{1}{4}(a+b)(a_1+b_1)(a_2+b_2)\cdots\right].$$

In (7.15), the proportions a and b are, respectively, independently drawn from $f(a)$ and $f(b)$ of (7.2). It is important to note that the derivation of the DFPE (7.15) is independent of those for the GSD. This raises the possibility of constructing a similar DFPE for higher dimension substrates without having to rely on the GSD.

An equivalent IE, like that of (7.3), can be identified for (7.15). Then we have the IE for the CZD, $P(s)$

$$P(s) = \int_0^{\min(s,1)} P\left(\frac{s}{a_s} - 1\right) \frac{f_s(a_s)}{a_s}\, da_s. \tag{7.16}$$

The exact form of $f_s(a_s)$ is unknown but we can calculate numerically a_s by the following formula

$$a_s = \frac{(a+b)}{2},$$

such that a and b are drawn from (7.2). The function $f_s(a_s)$ is obtained by generating a set of MC values of a and b using simulations such that

$$a_{s,j} = \frac{(a_j + b_j)}{2}.$$

We can easily quantify the performance of the solutions to (7.16) using the m^{th} moments S_m for the CZDs. Following the analysis in [44], from (7.15)

$$\begin{aligned} S_m = \langle s^m \rangle &= \langle \left(\frac{1}{2}(a+b)(1+s) \right)^m \rangle \\ &= \frac{1}{2^m} \sum_{k=0}^{m} \frac{m!}{k!(m-k)!} \langle a^{m-k} \rangle \langle b^k \rangle \sum_{p=0}^{m} \frac{m!}{p!(m-p)!} \langle s^p \rangle. \end{aligned} \tag{7.17}$$

Here, we have

$$\langle a^{m-k} \rangle = \int_0^1 a^{m-k} f(a) \, da = \frac{B(m-k+i+2, i+2)}{B(i+2, i+2)} = B_{m-k},$$

where B_{m-k} is defined by (7.6). Similarly, we also have $\langle b^k \rangle = B_k$. Referring back to (7.17) we find the following recursive relationship, with $\langle s^p \rangle = S_p$,

$$S_m = \left(\frac{1}{2} \right)^m \sum_{k=0}^{m} \frac{m!}{k!(m-k)!} B_{m-k} B_k \sum_{p=0}^{m} \frac{m!}{p!(m-p)!} S_p. \tag{7.18}$$

For obtaining the moments of the GWS, $P_\beta(s)$, by a similar analysis to that used for the moment of (7.15),

$$\begin{aligned} G_m &= \int_0^\infty s^m P_\beta(s) \, ds \\ &= a_\beta \int_0^\infty s^{m+\beta} e^{-b_\beta s^2} \, ds \\ &= \frac{a_\beta}{2 b_\beta^{(m+\beta+1)/2}} \int_0^\infty u^{(m+\beta+1)/2-1} e^{-u} \, du \\ &= \frac{a_\beta \Gamma\left(\frac{1}{2}(m+\beta+1) \right)}{2 b_\beta^{(m+\beta+1)/2}}. \end{aligned} \tag{7.19}$$

Recall from Chapter 3 that

$$a_\beta = \frac{2\Gamma\left(\frac{\beta+2}{2}\right)^{\beta+1}}{\Gamma\left(\frac{\beta+1}{2}\right)^{\beta+2}};\ b_\beta = \left(\frac{\Gamma\left(\frac{\beta+2}{2}\right)}{\Gamma\left(\frac{\beta+1}{2}\right)}\right)^2,$$

and, from this, we can write the following expression

$$\frac{a_\beta}{2b_\beta^{(m+\beta+1)/2}} = \frac{2\Gamma\left(\frac{\beta+2}{2}\right)^{\beta+1}/\Gamma\left(\frac{\beta+1}{2}\right)^{\beta+2}}{2\Gamma\left(\frac{\beta+2}{2}\right)^{m+\beta+1}/\Gamma\left(\frac{\beta+1}{2}\right)^{m+\beta+1}}.$$

Thus, from (7.19) and the definition of $\beta = 2(i+1)$ for the 1-D model, we obtain the moments of the GWS

$$G_m = \frac{\Gamma(i+3/2)^{m-1}\Gamma(i+(m+3)/2)}{(i+1)!^m}. \tag{7.20}$$

In the Results section, we discuss how well the moments, small- and large-size asymptotics of both (7.16) and the GWS compare with those of the MC data for the CZD.

7.4 Monte Carlo Simulation

This is essentially the same simulation as the one used in Chapter 6. Recall that monomers are deposited onto an initially empty 1-D array of sites representing the substrate at a rate F monolayers per unit time. Deposited monomers perform random hops between nearest neighbour lattice sites within periodic boundary conditions; this diffusion occurs at the rate D. In the case $i > 0$, a new island is nucleated when the number of monomers at any one site exceeds the critical island size. The $i = 0$ case represents spontaneous nucleation, and in this case monomers have a small probability p_n of nucleating a new island whenever they hop. Once nucleated, the new island absorbs monomers that hop onto it from a nearest neighbour site, therefore increasing in size.

Since we assume that any monomer cannot evaporate from the substrate, the deposition process can be measured by the nominal substrate coverage, $\theta = Ft$. Note that in the case of point islands, the coverage can exceed 100% even whilst most of the substrate remains free for monomer diffusion. The value of θ for which the aggregation regime (where scale-invariance is found) starts is dependent on i and R; we check that the values for θ are sufficiently high to ensure that we are in the aggregation regime.

As before, our simulations were performed on lattices with 10^6 sites, with $R = 8 \times 10^6$ up to coverage $\theta = 100\%$, averaging results over 100 runs. For $i = 0$ we set the spontaneous nucleation probability to $p_n = 10^{-7}$.

7.5 Results

7.5.1 Comparisons of the Integral Equation and Monte Carlo Data for the Gap Size Distribution

In Figure 7.5 we compare the converged form of the GSDs from equation (7.3), which we denote as $\phi_{\alpha_n}(x)$, with those found in our MC simulations for various critical island size i. For $i = 1-3$, we see that the observed GSD lies between that of the $\alpha_n = i + 1$ and $\alpha_n = i$ distributional fixed point solutions. This is expected since we have found elsewhere that island nucleation is driven by both deposition events and purely diffusional fluctuations in monomer density in Chapter 6. For spontaneous nucleation where $i = 0$, only the $\alpha_n = i + 1 = 1$ model is physically reasonable.

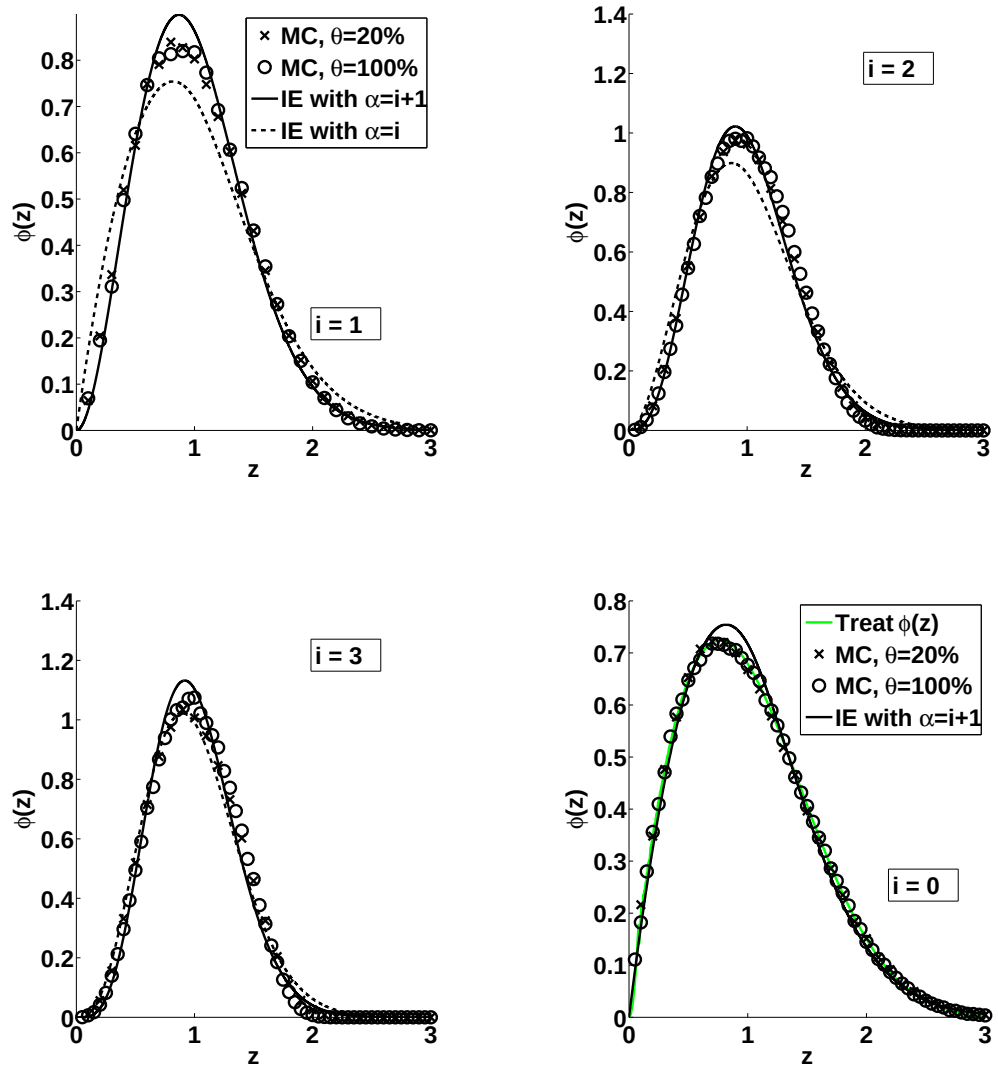

Figure 7.5: The GSDs compared to histograms of MC data for various critical island size i, taken at nominal coverage $\theta = 20\%$ and $\theta = 100\%$. The solid curve are the converged solutions to (7.3) with $\alpha_n = i + 1$ with $i = 0, 1, 2, 3$, and the broken lines are for $\alpha_n = i$ with $i = 1, 2, 3$.

Recall that for small z we have $\phi(z) \sim kz^{\alpha_n}$ for some constant k. This is essentially the same small-size asymptotic behaviour found in the fragmentation theory approach (6.3) in Chapter 6. It is not possible to obtain the large-size asymptotics for $\phi_{\alpha_n}(x)$. However, numerical analysis of the solutions in Figure 7.5 shows that

they differ from the fragmentation equation approach and we will further analyse this later in this chapter. The reason for this can be traced to the derivation of equation (7.3), where not only do we adopt a mean field approximations for nearest neighbour gap sizes, but we also neglect long-range correlations which are expected to be more prominent for larger gaps created early in the growth process. An example of this effect is the creation of g_4 which arose from the nucleation of I_4 and the fragmentation of gap of size $(g_5 + g_4 + g_3)$. This type of nucleation event is not included in the DFPE, which assumes that the gaps arise from the fragmentation of only two parents. Note that these events, arising from next-nearest-neighbour (or even longer) inter-gap correlations, will tend to involve large gaps rather than small ones. Nevertheless, the results in Figure 7.5 show that the solutions capture much of the essential physics for the GSDs.

In Figure 7.5, we also compare Treat's $i = 0$ $\phi(z)$ in (7.12) derived from the traditional fragmentation theory approach as discussed in Chapter 5. This is a useful benchmark to the MC data. As we see, for the $i = 0$ case (7.12) does fits the MC data quite well.

In the next subsection we argue that the mean-field DFPE (7.1) in fact provides a more realistic picture of the GSD than does the *a priori* more natural DFPE (7.9).

7.5.2 Fragmentation Bias for the DFPE with a Non Mean-Field Approximation Assumption

The model presented given by (7.9) and (7.10) for the GSD is not appropriate for the island nucleation process, since we know from MC simulations, in Chapter 6, that larger gaps are fragmented by nucleation events more often than smaller ones. We can account for this fragmentation bias by including the fragmentation probability $z^{2\alpha+1}$, which comes from the integral of equation (6.1). Incorporating

this bias in equation (7.10) we find

$$\phi(z) = \int_0^1 \int_0^{z/a} \phi\left(\frac{z}{a} - z_1\right) \phi(z_1) \frac{f(a)}{a^{2\alpha+2}} z^{2\alpha+1} \, da \, dz_1. \tag{7.21}$$

Note that we do not obtain this from a DFPE directly since the DFPE equivalent of (7.21) is unknown.

We now compare the fixed point probability distribution of equation (7.21) with those from the mean-field approximation (7.3) and from (7.10) above; see Figure 7.6. Note that the effect of the bias is to skew the distribution away from that of equation (7.10), which over-represents small gaps, towards that of the mean-field approximation – see Figure 7.5. This shows that the correct inclusion of the fragmentation bias justifies the mean-field approximation used for the gaps.

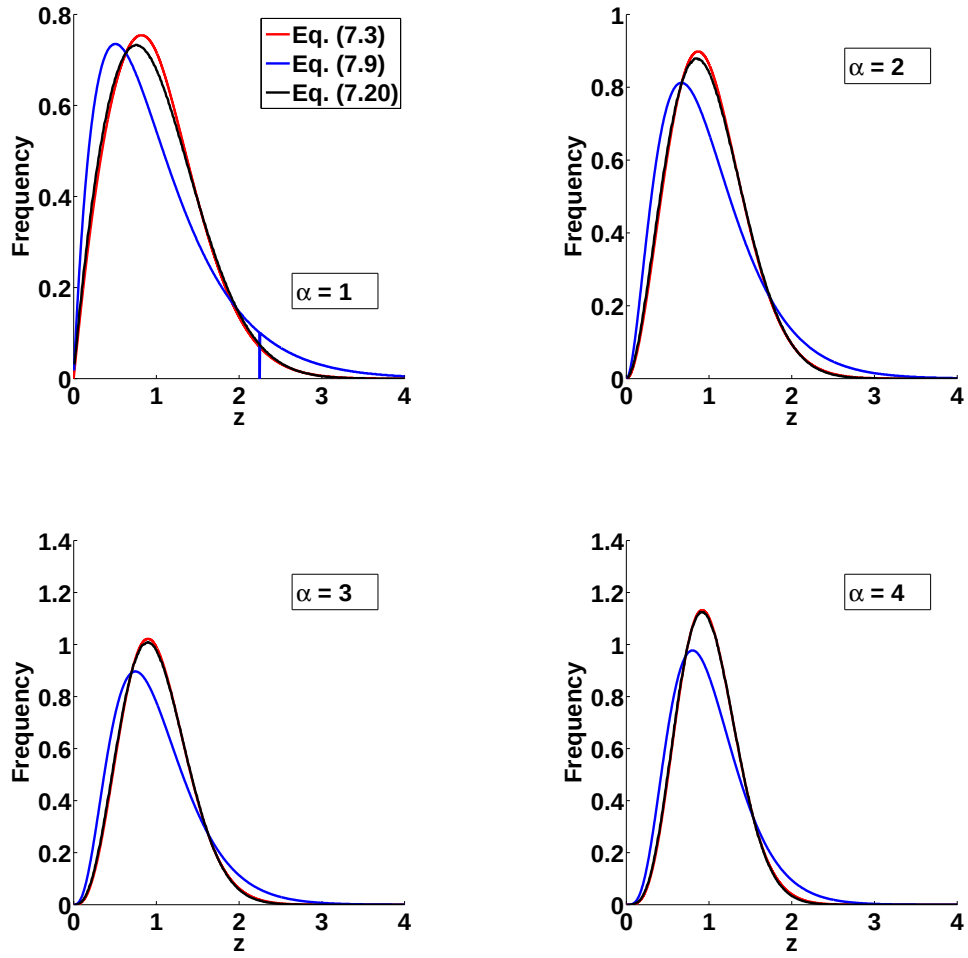

Figure 7.6: Comparison of the integral equations (7.3), (7.10) and (7.21) for the various gap size models with $\alpha = 1 - 4$.

7.5.3 Comparisons of the Integral Equation, Monte Carlo Data and the Generalised Wigner Surmise for the Capture Zone Distribution

In Figure 7.7 we compare the converged form of the CZD of (7.15) with those from the MC simulations. Again we find some excellent comparisons, particularly for $i = 0$ and $i = 1$. We also plot the GWS as a convenient analytical form for the

CZD whose parameters depend on i. Visually we see that our solutions work at least as well as, and in the case of $i = 0$ much better than the GWS.

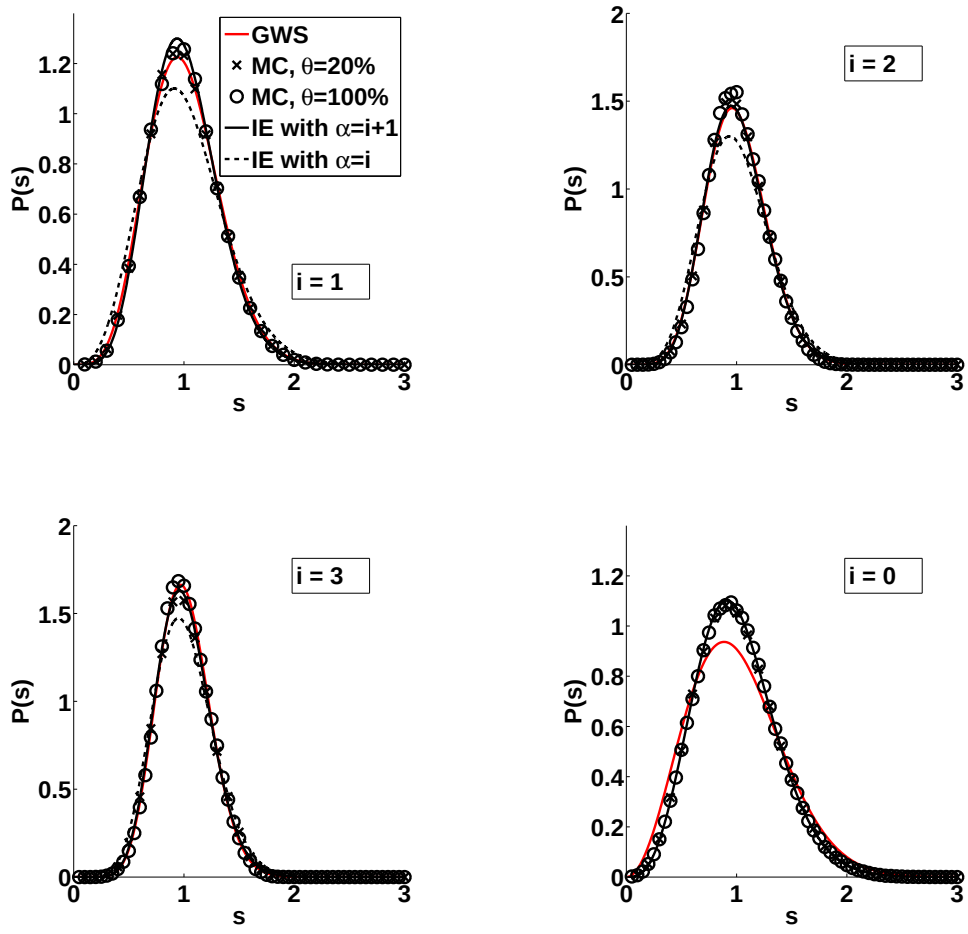

Figure 7.7: The CZDs compared to histograms of MC data for various critical island size i, taken at nominal coverage $\theta = 20\%$ and $\theta = 100\%$. The solid curve are the solutions to (7.3) for $\alpha_n = i + 1$ with $i = 0, 1, 2, 3$, and the broken lines are for $\alpha_n = i$ with $i = 1, 2, 3$.

7.5.4 Moments of the Gap Size Distribution

Here, we compare the moments of the IEs (7.8) and, for $i = 0$ only, (7.13) with the data from the full MC simulations at $\theta = 20\%$ and $\theta = 100\%$ for the GSD. Using bootstrap methods with 1000 samples of size as big as the original sample,

we consider the average moments of the MC data for the general case of $i \geq 0$, and therefore find the approximate 95% confidence interval of these averages. These errorbars are very small due to very large number of bootstrap samples. We have presented these results in Table 7.1 for all cases of $i = 0$, 1, 2 and 3.

By obtaining the moment of the MC data per simulation run, we consider the average moment of the MC data for the GSD over 100 simulation runs, and therefore find the approximate 95% confidence interval of these averages. Moreover, we have confirmed that these results in Table 7.2 is fairly consistent with the results in Table 7.1.

m	T_m	Z_m [a]	Z_m [b]	MC [c]	MC [d]
$\underline{i=0}$					
2	1.290	-	1.286	1.296 ± 0.001	1.290 ± 0.001
3	1.962	-	1.964	1.989 ± 0.001	1.963 ± 0.001
4	3.363	-	3.429	3.456 ± 0.001	3.365 ± 0.001
$\underline{i=1}$					
2	-	1.286	1.200	1.213 ± 0.001	1.206 ± 0.001
3	-	1.964	1.652	1.685 ± 0.001	1.659 ± 0.001
4	-	3.429	2.542	2.598 ± 0.001	2.520 ± 0.001
$\underline{i=2}$					
2	-	1.200	1.154	1.146 ± 0.001	1.139 ± 0.001
3	-	1.652	1.492	1.453 ± 0.001	1.427 ± 0.001
4	-	2.542	2.123	1.991 ± 0.001	1.924 ± 0.001
$\underline{i=3}$					
2	-	1.154	1.125	1.130 ± 0.001	1.118 ± 0.001
3	-	1.492	1.395	1.400 ± 0.001	1.360 ± 0.001
4	-	2.123	1.881	1.863 ± 0.001	1.766 ± 0.001

[a] $\alpha_n = i$
[b] $\alpha_n = i + 1$
[c] Point islands, $\theta = 20\%$
[d] Point islands, $\theta = 100\%$

Table 7.1: Moments of the GSDs for $i = 0$, 1, 2 and 3 from the DFPE (7.8) with $\alpha_n = i + 1$ or $\alpha_n = i$ (if appropriate), and from the MC simulations taken at $\theta = 20\%$ and $\theta = 100\%$ (θ is deposition rate times elapsed time).

In Table 7.1 we compare the moments calculated from (7.8) alongside those

m	T_m	Z_m [a]	Z_m [b]	MC [c]	MC [d]
$\underline{i=0}$					
2	1.290	-	1.286	1.269 ± 0.004	1.259 ± 0.003
3	1.962	-	1.964	1.948 ± 0.009	1.915 ± 0.007
4	3.363	-	3.429	3.385 ± 0.026	3.282 ± 0.018
$\underline{i=1}$					
2	-	1.286	1.200	1.200 ± 0.001	1.195 ± 0.001
3	-	1.964	1.652	1.668 ± 0.003	1.643 ± 0.003
4	-	3.429	2.542	2.572 ± 0.008	2.496 ± 0.006
$\underline{i=2}$					
2	-	1.200	1.154	1.127 ± 0.002	1.128 ± 0.002
3	-	1.652	1.492	1.429 ± 0.003	1.413 ± 0.003
4	-	2.542	2.123	1.958 ± 0.007	1.905 ± 0.006
$\underline{i=3}$					
2	-	1.154	1.125	1.110 ± 0.003	1.101 ± 0.002
3	-	1.492	1.395	1.375 ± 0.005	1.340 ± 0.004
4	-	2.123	1.881	1.829 ± 0.009	1.739 ± 0.007

[a] $\alpha_n = i$
[b] $\alpha_n = i + 1$
[c] Point islands, $\theta = 20\%$
[d] Point islands, $\theta = 100\%$

Table 7.2: Average moments of the GSDs for $i = 0$, 1, 2 and 3 from (7.8) with $\alpha_n = i+1$ or $\alpha_n = i$, and from the MC simulations taken at $\theta = 20\%$ and $\theta = 100\%$.

taken from our MC simulations for $i = 0$ and $i = 1$. These confirm the competitive performance of the DFPEs. It is interesting to note that the moments of Treat's $\phi(z)$ in (7.13) for $i = 0$ are similar to Z_m and notably compare with the MC data at $\theta = 100\%$ very well. This, along with the visual evidence from Figure 7.5, may not be surprising since (7.12) satisfies the small- and large-size asymptotics of the GSD extremely well as confirmed in Chapter 6.

Similarly, in Table 7.1 the moments of (7.8) for $i \geq 2$ seem to satisfy the MC data at both $\theta = 20\%$ and $\theta = 100\%$ fairly well. Furthermore, according to Table 7.1, the moments of the MC data seems to fit (7.3) in the form of $\alpha_n = i+1$ better than those in the form of $\alpha_n = i$ which may suggests that in terms of

nucleation mechanisms the diffusion process is more dominant than the deposition process.

7.5.5 Moments of the Capture Zone Distribution

Here we compare the moments of the IEs (7.18) and the GWS (7.20) with the data from the full MC simulations at $\theta = 20\%$ and $\theta = 100\%$ for the CZD. As before, we have used bootstrap methods with 1000 samples of size as large as the original sample size to consider the average moments of the MC data for the general case of $i \geq 0$, and therefore find the approximate 95% confidence interval of these averages. We have presented these results in Table 7.3 for all cases of $i = 0$, 1, 2 and 3.

Again, as before, to stay consistent with the results in Table 7.3, we have calculated the average moment of the MC data by obtaining the moment per simulation run. In Table 7.4, we also have confirmed good consistency between both set of results.

In Table 7.3 we compare the moments calculated from (7.18) and (7.20) alongside those taken from our MC simulations for $i = 0 - 3$. These confirm the competitive performance of the DFPEs, meaning that the solution of the DFPEs do describe the CZD well.

7.5.6 Small-Size Scaling of the Integral Equation

In Figure 7.8, as an alternative approach to the data analysis, we report the small-size behaviour of the converged solutions to the IEs (7.3) and (7.16) for the GSD ($\phi(z)$) and CZD ($P(s)$) in logarithmic scale. We are able to calculate the gradients for small-size scaling of (7.3) and (7.16). The results of this fitting procedure are shown in Tables 7.5 and 7.6. For the small-size asymptotic behaviour of the GSD

m	G_m	S_m [a]	S_m [b]	MC [c]	MC [d]
$\underline{i=0}$					
2	1.178	-	1.138	1.137 ± 0.001	1.134 ± 0.001
3	1.571	-	1.439	1.435 ± 0.001	1.425 ± 0.001
4	2.313	-	1.989	1.977 ± 0.001	1.949 ± 0.001
$\underline{i=1}$					
2	1.105	1.138	1.098	1.101 ± 0.001	1.098 ± 0.001
3	1.325	1.439	1.305	1.316 ± 0.001	1.307 ± 0.001
4	1.708	1.989	1.665	1.690 ± 0.001	1.666 ± 0.001
$\underline{i=2}$					
2	1.074	1.098	1.076	1.069 ± 0.001	1.066 ± 0.001
3	1.227	1.305	1.234	1.212 ± 0.001	1.202 ± 0.001
4	1.483	1.665	1.500	1.448 ± 0.001	1.425 ± 0.001
$\underline{i=3}$					
2	1.057	1.076	1.062	1.062 ± 0.001	1.056 ± 0.001
3	1.175	1.234	1.190	1.189 ± 0.001	1.169 ± 0.001
4	1.366	1.500	1.401	1.395 ± 0.001	1.352 ± 0.001

[a] $\alpha_n = i$
[b] $\alpha_n = i + 1$
[c] Point islands, $\theta = 20\%$
[d] Point islands, $\theta = 100\%$

Table 7.3: Moments of the CZDs for $i = 0$, 1, 2 and 3 from the DFPE (7.18) with $\alpha_n = i + 1$ or $\alpha_n = i$ (if appropriate), and from the MC simulations taken at $\theta = 20\%$ and $\theta = 100\%$ (θ is deposition rate times elapsed time).

and CZD we compare (7.3) and (7.16) with the data from MC simulations and the fragmentation equation approach predictions of Section 6.3. The values from these theories are also displayed in Tables 7.5 and 7.6. These tables are extensions of the original Tables 6.13 and 6.14 presented in Chapter 6, allowing us to easily compare the results of (7.3) and (7.16) with the previous results. We also recall a few of conclusions from Chapter 6 for convenience.

In Table 7.5, for the GSD we see that in the case of $i \geq 1$ the MC data exponent at $\theta = 100\%$ lies between the two possible values $\alpha_n = i$ and $\alpha_n = i + 1$ which show that both the deposition- and diffusion-driven nucleation mechanisms are at play in the simulations. We also see that for $i = 0$, the exponent is close to the

m	G_m	S_m [a]	S_m [b]	MC [c]	MC [d]
$\underline{i=0}$					
2	1.178	-	1.138	1.114 ± 0.003	1.107 ± 0.002
3	1.571	-	1.439	1.405 ± 0.005	1.389 ± 0.004
4	2.313	-	1.989	1.936 ± 0.012	1.901 ± 0.008
$\underline{i=1}$					
2	1.105	1.138	1.098	1.090 ± 0.001	1.088 ± 0.001
3	1.325	1.439	1.305	1.303 ± 0.002	1.295 ± 0.002
4	1.708	1.989	1.665	1.673 ± 0.004	1.651 ± 0.003
$\underline{i=2}$					
2	1.074	1.098	1.076	1.051 ± 0.001	1.056 ± 0.001
3	1.227	1.305	1.234	1.192 ± 0.002	1.190 ± 0.002
4	1.483	1.665	1.500	1.424 ± 0.004	1.411 ± 0.003
$\underline{i=3}$					
2	1.057	1.076	1.062	1.043 ± 0.002	1.040 ± 0.002
3	1.175	1.234	1.190	1.167 ± 0.003	1.152 ± 0.002
4	1.366	1.500	1.401	1.370 ± 0.005	1.332 ± 0.003

[a] $\alpha_n = i$
[b] $\alpha_n = i + 1$
[c] Point islands, $\theta = 20\%$
[d] Point islands, $\theta = 100\%$

Table 7.4: Average moments of the CZDs for $i = 0$, 1, 2 and 3 from (7.18) with $\alpha_n = i+1$ or $\alpha_n = i$, and from the MC simulations taken at $\theta = 20\%$ and $\theta = 100\%$.

i	${\alpha_n}^{\text{a}}$	${\alpha_n}^{\text{b}}$	$(7.3)^{\text{a}}$	$(7.3)^{\text{b}}$	GSD[c]	GSD[d]
0	-	1	-	0.946	0.876 ± 0.033	0.905 ± 0.029
1	1	2	0.946	1.853	1.701 ± 0.045	1.579 ± 0.105
2	2	3	1.853	2.697	2.789 ± 0.080	2.718 ± 0.074
3	3	4	2.697	3.489	2.719 ± 0.082	3.271 ± 0.056

[a] $\alpha_n = i$
[b] $\alpha_n = i + 1$
[c] $\theta = 20\%$
[d] $\theta = 100\%$

Table 7.5: Average gradient for the small-size scaling of the GSD using different bin-widths at coverages $\theta = 20\%$ and 100%.

$\alpha_n = i + 1 = 1$ prediction at both $\theta = 20\%$ and $\theta = 100\%$. The results show that the small-size asymptotics of (7.3) seem to underestimate the expected gradients

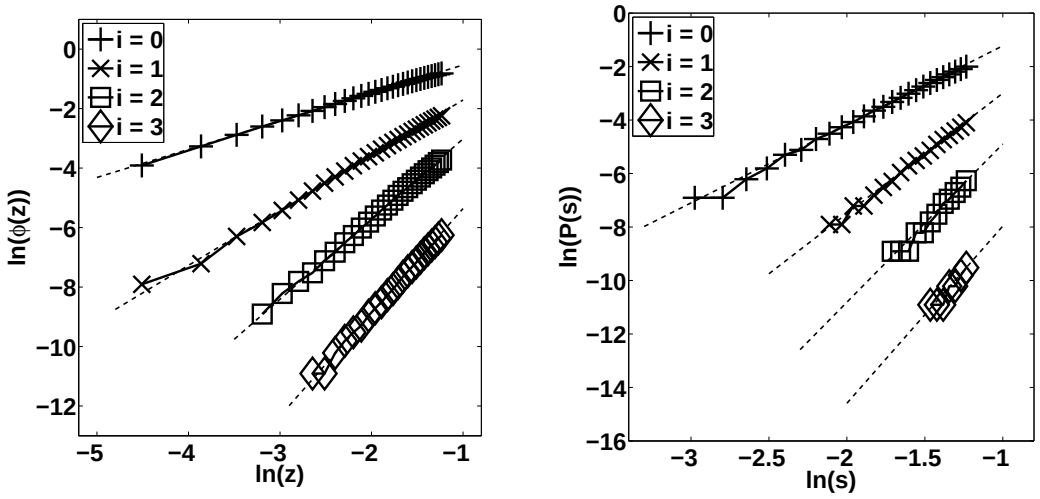

Figure 7.8: Small-size form of the IEs (7.3) and (7.16) for the GSD and CZD respectively in logarithmic scale for $i = 0$, 1, 2 and 3. The dashed line is the straight-line fit to data.

i	$2\alpha_n + 1$[a]	$2\alpha_n + 1$[b]	GWS[c]	(7.16)[a]	(7.16)[b]	CZD[d]	CZD[e]
0	-	3	2	-	2.938	2.730 ± 0.030	2.751 ± 0.086
1	3	5	4	2.938	4.503	4.187 ± 0.050	4.372 ± 0.149
2	5	7	6	4.503	5.915	5.883 ± 0.207	5.957 ± 0.187
3	7	9	8	5.915	6.627	7.200 ± 0.382	6.138 ± 0.124

[a] $\alpha_n = i$
[b] $\alpha_n = i + 1$
[c] $\beta = 2(i + 1)$
[d] $\theta = 20\%$
[e] $\theta = 100\%$

Table 7.6: Average gradient for the small-size scaling of the CZD using different bin-widths at coverages $\theta = 20\%$ and 100%.

consistently for each value of i.

For the CZD, in Table 7.6, we see that the $i = 0$ data are close to the $\lambda = 2i + 3 = 3$ prediction of the fragmentation equation approach, being somewhat larger than the $\beta = 2(i+1) = 2$ predicted by the GWS. The GWS exponent which appears to present a reasonable compromise given the two possible nucleation

mechanisms. As in the case of the small-size asymptotics of the GSD, for $i \leq 2$, we have confirmed that the MC data at $\theta = 20\%$ and $\theta = 100\%$ satisfies the small-size asymptotics of (7.16) for $\alpha_n = i + 1$ well. It is worth noting that the performance of (7.16) in this analysis does closely follow the GWS. For $i = 3$ at $\theta = 100\%$, it is notable that (7.16) seems to fare better than both the predictions of fragmentation theory approach and the GWS for the CZD.

7.5.7 Large-Size Scaling of the Integral Equation

In Figure 7.9 we present the large-size behaviour of the IEs (7.3) and (7.16) for the GSD and CZD respectively. As before in Chapter 6, the data are plotted in order to test the common large-size functional form of (6.6) and the GWS and compare these results to the fragmentation equation approach for the GSD and the GWS for the CZD as well as the MC data. In addition, we perfom fits to find the exponents of (7.3) and (7.16) on these plots. The results of this fitting procedure are presented in Tables 7.7 and 7.8 for the GSD and CZD respectively. As noted earlier, Tables 7.7 and 7.8 are simply extensions of the original Tables 6.17 and 6.18 in Chapter 6. Again, we recall the conclusions from Chapter 6.

Once again we compare the exponents of (7.3) and (7.16) with the MC simulation data and the fragmentation equation theoretical predictions. Recall, from Chapter 6, that for the GSD, the fragmentation equation approach predicts values of $2\alpha_n + 1$. For the CZD, the fragmentation theory prediction is 3 for $i = 0$ (see (6.6)). In contrast, the GWS prediction for the CZD is the universal value 2. The values from these theories are displayed in Tables 7.7 and 7.8.

For the GSD, as discussed in Chapter 6, we see values bracketed by the two possible nucleation mechanisms for $i = 1$ and 2. The prediction exponent for $i = 0$ is 3 but the actual behaviour is slightly below this. The data's exponent is below

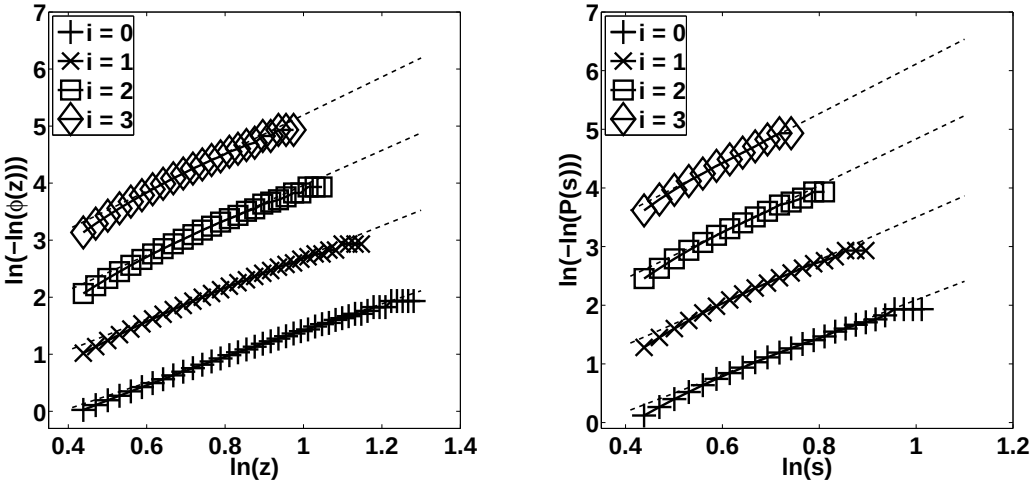

Figure 7.9: Large-size form of the IEs (7.3) and (7.16) for the GSD and CZD respectively in logarithmic scale for $i = 0$, 1, 2 and 3. The dashed line is the straight-line fit to data.

i	α_n [a]	α_n [b]	(7.3)[a]	(7.3)[b]	GSD[c]	GSD[d]
0	-	3	-	2.301	2.515 ± 0.006	2.665 ± 0.007
1	3	5	2.301	2.730	3.130 ± 0.009	3.383 ± 0.008
2	5	7	2.730	3.065	4.364 ± 0.020	5.112 ± 0.025
3	7	9	3.065	3.335	5.094 ± 0.026	6.437 ± 0.034

[a] $\alpha_n = i$
[b] $\alpha_n = i + 1$
[c] $\theta = 20\%$
[d] $\theta = 100\%$

Table 7.7: Average exponents for the large-size scaling of the GSD using different bin-widths at coverage $\theta = 20\%$ and 100%.

even that of the deposition-induced nucleation case for $i = 3$. It is notable that the IE (7.3) is consistently below the prediction of the fragmentation theory approach and the MC data. This strongly suggests that the large-size predictions of both are not the same, unlike the small-size predictions. For $i = 0$ and $i = 1$ the IE (7.3) seems to compare well with the MC data for the GSD. The results are rather mixed – in conclusion neither the IE (7.3) nor the fragmentation theory approach

i	$2i+3$[a]	GWS	(7.16)[a]	CZD[b]	CZD[c]
0	3	2	3.180	3.108 ± 0.012	3.043 ± 0.043
1	-	2	3.639	3.721 ± 0.020	3.826 ± 0.021
2	-	2	3.967	4.946 ± 0.029	5.536 ± 0.033
3	-	2	4.231	5.464 ± 0.041	6.530 ± 0.042

[a] $\lambda = 2i + 3$
[b] $\theta = 20\%$
[c] $\theta = 100\%$

Table 7.8: Average exponents for the large-size scaling of the CZD using different bin-widths at coverage $\theta = 20\%$ and 100%.

predict the large-size asymptotics of the GSD obtained from the MC simulation for $i \geq 2$.

For the CZD we observe that the MC data exponents Table 7.8 do indeed mirror those of the GSD in Table 7.7 quite well. We also see that the concrete prediction for $i = 0$ from the fragmentation theory, namely 3, is well supported by the simulation data. Similarly, for $i = 0$ the IE (7.16) seems to compare very well along with the MC data and the fragmentation theory prediction for the CZD. As the case for the GSD above, the large-size asymptotics of (7.16) is consistently below the MC data. We could say the same for the prediction of the fragmentation theory if, as discussed in Chapter 6, the conjecture that the $2i + 3$ prediction of large-size asymptotics for the CZD is correct. Despite the fact that (7.16) does not satisfy the MC data for $i > 1$, it is observed that (7.16) fares better than the universal prediction of the GWS, that is 2, and the conjecture described above.

7.6 Conclusions

In summary, we have presented distributional fixed point equations (DFPEs) for the nucleation of point islands in one dimension. The approach develops a new retrospective view of how the inter-island gaps and capture zones have developed

from the fragmentation of larger entities. The fixed point of the resulting integral equations (IEs) offers a new perspective on why scale-invariant distributions arise from the nucleation process. This approach was inspired by Seba's one-dimensional (1-D) car-parking model and, despite the reversibility of the Seba case, we were able to overcome the irreversibility barrier of our model.

We have considered three gap size models as presented in (7.1), (7.9) and (7.21). The DFPE (7.9) may be considered as the non mean-field version of (7.1). In fact, the fixed point for the former DFPE is given by a gamma distribution. However, we show that this model is not suitable for the island nucleation and growth processes as evidenced by the MC data for the gap size distribution (GSD). It is suggested that this particular model ignores the fact that larger gaps are more likely to be fragmented by nucleation events than smaller gaps. In other words, this model has over-represented smaller gaps.

In Chapter 6, under the assumption that the island nucleation and growth stage is in the aggregation regime, the probability of a new nucleation occuring in a gap of width z is proportional to $z^{2\alpha_n+1}$. If we incorporate this fragmentation bias in the IEs for the non mean-field model, then we see that the IEs (7.21) follow the mean-field IEs (7.3) closely. Interestingly, the former seems to be strongly related to Treat's solution for the $i = 0$ case. This creates a few questions – since we have used same assumptions in the same fragmentation model, are the IEs (7.21) the same as Treat's solution? Usually, physical intuition leads to the DFPEs, and, in turn, IEs follow algorithmically. So, what is the DFPE equivalent of (7.21)? Can one work out the DFPEs from the IEs by working backwards?

We now turn our attention to the IEs (7.3) for the GSD; we then presented the same data as shown in Chapter 6 for the nucleation and growth simulation. Numerical analysis of the solutions in Figure 7.5 show that the IEs differ from the

fragmentation theory approach. The reason for this is that we neglect longer-range correlations which are expected to be more prominent for larger gaps created early on in the growth process. Nevertheless, the results in Figure 7.5 show that the solutions capture much of the essential physics for the gap size distribution (GSD). Moreover, for $i = 0$ in Figure 7.5, we also compare the moments of Treat's $\phi(z)$ in (7.13) derived from the traditional fragmentation theory approach to those of the IEs (7.3). It is confirmed that Treat's (7.12) does fit the Monte Carlo (MC) data quite well. In the case of $i = 0$, this vindicates the whole fragmentation theory structure outlined in Chapter 5 although the fragmentation theory has limitations due to, for example, a significant decrease in the nucleation rate for higher critical island sizes; see Chapter 6 for further detail.

We note that the moments for the MC data seem to fit the IEs in the form of $\alpha_n = i + 1$ better than those in the form of $\alpha_n = i$, which may suggest that the diffusion process is more likely to be dominant than the deposition process due to the large value of $R = D/F$. For the small-size GSD scaling, the IEs predict the MC data well for $i \geq 0$ except possibly the $i = 3$ case. A possible explanation for this exception may be that, as mentioned in Chapter 6, the simulation does not enter the aggregation regime at low coverage in the $i = 3$ case.

For the large-size asymptotics of the GSD, we note that the IEs consistently predict below that of the fragmentation theory approach and the MC data. This is a strong suggestion that the large-size predictions of both are not the same, in contrast to the small-size predictions. For $i = 0$ and $i = 1$, the IEs compare well with the MC data. In contrast, for higher critical island sizes, neither the IEs nor the fragmentation theory approach predicts the large-size asymptotics we obtain from MC simulations for $i \geq 2$.

We now consider the IEs (7.16) for the capture zone distribution (CZD). The

construction of the IEs for the CZD is independent of those for the GSD, which is possibly a major conceptual advance to be discussed later in this section. In order to support the performance of the DFPEs (or its counterpart IEs), as in the case for the GSD we also have considered the moments and small- and large-size asymptotics of the IEs and the Generalised Wigner Surmise (GWS) alongside those taken from our MC simulations for $i \geq 0$.

The moment of the IEs performs notably better than the GWS in two cases of $i = 0$ and $i = 1$, and at least as well as the GWS for $i \geq 2$. We also confirm that the MC data satisfy the small-size asymptotics of the IE for $\alpha_n = i+1$ in the case of $i \leq 2$. The performance of the IEs competes well with the GWS and seems to fare better with $i = 3$ in comparisons to the predictions of the fragmentation theory approach (in the $\alpha_n = i + 1$ case) and the GWS.

For $i = 0$ and $i = 1$ in the case of large-size CZD scaling, the IEs (7.16) appears to compare very well along with the MC data and the fragmentation theory prediction. As for the GSD case, however, the large-size asymptotics of (7.16) consistently gives results that are below the MC data. If the conjecture is correct that the prediction of large-size asymptotics for the CZD is $2i + 3$, as discussed in Chapter 6, then we could say the same for (7.16) being consistently below the predictions. Despite the fact that (7.16) does not satisfy the MC data for $i > 1$, we observe that (7.16) fares better than the universal prediction of the GWS – that is, 2 – and the conjecture described above.

In conclusion, this promising approach clearly needs further investigation, especially for the GSD. Nevertheless, we have shown how the solutions of DFPEs, or their counterpart IEs, compare well to MC simulation data – performing at least as well as the GWS, and notably better for the case of $i = 0$.

One key outcome of our approach is that it allows one to construct the DFPEs

for the CZD directly. Recall, in Chapters 5 and 6, the CZD has been obtained from the GSD via the convolution equation (3.22). This provides a fresh perspective for capture zones; the retrospective approach might also help in higher dimensions where equivalents to the GSD do not exist – this could be considered as future work.

Chapter 8

Conclusions and Future Directions

8.1 Conclusions

For decades, considerable effort has been expended in trying to develop theories of nucleation and growth processes during submonolayer deposition. The aim of this work is to find a modelling framework that allows us to explain the island size distributions (ISDs) found both experimentally and in Monte Carlo (MC) simulation. A validated modelling framework would also provide predictive capabilities for the design of new experiments and material processes.

In Chapter 4, for a restricted class of solutions, we have obtained the long time behaviour of the monomer and island size distributions for rate equations with constant coefficients and the concept of a 'river' for the point-island case of general critical island size $i \geq 1$. To relax the aforementioned restriction, we requires that all solutions in the first quadrant are attracted to the river. Also, we have proved the convergence of the ISD to a self-similar profile where there is a

discontinuity at scaled island size of $(i+2)/(i+1)$. This is confirmed by the work of Bartelt and Evans who also studied the $i = 1$ model closely related to the one considered by da Costa *et. al.* [25]. However, the data from the MC simulation shows that there is no discontinuity for the ISD and hence the divergence discussed does not exist in reality. For consistency check, if one sets $i = 1$, then the results obtained in Chapter 4 will be collapsed to restricted versions of the results obtained by da Costa *et. al.* [25]. Furthermore, our weaker versions of the results obtained by da Costa *et. al.* provide confirmation that our results are consistent with the results in the work of Blackman and Wilding with $p = 0$ (the constant capture rate coefficients).

The Generalised Wigner Surmise (GWS) was proposed by Pimpinelli and Einstein to describe better the capture zone distribution (CZD). In Chapters 5 and 6, we have discussed the differences between the Blackman and Mulheran fragmentation theory and the GWS for the one-dimensional (1-D) point island nucleation and growth model. Since these two theoretical approaches are based on the same physical intuition, it is useful to confront these predictions together by means of the MC data. Essentially, in Chapter 5, we have shown that the GWS does not correspond with the small- and large-size asymptotic solutions to the Blackman and Mulheran (BM) fragmentation theory analysis. We have concluded that the BM theory and the GWS cannot be simultaneously correct. In Chapter 6, we presented MC data for the point island nucleation and growth simulation. We show that the fragmentation theory provides a good theoretical framework in which to understand the MC simulation results. Moreover, for the large-size CZD, the GWS is not successful when confronted with our 1-D simulation data since the Gaussian tail of the GWS is not observed in the simulation data. However, there are a few limitations of the BM fragmentation theory, such as its failure to capture the

time-dependent nature of the monomer density profile within gaps.

Nevertheless, this theory provides an useful theoretical framework from which to consider the island nucleation process – the deposition process or the diffusion process. It is important to note that similarity solutions correspond to $t \to \infty$, which implies that one mechanism will completely dominate another. This is true, at the asymptotic limit of large $R = D/F$ where $\theta = Ft$, the diffusion mechanism will dominate the deposition one. However, in practice, once cannot get to this limit in simulations or experiments (nor can we get to $t \to \infty$). Therefore, it is still valid to consider the behaviour whether one mechanism or the other dominates because this provides a good bracket to understand our MC data.

We have presented distributional fixed point equations (DFPEs) for the nucleation of point islands in one dimension. The approach develops a new retrospective view of how the inter-island gaps and capture zones have developed following the fragmentation of larger entities. Numerical analysis of the solutions in Chapter 7 demonstrate that the IEs differ from the results obtained from fragmentation theory approach. The reason for this is we neglect longer-range correlations – they are expected to be more prominent for larger gaps created early in the growth process. Nevertheless, the results show that the solutions capture much of the essential physics for the gap size distribution (GSD).

We focus our attention on the IEs for the CZD. The moment of the IEs performs notably better than the GWS in two cases – namely, $i = 0$ and $i = 1$ – and at least as well as the GWS when $i \geq 2$. The performance of the IEs competes well with the GWS and seems to fare better with $i = 3$ when compared to the predictions obtained by the fragmentation theory approach (in the $\alpha_n = i + 1$ case) and the GWS. In the $i = 0$ and $i = 1$ cases for the large-size CZD scaling, the IEs (7.16) appear to compare very well along with the MC data and the fragmentation theory

prediction. However, the large-size asymptotics of (7.16) consistently give results that are below the MC data. Despite the fact that the IEs do not satisfy the MC data for $i \geq 2$, we observe that the IEs fares better than the universal prediction of the GWS.

Despite this promising approach requiring further investigation – especially for the GSD – we have shown how the solutions of DFPEs, or their counterpart IEs, compare well to the MC simulation data; performing at least as well as the GWS, and notably better for the case of $i = 0$. A key advantage of this approach is that it allows the construction of the DFPEs for the CZD without having to rely on the GSD via the convolution equation. This raises the possibility of constructing a similar DFPE for the CZD in higher dimensional systems.

8.2 Future Directions

In order to establish the global asymptotic result that confirms the results obtained by Blackman and Wilding [16] and da Costa *et. al.* [25], we need to prove that all solutions in the first quadrant are attracted to the river $R(X)$. Due to the discontinuity found in the analysis for rate equations with constant capture rate coefficients, we need to consider the conditions on the coefficients of rate equations which will ensure a continuous scaling solution. Moreover, in the work of Blackman and Wilding, they had assumed that all islands of sizes $1 < j \leq i$ were allowed to fragment. Despite the fact that our case only assume that islands of sizes $1 < j \leq i$ simply do not arise, the asymptotic behaviour is the same in both cases, which is remarkable and merits further analytical work. Moreover, da Costa *et. al.* and we have considered the $\eta = 1$ case, which leads to a self-similar function, $\Phi_2(\xi)$. This raises a question – what is the physical meaning of this function in terms of the

modelling of submonolayer deposition?

In the fragmentation theory approach, it was observed that the nucleation rate slowed down over time in the higher critical island sizes, which could suggests less well-mixed systems. Along with this, a better fragmentation kernel that can incorporate this time dependency is required – this implies that the fragmentation equation will be nonlinear.

The DFPE approach is novel and, clearly, this needs further investigation. We might need to derive a better DFPE for the GSD that will incorporate long-range correlations. Note that the other two (non mean-field) gap size models are based on nonlinear IEs, which then could have to come from a nonlinear fragmentation equation. So, two interesting questions here are: what are the fragmentation equations and the similarity solutions of the aforementioned gap size models. Also, another future direction is to extend the DFPE for the CZD to higher dimensional cases; note that it is not possible to extend the DFPE for the GSD since the GSD only makes sense in the 1-D case and the derivation of the DFPE for the CZD is independent of those for the GSD which is one of key outcomes raised in Chapter 7.

In general, these conclusions and future directions are for the irreversible case, that is, no attached monomer can leave away from an island – this is one of the main assumptions we have adopted in this thesis. It is natural to consider the reversible case as studied in the past by several authors, such as Blackman and Wilding [16], Mulheran and Blackman [54], and Ratsch, Zangwill, Smilauer and Vvedensky [67]. However, we need to ask carefully: what do we mean by *reversibility* in this research field? As mentioned in Chapter 1, monomers can re-evaporate from the substrate at high temperatures, as observed by experiment – such process is known as desorption, which is one of the important processes for the nucleation and growth stage in some cases. We must note that this is not the

only possible scenario of reversibility – other possibilities are:

- Using the critical island size $i > 1$ already implies some reversibility – smaller (unstable) islands of size at most $i+1$ disassociate as soon as they form, or at least do so quickly compared to the average lifetime of a deposited monomer before either being captured by an existing island or join other monomer to nucleate a new island in the aggregation regime;

- Allowing small or all islands to diffuse – we have not looked at this possibility in this thesis;

- Islands of size, say, $k + m < i + 1$ breaking into two islands of size k and m respectively, which is the possibility of more complex pathways for disassociation.

As we see, this research field is rapidly evolving and it is difficult to mention all works especially in the case of some authors, such as Amar, Evans, Körner, Mulheran and so on. Here, we will only include a few recent papers (that are not related to any theory developed in this thesis) based on the theory of nucleation and growth of islands only as a way of providing a (small) snapshot of what is happening elsewhere prior to the publication of this thesis.

For the general survey on the submonolayer deposition and multilayer epitaxial thin film growth, a recent paper is written by Evans, Thiel and Bartelt [33]. This is not only focused on the theory of epitaxial growth but also on several case studies, which are relevant to the aforementioned theory. This is a good survey for both interested readers and experts.

Petrov, Miller, Rehse and Fornari [60] propose a new mathematical approach for the ISD in the $i = 1$ case of 1-D submonolayer deposition. This approach is based on exact difference-differential rate equations. The next step is to generalise

this approach for higher critical island sizes; they believe that this approach can be extended for the two-dimensional (2-D) case.

It was recognised that both islands and deposited monomers may diffuse, which influences the island density and the ISD. This motivates the work of Mulheran and Robbie [56]. Their simulations are similar to the one considered in this thesis with some differences: in a 2-D substrate, monomers are deposited randomly at a rate of F. These deposited monomers then diffuse and when monomers join, the island is irreversibly nucleated. The critical island size, i is 1 and the shape of islands is fractal unlike point and extended islands. These islands diffuse with the diffusion rate $Dj^{-\mu}$, where D is the monomer diffusion rate, j is the number of monomers in an island and μ is the exponent to be determined by experiments and simulations. Once the perimeters of islands meet, these islands coalesce into a larger island. It was noted that the value of the exponent μ lies typically in the range $1 < \mu < 2$ for 2-D islands on a 2-D substrate. Mulheran and Robbie have considered self-consistent rate equations in a similar manner as the work of Bales and Chrzan [6]. This work also leads to the following two papers [38, 43], which we discuss next.

Motivated by experiments on colloidal nanoparticles, Kryukov and Amar consider the case where islands are allowed to diffuse in the irreversible nucleation and growth stage [43] to study the effects on the island density and the ISD. They have confirmed that their island-density results are in good agreement with the results of Mulheran and Robbie [56]. Also, Hubartt, Kryukov and Amar present a generalisation of the self-consistent rate-equation approach originally developed by Bales and Chrzan [6] to the case of irreversible growth and island mobility. Hubartt *et. al.* [38] assume that islands diffuse with the rate $Dj^{-\mu}$, which is essentially the same as the one considered by the work of Mulheran and Robbie

as mentioned above. Hubartt *et. al.* have concluded that, in studying the ISD for few values of $\mu < 3$, their self-consistent rate-equation approach is in better agreement with their simulation data than the traditional rate-equation approach. This is expected since the presence of cluster mobility would reduce the effects of correlations, which influence the ISD. However, correlations are important for larger islands in the case of $\mu \geq 3$ and so the agreement with their simulation data is not good.

In [42], Körner, Einax and Maass consider rate equations in the case of irreversible nucleation and island growth along with direct impingement of arriving monomers. The authors obtain capture numbers $\sigma_j(\theta)$ which depend on both island size j and θ by collecting data for σ from MC simulations for constant θ, approximating the average σ as a function of j and θ and formulating rate equations using these averaged σ. Körner *et. al.* conclude that coefficients σ_j with no θ dependence lead to a poor prediction of ISD and thus there is a rate-equation model for submonolayer deposition that behaves just like the data from MC simulation if one takes into account the correct dependence of σ_j on both j and θ. More details can be found in [42].

Despite the fact that there is a wide range of works raising several different questions that may, or may not, be related to each other, these all have one common goal – obtaining reliable formulation for the all-important ISDs. On a final note, the structure of islands, capture zones surrounding each island and gaps between two neighbouring islands in the 1-D case – in any size and model – are clearly examples of coagulation-fragmentation processes as introduced in the very beginning of this thesis.

Bibliography

[1] A. Y. Abul-Magd, Modelling gap-size distribution of parked cars using random-matrix theory, Physica A **368** (2006), 536–540.

[2] J. G. Amar and F. Family, Critical cluster size: island morphology and size distribution in submonolayer epitaxial growth, Phys. Rev. Lett. **74** (1995), 2066–2069.

[3] J. G. Amar, F. Family and P.-M Lam, Dynamic scaling of the island-size distribution and percolation in a model of submonolayer molecular-beam epitaxy, Phys. Rev. B **50** (1994), 8781–8800.

[4] J. G. Amar, M. N. Popescu and F. Family, Rate-equation approach to island capture zones and size distributions in epitaxial growth, Phys. Rev. Lett. **86** (2001), 3092–3095.

[5] J. R. Arthur, Molecular beam epitaxy, Surf. Sci. **500** (2002), 189–217.

[6] G. S. Bales and D. C. Chrzan, Dynamics of irreversible island growth during submonolayer epitaxy, Phys. Rev. B **50** (1994), 6057–6067.

[7] M. Balluff and B. A. Wolf, Degradation of chain molecules. 1. Exact solution of the kinetic equations, Marcomolecules **14** (1981), 654–658.

[8] A. -L. Barabási and H. E. Stanley, *Fractal Concepts in Surface Growth*, Cambridge University Press, Cambridge 1995.

[9] J. D. Barrow, Coagulation with fragmentation, J. Phys. A: Math. Gen. **14** (1981), 729–733.

[10] M. C. Bartelt and J. W. Evans, Scaling analysis of diffusion-mediated island growth in surface adsorption processes, Phys. Rev. B **46** (1992), 12675–12687.

[11] M. C. Bartelt and J. W. Evans, Exact island-size distributions for submonolayer deposition: influence of correlations between island size and separation, Phys. Rev. B, **54** (1996), R17359-R17362.

[12] M. C. Bartelt, J. B. Hannon, A. K. Schmid, C. R. Stoldt and J. W. Evans, Island formation during deposition or etching, Colloids Surf. A **165** (2000), 373–403.

[13] R. Becker and W. Döring, Kinetische behandlung der keimbildung in übersättigten dämpfen, Ann. Phys. **24** (1935), 719–752.

[14] J. A. Blackman and P. A. Mulheran, Scaling behaviour in submonolayer film growth: a one-dimensional model, Phys. Rev. B **54** (1996), 11681–11692.

[15] J. A. Blackman and P. A. Mulheran, Growth of clusters on surfaces: Monte Carlo simulations and scaling properties, Comput. Phys. Commun. **137** (2001), 195–205.

[16] J. A. Blackman and A. Wilding, Scaling theory of island growth in thin films, Europhys. Lett. **16** (1991), 115–120.

[17] F. Blais, Asymptotic expansion of rivers, in: *Dynamic Bifurcations*, E. Benoît, ed., LNM 1493, Springer-Verlag, Berlin 1991, 181–189.

[18] K. Binder, *Monte Carlo and Molecular Dynamics Simulations in Polymer Science*, Oxford University Press, New York 1995.

[19] A. Bouhassoun, Asymptotic properties of some plane polynomial vector fields, Internat. Math. Forum **3** (2008), 1481–1488.

[20] A. D. Bruno, Power geometry as a new calculus, in: *Analysis and Applications, ISAAC 2001*, P. Kuchment, ed., Kluwer Academic, Dordrecht 2003, 51–71.

[21] J. Cano, The Newton polygon method for differential equations, in: *Computer Algebra and Geometric Algebra with Applications*, H. Li, ed., Springer Berlin/Heidelberg 2005, 18–30.

[22] Z. Cheng and S. Redner, Scaling theory of fragmentation, Phys. Rev. Lett. **60** (1988), 2450–2453.

[23] Z. Cheng and S. Redner, Kinetics of fragmentation, J. Phys. A: Math. Gen. **23** (1990), 1233–1258.

[24] J. F. Collet, Some modelling issues in the theory of fragmentation-coagulation systems, Commun. Math. Sci. **1** (2004), 35–54.

[25] F. P. da Costa, H. J. van Roessel, and J. A. D. Wattis, Long-time behaviour and self similarity in a coagulation equation with input of monomers, Markov Proc. Related Fields **12** (2006), 367–398.

[26] F. Diener, Fleuves et variétés centrales, Asterisque **150-151** (1987), 59–66.

[27] M. Diener, Détermination et existence des fleuves en dimension 2, Comptes Rendus Acad. Sci. Paris, série I, **301** (1985), 899–902.

[28] N. M. Donahue, A. L. Robinson and S. N. Pandis, Atmospheric organic particulate matter: From smoke to secondary organic aerosol, Atmos. Environ. **43** (2009), 94–106.

[29] D. Dufresne, On the stochastic equation $\mathscr{L}(X) = \mathscr{L}[B(X + C)]$ and a property of gamma distributions, Bernoulli **2** (1996), 287-291.

[30] R. Eckhardt, Stan Ulam, John von Neumann and the Monte Carlo method, Los Alamos Science **15** (1987), 131–141.

[31] M. Escobedo, S. Mischler, M. Rodriguez Ricard, On self-similarity and stationary problem for coagulation and fragmentation models, Ann. H. Poincaré Anal. Nonlin. **22** (2005), 99–125.

[32] J. W. Evans and M. C. Bartelt, Island sizes and capture zone areas in submonolayer deposition: scaling and factorization of the joint probability distribution, Phys. Rev. B **66** (2002), 235410-1–12.

[33] J. W. Evans, P. A. Thiel and M. C. Bartelt, Morphological evolution during epitaxial thing film growth: Formation of 2D islands and 3D mounds, Surf. Sci. Rep. **61** (2006), 1–128.

[34] G. Gartrell Jr. and S. K. Friendlander, Relating particulate pollution to sources: The 1972 California aerosol characterization study, Atmos. Environ. **9** (1975), 279–299.

[35] D. L. González, A. Pimpinelli and T. L. Einstein, Spacing distribution functions for the one-dimensional point-island model with irreversible attachment, Phys. Rev. E **84** (2011), 011601-1–10.

[36] D. Yu. Grigori'ev and M. F. Singer, Solving ordinary differential equations in terms of series with real exponents, Trans. AMS, **327** (1991), 329-351.

[37] M. Grinfeld, W. Lamb, K. P. O'Neill and P. A. Mulheran, Capture-zone distribution in one-dimensional sub-monolayer film growth: a fragmentation theory approach. J. Phys. A: Math. Theor. **45** (2012), 1–10.

[38] B. C. Hubartt, Y. A. Kryukov and J. G. Amar, Rate-equation approach to irreversible island growth with cluster diffusion, Phys. Rev. E **84** (2011), 021604-1–8.

[39] Y. Jiang, Instantaneous gelation in the generalized Smoluchovski coagulation equation, J. Phys. A: Math. Gen. **29** (1996), 7893–7901.

[40] Y. Jiang and F. Leyvraz, Scaling theory for ballistic aggregation, J. Phys. A: Math. Gen. **26** (1993), 179–186.

[41] A. Johansen, F. Brauer, C. P. Dullemond, H. Klahr and T. Henning, A coagulation-fragmentation model for the turbulent growth and destruction of preplanetesimals, Astronomy and Astrophysics **486** (2008), 597–613.

[42] M. Körner, M. Einax and P. Maass, Island size distributions in submonolayer growth: successful prediction by mean field theory with coverage dependent capture numbers, Phys. Rev. B **82** (2010), 201401-1–4.

[43] Y. A. Kryukov and J. G. Amar, Effects of cluster diffusion on the island density and size distribution in submonolayer island growth, Phys. Rev. E **83** (2011), 041611-1–10.

[44] M. Lallouache, A. Jedidi and A. Chakraborti, Wealth distribution: to be or not to be a Gamma?, arXiv:1004.5109.

[45] W. Lamb, Existence and uniqueness results for the continuous coagulation and fragmentation equation, Math. Meth. Appl. Sci. **27**, 703–721 (2004).

[46] F. Leyvraz, Scaling theory and exactly solved models in the kinetics of irreversible aggregation, Phys. Rep. **383** (2003), 95–212.

[47] M. Li, Y. Han and J. W. Evans, Comment on "Capture-zone scaling in island nucleation: universal fluctuation behaviour", Phys. Rev. Lett. **104** (2010), 149601.

[48] N. Madras, *Lectures on Monte Carlo Methods*, Field Institute Monographs, Amer. Math. Soc. **16**, 2002.

[49] G. Menon and R. L. Pego, Approach to self-similarity in Smoluchowski's coagulation equations, Comm. Pure Appl. Math. **57** (2004), 1197–1232.

[50] G. Menon and R. L. Pego, Dynamical scaling in Smoluchowski's coagulation equations: uniform convergence, SIAM J. Math. Anal. **36** (2005), 1629–1651.

[51] N. Metropolis and S. Ulam, The Monte Carlo method, J. Amer. Statist. Assoc. **44** (1949), 335–341.

[52] P. A. Mulheran, The dynamics of island nucleation and growth - beyond mean-field theory, Europhys. Lett. **65** (2004), 379–385.

[53] P. A. Mulheran, Theory of cluster growth on surfaces, in: *Metallic Nanoparticles (Handbook of Metal Physics vol 5)*, J. A. Blackman, ed., Amsterdam: Elsevier 2009, 73–111.

[54] P. A. Mulheran and J. A. Blackman, Capture zones and scaling in homogeneous thin-film growth, Phys. Rev. B **53** (1996), 10261–10267.

[55] P. A. Mulheran and D. A. Robbie, Theory of the island and capture zone size distributions in thin film growth, Europhys. Lett. **49** (2000), 617–623.

[56] P. A. Mulheran and D. A. Robbie, Island mobility and dynamic scaling during thin film deposition, Phys. Rev. B **64** (2001), 115402-1–5.

[57] T. J. Oliveira and F. D. A. Aarao Reis, Scaling of island size and capture zone distributions in submonolayer growth, Phys. Rev. B **83** (2011), 201405-1–4.

[58] F. Oosawa and S. Asakura, *Thermodynamics of the Polymerization of Protein*, New York: Academic Press, 1975.

[59] M. D. Penrose and A. R. Wade, Random minimal directed spanning trees and Dickman-type distributions, Adv. Appl. Prob. **36** (2004), 691–714.

[60] P. P. Petrov, W. Miller, U. Rehse and R. Fornari, A new method for calculation of island-size distribution in submonolayer epitaxial growth, App. Math. Mod. **35** (2011), 1331–1336.

[61] A. Pimpinelli and T. L. Einstein, Capture-zone scaling in island nucleation: universal fluctuation behaviour, Phys. Rev. Lett **99** (2007), 226102-1–4.

[62] A. Pimpinelli and T. L. Einstein, Response to comment on "Capture-zone scaling in island nucleation: universal fluctuation behaviour", Phys. Rev. Lett **104** (2010), 149602-1.

[63] S. E. Pratsinis, Flame aerosol synthesis of ceramic powders, Prog. Energy Combust. Sci. **24** (1998), 197–219.

[64] W. H. Press, S. A. Teukolsky, W. T. Vetterling and B. P. Flannery, *Numerical Recipes in FORTRAN – The Art of Scientific Computing*, Cambridge University Press, Cambridge 1992.

[65] C. Ratsch, Y. Landa and R. Vardavas, The asymptotic scaling limit of point island models for epitaxial growth, Surf. Sci. **578** (2005), 196–202.

[66] C. Ratsch and J. A. Venables, Nucleation theory and the early stages of thin film growth, J. Vac. Sci. Technol. A **21**(5) (2003), S96-S109.

[67] C. Ratsch, A. Zangwill, P. Smilauer, and D. D. Vvedensky, Saturation and scaling of epitaxial island densities, Phys. Rev. Lett. **72** (1994), 3194–3197.

[68] R. Y. Rubinstein, *Simulation and The Monte Carlo Method*, Wiley, New York 1981.

[69] R. W. Samsel and A. S. Perelson, Kinetics of rouleau formation, Biophys. J. **37** (1982), 493–514.

[70] P. Seba, Parking in the city, Acta Physica Polonica A **112** (2007), 681–690.

[71] F. Shi, Y. Shim and J. G. Amar, Capture-zone areas in submonolayer nucleation: effects of dimensionality and short-range interactions, Phy. Rev. E **79** (2009), 011602-1–6.

[72] I. W. Stewart, A uniqueness theorem for the coagulation-fragmentation equation, Camb. Phil. Soc. **107** (1990), 573–578.

[73] C. Thompson, C. Palasantzas, Y. P. Feng, S. K. Sinha and J. Krim, X-ray reflectivity study of the growth kinetics of vapor-deposited silver films, Phys. Rev. B **49** (1994), 4902–4907.

[74] V. I. Tokar and H. Dreyssé, Universality in size distributions of irreversibly grown epitaxial islands: kinetic Monte Carlo simulations and the rate equations study, Phys. Rev. B **80** (2009), 161403-1–4.

[75] R. P. Treat, On the similarity solution of the fragmentation equation, J. Phys. A **30** (1997), 2519–2543.

[76] I. P. van den Berg, Macroscopic rivers, in: *Dynamic Bifurcations*, E. Benoît, ed., LNM 1493, Springer-Verlag, Berlin 1991, 190–209.

[77] P. G. J. van Dongen and M. H. Ernst, Cluster size distribution in irreversible aggregation at large times, J. Phys. A: Math. Gen. **18** (1985), 2770–2793.

[78] J. A. Venables, G. D. T. Spiller and M. Hanbücken, Nucleation and growth of thin films, Rep. Prog. Phys. **47** (1984), 399–459.

[79] R. D. Vigil and R. M. Ziff, On the stability of coagulation-fragmentation population balances, J. of Coll. Interf. Sci. **133** (1989), 257–264.

[80] B. Voigtländer, Fundamental processes in Si/Si and Ge/Si epitaxy studied by scanning tunneling microscopy during growth, Surf. Sci. Rep. **43** (2001), 128–254.

[81] D. D. Vvedensky, C. Ratsch, F. Gibou and R. Vardavas, Singularities and spatial fluctuations in submonolayer epitaxy, Phys. Rev. Lett. **90** (2003), 189601-1–2.

[82] J. A. D. Wattis, Similarity solutions of a Becker-Döring system with time-dependent monomer input, J. Phys. A: Math. Gen. **37** (2004), 7823–7841.

[83] J. A. D. Wattis, An introduction to mathematical models of coagulation–fragmentation processes: a discrete deterministic mean-field approach, Physica D **222** (2006), 1–21.

[84] R. Wong, *Asymptotic Approximations of Integrals*, SIAM, Philadelphia 2001.

[85] P. -z. Wong and A. J. Bray, Scattering by rough surfaces, Phys. Rev. B **37** (1988), 7751–7758.

[86] R. M. Ziff, An explicit solution to a discrete fragmentation model, J. Phys. A: Math. Gen. **25** (1992), 2569–2576.

[87] R. M. Ziff and E. D. McGrady, Kinetics of polymer pegradation, Marcomolecules **19** (1986), 2513–2519.

[88] A. Zsom and C. P. Dullemond, A representative particle approach to coagulation and fragmentation of dust aggregates and fluid droplets, Astronomy and Astrophysics **489** (2008), 931–941.